

Role of Clays in Bitumen Extraction of Water-Based Oil Sands Processing

by

An Li

A thesis submitted in partial fulfillment of the requirements for the degree of

Doctor of Philosophy

in

Chemical Engineering

Department of Chemical and Materials Engineering
University of Alberta

© An Li, 2019

ABSTRACT

Fines ($< 44 \mu\text{m}$), especially clays ($< 2 \mu\text{m}$), in oil sands ores have a significant impact on the processability of the ore, or performance of bitumen extraction from the ore. The main focus of this research is to understand the effects of the type and wettability of clays on the performance of bitumen extraction from mined oil sands to develop a viable solution in dealing with clay/fines in operations.

The results from batch extraction tests showed a detrimental role of doping hydrophilic clays (kaolinite, illite, and montmorillonite) in suppressing bitumen recovery with montmorillonite being the worst. With 1 ~ 5 wt.% of clays addition, bitumen recovery reduced from the baseline of 88% to 78 ~ 25, 73 ~ 13, and 61 ~ 4% when doped with kaolinite, illite, and montmorillonite, respectively. The presence of clays in bitumen froth was found to be carried over by their attachment to bitumen. The crucial role of clays in bitumen slime-coating was studied through atomic force microscopy (AFM), ζ potential distribution measurement, and clay deposition test. For the hydrophilic clays, repulsive long-range forces with small adhesions between bitumen and the model basal planes of clays were measured by AFM. These forces could not explain the bitumen-clay hetero-coagulation observed in ζ potential distribution measurements in solutions of high clay to bitumen ratios. The deposition tests showed that clay concentration was an essential parameter in determining the bitumen-clay hetero-coagulation process. Strong slime-coating of clay particles on bitumen droplets occurred only above a critical clay concentration for a given type of clays. This critical concentration varied with clay type and water chemistry. In contrast to the results from earlier studies, kaolinite in this study was found to deposit strongly on bitumen surfaces. Under the conditions of extraction tests, the critical concentrations for kaolinite, illite, and montmorillonite were determined to be 12.9, 8.6, and 5.8 g/L, respectively. Increasing pH of

the slurry could improve the critical clay concentrations while the presence of monovalent or divalent cations was found to reduce the critical clay concentrations. To reduce slime-coating in oil sands operations, the concentration of clays in process water should be controlled to be lower than the critical concentration.

Hydrophilic clays were contaminated by soaking in toluene-diluted-bitumen solutions to examine the effect of solid hydrophobicity on bitumen extraction. In this case, different clays had a similar impact on bitumen extraction performance with a bitumen recovery of 68 ~ 29% because their surfaces were covered with similar materials during the soaking process. Due to different surface properties, hydrophobic clays had a less significant depression on bitumen recovery but a more significant deterioration on froth quality than hydrophilic clays. Similar slime-coating was observed among the different clays once contaminated by diluted bitumen, with the results being closely related to the hydrophobicity of contaminated clays. Furthermore, the presence of a large number of clays in bitumen extraction could result in excessive emulsification of bitumen into small droplets, contributing to low bitumen recovery.

A simple and robust method based on the use of X-ray fluorescence (XRF) spectroscopy to measure potassium content was developed as a tool for the determination of the clay/fines content in oil sands. Both the XRF method and the conventional methylene blue titration (MBT) method were used to analyze various solid samples, including model solids with and without surface contamination as well as the solids extracted from bitumen froth and tailings stream. The results showed that the XRF method was more tolerant to surface contamination and therefore more reliable in characterizing clay/fines content in oil sands and relevant processing streams than the MBT method. The high potassium content of froth solids determined by the XRF method served as a marker of low bitumen recovery discussed in this study.

To alleviate or eliminate the negative impact of high fines (clay) content in oil sands on bitumen extraction, NaOH addition and ore blending were tested as the coping strategies. It was found that both were effective in enhancing bitumen recovery.

PREFACE

The research proposal, experimental design, experiments, data analysis, and the preparation of this dissertation were performed by the author under the supervision of Dr. Zhenghe Xu. Except for the below-mentioned experiments, all other experiments were conducted by the author in Dr. Zhenghe Xu's labs at the University of Alberta.

– Bitumen extraction tests using process water at different levels of NaOH addition in Chapter 6 were performed by Mr. Han Wang, MSc. student at the University of Alberta, Department of Chemical and Materials Engineering.

– Surface tension measurements were performed by Dr. Ci Yan at the University of Alberta, Department of Chemical and Materials Engineering.

Manuscripts based on Chapters 3 and 4 are in preparation for publication.

A version of Chapter 5 has been accepted for publication in the Canadian Journal of Chemical Engineering.

ACKNOWLEDGEMENTS

I would like to sincerely thank all the people who have helped me during my Ph.D. study. I managed to complete my journey toward graduation with the support and encouragement of countless people.

First of all, I am full of gratitude to my research supervisor Dr. Zhenghe Xu, for his guidance, motivation, and invaluable suggestions which have not only contributed greatly to my research but also to my life. I appreciate his tolerance and patience to help me to finish my program and to train me to be a better researcher.

I also gratefully acknowledge Dr. Jun Long for his advice and support on my research, especially the writing of this thesis. His encourage and kindly sharing decades of wisdom benefit me a lot.

Special thanks to Dr. Qingxia Liu, Dr. Ci Yan, Dr. Chen Wang, Dr. Deepak Pudasainee, Mr. Shiraz Merali, and Ms. Ni Yang, who has been a source of ideas and help.

I am most grateful to Mr. Jim Skwarok, Ms. Jie Ru, Ms. Lisa Carreiro, Ms. Lily Laser, and all staff in lab and office for their instances and assistance along the way.

Many thanks go to my research colleagues in our oilsands group especially those whom I had the pleasure to collaborate with, Zhen Niu, Xiao He, Yelin Zhu, Yang Tan, Jing Chang, Rui Li, Yi Lu, Derek Russell, and Nina Ivanova. In particular, it would have been much difficult for me to handle the heavy equipment without Han Wang's help, thank you, Han.

It is not an easy feat to set up or carry out an experiment. I thank Ms. Adriana Briones, Dr. Lan Liu, Ms. Nan (Nancy) Zhang, Dr. Zuoli Li, Dr. Zhenzhen Lu, and Dr. Yuechao Tang, for their guidance and training.

I am grateful for the fund support from the Natural Sciences and Engineering Research Council (NSERC) Industrial Research Chair (IRC) Program in Oil Sands Engineering. I acknowledge the use of the samples provided by Syncrude Canada Ltd. and Teck Resources Ltd.

Anyone would be proud of calling them friends, Le Liu, Sangni Wang, Bingjie (Mandy) Ma, Xinrui Ma, and Bailin Xiang. They helped my time during the Ph.D. program to make it more exciting and enjoyable. I truly appreciate and love all my friends.

Finally, my eternal thanks go to my husband Tao Shui and my parents, Shuliang Chen and Jiugen Li, for their companionship, sharing, and encouragement when the going was smooth. And their consolation, prayers, and support when the going was tough. Thank you for never stop loving me.

Table of Contents

CHAPTER 1 INTRODUCTION.....	1
1.1 BACKGROUND	1
1.2 RESEARCH OBJECTIVES.....	3
1.3 THESIS OUTLINE.....	4
CHAPTER 2 LITERATURE REVIEW.....	7
2.1 THE OIL SANDS FORMATION	7
2.1.1 Composition of oil sands	8
2.2 WATER-BASED BITUMEN EXTRACTION PROCESS.....	9
2.2.1 Small-scale bitumen recovery.....	11
2.2.1.1 Liberation and coalescence	12
2.2.1.2 Aeration and flotation.....	14
2.2.2 NaOH addition.....	15
2.3 FINES AND CLAYS.....	18
2.3.1 Fines.....	19
2.3.2 Properties of clay mineral	20
2.3.3 Kaolinite.....	22
2.3.4 Illite	23
2.3.5 Montmorillonite.....	25

2.3.6 Important clay properties	26
2.3.6.1 Zeta (ζ) potential	26
2.3.6.2 Methylene blue index (MBI).....	28
2.4 EFFECT OF FINES/CLAYS ON ORE PROCESSABILITY	31
2.4.1 Bitumen slime coating	32
2.4.2 Wettability control	36
2.5 THE MINERALOGICAL METHODS	37
2.5.1 Optical mineralogy.....	38
2.5.2 Automated mineralogy.....	38
2.5.3 X-ray diffraction (XRD)	39
2.5.4 Element analysis	41
2.5.4.1 X-ray fluorescence (XRF)	43
CHAPTER 3 UNDERSTANDING THE EFFECT OF CLAY TYPE AND SOLID WETTABILITY ON BITUMEN EXTRACTION FROM CANADIAN OIL SANDS	46
3.1 INTRODUCTION	46
3.2 MATERIALS AND METHODS.....	50
3.2.1 Materials	50
3.2.2 Bitumen extraction test	51
3.2.3 Wettability modification of clay particles.....	52
3.2.4 ζ potential distribution measurement	53

3.2.5 Colloidal force measurement using scanning probe microscope (SPM)	53
3.2.5.1 <i>Sample preparation</i>	53
3.2.5.2 <i>Colloidal force measurement</i>	54
3.2.6 Clay deposition measurement	55
3.2.7 Contact angle measurement	57
3.3 RESULTS AND DISCUSSION.....	57
3.3.1 Effect of hydrophilic clays on bitumen extraction.....	57
3.3.1.1 <i>Bitumen recovery</i>	57
3.3.1.2 <i>Froth quality</i>	59
3.3.2 Effect of hydrophobic clays on bitumen extraction	61
3.3.2.1 <i>Bitumen recovery</i>	61
3.3.2.2 <i>Froth quality</i>	62
3.3.3 Mechanistic study on the effect of clays content on bitumen extraction.....	64
3.3.3.1 <i>ζ potential distributions</i>	64
3.3.3.2 <i>Clay deposition on diluted bitumen droplets.</i>	67
3.3.4 Interaction forces between bitumen and clays	71
3.3.4.1 <i>Interaction forces between bitumen and hydrophilic clays</i>	71
3.3.4.2 <i>Interaction forces between bitumen and hydrophobic clays</i>	73
3.3.5 System stability	75
3.3.6 Bitumen droplet size	78
3.4 CONCLUSIONS.....	79

CHAPTER 4 DEPOSITION AND SEPARATION OF CLAY PARTICLES AT THE BITUMEN-WATER INTERFACE	81
4.1 INTRODUCTION	81
4.2 MATERIALS AND METHODS.....	84
4.2.1 Materials	84
4.2.2 Methods.....	84
4.2.2.1 <i>Emulsion preparation</i>	84
4.2.2.2 <i>Deposition of kaolinite particles on bitumen surfaces</i>	85
4.2.2.3 <i>Separation of kaolinite particles from bitumen surfaces</i>	86
4.3 THEORETICAL BASIS.....	87
4.4 RESULTS AND DISCUSSION	88
4.4.1 Effect of pH.....	88
4.4.2 Effect of NaCl concentration	90
4.4.3 Effect of CaCl ₂ concentration	93
4.4.4 Separation	94
4.5 INDUSTRIAL IMPLICATIONS	96
4.6 CONCLUSIONS.....	97

CHAPTER 5	DETERMINATION OF CLAY CONTENT IN CANADIAN OIL SANDS USING X-RAY FLUORESCENCE SPECTROSCOPY FOR DIAGNOSIS OF ORE PROCESSABILITY	99
5.1	INTRODUCTION	99
5.2	MATERIALS AND METHODS.....	104
5.2.1	Materials	104
5.2.2	Methods.....	106
5.2.2.1	<i>Methylene blue titration</i>	106
5.2.2.2	<i>X-ray fluorescence analysis</i>	107
5.2.2.3	<i>Bitumen contamination and toluene washing</i>	107
5.2.2.4	<i>Low temperature ashing (LTA)</i>	108
5.2.2.5	<i>Contact angle measurement</i>	108
5.2.2.6	<i>Oil sands extraction</i>	109
5.2.2.7	<i>Wet sieving</i>	110
5.3	RESULTS AND DISCUSSION	111
5.3.1	Sensitivity of potassium content to illite ratio in the mixture.....	111
5.3.2	Correlation of potassium contents measured by XRF and MBI.....	113
5.3.3	Effects of bitumen contamination.....	116
5.3.4	Hydrophobicity of clays.....	122
5.3.5	Application to oil sands	124
5.4	CONCLUSIONS.....	126

CHAPTER 6	STRATEGIES FOR IMPROVING THE PROCESSABILITY OF OIL SANDS ORES OF HIGH FINES CONTENT	128
6.1	INTRODUCTION	128
6.2	MATERIALS AND METHODS.....	131
6.2.1	Materials	131
6.2.2	Methods.....	132
6.2.2.1	<i>Bitumen extraction test</i>	132
6.2.2.2	<i>ζ potential distribution measurement</i>	133
6.2.2.3	<i>Carboxylic surfactant analysis</i>	133
6.2.2.4	<i>Surface tension</i>	134
6.2.2.5	<i>X-ray fluorescence</i>	134
6.3	RESULTS AND DISCUSSION.....	135
6.3.1	Effect of doped fines on extraction performance.....	135
6.3.2	Effect of caustic addition on extraction performance	136
6.3.2.1	<i>Slime coating</i>	139
6.3.3	Effect of ore blending on extraction performance	142
6.3.3.1	<i>Water chemistry</i>	144
6.4	EVALUATION STRATEGY: XRF DETERMINED POTASSIUM CONTENT	146
6.5	CONCLUSIONS.....	147
CHAPTER 7	OVERALL CONCLUSIONS AND FUTURE WORK	149

7.1 OVERALL CONCLUSIONS.....	149
7.2 FUTURE WORK.....	151
REFERENCE.....	153
APPENDIX A: EFFECT OF CLAYS ON FROTH SOLIDS PARTICLE SIZE DISTRIBUTION.....	197
APPENDIX B: ZETA POTENTIAL DISTRIBUTIONS	202
APPENDIX C: DLVO/EDLVO FITTING EQUATIONS AND PARAMETERS	210
APPENDIX D: XRF ELEMENT ANALYSIS FOR ESTIMATING ORE PROCESSABILITY	214

List of Tables

Table 2.1. Classification of oil sands according to bitumen content	9
Table 2.2. Mineral components in total oil sand solids (Hepler and Smith, 1994)	18
Table 3.1. Volume-based passing size (d_{50} and d_{90}) of clays used in this study before and after homogenizing by a 500 ultrasonic dismembrator	50
Table 3.2. Results of BEU tests with the addition of hydrophilic solids	59
Table 3.3. Contact angles of water on various solids before and after wettability modification..	61
Table 3.4. Results of BEU tests with the addition of hydrophobic solids	63
Table 3.5. Solids-to-bitumen ratio for slime-coating of bitumen by fine solids measured under various conditions	67
Table 3.6. Multilayer model parameters of particle deposition	70
Table 3.7. Hamaker constants	77
Table 4.1. Multilayer model parameters of particle deposition at different pH values	90
Table 4.2. Multilayer model parameters of particle deposition at pH 8.0 with NaCl addition.....	92
Table 4.3. Multilayer model parameters of particle deposition at pH 8.0 with CaCl_2 addition ...	94
Table 4.4. Separation percent of added clay particles at various C_{wi} values at pH 5.0~5.6	95
Table 4.5. Separation percent of added clay particles at $C_{wi} = 28.6$ g/L under various conditions	96
Table 5.1. 50% passing size (d_{50}) of model solids used in this study	104
Table 5.2. Ion concentration of process water used in this study	105
Table 5.3. Composition of oil sands ores used in this study	105
Table 5.4. Solids extracted from oil sands processing streams used in this study	110
Table 5.5. K content (measured by XRF) of typical solid types in oil sands solids	112

Table 5.6. Water contact angle of model illite before and after bitumen contamination	123
Table 5.7. Methylene blue index of model illite after several treatments.....	124
Table 6.1. Composition of three oil sands ore samples used in this study	131
Table 6.2. Ion concentration of process water used in this study	132

List of Figures

Figure 2.1. Model structure of oil sands (Madge et al., 2004).....	8
Figure 2.2. Generalized scheme for water-based extraction process (Masliyah et al., 2004).	10
Figure 2.3. Interfacial energies in bitumen-sand-water system.	13
Figure 2.4. Interfacial energies in bitumen-air-water system.	14
Figure 2.5. Optimized caustic control in relation to fines content and ore grade for bitumen extraction (Long, 2016).	19
Figure 2.6. The particle size range of gravel, sand, silt, and clay (Kaminsky, 2010).....	20
Figure 2.7. Composition of clay fraction (Kaminsky, 2010).....	21
Figure 2.8. Two basic layers in clay mineral structure (Jordán, 2014).....	22
Figure 2.9. Sketch of the structure of kaolinite (Poppe et al., 2001).	23
Figure 2.10. Sketch of the structure of illite (Poppe et al., 2001).	24
Figure 2.11. Sketch of the structure of montmorillonite (Poppe et al., 2001).	25
Figure 2.12. Illustration of ζ potential in electric double layers (Valiño et al., 2014).....	27
Figure 2.13. Structure of a methylene blue cation.	28
Figure 2.14. Effect of slime-coating on bitumen flotation (Wallace et al., 1989).....	33
Figure 2.15. Interaction forces and adhesion forces (inset) between bitumen and fines isolated from tailings of good (open symbol, white bars) and poor (filled symbol, shaded bars) processing ores in tailings water of pH 8.5 (Liu et al., 2004a).....	34
Figure 2.16. Schematic ζ potential distributions for a hypothetical bitumen-clay system. a) ζ potential distribution of two components measured individually, b) binary mixture without slime-coating, c) binary mixture with strong slime-coating (complete coverage), d) binary mixture with strong	

slime-coating (partial coverage due to insufficient clays), e) binary mixture with weak slime-coating (Liu et al., 2002).....	35
Figure 2.17. Typical EDXRF arrangement and principle (http://www.goldtester.in/introduction-of-XRF-technology.html).	43
Figure 3.1. Schematics of wettability modification of clay particles.	53
Figure 3.2. Effect of doping solids on bitumen recovery: a) hydrophilic solids and b) bitumen contaminated solids.....	58
Figure 3.3. Effect of doping solids on froth quality: a) hydrophilic solids and b) bitumen contaminated solids.....	60
Figure 3.4. ζ potential distributions of bitumen emulsion and illite suspension (a) and their mixtures at 5:1(b), 6:1(c), and 10:1 (d) clay to bitumen mass ratios in 1 mM KCl aqueous solutions of pH 8.0.....	65
Figure 3.5. Deposition isotherms of clays on diluted bitumen droplets in aqueous suspensions without pH control (pH=5.0~5.6).	68
Figure 3.6. ζ potential distributions of bitumen emulsion and kaolinite suspension (a) and their mixture at 1:1 kaolinite to bitumen mass ratio of 15 g/L kaolinite (b) in 1 mM KCl aqueous solutions without pH control (pH=5.0~5.6).....	70
Figure 3.7. Colloidal forces between bitumen probe and silica wafers in 1 mM KCl aqueous solutions of different pHs. (a) long-range force; and (b) adhesion force.....	71
Figure 3.8. Colloidal forces between bitumen probe and alumina wafers in 1 mM KCl aqueous solutions of different pHs. (a) long-range force; and (b) adhesion force.....	72
Figure 3.9. Colloidal forces between bitumen probe and hydrophobic silica wafers in 1 mM KCl aqueous solutions of different pHs. (a) long-range force; and (b) adhesion force.	74

Figure 3.10. Colloidal forces between bitumen probe and hydrophobic alumina wafers in 1 mM KCl aqueous solutions of different pHs. (a) long-range force; and (b) adhesion force.....	75
Figure 3.11. Bitumen droplet size in flotation slurry with (a) no clay addition; (b) 2 wt.% hydrophilic illite addition; (c) 5 wt.% hydrophilic illite addition; (d) 2 wt.% hydrophobic illite addition; (e) 5 wt.% hydrophobic illite addition.....	79
Figure 4.1. Schematic illustration for preparing diluted bitumen in water emulsion with kaolinite addition.....	85
Figure 4.2. Deposition isotherms of kaolinite particles on diluted bitumen droplets in aqueous suspensions of different pH values.....	89
Figure 4.3. Deposition states of kaolinite particles on diluted bitumen droplets.....	90
Figure 4.4. Deposition isotherms of kaolinite particles on diluted bitumen droplets in aqueous suspensions at pH 8.0 containing different levels of NaCl.....	92
Figure 4.5. Deposition isotherms of kaolinite particles on diluted bitumen droplets in aqueous suspensions at pH 8.0 containing different levels of CaCl ₂	94
Figure 4.6. Critical concentration diagram for kaolinite clays a) at different pH; and at a given pH of 8.0 with the addition of b) sodium ions; or c) calcium ions.....	97
Figure 5.1. Correlation between the K content measured by XRF and illite ratios in the illite (I)-Teck fines 1(T), illite (I)-kaolinite (K), and illite (I)-sand (S) mixtures.....	113
Figure 5.2. Correlation between MBI and illite ratios in the illite (I)-Teck fines 1 (T) and illite (I)-kaolinite (K) mixtures.....	114
Figure 5.3. Correlation between the K content measured by XRF and MBI of illite (I)-Teck fines 1(T) and illite (I)-kaolinite (K) mixtures (linear fitting).....	115

Figure 5.4. Effect of bitumen contamination, toluene washing, and LTA cleaning on K content measured by XRF and MBI of illite (I)-kaolinite (K) mixtures.....	118
Figure 5.5. FTIR spectra of illite (I)-kaolinite (K) mixtures before and after various treatments (TW=toluene washing).	119
Figure 5.6. TGA spectra of illite samples before and after various treatments.	120
Figure 5.7. Effect of bitumen contamination, toluene washing, and LTA cleaning on K content measured by XRF and MBI of illite (I)-Teck fines 1 (T) mixtures.	121
Figure 5.8. FTIR spectra of illite (I)-Teck fines 1 (T) mixtures before and after various treatments (TW=toluene washing).	121
Figure 5.9. Effect of toluene washing, Dean Stark, and LTA cleaning on the K content measured by the XRF and MBI of (a) primary froth solids and (b) tailings solids of ore A.	125
Figure 5.10. Correlation between the fines content and K content measured by XRF.....	126
Figure 6.1. Effect of fines on (a) bitumen recovery and (b) froth quality of ore G.	136
Figure 6.2. Effect of NaOH addition on (a) bitumen recovery and (b) froth quality of ore HF.	138
Figure 6.3. Effect of NaOH addition on (a) bitumen recovery and (b) froth quality of ore MF.	138
Figure 6.4. ζ potential distributions of bitumen emulsion and fines suspension (a) and their mixtures at 3:1(b), 4:1(c), and 5:1 (d) fines to bitumen mass ratios in 1 mM KCl aqueous solutions without pH control.	139
Figure 6.5. ζ potential distributions of bitumen emulsion and fines suspension (a) and their mixtures at 5:1(b), 6:1(c), and 8:1 (d) fines to bitumen mass ratios in 1 mM KCl aqueous solutions of pH 8.0.	140
Figure 6.6. ζ potential distributions of bitumen emulsion and fines suspension (a) and their mixture at 20:1 fines to bitumen mass ratio (b) in 1 mM KCl aqueous solutions of pH 10.8.	141

Figure 6.7. Effect of ore blending on (a) bitumen recovery and (b) froth quality of ore MF and ore HF with the addition of NaOH.....	142
Figure 6.8. Effect of blending ratio on (a) bitumen recovery and (b) froth quality of ore MF and ore HF at 0.05% caustic level.	144
Figure 6.9. Effect of ore blending on (a) carboxylic surfactant concentration and (b) surface tension of tailing water at 3 caustic levels.....	145
Figure 6.10. Correlation between overall bitumen recovery and XRF determined potassium content in froth solids.	147

NOMENCLATURE

Abbreviations

AFM	Atomic force microscopy
XRF	X-ray fluorescence
EDXRF	Energy dispersive XRF
WDXRF	Wavelength dispersive XRF
MBT	Methylene blue titration
SCO	Synthetic crude oil
MBI	Methylene blue index
SEM	Scanning electron microscopy
XRD	X-ray diffraction
QXRD	Quantitative XRD
PSV	Primary separation vessels
PSC	Primary separation cells
BEU	Batch extraction units
MBEU	Modified BEU
LHES	Laboratory hydrotransport extraction system
DCM	Dichloromethane
FTIR	Fourier transform infrared spectroscopy
T	Tetrahedron/ tetrahedral
O	Octahedron/ octahedral
PZC	Point of zero charge

IEP	Isoelectric point
meq	Milliequivalent
BET	Brunauer-Emmett-Teller
SSA	Specific surface area
UV-VIS	Ultraviolet visible
QCM-D	Quartz crystal microbalance with dissipation monitoring
OIA	Optical image analyses
MLA	Mineral liberation analyzer
QEMSCAN	Quantitative evaluation of minerals by scanning electron microscopy
XPS	X-ray photoelectron spectroscopy
INNA	Instrumental neutron activation analysis
LIBS	Laser-induced breakdown spectroscopy
ICP-MS	Inductively coupled plasma mass spectroscopy
PIXE	Particle induced X-ray emission
AAS	Atomic absorption spectrometer
API	American petroleum institute
S/B	Solids to bitumen
DLVO	Derjaguin-Landau-Verwey-Overbeek
SPM	Scanning probe microscope
E-DLVO	Extended DLVO
ppm	Parts per million
O/W	Oil-in-water

W/O	Water-in-oil
DP	Desorption percent
LTA	Low temperature ashing
I	Illite
K	Kaolinite
T	Teck fines 1
S	Sand
TGA	Thermal gravimetric analysis
IPA	Isopropyl alcohol
DTGS	Deuterated triglycine sulfate
CSC	Critical surfactant concentration

Symbols

ζ	Zeta potential
ΔG	Gibbs free energy
ΔA	Surface area
$\gamma_{S/W}$	Interfacial tension between solids and water
$\gamma_{B/W}$	Interfacial tension between bitumen and water
$\gamma_{B/S}$	Interfacial tension between bitumen and solids
$\gamma_{B/A}$	Interfacial tension between bitumen and air
$\gamma_{A/W}$	Interfacial tension between air and water
θ	Contact angle
d_b, d_a	Diameter

Ψ_s	Surface potential
X_m	Adsorbed molecules in mole/g
N	Avogadro number
A	Area
λ	Wavelength
n	Number of wavelengths
d	Distance
d	Diameter
M	Matrix of the element composition of minerals
x	Weight percentage
b	Element composition of the sample
C_{wi}	Initial concentration of clays in aqueous phase
C_w	Equilibrium concentration of clays in aqueous phase
C_b	Equilibrium concentration of clays on the bitumen droplets
$C_{cri,b}$	Critical concentration of clays at pH b
C_w^m	Equilibrium concentration of clays in aqueous phase at monolayer coverage
C_{wi}^m	Initial concentration of clays in aqueous phase at monolayer coverage
$W_t, W_o, W_i, W_w, W_{on}$	Weight
$V_t, V_w, V_o, V_{ea}, V_{wa}$	Volume
k_1, k_m	Equilibrium constants for deposition
C_m	Monolayer coverage

R	Clay to bitumen ratio
F_H	Hydrophobic force
C_0, D_0	E-DLVO fitting parameters
R	Radius
P_s, P_c, P_a, P_d	Probability
k_B	Boltzman constant
ε	Dielectric constant
h	Plank constant
ν_e	UV absorption frequency
n	Refractive index
S	Stability ratio

CHAPTER 1 INTRODUCTION

1.1 BACKGROUND

Oil sands are comprised of mineral solids, bitumen, and water. The deposit of oil sands in northern Alberta represents a vast unconventional petroleum resource. The oil sands can be processed to recover the bitumen, which can then be upgraded into synthetic crude oil (SCO) to be fed to refineries to produce gasoline, diesel fuel, jet fuel, and heating oil. Alberta's oil sands deposit can potentially provide Canada with a stable supply of SCO for more than 200 years (Masliyah et al., 2011). Depending on the depth of the deposit, the bitumen can be recovered through either open-pit mining (for deposition depth <75 m) or in-situ drilling (for deposition depth >75 m) (Chew, 2014; Chalaturnyk et al., 2002; Rosa et al., 2017). It was estimated that around 45 % of the bitumen production was from surface mining (AER report, 2018). In a surface mining operation, the ore is mined from an open pit first. The mined ore is then processed through ore preparation and bitumen extraction to produce a bitumen froth product for further treatment. The bitumen extraction process involves a few elemental steps, including the liberation of the bitumen from the sand grains and the coalescence, aeration, and flotation of the bitumen droplets (Takamura and Wallace, 1988; Basu, et al., 1997; Moran et al., 2000; Gu et al., 2004; Alexander and Li, 1996). The efficiency and success of these steps are critical to bitumen recovery and froth quality, which are the key performance indicators for the evaluation of an extraction process.

To maximize bitumen recovery is very important for the oil sands industry from the perspective of both economic and resource utilization. It has been estimated that a 1% reduction in bitumen recovery at the present rate of bitumen production in Canada is equivalent to about \$ 442 million loss annually (Millington, 2018). Industrial experience and laboratory research have shown that the fines (<44 μm) content of the ore is one of the most important parameters that affect bitumen

extraction performance. Fine particles, especially clays, are reported to be detrimental to bitumen recovery. (Sanford, 1983; Tu et al., 2005; Kasongo et al., 2000; Ding et al., 2006; Zhou et al., 1999, 2017a, 2017b). The tests by Fong et al. (2004) showed that bitumen recovery was sharply decreased when 1 to 5 wt.% of kaolinite was added to the ore feed or 0.05 to 1 wt.% of montmorillonite was added. The detrimental effect of clays in bitumen extraction was mainly due to the coating of the bitumen droplets by the clay particles, aka slime-coating (Liu et al., 2005b). Slime-coating leads to worse bitumen coalescence, aeration, and flotation, and eventually bitumen recovery and froth quality (Masliyah et al., 2004). This detrimental effect was found to become worse in the presence of divalent cations such as calcium or magnesium ions or high salinity environment (Kasongo et al., 2000; Liu et al., 2004b; Chen et al., 2017). The introduction of chemical aids, such as NaOH was capable of alleviating or eliminating the negative effects of clays to optimize extraction performance (Schramm et al., 2003; Masliyah et al., 2004).

In the oil sands industry, mineralogical methods have been extensively used to characterize the fine solids (clays), with the results being correlated with the ore processability (Kaminsky, 2014; Parian et al., 2015; Donkor et al., 1996; Harhira et al., 2018). Traditionally used methylene blue index (MBI) was one of the early indicators of ore processability (Kaminsky, 2014). Ores with an MBI less than or equal to 0.6 meq/100g are usually processed well. While poor processing ores typically have an MBI greater than 1.3 meq/100g. Ores with an MBI between 0.6 and 1.3 meq/100g are very sensitive to process water chemistry. However, the determination of MBI depends greatly on operators and varies from one operator to another. Other mineralogy methods such as scanning electron microscopy (SEM) and X-ray diffraction (XRD) are expensive, time-consuming, and require tedious sample preparation (Omotoso and Eberl, 2009; Lastra and Petruk, 2014). To find

a simple and robust method to measure clay/fines related properties and to correlate them with oil sands processability is therefore of great importance.

1.2 RESEARCH OBJECTIVES

This research focuses on the influence of clays on bitumen extraction. Fines and clays are known to be detrimental to bitumen extraction, mainly due to their attachment on bitumen droplets that causes slime-coating. It was found that the degree of slime-coating depends on both the type of clays and water chemistry. However, the roles of clay concentration and solid wettability in bitumen-clay hetero-coagulation have not been well studied. Also, fast and reliable techniques for measuring the clay content in the ores have not been readily available. The overall goal of the current research is to further understand the impact of clays on bitumen extraction, and to explore new methods for measuring clays in oil sands, and to develop coping strategies to counteract the negative impact of clays on bitumen extraction. More specifically, the objectives of this Ph.D. thesis research include:

(1) To investigate the effects of various types of clays and their surface wettability on bitumen extraction by performing extraction tests with doping clays of varying surface properties.

(2) To understand the role of clay concentration in bitumen-clay interactions (slime-coating) and to determine the threshold concentrations of clays in processing streams with different water chemistry.

(3) To demonstrate the feasibility of using XRF to determine potassium content so as to provide a measurement of clay/fines content in oil sands.

(4) To explore the use of NaOH and ore blending to alleviate the negative impacts of clays or fine solids on bitumen extraction.

1.3 THESIS OUTLINE

Chapter 1

- Introduces the areas, statement of problems, objectives, and organization of this thesis.
- A brief background on oil sands and clay mineralogy are discussed.

Chapter 2

- The formation and composition of oil sands and the elementary steps in a water-based bitumen extraction process are reviewed.
- The components, structures, and properties of fines and clays, and their roles in determining oil sands processability are reviewed.
- Mineralogic methods for characterizing oil sands solids and their applications in various fields discussed in previous studies are reviewed.

Chapter 3

- Presents the results of bitumen extraction test with clays addition for understanding the effects of clays on bitumen recovery and froth solids/bitumen ratios.
- Shows the impacts of clay mineralogy and surface wettability on bitumen extraction, bitumen-clay interaction, and bitumen droplet size in flotation.
- Develops the strategy of clay deposition test in the diluted bitumen-in-water emulsion to investigate the role of clay concentration in bitumen slime-coating.

- Provides critical concentrations of kaolinite, illite, and montmorillonite clays in aqueous solution to produce slime-coating in the absence of cations without pH control.

Chapter 4

- Compares the deposition isotherms of kaolinite clays from aqueous phase to bitumen-water interface at different pH and at a given pH with different water chemistry.

- Studies the separation characteristics of kaolinite clays from bitumen surfaces to evaluate the strength of the clay-bitumen attachments.

- Further provides critical concentrations of kaolinite clays at different aqueous pH and various levels of monovalent or divalent cations in oil sands processing.

Chapter 5

- Compares the XRF determined potassium content with the traditional MBT method to indicate clay/fines concentrations in the clean system.

- Examines the tolerance of the two methods to surface contamination by organic compounds to find a more appropriate method to determine clay/fines contents in oil sands.

Chapter 6

- Evaluates the effectiveness of NaOH addition and ore blending to improve the processability of ores with high fines content by considering slime-coating control and water chemistry.

- Correlates potassium content of froth solids determined by XRF with overall bitumen recovery.

Chapter 7

- Summarizes the overall conclusions from this work. The contributions and possible extensions of this investigation are presented.

Appendixes

- Provide the additional results of this thesis.

CHAPTER 2 LITERATURE REVIEW

2.1 THE OIL SANDS FORMATION

Canadian oil sands represent the third-largest petroleum reserves in the world, ranking behind Saudi Arabia and Venezuela. Over 1 trillion barrels of heavy oil or bitumen are locked at relatively shallow depth deposits in several areas within the province of Alberta (Janeth, 2005): Athabasca, Peace River, and Cold Lake.

As now delineated, oil sands, tar sands, and bituminous sands are all used to refer to sand beds saturated with various carbon disulphide soluble bitumen that are heavy, viscous, and cannot be extracted by conventional petroleum recovery methods (Berkowitz and Speight, 1975). To date, there are two main ways to recover the bitumen from the oil sands: open-pit mining and in-situ drilling (Masliyah et al., 2011). Surface mining is generally limited to ores with less than 75 m of overburden. The mined oil sands are further treated in a water-based extraction process to recover the bitumen. In situ bitumen recovery is required to tap the deposits that are too deeply buried to be produced by the mining operation. In general, more than 90 percent of the oil sands reserves in Alberta are considered potentially recoverable by in-situ drilling only (Mossop, 1980).

Global demand for oil and its economic potential drive the development of oil sands to continue. It is essential to alleviate any detrimental effects as much as possible to proceed this development in a manner to minimize impacts on the health and welfare of the humans, wildlife, and environment (Giesy et al., 2010).

2.1.1 Composition of oil sands

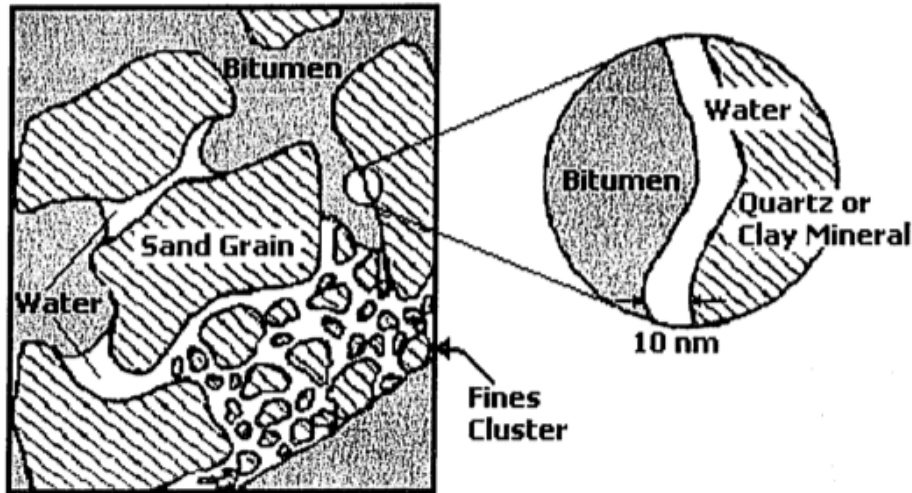


Figure 2.1. Model structure of oil sands (Madge et al., 2004).

Typical oil sands contain an intimate mixture of sand grains of various particle sizes, bitumen, water, and other minerals. As described in Figure 2.1, bitumen is hypothetically isolated from the solid matrix by a thin layer of connate water that is ~10 nm thick (Madge et al., 2004). This connate water film envelops the surfaces of individual sand grains and clay minerals are suspended in the water phase (Takamura, 1982; Mossop, 1980; Hall et al., 1983). The sand grains in oil sands are believed to be hydrophilic or water wet, providing a significant basis for a water-based bitumen extraction process to be workable (Ball, 1935; Clark and Pasternack, 1932). The hydrophobic bitumen surrounding the water encapsulates solid grains and fills the void volume.

The bitumen content in Alberta oil sands ranges from ~0 to ~16 wt.%. Table 2.1 summarizes the general classification of oil sands according to the bitumen content (Masliyeh et al., 2011). Typically, the mined oil sands fall in the range of 9~13 wt.% bitumen.

Table 2.1. Classification of oil sands according to bitumen content

Grade	Bitumen content (wt.%)
Low	<8
Average	8~11
High	>11

In the oil sands industry, mineral fines are referred to as solids smaller than 44 μm while clays are particles of sizes smaller than 2 μm . Their contents are expressed as the fraction of the total solids. Generally, there is a positive correlation between the contents of fines and clays in oil sands solids. The fines percent in an oil sands ore is an important ore characteristic (Sanford, 1983). By and large, there is an inverse correlation between fines content and bitumen grade in oil sands (Hendrickson, 1975), and a reasonable correlation exists between fines content and bitumen recovery. Other parameters being equal, a high fines content in the ore leads to a low bitumen recovery (Sanford, 1983; Kasongo, 2006). The particle sizes of oil sands solids can vary over quite a large range. The corresponding fines content in mineral solids ranges from ~5 to ~60%. The chemistry of the water associated with the sand grains is similar to that of sea water. In summary, the properties of ore determine its processability, which can also be affected by the addition of chemical aids, energy consumption, and process optimization.

2.2 WATER-BASED BITUMEN EXTRACTION PROCESS

Currently, around 45% of the bitumen production in Alberta is from surface mining with water-based extraction processes (AER report, 2018). The hot water extraction process operating at 70~80 $^{\circ}\text{C}$ was first developed by Karl Clark (Clark, 1929, 1944; Clark and Pasternack, 1932). To reduce operation costs and greenhouse gas emissions, a cold water extraction process was developed to produce bitumen at lower temperatures (e.g., 35 $^{\circ}\text{C}$) (Sury, 1990). In recent years, the

warm water extraction processes operating at $\sim 55^\circ\text{C}$ are widely used in industrial operations (Long et al., 2007).

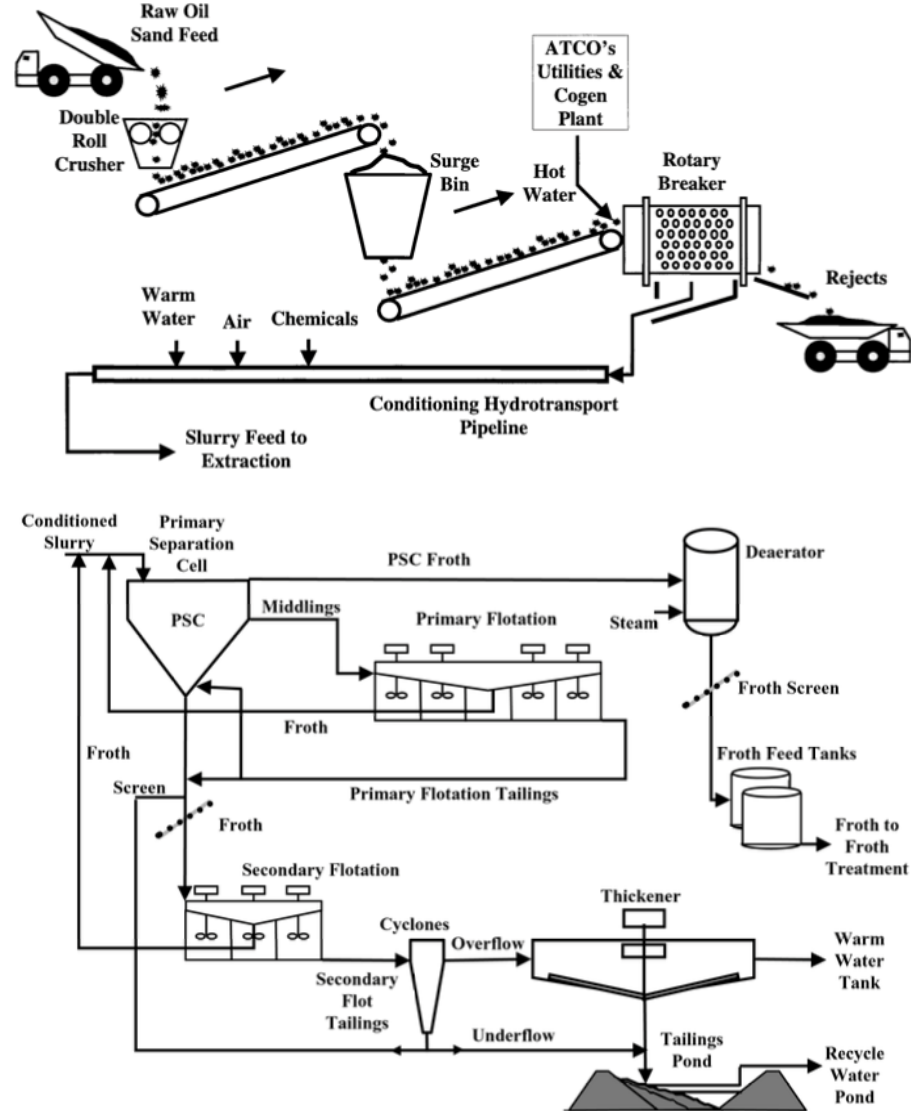


Figure 2.2. Generalized scheme for water-based extraction process (Masliyah et al., 2004).

An example of commercial water-based ore preparation and bitumen extraction circuits is shown in Figure 2.2. The oil sands mined by trucks and shovels are crushed and mixed with process water in mixing boxes, stirred tanks, cyclo-feeders (Syncrude) or rotary breakers (Suncor and

Albian) with the addition of chemical additives (e.g., NaOH). The formed oil sands slurry is then transferred through hydro-transport pipelines to primary separation vessels/cells (PSV/PSC). During transportation, oil sand lumps are sheared, and bitumen is released from the sand grains and attached to entrained or introduced air bubbles. In PSV/PSC, the aerated bitumen floats to the top (bitumen froth), while solids settle to the bottom as a result of gravity separation and are drained as tailings. The bitumen froth, typically comprised of 60% bitumen, 30% solids, and 10% water, is diluted by solvents to lower its viscosity and to increase the density difference between the bitumen and the water to allow the bitumen to be separated from solids and water. Then the treated bitumen is ready for upgrading and refining. The tailings slurry is discharged to thickeners and then to tailings pond for further treatment and water recycle. This general process with some modifications and improvements has been widely employed for oil sands processing.

2.2.1 Small-scale bitumen recovery

Generally, the bitumen recovery process involves a few elementary steps: liberation, coalescence, aeration, and flotation. Under the synthetic effect of process water chemistry and operational conditions, bitumen layers on sand surfaces rupture to form droplets. The liberated bitumen droplets partially coalesce. Air is introduced into the system to float the bitumen droplets. Bitumen droplets attach to ($< 35\text{ }^{\circ}\text{C}$) or engulf ($45\text{--}80\text{ }^{\circ}\text{C}$) air bubbles to be recovered in bitumen froth (Masliyah et al., 2004).

Small-scale batch extraction units were built to simulate bitumen recovery from oil sands. There are two primary laboratory-scale devices for oil sands processability evaluation: Denver flotation cells (Zhou et al., 2004; Kasongo et al., 2000) and batch extraction units (BEU) (Sanford and Syer, 1979; Romanova et al., 2006; Mikula et al., 2007). For these lab-scale tests, oil sands ore of $\sim 500\text{ g}$ and process water of $900\text{--}1000\text{ mL}$ are used in one test. It was found that a Denver

flotation cell test was more sensitive to temperatures below 50 °C and a BEU test was more sensitive to chemical aids (Romanova et al., 2006; Bakhtiari, 2015). Besides, laboratory-scale pipeline loops, or laboratory hydro-transport extraction systems (LHES) have been developed to investigate bitumen liberation, bitumen aeration, and bitumen recovery (Wallwork et al., 2003; Wallwork et al., 2004).

2.2.1.1 Liberation and coalescence

Bitumen liberation, i.e., the separation of bitumen from the sand grains in aqueous solution, is an essential step in bitumen extraction. In this process, the bitumen-sand interface is replaced by the sand-water and bitumen-water interfaces. To quantify the interfacial energy associated with bitumen recession and detachment from sand surfaces, Eq. 2.1 is obtained:

$$\frac{\Delta G}{\Delta A} = \gamma_{S/W} + \gamma_{B/W} - \gamma_{B/S} \quad (2.1)$$

Here, ΔG is Gibbs free energy, ΔA is the surface area, and $\gamma_{S/W}$, $\gamma_{B/W}$ and $\gamma_{B/S}$ are the interfacial tensions between sand/water, bitumen/water, and bitumen/sand, respectively. It is clear that a decrease in the sand-water and bitumen-water interfacial tensions and an increase in the bitumen-sand interfacial tension promote bitumen liberation. Since the bitumen-sand interfacial tension is difficult to alter, it is desirable to increase pH in liberation step not only to reduce the sand-water interfacial tension by facilitating the hydrolysis of sands, but also to lower the bitumen-water interfacial tension through the release of natural surfactants.

The corresponding schematic of interfacial energies is shown in Figure 2.3. The wettability of sand surfaces, indicated by the contact angle θ , plays a significant role in bitumen recession and

separation. By inserting Young's equation (Eq. 2.2) into Eq. 2.1, a simplified governing equation for bitumen liberation is then given by Eq. 2.3:

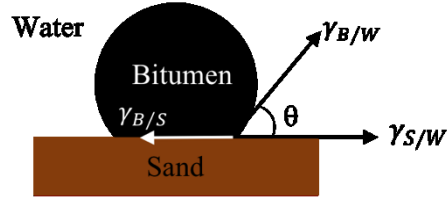


Figure 2.3. Interfacial energies in bitumen-sand-water system.

$$\cos\theta = \frac{\gamma_{B/S} - \gamma_{S/W}}{\gamma_{B/W}} \quad (2.2)$$

$$\frac{\Delta G}{\Delta A} = \gamma_{B/W}(1 - \cos\theta) \geq 0 \quad (2.3)$$

It is seen that bitumen separation from the sand grains is thermodynamically unfavorable. A complete detachment can only be achieved when the sand grains are extraordinary hydrophilic ($\theta=0$). Therefore, external mechanical energy is required to compensate for the interfacial energy gain (Masliyah et al., 2011).

The coalescence of bitumen droplets to grow to a critical size (>1 mm) is important to maximize bitumen recovery (Wik et al., 2008). The increases in pH values and the concentration of divalent cations led to a hindered coalescence between bitumen droplets. Also, the addition of montmorillonite into the system has been shown to depress the bitumen coalescence (Liu et al., 2005a). Stronger repulsion and weaker adhesion between bitumen droplets were measured with the introduction of montmorillonite. This depressing effect became severer in the presence of calcium ions.

2.2.1.2 Aeration and flotation

For bitumen aeration, an attachment between bitumen and air bubbles should occur. The strength of bitumen attaching to air bubbles can be analyzed in terms of interfacial energies, as shown in Eq. 2.4, where A represents air:

$$\frac{\Delta G}{\Delta A} = \gamma_{B/A} - (\gamma_{B/W} - \gamma_{A/W}) \quad (2.4)$$

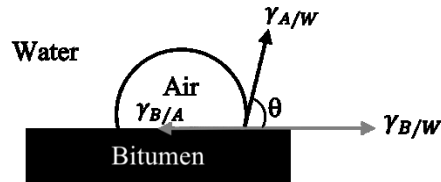


Figure 2.4. Interfacial energies in bitumen-air-water system.

The involved energies are described in Figure 2.4. Once again, we introduce Young's equation (Eq. 2.5) for this system to derive the governing relation, Eq. 2.6, for bitumen aeration:

$$\cos\theta = \frac{\gamma_{B/A} - \gamma_{B/W}}{\gamma_{A/W}} \quad (2.5)$$

$$\frac{\Delta G}{\Delta A} = \gamma_{A/W}(\cos\theta - 1) \leq 0 \quad (2.6)$$

Clearly, at contact angles greater than zero, $\frac{\Delta G}{\Delta A}$ is negative, suggesting a thermodynamically favorable tendency for bitumen-air bubble attachment. The larger the contact angle θ from the aqueous phase, the more negative the $\frac{\Delta G}{\Delta A}$, the more beneficial it is for aeration. In this step, increasing pH is not favorable since it decreases the contact angle θ of water on bitumen (Masliyah et al., 2011).

It is important to note that increasing pH provides a favorable condition for bitumen liberation but an unfavorable condition for bitumen coalescence and aeration. Controlling pH is important to optimize recovery.

Following aeration, the flotation of bitumen-air aggregates takes place. The efficiency of this step depends on the fluid viscosity and the density difference between the fluid and the aggregates. It was found that an increase in fluid viscosity with the presence of fine particles hindered bitumen recovery (Schramm, 1989). The use of NaOH had a significant impact on viscosity. A higher NaOH concentration led to a lower viscosity (Schramm, 1989).

The formation of colloidal clay gels will occur if high levels of ultrafine particles ($<0.3 \mu\text{m}$) are presented in the system (Mercier et al., 2012). Even at low levels, ultrafines are detrimental to bitumen recovery. The addition of divalent cations enhances gelation of ultrafine particles so that such gels can form at lower concentrations of ultrafines.

Finally, hydrodynamic analysis of flotation suggests that large bitumen droplets are much easier to be carried over to bitumen froth while small air bubbles are more effective in collecting bitumen droplets. In general, the collision rate between bitumen droplets and air bubbles of diameters d_b and d_a , respectively, is scaled by $(\frac{d_b}{d_a})^2$ (Yoon and Luttrell, 1989). Moreover, large bitumen droplets and small air bubbles also facilitate bitumen-air attachment upon collision (Moran et al., 2000; Yeung and Moran, 2000; Gu et al., 2004).

2.2.2 NaOH addition

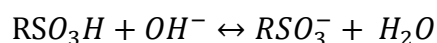
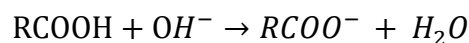
The performance of bitumen extraction is significantly influenced by the process temperature, chemical aids, mechanical agitation, and interfacial properties (Masliyah et al., 2004). Chemical aids are added into the system to improve the bitumen recovery. The commonly used process aid

is caustic (NaOH), even though other chemicals were tested (Clark and Pasternack, 1932; Schramm, 2000; Flury et al., 2014; Long et al., 2011; Hupka et al., 1983; Li et al., 2008).

The addition of NaOH to the process water helps to obtain optimal bitumen recovery by altering the following characteristics:

a. increasing pH of the slurry. The increase in the slurry pH leads to more negatively charged bitumen and sand surfaces, and thus increases the electrostatic repulsive force between them (Liu et al., 2002, 2003, 2004a, 2004b). As expected, bitumen liberation was observed to be improved with higher pH by an online visualization technique (Srinivasa et al., 2012; Bakhtiari, 2015). However, increasing pH has a negative impact on bitumen aeration. It was found that the induction time required for bitumen attaching to air bubbles increased with increasing pH (Flury et al., 2014; Chen et al., 2017). Also, the ionization of natural surfactants at the bitumen-water interface with higher pH reduced bitumen-water interfacial tension and made bitumen surfaces less hydrophobic, which were unfavorable for bitumen-air attachment. Therefore, overdosing NaOH extraction system should be avoided.

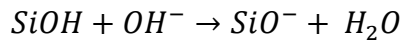
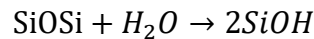
b. extracting the natural surfactants from bitumen. NaOH is capable of promoting the release of surfactants existing naturally in bitumen. There are two main types of natural surfactants found in oil sands bitumen: carboxylic (RCOO^-) and sulfonic (RSO_3^-). The reactions for how base ionizes natural surfactants are shown as follows (Baptista and Bowman, 1969; Bowman, 1967; Sanford and Syer, 1979; Sanford, 1983; Bakhtiari, 2015):



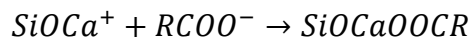
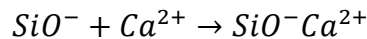
As early as 1981, carboxylate surfactants were reported as the primary surfactants found in processing oil sands (Mistra et al., 1981). Shortly after, isolation and quantification methods of

natural surfactants were developed, and their correlation with bitumen recovery were observed by Schramm and his colleagues (Schramm et al., 1984a, 1984b; Schramm and Smith, 1985, 1987). In their research, natural surfactants were separated from processing slurry by centrifugation, ultra-filtration and foam fractionation. H and C¹³ NMR were used to characterize the isolated surfactants. A critical concentration of natural surfactants was observed to achieve maximum bitumen recovery. Too much or too little natural surfactants were both unfavorable for bitumen extraction performance (Schramm and Smith, 1987). Recently, Dichloromethane (DCM) extraction method with Fourier transform infrared spectroscopy (FTIR) quantification was demonstrated to be suitable to measure the concentration of natural surfactants in oil sands tailings (Bakhtiari, 2015).

c. hydrolyzing sand surfaces. The hydrolysis of sand grains can be promoted by increasing pH with NaOH addition. At high pH, the hydrolyzed sand surfaces deprotonate and become negatively charged, which, in turn, supports bitumen liberation from sand grains. The involved reactions are presented below:



d. scavenging divalent cations. In the presence of divalent cations, usually calcium or magnesium ions, the deprotonated sites on solid surfaces adsorb them to become more positively charged and thus making it easier for fine particles to deposit on bitumen droplets, which is detrimental to bitumen recovery and froth quality:



Experimental results confirmed the negative role of divalent cations in bitumen extraction (Kasongo et al., 2000; Basu et al., 2004). At pH<9, the influence of divalent cations was significant in processing oil sands. While in an environment with sufficiently high pH with the addition of NaOH, precipitation of divalent cations occurred. Hence they were less impactful to bitumen extraction (Dai et al., 1992; Fong et al., 2004).

2.3 FINES AND CLAYS

Table 2.2. Mineral components in total oil sand solids (Hepler and Smith, 1994)

Component	Weight percent (%)
Quartz	82
K-feldspar	5
Calcite	trace
Dolomite	nil
Siderite	trace
Pyrite	nil
Kaolinite	4
Illite	7
Chlorite	1
Smectite	trace
Mixed layer clays	1
Anhydrate	trace

In oil sands, solids are mostly comprised of quartz with a small amount of feldspar, clay minerals, and other trace minerals, as indicated qualitatively in Table 2.2. It should be noted that the ratio of kaolinite to illite is not uniform, depending on the origin of ore samples being used.

By and large, kaolinite is the dominant clay. The fine solids are mainly kaolinite, illite, and other clays as well as non-clay minerals such as quartz.

2.3.1 Fines

The term, fines, is adopted to describe the mineral solids that are smaller than 44 μm in oil sands. Fines content or fines percent in oil sands is an important ore characteristic. Generally speaking, the fines content in an oil sands ore can vary in a broad range. A high fines ore typically requires more energy and larger dosage of chemical aids to maximize recovery than a low fines ore (Sanford, 1983). Long (2016) proposed a linear equation to estimate the required NaOH amount based on the fines content and bitumen content of the ore, as shown in Figure 2.5.

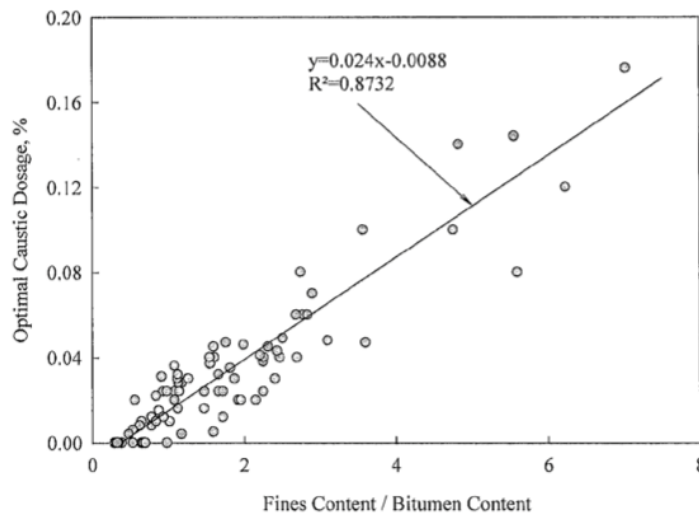


Figure 2.5. Optimized caustic control in relation to fines content and ore grade for bitumen extraction (Long, 2016).

Fines content and bitumen grade in an ore sample are not independent of each other. They are, to some degree, correlated. High fines ore normally has a low grade of saturated bitumen (Hendrickson, 1975; Cuddy, 2004). The impacts of fines content on bitumen recovery depend on

the mineralogy of fines and water chemistry. In general, a high bitumen recovery can be achieved for low fine ore (Sanford, 1983; Kasongo, 2006; Tipman, 2000; Wallace et al., 2001).

2.3.2 Properties of clay mineral

The fines in oil sands solids contain various types of clays. Gillott (1987) defined the term clay as a “natural, earthy, fine-grained material, largely composed of hydrous aluminum and magnesium silicates, which develops plastic properties when mixed with a limited amount of water.” Some other definitions emphasize the shape retention property of clays during drying and the conservation of shape with the increase of strength during firing (Grim, 1953). In oil sands, fine particles smaller than 2 μm are commonly referred as clays. Clays, along with terms such as sand and silt to describe mineral solids are shown in Figure 2.6.

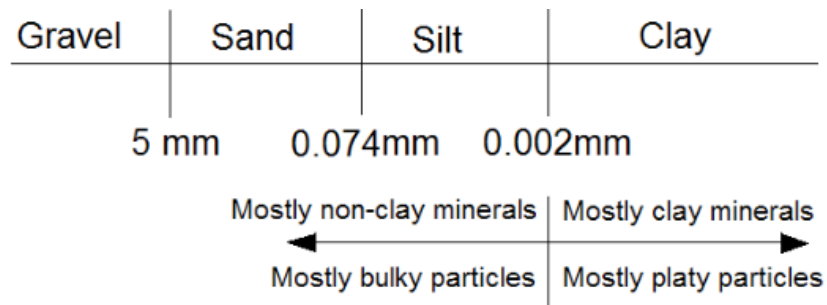


Figure 2.6. The particle size range of gravel, sand, silt, and clay (Kaminsky, 2010).

Figure 2.7 shows the composition of the clay fraction in oil sands, which contains about 90% clay minerals. The most common clays in oil sands are kaolinite and illite. Other clays such as montmorillonite could also exist but in small amounts.

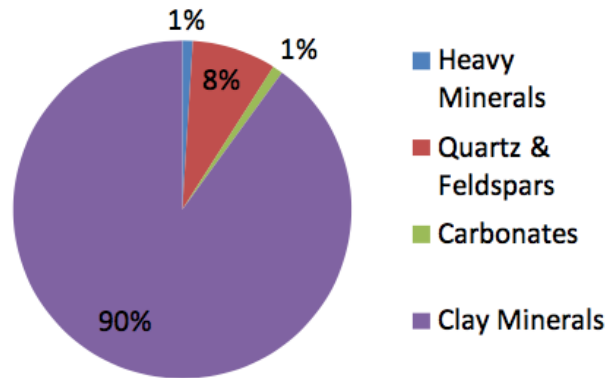


Figure 2.7. Composition of clay fraction (Kaminsky, 2010).

Clay minerals are composed of two main building blocks: silicon-oxygen tetrahedron sheets (T) and octahedron sheets (O) made of aluminum-oxygen-hydroxyl (known as gibbsite) or magnesium hydroxide (known as brucite) (Pauling, 1930). Tetrahedron and octahedron are used to describe how oxygen atoms gather around a central atom. Schematic representations of the tetrahedron and octahedron layers are shown in Figure 2.8. Different arrangements of two basic layers result in varieties of clay minerals, such as 1:1 layering structured kaolinite (-TO-TO-), and 2:1 layering structured illite and smectite (-TOT-TOT-). The bindings between tetrahedron and octahedron sheets are achieved by sharing the apex oxygen atoms from the tetrahedron sheet.

The ideal tetrahedron and octahedron sheets are electrically neutral. However, the basal surfaces carry a permanent negative charge caused by isomorphic substitution of one cation by another with similar size and usually lower valence such as Si^{4+} by Al^{3+} in the tetrahedron sheet and Al^{3+} by Mg^{2+} , Fe^{2+} , or Mn^{2+} in the octahedron sheet. The charge deficiency is balanced by compensating ions, such as K^+ and Na^+ , to make the clay minerals electrically neutral as a whole (Masliyeh et al., 2011).

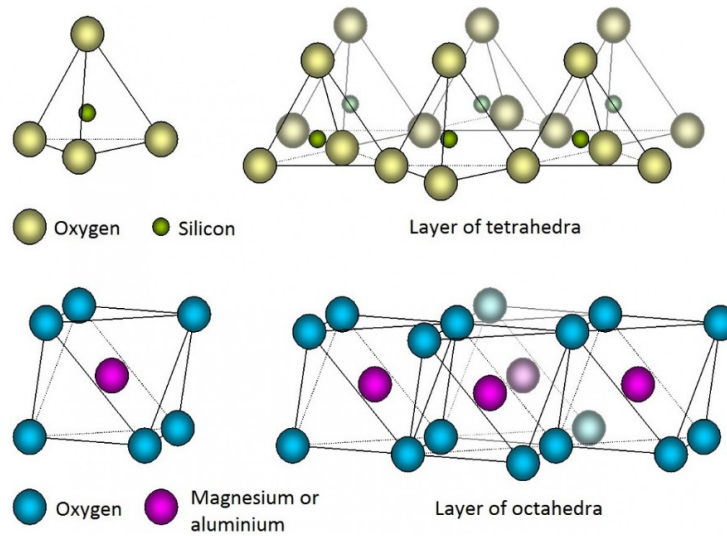


Figure 2.8. Two basic layers in clay mineral structure (Jordán, 2014).

2.3.3 Kaolinite

Kaolinite ($\text{Si}_2\text{Al}_2\text{O}_5(\text{OH})_4$) is the most abundant clay minerals found in oil sands (Masliyah et al., 2013). It is a two-layer type with one tetrahedron sheet and one octahedron sheet. A sketch of the lattice structure of kaolinite is shown in Figure 2.9. The almost perfect 1:1-layer structure has basal oxygen in the tetrahedron sheet and hydroxyls in the octahedron sheet. As the hydrogen bonding between the unit layers of kaolinite is quite strong, this type of clay is rigid and difficult to delaminate. Using a computational structure model, White et al. (2009) found that the bond lengths of the hydroxyl groups in the octahedron sheet, which form hydrogen bonds with adjacent oxygens in the tetrahedron sheets, vary from 0.970\AA to 0.974\AA . Although some swelling phenomena have been observed in kaolinite when combined with compounds with certain strong hydrogen bonds (van Olphen, 1963), kaolinite is commonly considered as non-swelling in water.

In addition to the above mentioned two basal planes, clay particles also have edge surfaces containing broken Si-O and Al-O bonds. These broken bonds are hydrolyzed when immersed in water. The cation exchange capacity of kaolinite clay is meager and occurs mainly at the edge of

the layers. The cation exchange capacity of clays is of great importance (Stumm and Morgan, 1996; Essington, 2004).

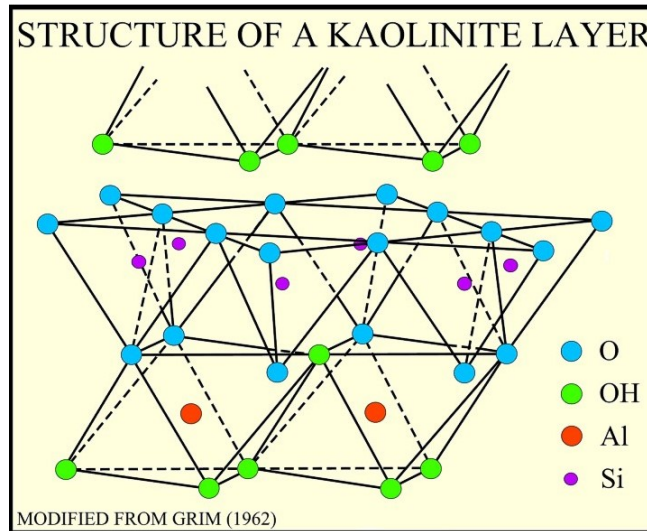


Figure 2.9. Sketch of the structure of kaolinite (Poppe et al., 2001).

The number of isomorphic substitutions in kaolinite structure, mainly in the tetrahedron sheet, is normally small, resulting in a low permanent charge on its basal planes. Clay particles could carry charges on the edges, depending on the solution pH. The point of zero charge (PZC) of kaolinite edges falls in the range of pH 6 to pH 6.5 (Tombácz and Szekeres, 2006). The ζ potential of kaolinite is also known to be strongly pH-dependent. Those charge characteristics of kaolinite clay indicate that we could control dispersion or flocculation of clays by adjusting pH (Moore and Reynolds, 1997).

2.3.4 Illite

Illite is a dioctahedral 2:1-layer structured clay. The main differences among various types of three-layer clays (such as illite and montmorillonite) are the number and location of isomorphic substitution and the type of compensating ions. For illite, as shown in Figure 2.10, the isomorphic

substitution occurs mainly in the tetrahedron sheet where $\sim 1/4$ of Si atoms are replaced by Al atoms, causing its basal planes to be negatively charged. These charges are balanced mainly by compensating potassium ions. Gaudette et al. (1966) calculated that the Al assigned to the tetrahedron sheet ranged from 0.9 to 1.6 per unit cell with the Al substitution in the tetrahedron sheet varied between 11.0 and 19.5%. Since illite is also non-swelling in water, the interlayer potassium cations are not exchangeable. The non-swelling illite could become swelling when it is degraded, making its cation exchange capacity slightly higher than kaolinite (Gillott, 1987; Masliyah et al., 2011; Moore and Reynolds, 1997). Wallace et al. (2004) suggested the use of soluble potassium as an indicator of illite degradation to account for the poor processing behavior of oil sands.

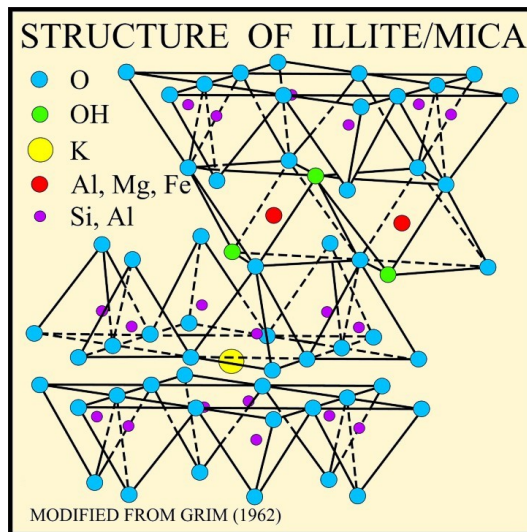


Figure 2.10. Sketch of the structure of illite (Poppe et al., 2001).

Due to a greater isomorphous substitution and a larger Si/Al ratio on the edges, illite is generally more negatively charged than kaolinite. There is no isoelectric point (IEP), where ζ potential is zero, for illite in solution from pH 2 to pH 11. This indicates that basal planes become a dominant contributor to the overall charge of illite, which is pH-independent.

The structural formula for illite is $(K, H)(Al, Mg, Fe)_2(Si, Al)_4O_{10}(OH)_2 \cdot nH_2O$ (Janeth, 2005).

Illite minerals are presented in tiny particles mixed with other clays.

2.3.5 Montmorillonite

Montmorillonite, a typical clay mineral in smectite group, is another type of three-layer clays occasionally present in oil sands. Chemically, it is described as $(Na, Ca)_{0.33}(Al, Mg)_2(Si_4O_{10})(OH)_2 \cdot nH_2O$. Like illite, montmorillonite also occurs in small particle size, making this clay susceptible to mineral impurities (Grim, 1953).

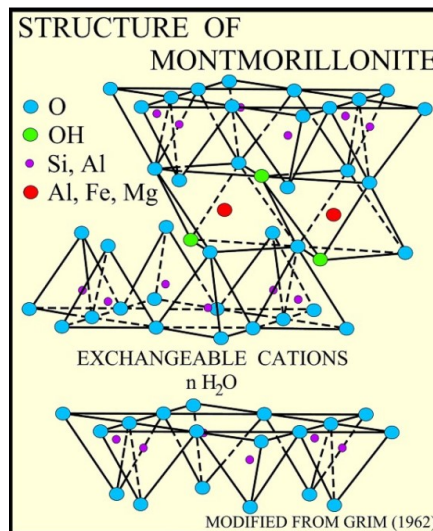


Figure 2.11. Sketch of the structure of montmorillonite (Poppe et al., 2001).

A representation of the repeating unit in the montmorillonite structure is sketched in Figure 2.11. The isomorphous substitution occurs in both the tetrahedron and octahedron sheets. The substitution in tetrahedron sheet is similar to that occurs in kaolinite and illite, while the substitution in octahedron sheet makes this layer delocalized. As a result, the compensating ions move towards the tetrahedron sheet. Such compensating ions between the unit layers weaken the

interlayer binding and are available for ion exchange. Hence, the cation exchange capacity is high in montmorillonite (Gillott, 1987).

The appearance of interlayer swelling with water in montmorillonite has attracted extensive attention. The first region of swelling, or crystalline swelling, take up ~0.5 g water/g clay with the interlayer spacing increased from 9.5 Å to 20 Å. Then the second region of swelling, which occurs when placing Na-montmorillonite in water, adsorbs 10 g water/g clay and expands the interlayer spacing to greater than 30 Å (Falconer and Mattson, 1933; Norrish, 1954).

A unique feature of swelling clays is that the total surface charge is governed by the basal planes, and therefore the ζ potential of montmorillonite is insensitive to pH, and a flat ζ potential profile with negligible variation is observed for this type of clay. Such a conclusion can be anticipated by comparing the less than 1% edge surface area with 1 nm thickness in montmorillonite clays with the corresponding ~20% edge surface area with 40 nm thickness in non-swelling kaolinite clays (Wan and Tokunaga, 2002).

2.3.6 Important clay properties

2.3.6.1 Zeta (ζ) potential

The origin of electric charges on boundaries between the solid (sand/clay) surfaces and the solution (water/electrolyte) can be explained by the following mechanisms: a) isomorphic substitution; b) hydrolysis of broken surfaces; c) unequal dissolution of lattice-forming ions; d) adsorption of molecules onto the surface or interface.

Regardless of the formation of the surface charge, the system of a solid particle in a solution should be electrically neutral. Therefore, both the solid particle and the solution in contact with the particle carry charges, which are equal in value and opposite in sign (Masliyeh et al., 2011).

The charges on the surface and in the solution form a system of the so-called “electric double layer,” as shown in Figure 2.12. The charged ions in solution consist of two regions separated by a stern plane: an inner stern layer of counter ions bound relatively tightly to the particle surface, and an outer diffuse layer where a balance of electric forces and thermal molecular motions determines the ion distribution (Debye and Hückel, 1923).

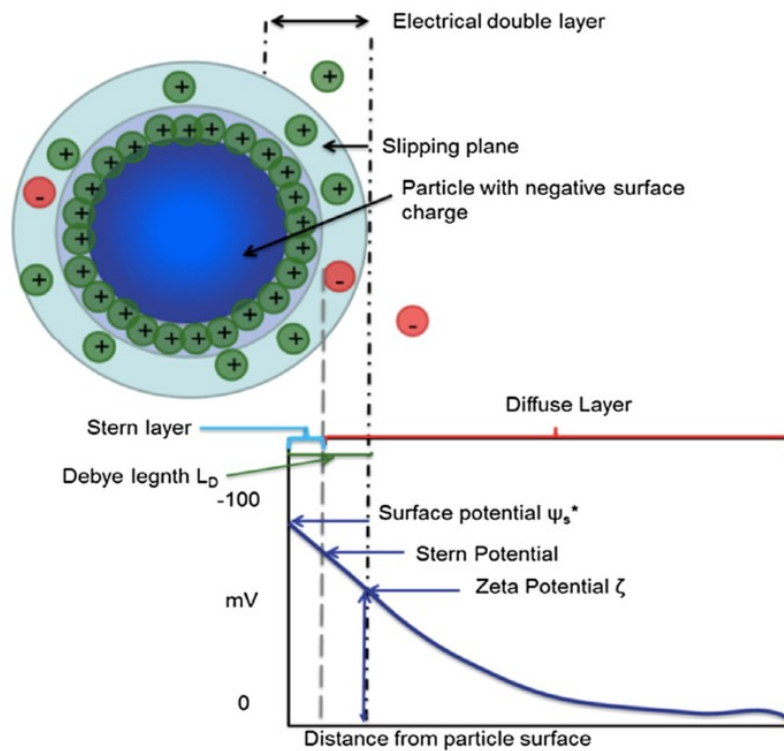


Figure 2.12. Illustration of ζ potential in electric double layers (Valiño et al., 2014).

The plot of electric potential in the double layer is also shown in Figure 2.12. The potential decays exponentially versus the distance from the particle surface, with a characteristic scale: the Debye length. Since the surface potential Ψ_s cannot be measured experimentally, the ζ potential, which is close to the surface potential and measurable, serves as a very important parameter for colloidal particles. By definition, ζ potential is the potential on the slipping/shear plane which refers to as the separatrix between the mobile part and the immobile part in the diffuse double layer.

The position of the slipping/shear plane is considered to be far away from the stern plane and close to the Gouy plane where the distance equals to the Debye length (Li et al., 2003).

2.3.6.2 Methylene blue index (MBI)

Methylene blue ($C_{16}H_{18}ClN_3S$, 319.86) is an organic polar molecule capable of forming face-to-face dimers in dilute aqueous solutions and higher aggregates with rising concentration (Fornili et al., 1981). Cenens and Schoonheydt (1988) indicated its cation structure as below:

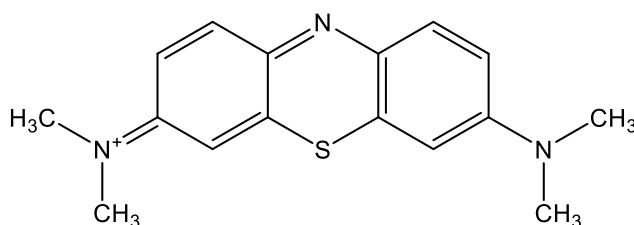


Figure 2.13. Structure of a methylene blue cation.

In the oil sands industry, methylene blue index (MBI) is widely used as an indicator of clay activity or cation exchange capacity and specific surface area of the solids (clays) in various process streams, such as ores, bitumen froth, tailings (Boxill, 2011).

Cation exchange capacity. Cations are positively charged ions such as H^+ , Mg^{2+} , K^+ , Ca^{2+} , and Na^+ that are present in clay minerals. The capacity of a clay mineral to accommodate these cations on its surface is called cation exchange capacity. Methylene blue adsorbs onto the clay minerals mainly by cation exchange together with supplementary hydrogen bonding since it is able to attach itself to the exchangeable sites on the clay surfaces, while a small amount of it adsorbs physically (Yuner et al., 2012; Kelly, 1984; Kahr and Madsen, 1995; Li et al., 2010).

For the five cations mentioned above, the cation exchange capacity decreases in the following order: $H^+ > Na^+ > K^+ > Mg^{2+} > Ca^{2+}$ (Taylor, 1985). The MBI values of clays depend on their properties, the pretreatment of the samples, as well as the method used.

Usually, we use MBI, i.e., milliequivalent methylene blue adsorbed on 100 g of sample, to indicate the cation exchange capacity of clay minerals (CONRAD Clay Focus Group, 2012):

$$MBI \left(\frac{meq}{100g} \right) = \frac{mls\ of\ MB \times Normality\ of\ MB}{mass\ of\ dried\ sample\ (g)} \times 100 \quad (2.7)$$

Specific surface area. MBI measurement has been used as a substitute for the Brunauer-Emmett-Teller (BET) method to indicate the specific surface area of clay minerals and other solids. Assuming a full coverage of the clay surface by the methylene blue molecules, the specific surface area is calculated by (Hang and Brindley, 1970; Tewari and Thornton, 2010):

$$SSA(Specific\ Surface\ Area) = X_m \cdot N \cdot A \quad (2.8)$$

where X_m is the adsorbed methylene blue in mole/g, and N is Avogadro number, and A is the area per molecule on the surface.

There is no doubt that the area covered by the methylene blue cations per molecule on the clay surface depends mainly on the cation orientations and the thickness of the layers. For an ideal assumption of monolayer adsorption and flat orientations, the A is 130 \AA^2 (Hang and Brindley, 1970).

Titration is commonly used to measure the adsorption of methylene blue cations on clay surfaces. To obtain accurate and reproducible methylene blue titration results, a good dispersion of clay samples and a precise determination of titration endpoint are of crucial importance.

There are many ways to enhance the dispersion of the samples, such as soaking, heating, stirring, and sonication. pH also affects dispersion. According to [Vietti \(2011\)](#), clay particles would associate due to their edge-face interactions at a low pH (<8) and aggregate at a high pH (>11.5). A fine dispersion of clays can only be achieved in the pH range of 8 to 11 when a strong repulsion between particles leads to a stable colloidal state. Similar results were obtained by [Currie et al. \(2014\)](#), where the desirable basic pH range was 9.5 to 10.5. Magnetic stirring and ultrasonic bathing are often used to further disperse the samples. [Omotoso \(2011\)](#) showed that at least 20 min of both stirring and sonication is required to enhance dispersion. Other techniques such as hydrogen peroxide treatment ([Robertson et al., 1984](#); [Di Stefano et al., 2010](#)) are also used for the dispersion of the solid samples.

The identification of the titration endpoint can be achieved by the use of either a filter paper or an ultraviolet-visible (UV-VIS) spectrophotometer. When using a filter paper, the endpoint is indicated by a light blue halo formed around the center dark blue drop on the filter paper ([ASTM C837-09](#)). Even though the determination of the endpoint is somewhat operator-dependent, an experienced operator could obtain results similar to those obtained by more complicated methods ([Yukselen and Kaya, 2008](#)). The selection of filter paper varies among different standards. In ASTM C837-09, Baroid No. 987 filter paper is recommended, whereas the CONRAD Clay Focus Group prefers the Whatman 42 filter paper. [Fityus et al. \(2000\)](#) indicated that large 1, 4, 5A, 30, or 41-grade filter papers were all suitable, but grade 5, 30, and 40 should be avoided. Nevertheless, [Currie et al. \(2014\)](#) found that the Whatman 42 filter paper was better than the Whatman 41 filter paper. On the other hand, [Potgieter \(1990\)](#) pointed out that the maximum absorbance of methylene blue occurred at a wavelength of 630 nm, indicating the possibility of using spectroscopy to detect the adsorption state. A calibration curve of maximum absorbance (at 663 nm in this study) against

methylene blue concentration (Ramasamy and Anandalakshmi, 2008) exhibited a linear correlation at a low concentration range (< 25 mg/L). By adding methylene blue solution (< 25 mg/L) to the clay suspension with known concentration (methylene blue should be excessive), it is suitable to determine the adsorption of methylene blue on clay surfaces by comparing the maximum absorbance of remaining suspension after complete adsorption with calibration curve (Ramasamy and Anandalakshmi, 2008; Potgieter and Strydom, 1999). The adsorption may differ for various types of clays (Searle, 1996; Grim, 1968).

The MBI titration method can also be used to distinguish montmorillonite from illite and kaolinite. The methylene blue solution appears purple with the addition of montmorillonite but presents blue with the addition of the other two clays (Hang and Brindley, 1970).

2.4 EFFECT OF FINES/CLAYS ON ORE PROCESSABILITY

One of the challenges to recover bitumen efficiently and effectively from poor ores is the detrimental effect of the relatively large fraction of fines and clays in these ores. Fines and clays are problematic in bitumen extraction for the following reasons (Wallace, 2015; Masliyah et al., 2004; Zhou et al., 2017b):

- They coat or accumulate on bitumen droplets and bubble surfaces, forming steric barriers for bitumen-bitumen coalescence and bitumen-air attachment, resulting in small bitumen droplets that are difficult to be recovered and poor bitumen aeration, flotation, and recovery.
- A high concentration of clays/fines results in increased slurry viscosity, which leads to difficulties for bitumen droplets to rise and solids to settle in a separation vessel, and thus poor recovery.

To improve bitumen recovery, it is desirable to disperse the fine solids (clays) to prevent their hetero-coagulation with bitumen droplets. A stable dispersion of fine particles can be achieved by adjusting pH and the sodium concentration of the aqueous phase (Takamura and Wallace, 1988).

In normal extraction operations, there are always some fines and clays that report to the bitumen froth, due to the following mechanisms (Masliyah et al., 2004):

a) Mechanical entrainment of fines solids (clays) in water, depending on particle size and slurry hydrodynamics;

b) Mechanical entrapment of fines solids (clays) squeezed/sandwiched between bitumen droplets;

c) Bitumen slime-coating;

d) Unliberated bitumen-solid aggregates attached to air bubbles (Zhou et al., 2017a);

e) Flotation of fines solids (clays) due to wettability change by ore aging/weathering, adsorbing surfactants or organic film coverage (Baptista and Bowman, 1969; Shaw et al., 1994; Itokumbul et al., 1985; Kotlyar et al., 1984b, 1985, 1987, 1988).

The detrimental effects of fines and clays on bitumen recovery also depend on solid mineralogy, process water chemistry, and operation conditions. Tests show that adding clays to an oil sands ore did reduce bitumen recovery (Kasongo et al., 2000; Repka, 2007; Ding et al., 2006; Zhou et al., 2017b; Fong et al., 2004). This detrimental effect became worse when divalent cations were presented (Kasongo et al., 2000; Ding et al., 2006; Liu et al., 2004b).

2.4.1 Bitumen slime coating

Fines and clays can collide with and then attach to bitumen surfaces. This phenomenon, i.e., the coverage of bitumen by fines/clays, is called slime-coating. Theoretically, if a bitumen droplet

is coated by hydrophilic particles, it will not be able to attach to air bubbles effectively, resulting in reduced bitumen recovery. Otherwise, if a bitumen droplet is covered by hydrophobic particles, the bitumen droplet is still able to attach to air bubbles and to be recovered. However, this could lead to high solids content in the bitumen froth (Masliyah et al., 2011). Slime-coating is one of the most prevalent mechanisms proposed for poor processability (Liu et al., 2005b). As illustrated in Figure 2.14, if too many fines and clays are attached to bitumen droplets, the bitumen does not float (Wallace et al., 1989).

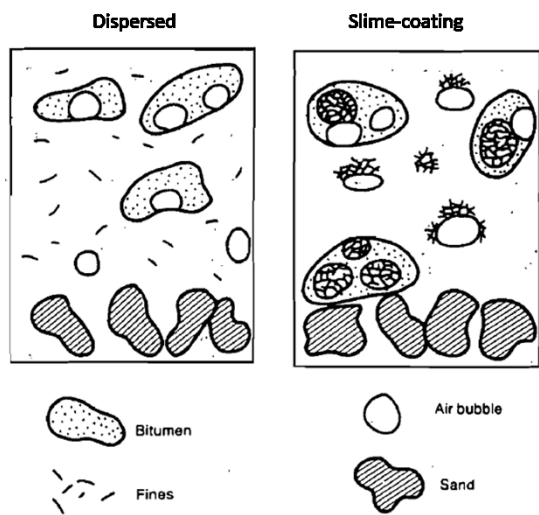


Figure 2.14. Effect of slime-coating on bitumen flotation (Wallace et al., 1989).

Slime-coating has been extensively studied by AFM and ζ potential distribution measurement (Liu et al., 2002, 2003, 2004a, 2004b, 2005b; Repka, 2007; Ding et al., 2006; Zhao et al., 2006). A repulsive force profile and weak adhesion force were measured for bitumen interacting with fines isolated from a good processing ore while an attractive force profile and strong adhesion force were observed between bitumen and fines from a poor processing ore (Figure 2.15). This may be explained by the increased hydrophobicity of fines isolated from the poor processing ores (Liu et al., 2004a). The role of clay type in slime-coating was also studied by the AFM technique.

It was concluded that in the presence of divalent cations, montmorillonite deposited on bitumen surface easily at pH 8 to 8.5, while kaolinite was found to attach only weakly to bitumen droplet (Liu et al., 2004b, 2005b). Divalent cations (Ca^{2+} , Mg^{2+}) acted as bridges for bitumen-clay hetero-coagulations (Masliyah et al., 2011). The different cation exchange capacity of different clays has been considered to account for their different responses in coagulating with bitumen in the presence of divalent cations (Wallace et al., 2004; Liu et al., 2002).

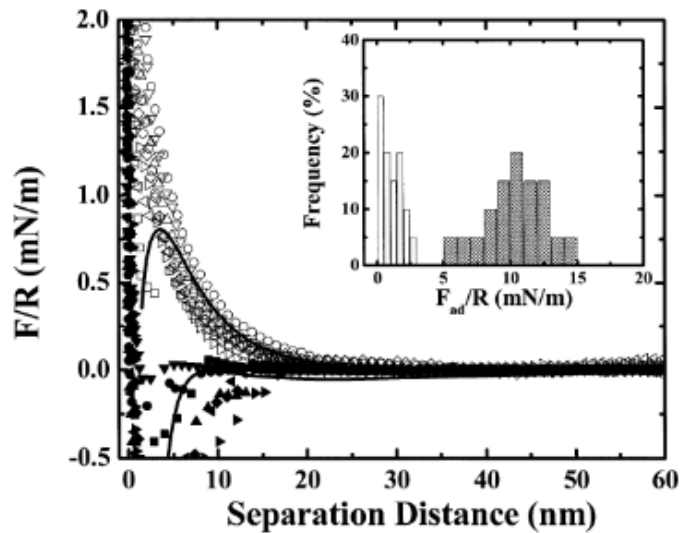


Figure 2.15. Interaction forces and adhesion forces (inset) between bitumen and fines isolated from tailings of good (open symbol, white bars) and poor (filled symbol, shaded bars) processing ores in tailings water of pH 8.5 (Liu et al., 2004a).

By measuring the ζ potential distributions of bitumen and clays, individually or as a mixture, the hetero-coagulation phenomena in these two-component systems were studied. Figure 2.16 is a schematic showing the use of the ζ potential distributions to indicate if slime-coating occurs (Liu et al., 2002). Deposition of montmorillonite on bitumen droplets with divalent cations acting as bridges was inferred from the results of ζ potential distribution measurements at pH 8 (Liu et al., 2002; Repka, 2007). In the bitumen-illite system, the slime-coating phenomenon was observed at pH 4.9 in the presence of divalent cations (Ding et al., 2006).

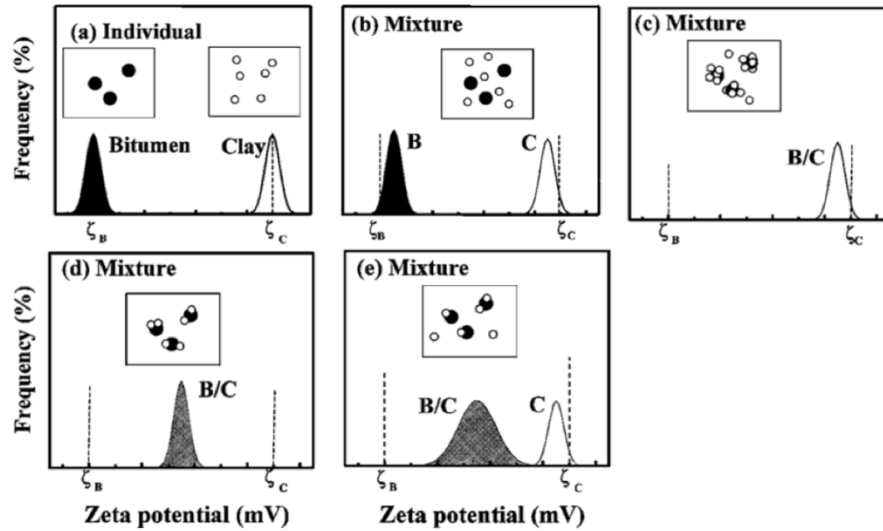


Figure 2.16. Schematic ζ potential distributions for a hypothetical bitumen-clay system. a) ζ potential distribution of two components measured individually, b) binary mixture without slime-coating, c) binary mixture with strong slime-coating (complete coverage), d) binary mixture with strong slime-coating (partial coverage due to insufficient clays), e) binary mixture with weak slime-coating (Liu et al., 2002).

More recently, Marjan et al. (2015) attempted to use a quartz crystal microbalance with dissipation monitoring (QCM-D) to monitor bitumen clay interactions. Illite clays were confirmed to slime-coat onto bitumen droplets in tailings water of pH 8.5 (containing $\text{Ca}^{2+}/\text{Mg}^{2+}$) after removal of humic acids. Kaolinite has not been measured to deposit strongly on bitumen surfaces, yet it hindered bitumen-air attachment as in the case of montmorillonite and illite clays (Moran et al., 2000).

Increasing pH and eliminating divalent cations were found to be able to minimize bitumen clay hetero-coagulations, due to a stronger repulsion between bitumen and clays (Liu et al., 2002, 2004b; Fong et al., 2004; Schramm et al., 1984a, 1984b, 2003; Long et al., 2007; Marjan et al., 2015).

2.4.2 Wettability control

The separation of bitumen from a hydrophobic solid matrix is more difficult than that from a hydrophilic solid matrix (Dang-Vu et al., 2009). Hydrophobic fine particles can attach to bitumen droplets and air bubbles, resulting in reduced bitumen recovery and froth quality.

During ore weathering or bitumen oxidation, the formation water between bitumen and solids was removed, resulting in close contact of bitumen with sand grains and contamination of grain surfaces by bitumen components to become hydrophobic (Ren et al., 2009a). Such a wettability conversion of solid surfaces has been widely reported in the literature (Liu et al., 2005c; Ren et al., 2009a, 2009b, 2009c; Wang et al., 2010; Yang et al., 2012; Ding et al., 2014). The hydrophobicity of particle surfaces promoted unfavorable hetero-coagulations between bitumen and the fine solids (clays) (Ren et al., 2009b, 2009c).

The adsorption of organic matters on clay surfaces was found to improve the hydrophobicity of clay particles (Kotlyar et al., 1984a; Jada and Debih, 2009; Chenu et al., 2000; Tu et al., 2006). Several mechanisms can account for the adsorption process:

- Organic molecules or ions from a gaseous/liquid phase accumulate onto the clay surfaces (Yariv, 2002). The union of inorganic clay mineral and organic matter forms a clay-organic complex or organic-mineral complex (Jacks, 1963). Their association varies from loosely bound organic and clay particles to tightly bound complexes, depending on the degree of physiochemical interactions (Chenu, 2006).
- Polyvalent cations form a bridge between organic anions and clay surfaces with negative charges (Stevenson, 1982). These polyvalent cations are usually Ca^{2+} , Al^{3+} , and Fe^{3+} (Evans and

Russell, 1959; Theng and Scharpenseel, 1975; Greenland, 1971). Organic matters bound with Al^{3+} and Fe^{3+} are stronger than that with Ca^{2+} (Stevenson, 1982).

- Strong coordination bond (ligand exchange) and simple anion exchange with hydrous oxides (iron and aluminum) present in clay minerals facilitate the adsorption of organic matters (Greenland, 1971; Stevenson, 1982).

- Aspartic acid-enriched organic matters prefer to be adsorbed on carbonate surfaces rather than on non-carbonate surfaces (Carter and Mitterer, 1978; Chave, 1965).

Furthermore, the surfactants in the slurry adsorbed onto the clay surfaces to make them hydrophobic (Zhao et al., 2006; Martin et al., 2006; Xu and Boyd, 1995). They are oriented in such a way that the hydrophilic polar heads of the surfactants are adsorbed on the particle surfaces with the hydrophobic tails facing the surrounding water. Clay particles are therefore present hydrophobic natures. Cationic surfactants do not necessarily attach to clay surfaces through solution but can also through a solid-liquid interface once bitumen contacted with clays (Aronson et al., 1978; Zhou et al., 1999). While surfactants with anionic and nonionic polar groups are less likely to approach clay surfaces (Mulligan et al., 2001). The deposition of calcium ions on clay surfaces triggers the adsorption of anionic surfactants onto clays (Zhou et al., 1999; Masliyah et al., 2011).

2.5 THE MINERALOGICAL METHODS

The mineralogical information forms a vital basis for designing, diagnosing, and optimizing mineral-related processes (Lamberg et al., 2013). A proper quantitative mineral characterization of the ore is required when evaluating the ore, mapping the variation in the ore body (Lund, 2013), estimating the optimal dosage of process aids, and designing the reasonable process conditions. Mineralogical information can be divided into different levels depending on the increasing

complexity and details (Lamberg et al., 2013). The simplest approach is to qualitatively identify the lithology and mineral types in bulk samples. The quantitative approach provides detailed mineralogical information on particles, and its accuracy and efficiency depends greatly on the selection of the techniques.

2.5.1 Optical mineralogy

Traditionally, modal mineralogy or mineral grades have been determined by the optical microscopy with point counting (Lund, 2013), which is time-consuming (Petruk, 2000) and relies largely on the experience of the mineralogist (Henley, 1992). In a word, the classification of silicate minerals is dependent on the polymerization degree of constitutive tetrahedral units. Mineralogists turn upon how many oxygens are shared with other tetrahedra in each tetrahedron to determine the system for classification. While for non-silicate minerals, the relationship between the optical and physical properties and the chemical composition and structure of materials is difficult to identify. Hence, they are only outlined for the four major groups: halides, carbonates, oxides, and sulfides (Gribble et al., 1992). Nevertheless, optical parameters (e.g., refractive index, extinction coefficient, reflectance) can be used to evaluate chemical composition powerfully and cost-effectively (Rouzaud et al., 1989; Reinhardt, 2004).

2.5.2 Automated mineralogy

The appearance of computer-based systems has freed researchers from the labor-intensive works. Automated mineralogy, commonly based on the scanning electron microscopy (SEM) and optical image analyses (OIA), provides a quantitative analysis of textures, grain sizes, and mineral grades (Jones et al., 1970; Sutherland et al., 1991, 2007; Parian et al., 2015). On the one hand, SEM-based automated mineralogy can be used to differentiate minerals to support the mineral liberation analyzer (MLA) (Gu, 2003; Fandrich et al., 2007; Figueroa et al., 2012) and the

quantitative evaluation of minerals by scanning electron microscopy (QEMSCAN) (Goodall, 2008; Ayling et al., 2012; Little et al., 2015) for mineral and ore characterization, process design, and process optimization. It is generally regarded as the most reliable method for estimating mineral grades (Parian et al., 2015). However, SEM-based automated mineralogy requires cautious and tedious sample preparation procedure and is expensive and time-consuming (Lastra and Petruk, 2014). On the other hand, OIA-based automated mineralogy can also be used to improve the mineral characterization of ore deposits, providing representative and accurate numeric support to the petrology studies and process improvement (Berrezueta, et al., 2016, 2017; Poliakov, et al., 2014; Donskoi et al., 2015 (1)). OIA-based analysis reduces the cost, increases the speed, and shows higher resolution compared to SEM-based analysis (Donskoi, et al., 2015 (2)), while it is less sensitive to non-opaque minerals and ores or tailings with low iron content (Donskoi, et al., 2013). The limitations of automated mineralogy exist in problematic results for very fine particles (Kwitko-Ribeiro, 2012), and undistinguishable identification of similar chemical compositions, such as magnetite and hematite (Gomes et al., 2013).

2.5.3 X-ray diffraction (XRD)

It has been a century since the XRD experiment was first discovered (Friedrich et al., 1912). Today, XRD has become one of the most powerful technique for qualitative and quantitative identification and characterization of materials and its future development is promising (Sharma et al., 2012; Lavina et al., 2014).

The principle behind the XRD is the diffraction event. Mathematically, diffraction will occur if and only if the path difference between the two scattered beams is equal to a whole number n of the wavelength (λ) of the beams. Bragg's law (Bragg, 1913) is useful to explain the diffraction in an intuitive way and to provide a mathematical strategy for figuring diffraction directions:

$$n\lambda = 2d\sin\theta \quad (2.9)$$

In a crystal which is composed of a set of parallel planes of atoms, the path difference is equivalent to twice the d-spacing between planes times the sine of the angle θ formed between the incident beam and the planes of atoms.

In general, the XRD analysis follows the procedures described below: a) measure the XRD patterns of a sample; b) determine the d-spacing based on Bragg's law; c) obtain integrated intensities; d) compare the measured patterns with standard database (ICDF cards); e) a typical XRD pattern is characterized for peak position, peak intensity, and peak width.

Since the intensities of the diffraction peaks for a given component in a mixture are proportional to the concentration of this component in the mixture, XRD is readily adaptable to quantitative analysis (Ryland, 1958). No invariant method is available for the quantitative analysis of materials by XRD (Moore and Reynolds, 1997) and therefore at least four general approaches have been developed to date (Kahle et al., 2002). Among them, the Rietveld method (Rietveld, 1967) for full pattern fitting, capable of overcoming the peak overlap in XRD interpretation of powder diffraction results (Kaminsky, 2008), has been widely used in XRD for structural analysis. A detailed description of the Rietveld method can be found in "The Rietveld Method" edited by Young, 1993.

Quantitative XRD (QXRD) analysis is mainly used for quantifying the phase weight fractions in powdered/thin film samples. Although it is inevitably sensitive to the preferred orientation, crystallinity, crystal size, and variation in the chemical composition of the contributing phases present in the material (Lund, 2013), QXRD maintains its unshakable position in mineralogy determination through its non-destructive features, capability to model sample, specimen, and

instrumental problems, and accurate and precise quantification results (Nayak et al., 2007; Hutton et al., 1996; Scrivener et al., 2004; Winburn et al., 2000; Bish et al., 2013; Ryan et al., 2002).

2.5.4 Element analysis

Element composition has been widely used in various fields for enriching the understanding of mineralogy and chemical composition of the solid samples. Determination of the mineralogy from the element analysis directly provides geoscientists and engineers with a powerful tool. To convert the measured element composition to the quantity of desired minerals in bulk samples, a multicomponent mass balancing method, “element to mineral conversion”, is often used (Lamberg et al., 1997; Paktunc, 1998; Whiten, 2007).

The “element to mineral conversion” is a simple way to estimate the mineral composition of the samples by solving multiple mass balance equations formulated between the elements and minerals simultaneously. The method is restricted to the solution of multiple equations where the number of minerals must be no larger than the number of analyzed element components (Spencer et al., 2016; Parian et al., 2015). Mathematically it can be written in matrix form as $M \cdot x = b$, i.e. (Parian et al., 2015; Lamberg et al., 1997)

$$\begin{bmatrix} M_{11} & \cdots & M_{1n} \\ \vdots & \ddots & \vdots \\ M_{n1} & \cdots & M_{nn} \end{bmatrix} \times \begin{bmatrix} x_1 \\ \vdots \\ x_n \end{bmatrix} = \begin{bmatrix} b_1 \\ \vdots \\ b_n \end{bmatrix} \quad (2.10)$$

where M is the matrix of the element composition of minerals, x is the vector of unknown weight percentage of minerals in bulk sample, and b is the vector representing analyzed element composition of the sample.

Although the “element-to-mineral conversion” method has been proposed for decades, it is systematically applied in academic or industrial operations very rarely (Lamberg, 2011). There is

no denying that this method provides accurate and precise results for mineral characterization, and it is fast and easy to include in the industry (Hestnes et al., 2012). More often, the element analysis was used as an evaluation strategy for estimating the assay-dependent parameters. In nanomaterials, X-ray photoelectron spectroscopy (XPS) determined target elements intensities can be used as a quantitative approach for evaluating the ligand densities (number/unit area) on nanoparticles even at very small diameters (Katari et al., 1994; Torelli et al., 2015; Smith et al., 2017). In oil sands, instrumental neutron activation analysis (INNA) has been used to establish the correlations between the fines content and 11 types of individual elements in 23 oil sands samples (Donkor et al., 1996). Potassium content measured by K-40 gamma spectroscopy has been commercially applied for the clay/fines determinations (Dougan et al., 1997). Also, light elements concentrations ($Z < 12$) measured by laser-induced breakdown spectroscopy (LIBS) are used to estimate the bitumen content (Harhira et al., 2018). In food science, mineral and trace elements contents analyzed by inductively coupled plasma mass spectroscopy (ICP-MS) are served as indicators for the quality traits in rice (Batten, 2002; Jiang et al., 2007) and the geographic origin of the potatoes (Giacomo et al., 2007). In pharmaceuticals, particle-induced X-ray emission (PIXE) technique has been utilized for quantifying the trace elements concentrations in the medicinal plants to correlate with their curative ability (Devi et al., 2008; Rihawy et al., 2010; Raju et al., 2013).

There is, of course, no shortage of other instruments available for the elemental determination, for example, atomic absorption spectrometer (AAS) (Doesthale et al., 1979; Suárez et al., 2007; Chahid et al., 2014). More research should be done in the future to expand the applications of the instruments based on element analysis.

2.5.4.1 X-ray fluorescence (XRF)

XRF is a well-established analytical technique for estimating the element composition of rocks, sediments (De Vries et al., 2002; Weltje et al., 2008), and other solid/liquid samples. It is one of the most versatile techniques (He et al., 1991) for elemental identification due to its wide detection range from sodium to uranium with detection limits from ng/g to $\mu\text{g/g}$. Also, it is fast, non-destructive, and reliable, requires no or very little sample preparation, making it suitable for solid, liquid, and powdered samples (Cesareo, 2010). Modern X-ray spectrometers are divided into two groups based on their mechanism to characterize X-ray emission wavelength or energy. Unlike with wavelength dispersive spectrometry which uses the diffracting power of a single crystal to isolate the narrow wavelength bands, energy dispersive spectrometry uses a proportional detector to isolate the narrow energy bands, from the polychromatic radiation excited from the sample (Jenkins, 1999). A more detailed measurement theory of the energy dispersive X-ray fluorescence (EDXRF) analysis will be discussed in the following paragraph, and that of the wavelength dispersive X-ray fluorescence (WDXRF) can be found elsewhere (Helsen et al., 1993).

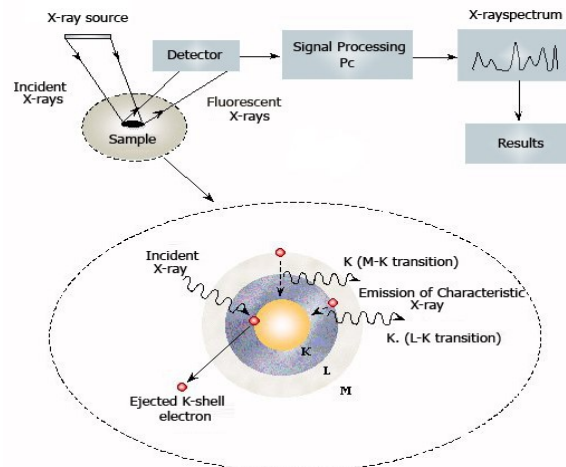


Figure 2.17. Typical EDXRF arrangement and principle (<http://www.goldtester.in/introduction-of-XRF-technology.html>).

EDXRF spectrometers consist of a source of excitation radiation (X-rays, gamma-rays, electrons, and photos), most commonly X-ray photos (Jenkins, 1999); a radiation detector; a display of the spectral output; and a computer for data processing. As shown in Figure 2.17, individual atoms in the sample material are excited by incident X-rays, and specific X-ray fluorescence signals are then emitted by the atoms after the photoelectric ionization. In brief, electrons from the outer orbit or shell tend to transit to the inner shell and eject electrons when excited by external high energy photons. Since the outer shell electrons are more energetic than the inner shell electrons, the relocated electrons expend excess energy as X-ray fluorescence photons. Each element generates a specific energy level during this transition process, and the corresponding energies are known as characteristic X-rays (Clapera, 2006). The detector converts these characteristic X-ray fluorescence signals into voltage pulses to obtain a spectrum of intensity against energy. The positions of the peaks identify the type of elements present, and the peak heights indicate the content of each element in the sample (Clapera, 2006).

A typical application of XRF is the determination of major, minor, and trace elements in materials such as rocks, ores, soils, ashes, and sewage sludges (Heckel et al., 1992). The accuracy and precision criteria are well met for the XRF technique to provide the element composition of the tested samples (Leake et al., 1969; Franzini et al., 1972; Wobrauschek et al., 1975; Ramsey et al., 1995; Xie et al., 1998; Dos Anjos et al., 2000; Twining et al., 2003; Meel et al., 2007; Rowe et al., 2012). The qualitative or semi-quantitative correlations between the concentrations of the elements determined by XRF and the important variables in a certain system have been established in thousands of scientific publications (e.g. Bloch, 1985; Neumann et al., 1991; Carlisle et al., 1995; Mantler et al., 2000; Paunesku et al., 2006; Allen et al., 2008; Melquiades et al., 2012; Alassane et al., 2013). Some of such applications are summarized. With the determination of

inorganic elements concentrations, XRF has been applied for the characterization of air particulate matter (PM_{2.5} and PM₁₀) in the Athabasca oil sands region (Wang et al., 2015; Landis et al., 2017). Levels of traffic, pedestrian flow, and contamination assessment of urban roads can be evaluated by measuring the concentrations of the chemical elements in the street dust samples using XRF (Yeung et al., 2003; Lu et al., 2009). Also, it is helpful to measure the nutrient and toxic elements levels in biopsy specimens by XRF to predict the cancer risks in humans (Abnet et al., 2005; Cui et al., 2007; Geraki et al., 2002). Combined with chemometric methods, XRF can be used to classify oils (Bortoleto et al., 2005; Henriques et al., 2013), plants (Alexandre et al., 2006; Calza et al., 2007), ceramics (Bakraji, 2006; Freitas et al., 2010), bricks (Bonizzoni et al., 2013), and sediments (Melquiades et al., 2015). Besides, XRF has become a standard method in archaeometry to analyze paintings, manuscripts, pottery, glasses, statues, metalworks, and other materials with the aim of restoring their appearance, recognizing their materials, origin, and production technologies, distinguishing authentic work from counterfeits, and understanding the culture and human activities at that time (Calza et al., 2007; Dik et al., 2008; Musílek et al., 2012; Marwick, 2005).

Like other instruments based on element analysis, the quantitative applications of XRF are underused. Recently, XRF Solutions Ltd. (Spenser et al., 2015, 2016; Weedmark et al., 2018) commercialized portable XRF as a technology to predict the mineralogy, permeability, porosity, bitumen/water contents, and bitumen quality in heavy oil reservoirs.

CHAPTER 3 UNDERSTANDING THE EFFECT OF CLAY TYPE AND SOLID WETTABILITY ON BITUMEN EXTRACTION FROM CANADIAN OIL SANDS

3.1 INTRODUCTION

Over the past two decades, the large-scale extraction of Canadian oil sands has significantly impacted the global energy landscape (Heyes et al., 2018). Oil sands are a mixture of water, sands and clays, with the oil or bitumen having a low API gravity and a high viscosity (Rui et al., 2018). These deposits require complex and advanced technologies to recover valuable commodity of bitumen. Depending on the depth of the oil sands reserves, two different recovery strategies are commonly used, including surface mining for deposits of depth <75m and in situ drilling for deposits of depth >75m (Chew, 2014; Chalaturnyk et al., 2002; Rosa et al., 2017). In 2017, an average of $451.1 \times 10^3 \text{m}^3$ of crude bitumen was produced per day in Canada, of which around 45% was from surface mining operations using water-based extraction processes (Alberta Energy Regulator, 2018). The performance of a water-based bitumen extraction process relies on the efficiency of bitumen separation from the sand grains known as liberation (Srinivasa et al., 2012; Basu et al., 1997) and the subsequent aeration of liberated bitumen attaching to air bubbles (Moran et al., 2000; Gu et al., 2004; Alexander and Li, 1996). The aerated bitumen droplets float to the top in a separation vessel under the natural gravity to form a bitumen froth which is collected and subjected to further treatments.

In a bitumen extraction process, clays are found to be problematic in a number of ways such as increasing slurry viscosity, reducing bitumen recovery, and deteriorating froth quality (Tu et al., 2005; Masliyah et al., 2004). In 2000, Kasongo et al. (2000) demonstrated that the addition of either kaolinite, illite, or montmorillonite clay alone at 1 wt.% of the processed ore or the addition

of divalent cations alone up to 40 ppm had little impact on bitumen recovery at 82 °C. A sharp reduction in bitumen recovery was observed only with the co-addition of 1 wt.% montmorillonite clay and divalent cations greater than 30 ppm. This finding suggests that the addition of 1 wt.% montmorillonite was only detrimental with the presence of divalent cations at processing temperature of 82 °C. A similar detrimental effect of illite and divalent cations on depressing bitumen recovery was measured at a much lower processing temperature (35 °C) and a higher illite addition (3 wt.%) (Ding et al., 2006). In the absence of divalent cations, a further decrease in temperature or increase in the amount of clays was required to result in a noticeable reduction in bitumen recovery. For example, 3 wt.% montmorillonite clays at 35 °C (Repka, 2007) or 5 wt.% illite clays at 25 °C (Ding et al., 2006) without introducing additional divalent cations were found to depress bitumen recovery significantly. For kaolinite at 50 °C, an 11 wt.% doping was needed to show a noticeable depression of bitumen recovery (Zhou et al., 2017b). The amount of clays required to show a similar impact on the reduction of bitumen recovery was found to vary significantly, depending on the type of ores and the processing temperatures (Fong et al., 2004). Early studies collectively showed that montmorillonite was the most detrimental clay, followed by illite and kaolinite. High processing temperatures and elimination of divalent cations were effective in alleviating the negative impact of clays on bitumen recovery.

Slime-coating, defined as the attachment of solid particles on bitumen droplets, has been long considered as a main cause for the low bitumen recovery and poor froth quality observed when processing oil sands of high clay contents often linked with high electrolyte contents (Liu et al., 2005b). The deposition of clay particles on bitumen droplets forms a layer of hydrophilic clays on bitumen surfaces, which hinders the attachment of air bubbles to the bitumen droplets. Slime-coating phenomenon has been studied extensively by researchers using AFM and ζ potential

distribution measurement (Ding et al., 2006; Liu et al., 2002, 2003, 2004b, 2005b). By analyzing the interaction forces between bitumen and clay particles, montmorillonite was found to attach on bitumen surface easily in the presence of calcium or magnesium ions at pH of 8~8.5 due to the presence of only small energy barriers, and exhibit strong adhesion forces with bitumen upon their attachment (Liu et al., 2004b). Deposition of montmorillonite on bitumen droplets with divalent cations acting as bridges was inferred from the results of ζ potential distribution measurements at pH 8 (Repka, 2007; Liu et al., 2002). In the bitumen-illite system, slime-coating phenomenon was observed early at acidic pH environment (pH=4.9) in the presence of divalent cations (Ding et al., 2006). Recently, QCM-D was used to monitor bitumen clay interactions and illite was confirmed to slime-coat onto bitumen droplets in tailings water (pH=8.5, containing $\text{Ca}^{2+}/\text{Mg}^{2+}$) after removal of humic acids from process water (Marjan et al., 2015). Kaolinite was found to attach only weakly to bitumen droplets even in the presence of divalent cations (Liu et al., 2004b; Marjan et al., 2015), yet it hindered bitumen-air attachment as in the case of montmorillonite and illite clays (Moran et al., 2000). To minimize slime-coating, chemical aids such as NaOH were often added to increase the solution pH and hence repulsive forces between bitumen and clays, which improved bitumen recovery and froth quality (Masliyah et al., 2004; Marjan et al., 2015; Long et al., 2007; Schramm et al., 2003).

Clays are hydrophilic by nature. However, the clays in oil sands could be hydrophobized due to natural weathering (Ren et al., 2009a, 2009c) which enhances the adsorption of surfactants (Zhao et al., 2006) and/or organic matters present in bitumen on clays (Sparks et al., 2003; Chen et al., 2017). The hydrophobic clay particles coagulate easily with bitumen to form aggregates. These slime-coated bitumen droplets remain hydrophobic and are able to be attached to air bubbles and recovered, although large aggregates may sink (Sparks et al., 2003). Slime-coating of bitumen

by hydrophobic clays was found to reduce both bitumen recovery and froth quality (Zhou et al., 2017b; Fu et al., 2010).

The detrimental impact of clays on bitumen recovery is clear, however the underlying mechanisms of the impact remain inconclusive due to the lack of understanding in the following areas:

- Slime-coating of clays on bitumen surfaces was only observed in the presence of divalent cations. This observation cannot explain the depression of bitumen recovery with the introduction of clays alone.
- Previous fundamental studies on bitumen slime-coating paid little attention to clay content in the slurry (suspension). In all early studies, particle-surface interactions were analyzed without considering the effect of clay concentration. Consideration of limited clay content to less than 10 g/L in ζ potential distribution measurements does not apply to extraction systems of high clay contents.
- Little/negligible deposition of kaolinite on bitumen droplets was observed. This is in conflict with the poor processabilities of ores with high clay contents of clays mainly from kaolinite.

The objective of the current study is to gain an in-depth understanding on the effect of various types of clays and their surface hydrophobicity on bitumen extraction. Slime-coating mechanism was investigated using AFM direct force measurement and ζ potential distribution measurement in conjunction with clay deposition tests. The effect of clay concentration and clay surface hydrophobicity on slime-coating was studied. Also studied was the effect of clays on the stability

of the bitumen-in-water emulsions by determining bitumen droplet size in flotation slurry with and without clay addition.

3.2 MATERIALS AND METHODS

3.2.1 Materials

A high-grade oil sands sample (ore G), provided by Syncrude Canada Ltd., was used in this study. The grade (or bitumen content) of this ore was 11.5% with a low fines content of only 15.4 wt.% (fines are defined by the oil sands industry as particles of sizes <44 μm).

Table 3.1. Volume-based passing size (d_{50} and d_{90}) of clays used in this study before and after homogenizing by a 500 ultrasonic dismembrator

Type	Original		After homogenizing	
	d_{50} (μm)	d_{90} (μm)	d_{50} (μm)	d_{90} (μm)
Kaolinite	5.86	10.63	1.66	5.26
Illite	5.77	17.39	2.89	9.47
Montmorillonite	4.23	11.25	1.65	5.14

Three clays were tested in this study to evaluate their impact on bitumen extraction: kaolinite (Edgar, Florida, U.S.A), illite (Rochester, New York, U.S.A.), and montmorillonite (Panther Creek, Colorado, U.S.A.). Kaolinite and montmorillonite came as fine powders and used as received while illite was ground first to sub-micrometer sizes. The particle size distribution of the clay particles was determined using a Malvin Mastersizer 3000. As shown in Table 3.1, the volume-based 50 and 90% passing sizes (d_{50} and d_{90}) of the clay particles were 4 to 6 and 11 to 17 μm , respectively. After homogenizing by a 500 ultrasonic dismembrator (Fisher) to prepare clay suspension for ζ potential distribution measurements and clay deposition tests, the measured d_{50} and d_{90} were reduced to 2 to 3 and 5 to 10 μm , respectively. Silica powders (Berkeley Springs,

West Virginia, USA) used in a few tests for comparison had d_{50} and d_{90} of 2 and 40 μm . All these clay and silica particles were 100% fines ($<44 \mu\text{m}$).

Coker feed bitumen from Syncrude Canada was used to prepare bitumen emulsions for ζ potential distribution measurement and clay deposition test. Certified ACS grade toluene (Fisher Scientific) was used as the diluent of bitumen. De-ionized water ($0.8 \mu\text{S}\cdot\text{cm}^{-1}$) with a pH of 5.0~5.6 was used throughout these fundamental measurements. High purity KCl ($>99.999\%$, Aldrich) was used as the background electrolyte in preparing aqueous solutions while NaOH (1N, Fisher Scientific) and HCl (1N, Fisher Scientific) standard aqueous solutions were used as pH modifiers. NaOH was also used as a process aid in a few extraction tests. In the tests without pH control, the pH was in the range of 5.0 to 5.6.

3.2.2 Bitumen extraction test

A modified Batch Extraction Unit (BEU) was used for bitumen extraction tests. For baseline tests, 150 mL de-ionized water ($98 \text{ }^\circ\text{C}$) were placed in the BEU cell. 500 g of oil sands ore were then added into the cell. Temperature of the cell was set at $55 \text{ }^\circ\text{C}$. After the slurry was conditioned with 150 mL/min air addition and mechanical stirring at 600 rpm for 10 min, 900 mL de-ionized water ($55 \text{ }^\circ\text{C}$) was added as flood water to the cell. Air was introduced during conditioning to produce bitumen-air aggregates with densities lower than the aqueous slurry to achieve acceptable levels of bitumen separation from slurry (Flynn et al., 2001). Primary froth was first collected while the slurry was continuously stirred without air addition for 10 min. The air was then introduced again at 50 mL/min for other 5 minutes with the slurry under stirring at 800 rpm, during which the secondary froth was collected. After each test, the suspension remained in the cell was preserved as tailings water with coarse solids being settled to the bottom of the cell. Dean Stark

refluxing method was used to obtain the contents of bitumen, water, and solids in the collected froths. The overall bitumen recovery was calculated by:

$$\begin{aligned} & \text{Overall Bitumen Recovery (\%)} \\ &= \frac{\text{Bitumen in primary and secondary froth (g)}}{\text{Bitumen in feed (g)}} \times 100\% \end{aligned} \quad (3.1)$$

The overall solids-to-bitumen ratio in bitumen froth was obtained as follows:

$$\begin{aligned} & \text{Overall solids to bitumen ratio (g/g)} \\ &= \frac{\text{Solids in primary and secondary froth (g)}}{\text{Bitumen in primary and secondary froth (g)}} \end{aligned} \quad (3.2)$$

Solids retained in the thimbles holding bitumen froth after Dean Stark reflux were dried and saved for further analysis. All the other extraction tests were performed similarly except for doping of solids by thorough mixing with the oil sands ore before introducing the mixtures as the “ore” into the cell.

3.2.3 Wettability modification of clay particles

To modify the surface hydrophobicity of clay particles, bitumen was dissolved in toluene to a bitumen concentration of 58.8 wt.%. The original solids in bitumen were removed by centrifuging the prepared bitumen-in-toluene solution at 20,000 g force for 3.5 h. Figure 3.1 describes the procedures of modifying the wettability of clays. Clay particles were dispersed in bitumen-in-toluene solutions under stirred for 24 h to maximize the contact between clay particles and bitumen. The suspension was then centrifuged to separate the solution from the solids. After decanting the supernatant, the solids were washed by fresh toluene multiple times until the supernatant became colorless. The solids collected were dried in a vacuum oven overnight.

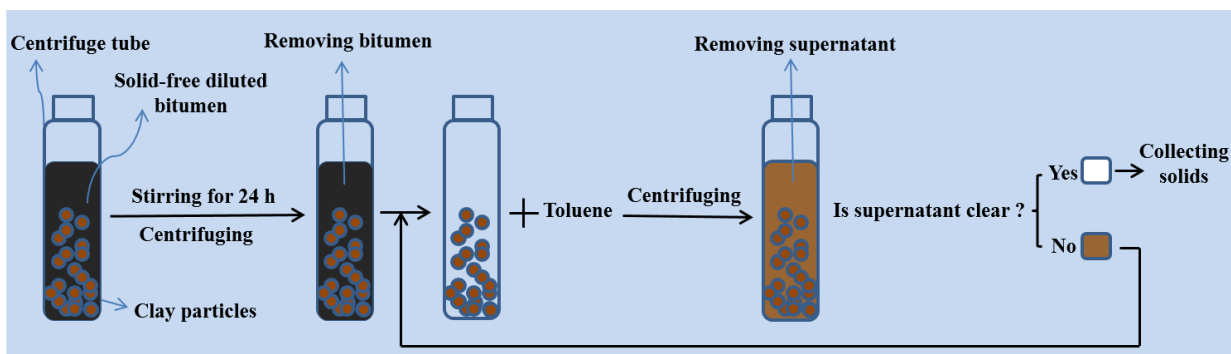


Figure 3.1. Schematics of wettability modification of clay particles.

3.2.4 ζ potential distribution measurement

ζ potential distribution was measured using a Zetaphoremeter III (SEPHY/CAD). 1 g of bitumen was emulsified in 100 mL KCl solution (1 mM) using a 500 ultrasonic dismembrator (Fisher). The clay suspension was prepared using similar procedures. Binary mixtures were obtained by mixing bitumen emulsion and clay suspension at a specific ratio and conditioned in an ultrasonic bath for five minutes. The samples prepared were then diluted to a concentration of 0.01–0.1 wt.% particles. Around 50–100 particles were traced for a given system to obtain ζ potential distribution histogram. ζ potential distributions of bitumen droplets and clay particles, either individually or in a mixture, were measured to provide a good estimation of hetero-coagulation in an aqueous medium by following the methodology reported elsewhere (Liu et al., 2002).

3.2.5 Colloidal force measurement using scanning probe microscope (SPM)

3.2.5.1 Sample preparation

Two types of substrates were used in this study: silica (simulating silica basal planes of clays) and alumina (simulating alumina basal planes of clays) (Alagha et al., 2011; Klein et al., 2013). A detailed description on procedures for preparing substrates and probe particles can be found

elsewhere (Liu et al., 2003). In brief, a silica (Nanofab, University of Alberta) or alumina (University Wafer Inc.) wafer was cut into 15 mm × 15 mm square pieces which were washed with chloroform and rinsed with de-ionized water and ethanol to remove organic contaminants. Ultrapure grade nitrogen was used to dry these washed square pieces of substrates.

To prepare bitumen probes, dip-coating technique was adopted (Liu et al., 2005a). Silica spheres with a diameter of $\sim 8\mu\text{m}$ were picked up using a micromanipulator under an optical microscope and glued onto the apex of a tipless cantilever using a two-component epoxy. (Ducker and Senden, 1992). Bitumen solution was prepared by dissolving 250 mg bitumen in 100 mL toluene. The glued silica particles on AFM cantilevers were dipped into the bitumen solution for ~ 1 min. The probes were then taken out and allowed for solvent evaporation and hence bitumen coating (referred to as bitumen probe) in a horizontal laminar hood for more than 1 h before used in colloidal force measurements.

3.2.5.2 Colloidal force measurement

The interaction forces between bitumen and silica/alumina in aqueous solutions of different pH were measured using a Multimode 8 AFM (Veeco). The principle of colloidal force measurement can be found elsewhere (Ducker and Senden, 1992) and is described only briefly here. Both the substrate and bitumen probe were immersed in 1 mM KCl solutions of different pH for 1 h to allow the system to reach an equilibrium prior to force measurement. A piezo translation stage was used to move the silica/alumina surface to approach or retract from the bitumen probe. The force between the bitumen probe and the substrate deflected the cantilever and the corresponding force-versus-distance curve was obtained by recording the deflection and calculating the force using carefully calibrated spring constant of the cantilever. The long-range interaction force was determined during the approaching stage and the adhesion force was

measured in the retraction stage. For the bitumen interacting with hydrophobic clays, silica and alumina wafers were hydrophobized by immersing in diluted bitumen solution using the procedure discussed earlier.

3.2.6 Clay deposition measurement

The deposition of clay particles from an aqueous phase onto a bitumen-water interface was determined to study the effect of clay concentration on bitumen-clay hetero-coagulation. A known amount of clay particles was first added into 175 mL of water and dispersed using an ultrasonic dismembrator for 15 min to break up any lumps. Then 25 mL of bitumen-in-toluene solution (450 g bitumen per L solution) were added to the prepared clay suspension and the mixture was homogenized using a magnetic stirrer at 600 rpm for 20 min. Once the emulsion was formed, it was left in a separating funnel for a period of 10-minute creaming time. The volumes of the obtained emulsion phase and aqueous phase were recorded using a graduated cylinder. A known volume of the aqueous phase was dried in an oven at 220 °C for 24 h to determine the weight of clays remaining in the aqueous phase. The concentration of clays (g/L) remained in the aqueous phase was calculated by:

$$C_w = \frac{W_t}{V_t} \quad (3.3)$$

where W_t and V_t were the weight of dried clay particles and the volume of the aqueous phase tested, respectively.

To determine the deposition of clays on bitumen, an assumption was made for the emulsion phase that the clay concentration in the water entrained between the diluted bitumen droplets was

the same as that in the aqueous phase (Yan and Masliyah, 1994). The weight of clays deposited on the surface of emulsified bitumen droplets was calculated by:

$$W_o = W_i - C_w V_w \quad (3.4)$$

where W_i was the initial weight of clays added into the water, and V_w was the volume of water used to prepare clay suspension prior to emulsification.

Finally, the surface concentration (g/cm^2) of clays on the diluted bitumen droplets was given by:

$$C_b = \frac{W_o}{A} = \frac{W_o}{V_o} \frac{d}{6} = \frac{W_i - C_w V_w}{V_o} \cdot \frac{d}{6} \quad (3.5)$$

where V_o was the volume of diluted bitumen solution added prior to emulsification and A was the total bitumen-water interfacial area. The diameter of diluted bitumen droplets, d , was determined by averaging sizes of 80–100 diluted bitumen droplets measured using an optical microscope.

For given clay particles, the deposition isotherm of C_b vs. C_w is fitted by the BET theory of a multilayer adsorption model (Oscik, 1982; Yan and Masli):

$$\frac{C_b}{C_w} = \frac{k_1 C_m}{(1 - k_m C_w)(1 - k_m C_w + k_1 C_w)} \quad (3.6)$$

where k_1 , k_m and C_m are fitting parameters. k_1 and k_m are the equilibrium constants for the 1st layer and the subsequent layers of deposition while C_m is the monolayer coverage of the clay particles at the diluted bitumen droplet-aqueous interface.

3.2.7 Contact angle measurement

A Theta Optical Tensiometer (T200) was used to measure the contact angles of water on solid surfaces using the sessile drop method (Drelich, 2013). 0.2 g of clay particles were dispersed in 20 mL toluene and sheared by a 500 ultrasonic dismembrator (Fisher) for about 15 min to prepare a clay suspension. A clean silica wafer was placed on a spin coater with vacuum being applied to hold the wafer firmly in place. Then 10 drops of clay suspensions were carefully added to the silica wafer spinning at 6000 rpm. After the evaporation of toluene, a layer of the solid particles remained on the silica wafer. A water droplet was placed on the solid surface and the contact angle from the aqueous phase was measured directly by the goniometer.

3.3 RESULTS AND DISCUSSION

3.3.1 Effect of hydrophilic clays on bitumen extraction

3.3.1.1 Bitumen recovery

To investigate the effect of clays on bitumen recovery, kaolinite, illite, and montmorillonite with similar particle size distributions were doped to ore G at clay to ore weight ratios of 1~5% to exam their effects on overall bitumen recovery. Silica was also tested as a representative of sand in oil sands. Figure 3.2a shows the results of bitumen recovery for ore G with the addition of different types of solids at different levels. For the baseline test (no solids addition), the bitumen recovery was 88%. The addition of hydrophilic silica at 1 and 5 wt.% of ore caused a small reduction in bitumen recovery to 80 and 70%. Such small effect of hydrophilic silica addition on bitumen recovery could be explained by weak attraction if any of silica to bitumen surfaces (Zhou et al., 1999; Dai and Chung, 1995), which was supported by results of early colloidal force measurements (Liu et al., 2003). The addition of clays led to a different story. The recovery was reduced to 78, 73, and 61% by the addition of 1 wt.% of hydrophilic kaolinite, illite, and

montmorillonite, respectively. These recovery reductions confirmed the negative role of clays played in bitumen extraction, due mainly to the hindered bitumen-air bubble attachment by slime-coating of hydrophilic clay particles on bitumen droplets. Montmorillonite was shown to be the most detrimental clays, leading to the highest reduction in bitumen recovery due to their strongest slime-coating as shown in earlier studies (Liu et al., 2004b, 2005b; Xu et al., 2003). When the addition of clay particles was increased to 2 and 5 wt.%, the bitumen recovery was further decreased to ~45% and below. This decreasing trend in bitumen recovery indicates clearly an increasing negative impact of clays on bitumen extraction with increasing the clays content. Between the two clays naturally present in oil sands, the reduction in bitumen recovery by illite addition is more severe than by kaolinite addition at all levels tested, indicating a more detrimental role of illite than kaolinite in suppressing bitumen recovery. Compared with kaolinite, illite could become weathered and hence swelling, making its affinity to divalent cations stronger than non-swelling kaolinite (Stumm and Morgan, 1996). The early study also showed a more severe slime-coating of illite clays than kaolinite clays on bitumen droplets (Marjan et al., 2015).

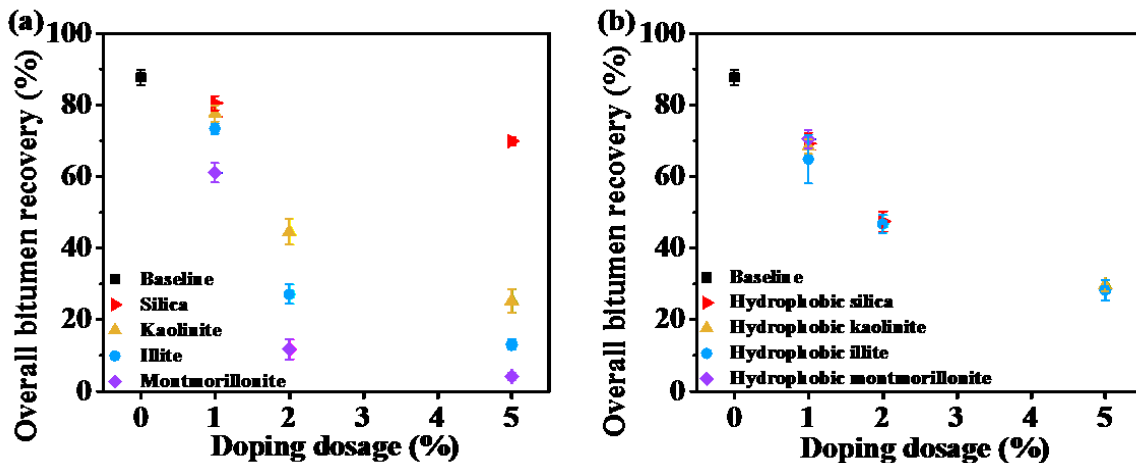


Figure 3.2. Effect of doping solids on bitumen recovery: a) hydrophilic solids and b) bitumen contaminated solids

3.3.1.2 Froth quality

Table 3.2. Results of BEU tests with the addition of hydrophilic solids

Condition	Recovery (wt.%)	Froth Composition (wt.%)			S/B ratio (g/g)
		Bitumen	Solids	Water	
Baseline	87.7	37.2	10.8	52.0	0.29
1 wt.% solids addition					
Silica	80.5	35.1	10.1	54.8	0.29
Kaolinite	77.6	33.8	10.1	56.1	0.30
Illite	73.3	32.6	10.6	56.8	0.33
Montmorillonite	61.1	22.3	8.4	69.3	0.37
2 wt.% solids addition					
Kaolinite	44.5	22.8	9.4	67.8	0.41
Illite	27.1	16.2	7.4	76.4	0.46
Montmorillonite	11.7	12.4	6.3	81.3	0.51
5 wt.% solids addition					
Silica	69.8	31.9	22.2	45.9	0.70
Kaolinite	25.2	14.6	11.7	73.6	0.80
Illite	13.0	8.9	7.4	83.7	0.83
Montmorillonite	4.1	5.9	5.2	88.9	0.87
5 wt.% illite addition + NaOH					
0.05% NaOH	30.5	18.8	14.3	66.9	0.76
0.15% NaOH	67.7	45.0	24.4	30.6	0.54

*S/B=solids/bitumen

The quality of bitumen froth for each test is summarized in Table 3.2. To understand the effect of solids addition on froth quality, the overall solids-to-bitumen ratio is plotted in Figure 3.3a.

Without solids addition, the solids-to-bitumen ratio of the froth was about 0.29. When fine particles were added, the froth quality decreased as less bitumen but more water were brought to the froth. As expected, less depression of froth quality was obtained by adding silica particles than by adding clays into the system due most likely to less slime-coating of silica on bitumen. At all levels of solids addition tested, montmorillonite led to the highest solids-to-bitumen ratio, indicating the strongest deterioration of froth quality by montmorillonite addition due to its strongest slime-coating. Poorer froth qualities (higher solids-to-bitumen ratios) were observed with more solids added into the system. Illite addition was found to cause a froth of higher solids-to-bitumen ratios than kaolinite addition. As shown in Figure 3.3a, the addition of a larger amount of clays caused a more significant reduction in froth quality as anticipated.

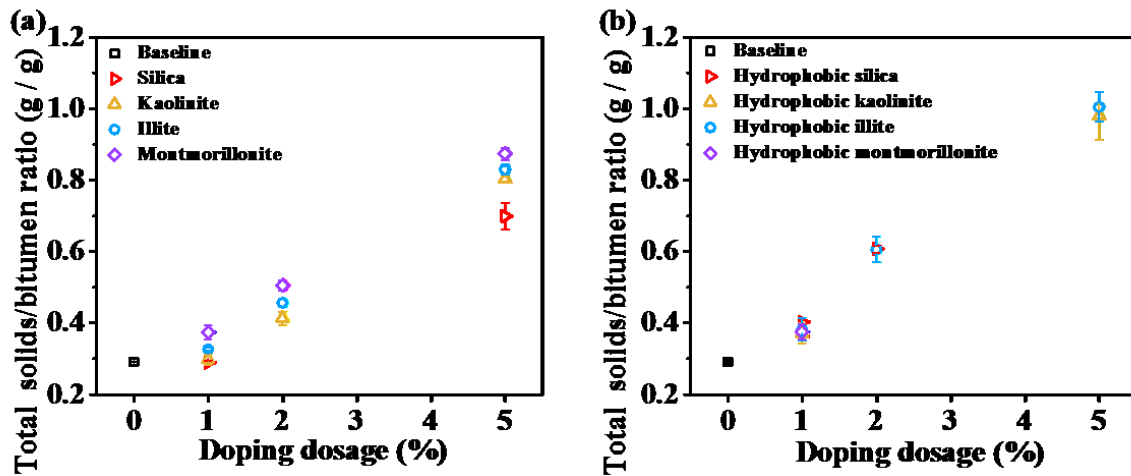


Figure 3.3. Effect of doping solids on froth quality: a) hydrophilic solids and b) bitumen contaminated solids.

As shown in Table 3.2, NaOH addition was able to improve bitumen recovery and to decrease the solids-to-bitumen ratio in froth. The addition of 0.05 wt. % and 0.15 wt. % NaOH increased pH of the (slurry) tailing water from 6.8–7.3 to ~8.0 and ~10.8, respectively. Both clay particles and bitumen droplets became more negatively charged in the elevated pH environment, depressing

the slime-coating by increasing electrostatic repulsion between clays and bitumen. The existence of more clays in the extraction system requires more NaOH to eliminate the negative effect of clays on bitumen extraction.

3.3.2 Effect of hydrophobic clays on bitumen extraction

3.3.2.1 Bitumen recovery

To understand the effect of solids hydrophobicity on bitumen recovery, solid surfaces were contaminated by immersing the solids in a solids-free diluted bitumen solution prior to their addition into the BEU tests. Here solids were contaminated in a diluted bitumen solution to mimic an oil sand slurry where solids are possibly in contact with bitumen. Contact angles of water on solid surfaces before and after bitumen contamination were measured to show the change in surface hydrophobicity. Table 3.3 shows the results of measured contact angles on different surfaces. The original clay and silica surfaces were hydrophilic with water contact angles at zero degree. After contamination by bitumen, the contact angles increased significantly to at least 84°, indicating hydrophobic nature of solids by contamination in diluted bitumen with kaolinite becoming the most oil wet at a water contact angle of 110°.

Table 3.3. Contact angles of water on various solids before and after wettability modification

Solid type	Contact angle (degree)	
	Original	After modification
Silica	0	84
Kaolinite	0	110
Illite	0	100
Montmorillonite	0	91

Figure 3.2b shows the results of bitumen recovery with hydrophobic solids addition. In general, there was a clear decreasing trend in bitumen recovery with the addition of hydrophobic solids. The bitumen recovery was reduced from the base case of 88 to ~68% with 1 wt.% solids addition. When solids addition increased to 2 and 5 wt.%, a further reduction in bitumen recovery to ~47 and ~29%, respectively, confirmed a more detrimental role of hydrophobic solids in bitumen extraction at higher solids contents. The decrease of ~59% (absolute) in recovery with 5 wt.% hydrophobic clays addition is lower than the recovery decrease of 63–84% obtained with 5 wt.% hydrophilic clays addition (Figure 3.2a). The results suggest that the hydrophobic clays were not as detrimental to bitumen recovery as the hydrophilic clays since the bitumen covered with hydrophobic slimes may still be recovered in bitumen froth. The results in Figure 3.2b also show a negligible difference in depressing bitumen recovery with the addition of contaminated solids, regardless the type of original solids. It appears that the surfaces of the different types of solids were covered by similar organic matter during the contamination process and the hydrophobicity of the solids at a given amount determined the degree of slime-coating.

3.3.2.2 Froth quality

Table 3.4 summarizes the total amount of bitumen, solids and water obtained from bitumen froth for each extraction test with hydrophobic solids addition. The results show that:

- The addition of hydrophobic solids in general resulted in poorer froth quality with lower bitumen content and higher water content in the froth;
- 2 wt.% or more hydrophobic solids addition increased significantly solids content in froth;

- 0.05 wt.% NaOH addition (tailings pH 8.0) led to lower bitumen recovery and poorer froth quality, while 0.15 wt.% NaOH addition (tailings pH 10.8) improved both bitumen recovery and froth quality.

Table 3.4. Results of BEU tests with the addition of hydrophobic solids

Condition	Recovery (wt.%)	Froth Composition (wt.%)			S/B ratio (g/g)
		Bitumen	Solids	Water	
Baseline	87.7	37.2	10.8	52.0	0.29
1 wt.% hydrophobic solids addition					
Silica	69.2	29.8	12.0	58.2	0.40
Kaolinite	68.3	29.1	10.8	60.1	0.37
Illite	64.8	29.6	11.3	59.1	0.38
Montmorillonite	70.4	27.2	10.2	62.6	0.38
2 wt.% hydrophobic solids addition					
Silica	47.4	26.6	16.2	57.2	0.61
Illite	46.7	27.0	16.3	56.7	0.61
5 wt.% hydrophobic solids addition					
Kaolinite	29.6	18.9	18.5	62.6	0.98
Illite	28.3	18.5	18.5	63.0	1.00
5 wt.% hydrophobic illite addition + NaOH					
0.05% NaOH	20.0	16.1	21.4	62.5	1.33
0.15% NaOH	70.6	48.6	25.1	26.3	0.52

*S/B=solids/bitumen

The corresponding solids-to-bitumen ratio (Figure 3.3b) in bitumen froth with the addition of bitumen-contaminated solids (clays and silica) confirmed the negative impact of hydrophobic particles on froth quality. Comparison of Figure 3.3 a and b shows that the addition of bitumen

contaminated solids led to a higher solids-to-bitumen ratio in the froth than the addition of hydrophilic solids. It appears that more solids were attached to bitumen when contaminated than its original of hydrophilic nature. Also, the hydrophobic particles were able to recover in bitumen froth by attaching to air bubbles directly (Zhou et al., 2017b). The bitumen coated by these contaminated (hydrophobic) solids appeared to some degree to be recoverable by flotation as shown by higher bitumen recovery at the same lever of particle addition. In commercial oil sands operations, the solids could become hydrophobized due to the contamination of the solid surfaces by organic matter. To sum up, hydrophobic solids were also detrimental to bitumen extraction.

3.3.3 Mechanistic study on the effect of clays content on bitumen extraction

3.3.3.1 ζ potential distributions

Figure 3.4a shows the ζ potential distributions of bitumen emulsion and illite suspension measured separately in 1 mM KCl solution of pH 8.0. Both bitumen and illite displayed a negative ζ potential with the peaks centered at -76 and -35 mV, respectively. For the mixture at the illite to bitumen ratio of 5, two distinct peaks centered at -60 and -36 mV were observed as shown in Figure 3.4b. The peak at -36 mV was nearly identical to that measured for illite alone while the peak at -60 mV shifted significantly from the peak at -76 mV for bitumen alone. This shift indicates a weak attraction between illite and bitumen. To confirm this argument, the illite to bitumen ratio was increased to 6. In this case, Figure 3.4c shows a further shift in the peak corresponding to bitumen emulsions, but the peak for illite remains although it is weaker now. The results indicate an increased illite coating on bitumen with increasing illite addition, accounting for increased depression of bitumen recovery and froth quality with increasing illite addition as shown in Figures 3.2a and 3.3a, respectively. When the illite to bitumen ratio was further increased to 10, the unimodal ζ potential distribution peaked around the original peak of illite at about -40 mV (Figure

3.4d), indicating a complete coverage of bitumen surface by illite particles. The results in Figure 3.4 confirm the deposition of illite on bitumen surfaces under the test conditions.

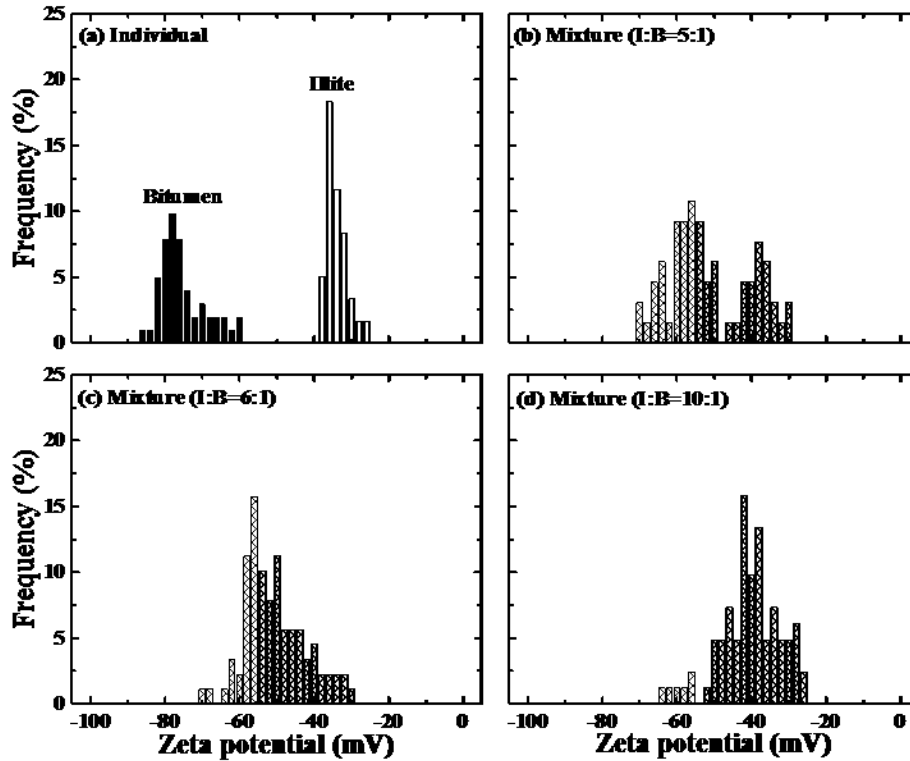


Figure 3.4. ζ potential distributions of bitumen emulsion and illite suspension (a) and their mixtures at 5:1(b), 6:1(c), and 10:1 (d) clay to bitumen mass ratios in 1 mM KCl aqueous solutions of pH 8.0.

Table 3.5 summarizes the clay to bitumen ratios at which strong slime-coating occurred between bitumen and various types of clays at different pH (see distributions in appendix B). For hydrophilic clays, kaolinite did not deposit on bitumen droplets in the measured pH range. Both illite and montmorillonite could deposit on bitumen surface without pH control. However, montmorillonite required a lower clay to bitumen ratio for slime-coating to occur than illite, indicating a stronger attraction between montmorillonite and bitumen droplets. The increase of pH to 8.0 could alleviate slime-coating as the required clay-to-bitumen ratios increased. A further

increase of pH to 10.8 was capable of eliminating bitumen slime-coating as no slime-coating was detected at the highest clay-to-bitumen ratio of 20. This finding accounts for improved bitumen recovery and froth quality with NaOH addition as shown in Tables 3.2 and 3.4. For hydrophobic clays, all 3 types of clays could slime-coat on bitumen droplets at the clay to bitumen ratios of 4 to 5 without pH control, indicating a stronger attraction between hydrophobic clays and bitumen than hydrophilic clays and bitumen most likely as a result of hydrophobic attraction. With the addition of NaOH to pH 8.0, the required clay to bitumen ratios were decreased to 2~3, indicating a stronger slime-coating than the cases without pH control. An increase in pH to 8.0 made both the bitumen and the hydrophobic clays more negatively charged, thus increasing the electrostatic repulsion between the two surfaces. However, the repulsive force is not sufficient to overcome the hydrophobic attractive force, while the improved dispersion of hydrophobic clay particles caused by the increase of pH would promote contacts between bitumen droplets and hydrophobic clays, thus intensifying the hetero-coagulation. Further increase in pH with NaOH addition to pH 10.8, no bitumen slime-coating was detected. At pH 10.8, both bitumen droplets and solids became more negatively charged to greatly increase the repulsive force that could overcome hydrophobic force, thus hindering hetero-coagulation between bitumen and hydrophobic clays. In summary, the results in Table 3.5 show the followings: a) hydrophilic kaolinite particles did not attach to bitumen unless their surfaces became hydrophobic by organic matter attachment; b) illite and montmorillonite clays slime-coated on bitumen droplets in acidic and weak alkaline conditions regardless of the surface hydrophobicity; c) the adsorption of organic matter modified clay surfaces and increased bitumen clay attachment; d) increasing pH was proved to be able to reduce slime-coating; and e) for hydrophobic clays, clay mineralogy showed little effect on slime-coating due to the coverage of their surface by similar organic matters. The measured clay to bitumen ratios

for slime-coating to occur as detected by ζ potential distribution measurement are much higher than in a real oil sands system where the clay to bitumen ratio is normally less than 2. One possible explanation is that the bitumen and clay concentrations used in the ζ potential measurements were much lower than that in the real cases. Smaller ratios are expected to be effective for bitumen clay hetero-coagulation in a system of higher bitumen and clay contents. The effect of clay concentration on bitumen slime-coating will be discussed later in this study.

Table 3.5. Solids-to-bitumen ratio for slime-coating of bitumen by fine solids measured under various conditions

Clay type	Clay to bitumen ratio (wt.)						
	No pH control			pH=8.0			pH=10.8
Kaolinite	20✘			20✘			20✘
Illite	5✘	6✓	10✓	5✘	6✓	10✓	20✘
Montmorillonite	3✘	4✓	5✓	3✘		4✓	20✘
Hydrophobic kaolinite	3✘	4✓	5✓	2✘	3✓	4✓	20✘
Hydrophobic illite	3✘	4✘	5✓	1✘	2✓	5✓	20✘
Hydrophobic montmorillonite	3✘	4✓	5✓	2✘		3✓	20✘

*Strong slime-coating ✓ No/weak slime-coating ✘

3.3.3.2 Clay deposition on diluted bitumen droplets.

Regarding the bitumen-clay hetero-coagulation, clay concentration can be an important factor, as increasing the number of clay particles would increase the frequency of clay-bitumen collisions. With no pH control, strong bitumen-illite hetero-coagulation was observed at 9 g/L illite concentration. Montmorillonite was easier to coat on bitumen surface, as indicated by the occurrence of strong bitumen-montmorillonite hetero-coagulation at 8 g/L montmorillonite concentration. Strong bitumen-kaolinite hetero-coagulation was not measured in 5 to 10 g/L

kaolinite suspensions. A hypothesis was then made that strong bitumen-clay hetero-coagulation occurs only above a critical clay concentration for a given type of clays. This critical concentration is expected to be different for different clays. We can estimate the critical concentration of clays at a given pH b ($C_{cri,b}$) from the clay to bitumen ratio (R) corresponding to the onset of strong slime-coating determined from ζ potential distribution measurement as:

$$C_{cri,b} = \frac{C_i \cdot R}{R + 1} \quad (3.7)$$

Here, initial clay concentration (C_i) was prepared at 10 g/L. It is important to note that the solutions were diluted for ζ potential measurements. Therefore, the critical concentrations obtained using this method were most likely an overestimate.

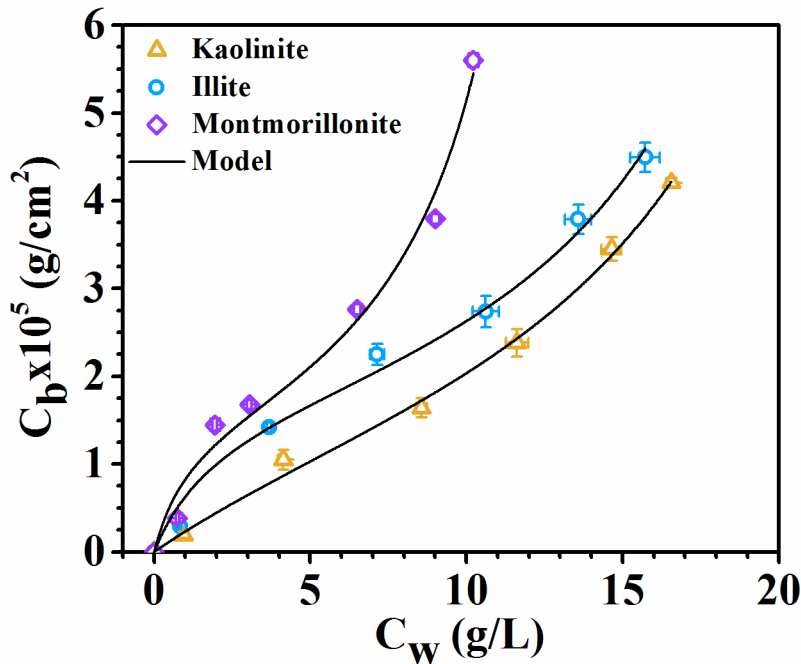


Figure 3.5. Deposition isotherms of clays on diluted bitumen droplets in aqueous suspensions without pH control (pH=5.0~5.6).

To estimate this critical concentration of slime-coating more accurately under the conditions pertinent to bitumen extraction, the deposition of clay particles from an aqueous phase onto a bitumen-water interface was determined. The BET theory for a multilayer adsorption model was used to fit the results of deposition experiments. As shown in Figure 3.5, the measured deposition of 3 clays on bitumen droplets can be fitted well with the BET adsorption model. The fitting parameters obtained are listed in Table 3.6. As expected, the equilibrium constant for the 1st layer (k_1) was much larger than that for the second and subsequent layers (k_m), indicating strong binding of clays on bitumen surfaces. Among the 3 types of clays, montmorillonite was found to be much easier to deposit on bitumen droplets as shown by the highest values of k_1 and k_m . The fitted monolayer coverage was found to be different for different types of clays as indicated by the variation in C_m values. The fifth column in Table 3.6 (C_w^m) is the fitted equilibrium clay concentrations in aqueous phase at the monolayer coverage. The corresponding initial clay concentrations in aqueous phase (C_{wi}^m) was calculated by linear interpolation between two adjacent experimental points, as listed in the last column. If we assume the clay concentration at monolayer coverage of clays on bitumen droplets as an indicator of strong slime-coating, it corresponds to 12.9 g/L for kaolinite, 8.6 g/L for illite, and 5.8 g/L for montmorillonite, indicating the strongest slime-coating by montmorillonite followed by illite and kaolinite. This trend agrees with that obtained from the ζ potential distribution measurement. Quantitatively, the critical concentrations observed from ζ potential distribution measurement is much higher than the values obtained from clay deposition experiment as anticipated. This finding confirms our hypothesis that any clay could slime-coat on bitumen droplets, and strong slime-coating could only be observed at concentrations higher than a critical value.

Table 3.6. Multilayer model parameters of particle deposition

Clay type	Fitting parameters			Model prediction	
	$C_m \times 10^5 (\text{g}/\text{cm}^2)$	$k_1 (\text{L}/\text{g})$	$k_m (\text{L}/\text{g})$	$C_w^m (\text{g}/\text{L})$	$C_{wi}^m (\text{g}/\text{L})$
Kaolinite	1.8902	0.1295	0.0374	9.346	12.90
Illite	1.7518	0.5051	0.0404	5.457	8.64
Montmorillonite	1.5572	0.9091	0.0707	3.084	5.77

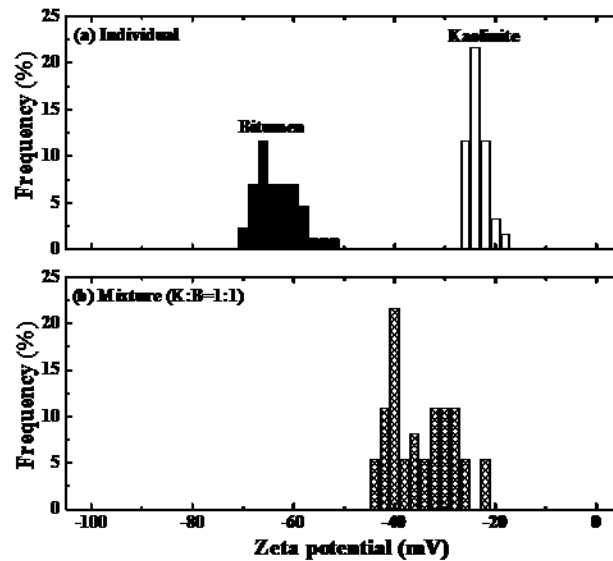


Figure 3.6. ζ potential distributions of bitumen emulsion and kaolinite suspension (a) and their mixture at 1:1 kaolinite to bitumen mass ratio of 15 g/L kaolinite (b) in 1 mM KCl aqueous solutions without pH control (pH=5.0~5.6).

To confirm the dependence of slime-coating on clay content, ζ potential distribution measurements were conducted at higher kaolinite concentration of 15g/L. As shown in Figure 3.6, strong slime-coating of bitumen by kaolinite was indeed observed at such high kaolinite concentration. This is the first-time strong kaolinite slime-coating on bitumen was detected experimentally, which is not surprising as slime-coating is a result of both collision and attachment. For a given probability of bitumen-particle attachment determined by the nature of colloidal

interactions, increasing concentration of clay particles would increase the collisions rate of bitumen droplets with clay particles, leading to more severe hetero-coagulation as observed.

3.3.4 Interaction forces between bitumen and clays

3.3.4.1 Interaction forces between bitumen and hydrophilic clays

To better understand the dominant factors that affect bitumen-clay attachment, interaction forces were measured for the current systems. In general, the Derjaguin-Landau-Verwey-Overbeek (DLVO) theory considering van der Waals forces and electrostatic double layer force has been considered to be adequate for describing colloidal forces between hydrophilic clays and bitumen in aqueous solutions (Liu, et al., 2003, 2004b, 2005b; Zhao et al., 2006). The corresponding equations for van der Waals forces and electrostatic double layer force can be found elsewhere (Hogg et al., 1966; Usui, 1973; Martines et al., 2008).

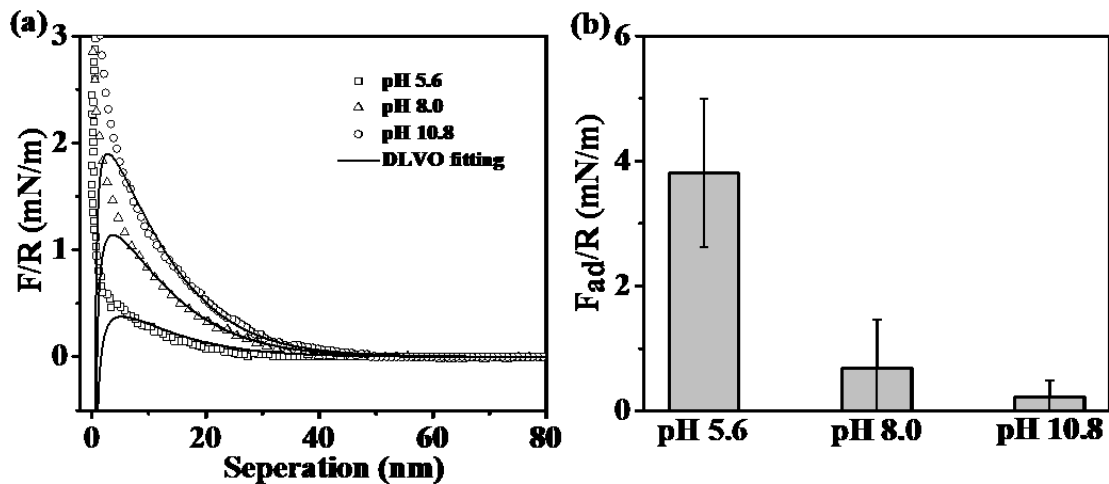


Figure 3.7. Colloidal forces between bitumen probe and silica wafers in 1 mM KCl aqueous solutions of different pHs. (a) long-range force; and (b) adhesion force.

Figure 3.7 shows the measured colloidal forces between bitumen probe and silica wafers in 1 mM KCl solutions of different pH. The long-range force profiles at separation distance greater

than 6 nm can be well fitted with the DLVO theory, as indicated by the solid lines in Figure 3.7a. The excellent fit between experimental results and DLVO theory suggests that the long-range repulsive forces were predominantly from the van der Waals forces and electrostatic double layer force. Within the pH range studied, the measured long-range forces between bitumen probe and silica wafer surfaces were monotonically repulsive, setting up an energy barrier for silica planes to approach the bitumen probe surface. The long-range repulsion with corresponding small adhesion forces (Figure 3.7b) of less than 4 mN/m support a weak tendency of hetero-coagulation between bitumen and silica surfaces. Increasing pH of aqueous solutions led to an increase in the energy barrier and a reduction in adhesion, indicating negligible hetero-coagulation between silica particles and bitumen droplets at higher pHs. This finding confirms the effectiveness of increasing pH to reduce slime-coating of bitumen by fine silica particles or clays through their silica basal planes in the pH range of 5.6~10.8.

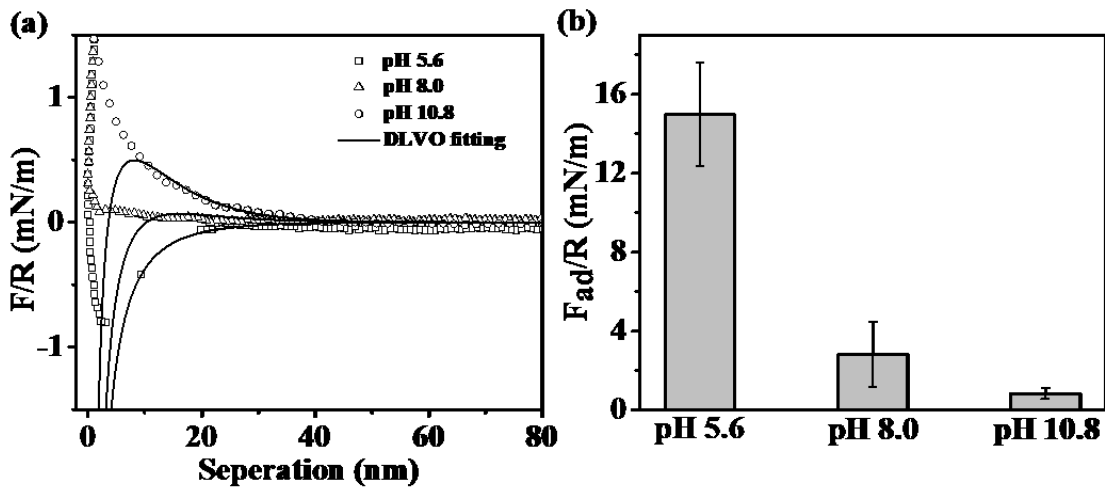


Figure 3.8. Colloidal forces between bitumen probe and alumina wafers in 1 mM KCl aqueous solutions of different pHs. (a) long-range force; and (b) adhesion force.

For bitumen probe and alumina wafers, attractive long-range forces were measured in 1 mM KCl solutions at pH 5.6, as shown in Figure 3.8a. The attraction between bitumen probe and alumina basal planes was reduced to ~ 0 at pH 8.0. When the pH was further increased to 10.8, the long-range forces between bitumen probe and alumina surfaces became repulsive. Again, the force profiles at separation distance greater than 10 nm can be well-described by the DLVO theory. From the measured long-range colloidal forces, one might expect slime-coating of bitumen droplets by kaolinite clays through the attachment by alumina basal planes of clays at pH lower than 8. However, the adhesion forces (Figure 3.8b) between bitumen droplets and alumina planes ranged from 4.2 mN/m at pH 5.6 to 1.2 mN/m at pH 8.0, which were only marginally stronger than those between bitumen droplets and silica basal planes. This finding suggests a weak attachment of alumina basal planes to bitumen droplet surface at pH 5.6~8.0. At high pH where there are only repulsive long-range forces and tiny adhesion forces, there thus were no slime-coating of bitumen droplets by kaolinite through alumina basal planes. Collectively, the results from the colloidal force measurement suggest minimal slime-coating of bitumen by clays if any.

3.3.4.2 Interaction forces between bitumen and hydrophobic clays

For systems of bitumen and hydrophobic clays, unfavorable attractive forces between the hydrophobic surfaces would lead to depression of energy barriers by attractive hydrophobic forces and an increase in adhesion between bitumen and the clays. The long-range hydrophobic force (F_H) was expected to exist between the two hydrophobic surfaces in an aqueous solution (Rabinovich and Yoon, 1994; Ralston et al., 2001; Nguyen et al., 2003), which could be described by an exponential form (Ralston et al., 2001): $\frac{F_H}{R} = C_0 \exp\left(\frac{-D}{D_0}\right)$, where C_0 and D_0 are fitting parameters depending on the hydrophobicity of interacting surfaces and solution conditions. The introduction of the hydrophobic force in the classical DLVO theory leads to a so-called extended DLVO

(EDLVO) theory. After introducing an extra hydrophobic force, the measured force profiles in Figure 3.9a for bitumen interacting with hydrophobic silica wafers in 1 mM KCl solutions can be fitted well with the EDLVO theory. At pH 5.6 and 8.0, the long-range forces between bitumen and hydrophobic silica planes were attractive and there were strong adhesions (Figure 3.9b) between them, suggesting that hydrophobic silica could easily coagulate with bitumen droplets. Increasing pH was able to decrease both the long-range attractive force and the adhesion force. When the pH was as high as 10.8, the long-range forces became repulsive with adhesion between bitumen and hydrophobic silica being depressed to 0.7 mN/m.

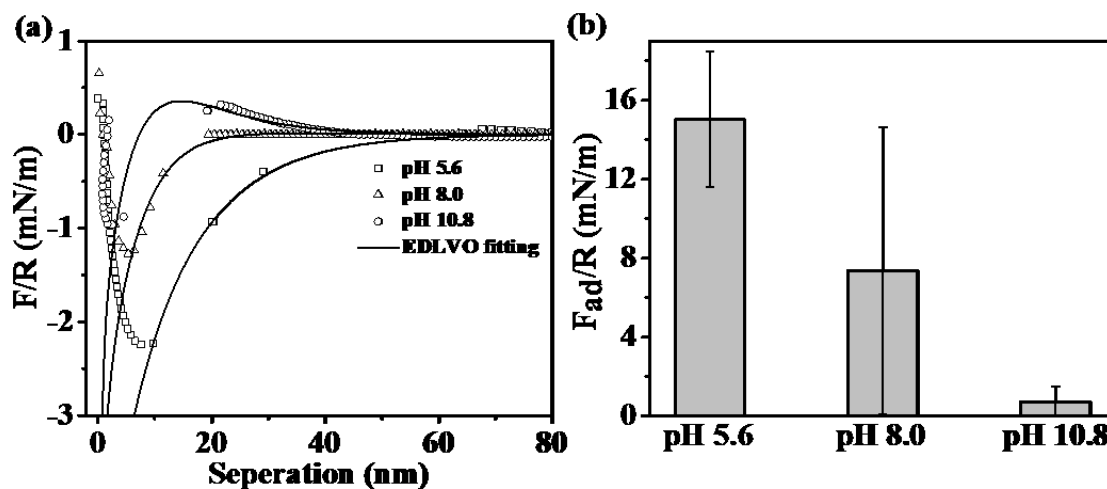


Figure 3.9. Colloidal forces between bitumen probe and hydrophobic silica wafers in 1 mM KCl aqueous solutions of different pHs. (a) long-range force; and (b) adhesion force.

Interaction forces for bitumen and hydrophobic alumina wafers in 1 mM KCl solutions are shown in Figure 3.10. As in the case of hydrophobic silica wafers, the long-range forces (Figure 3.10a) can be also suitably fitted with the EDLVO theory. It is not surprising to measure the attractive long-range forces with reasonable adhesion between bitumen and hydrophobic alumina at pH 5.6~8.0. This result indicates a strong tendency of slime-coating of bitumen by hydrophobic alumina particles under these conditions. At pH 10.8, negligible long-range forces coupled with

marginal adhesion between bitumen and hydrophobic alumina contributed to a negligible slime-coating of bitumen by hydrophobic clays. These results were consistent with the results of ζ potential distribution measurements and clay deposition tests.

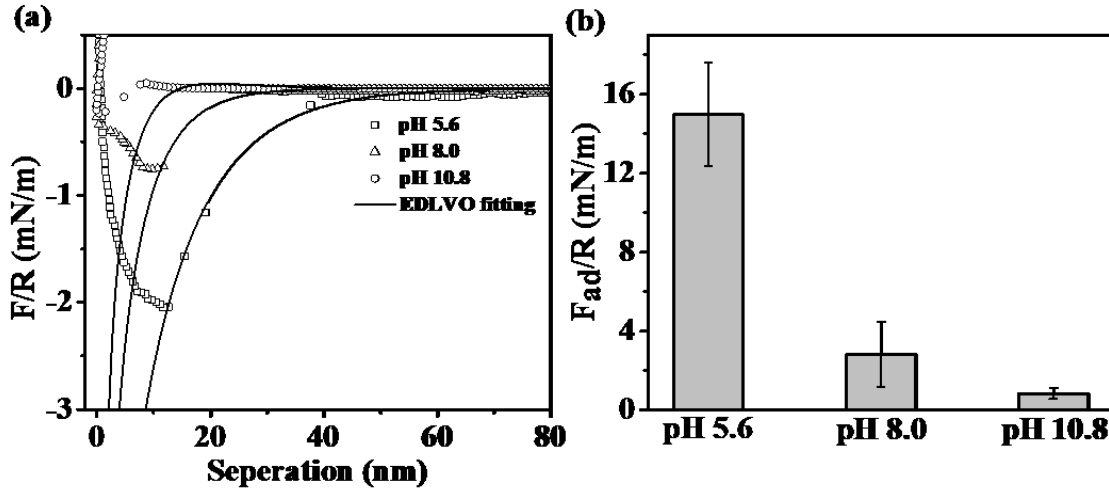


Figure 3.10. Colloidal forces between bitumen probe and hydrophobic alumina wafers in 1 mM KCl aqueous solutions of different pHs. (a) long-range force; and (b) adhesion force.

3.3.5 System stability

The success of bitumen slime-coating by clay particles relies on three distinct processes: collision, attachment, and detachment (Ralston et al., 1999). Conditions when the probability of bitumen-clay collision and attachment is high while the detachment of particles from bitumen is low facilitating the deposition of clay particles on bitumen surfaces. From this perspective, slime-coating can be considered as a random event, whose probability (P_s) is the result of probability of collision (P_c), attachment (P_a) and detachment (P_d) with the governing equation shown below:

$$P_s = (P_c) \cdot (P_a) \cdot (1 - P_d) \quad (3.8)$$

As we discussed earlier, a more severe hetero-coagulation between bitumen and clay particles could be achieved by increasing the clays content. This may be possibly due to the increased

collision rate of bitumen with clay particles at higher clay concentrations. For the probability of bitumen-particle attachment, it could be calculated from the energy barrier (E_b) determined from the colloidal interactions and the kinetic energy (E_k) imparted on particles by mechanical energy input (such as mixing and agitation) (Mao and Yoon, 1997):

$$P_a = \exp\left(-\frac{E_b}{E_k}\right) \quad (3.9)$$

It is evident that the higher the energy barrier, the lower the probability of bitumen-particle attachment. For slime-coating to occur, the energy barrier must be overcome (Oats et al., 2010; Warren, 1975). In this case, the mechanical energy input might provide external kinetic energy for particles to overcome the energy barrier to approach the bitumen surfaces, resulting in more severe slime-coating. On the other hand, high mechanical energy input could also promote the removal of slime-coated particles from bitumen surfaces unless there were sufficiently strong adhesion forces between them to prevent the detachment process (Yu et al., 2017). Overall, the intensity of the mechanical energy input should be cautiously determined to provide optimal conditions for slime-coating control.

When bitumen droplets and clay particles came sufficiently close to each other, van der Waals attraction became dominant. For clay particles of similar size, the van der Waals attractive forces between clays and bitumen depend on the Hamaker constant. The larger the Hamaker constant, the stronger the attraction. According to Lifshitz approach, Hamaker constant for substance 1 and 2 interacting in the presence of medium 3 (A_{132}) can be calculated by quantum physics (Yu et al., 2018):

$$A_{132} \approx \frac{3}{4} k_B T \left(\frac{\varepsilon_1 - \varepsilon_3}{\varepsilon_1 + \varepsilon_3} \right) \left(\frac{\varepsilon_2 - \varepsilon_3}{\varepsilon_2 + \varepsilon_3} \right) + \frac{3h\nu_e}{8\sqrt{2}} \frac{(n_1^2 - n_3^2)(n_2^2 - n_3^2)}{\sqrt{n_1^2 + n_3^2} \sqrt{n_2^2 + n_3^2} (\sqrt{n_1^2 + n_3^2} + \sqrt{n_2^2 + n_3^2})} \quad (3.10)$$

where k_B is the Boltzman constant, T is 293.15 K, ε is the dielectric constant ($\varepsilon_0 = 8.854 \times 10^{-12} \text{J} \cdot \text{V}^{-2} \cdot \text{m}^{-1}$), h is the Plank constant, ν_e is the UV absorption frequency ($\sim 3 \times 10^{15} \text{s}^{-1}$) and n is the refractive index. The calculated Hamaker constants for kaolinite, illite and montmorillonite interacting with bitumen in the aqueous medium are listed in Table 3.7 (Yu et al., 2018; Robinson, 2004; Taylor et al., 2001; Querry, 1987).

Table 3.7. Hamaker constants

	Bitumen	Water	Kaolinite	Illite	Montmorillonite
ε	2.8	80	5.1	5.8	5.5
n	1.584	1.333	1.362	1.381	1.426
$A_{\text{bitumen/water/clay}}$ ($\times 10^{-21} \text{J}$)			4.41	5.62	8.56

Obviously, the Hamaker constants in the aqueous medium decreased in the order bitumen-montmorillonite > bitumen-illite > bitumen-kaolinite. This explains the slime-coating tendency of three clays on bitumen surfaces to some degree.

We can define a concept of stability ratio (Masliyah et al., 2011) to understand the role of bitumen-clay hetero-coagulation in system stability:

$$S = \frac{\text{number of all collisions}}{\text{number of effective collisions}} \quad (3.11)$$

Under favorable conditions when there is a low tendency of slime-coating of bitumen by clay particles, the system is stable with better performance of bitumen extraction. Otherwise, if there is

a high tendency of slime-coating of clays on bitumen droplets, the presence of clays decreased the system stability by deteriorating bitumen flotation.

3.3.6 Bitumen droplet size

The effective aeration of bitumen depends on the success of liberated bitumen globules attaching to (<35 °C) or engulfing (45~80 °C) air bubbles in the extraction process (Masliyah et al., 2004). An important factor in determining the efficiency of bitumen-air bubble interaction is the size of bitumen droplets in oil sands slurry. In general, a smaller bitumen droplet is more difficult to attach to air bubbles in slurry due to lower collision rate of smaller bitumen droplets. Bitumen droplets of millimeters in size were found to be easily recovered (Moran et al., 2000; Yeung and Moran, 2000). Figure 3.11 shows the photos of bitumen droplets collected right below the froth layer with different clay additions. Without the addition of clays, the rising bitumen droplets were as large as 500~1500 µm. When 2~5 wt.% hydrophilic illite were added into the system, the bitumen droplets were reduced to 150~400 µm in size, contributing to the reduction in bitumen recovery as observe. A more serious decrease in bitumen droplet size to 50~200 µm was observed with the addition of 2~5 wt.% hydrophobic illite. Fundamentally, clays act as steric barriers for bitumen-bitumen coalescence, resulting in smaller bitumen droplets in the extraction system. Compared with hydrophilic clays, hydrophobic clay particles were able to make bitumen droplets smaller. However, such reduction does not contribute further to depressing bitumen recovery due to their hydrophobic nature of surfaces.

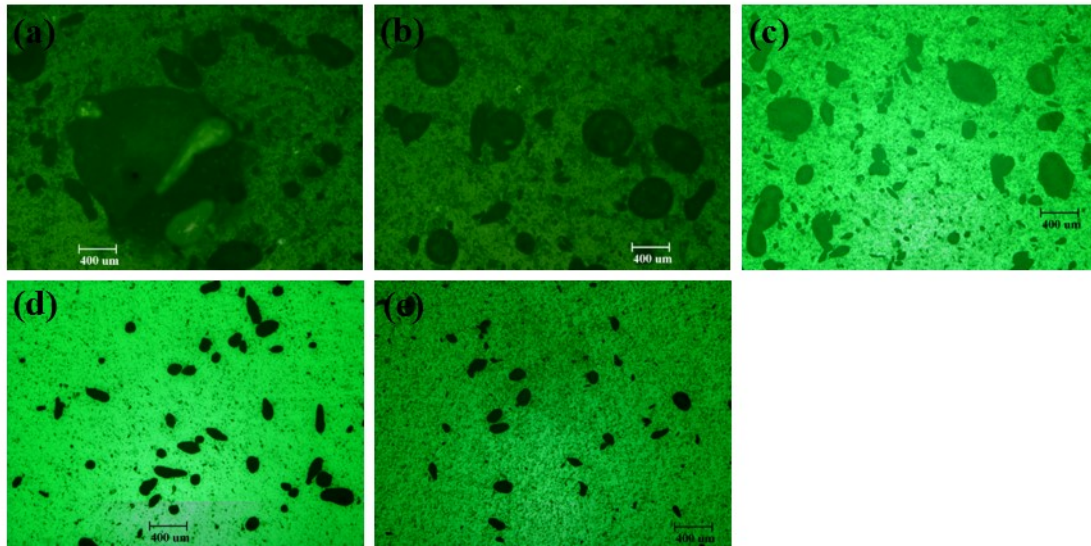


Figure 3.11. Bitumen droplet size in flotation slurry with (a) no clay addition; (b) 2 wt.% hydrophilic illite addition; (c) 5 wt.% hydrophilic illite addition; (d) 2 wt.% hydrophobic illite addition; (e) 5 wt.% hydrophobic illite addition.

3.4 CONCLUSIONS

The effects of original and hydrophobized kaolinite, illite, and montmorillonite clays on bitumen extraction were studied. It was found that clays were generally detrimental to bitumen extraction. Montmorillonite resulted in the highest bitumen recovery reduction. The total froth solids-to-bitumen ratio increased as the clay amount increased. Organic contaminants were able to attach to clay surfaces to render them hydrophobic. Less bitumen was lost in flotation while more solids were present in the produced bitumen froth when hydrophobic clays were added, and clay mineralogy was not important in this case due to the coverage of their surface by similar organic matter. Fundamentally, the existence of clays in extraction reduced bitumen recovery mainly by: (a) slime-coating; (b) decreasing bitumen droplet size. Bitumen clay hetero-coagulation was proved to be governed by clay concentration for hydrophilic clays. Full coverage of 3 types of clays on bitumen droplets was observed at clay concentrations exceeding a critical concentration. The critical concentrations were determined to be 12.9, 8.6, and 5.8 g/L for kaolinite, illite, and

montmorillonite, respectively. In this study, kaolinite was demonstrated to be able to slime-coat on bitumen droplets when its concentration was high. For hydrophobic clays, long-range attractive forces and strong adhesions between bitumen and the basal planes of clays accounted for their aggregation. Furthermore, bitumen droplet size decreased when more clay particles were in the system. Hydrophobic clays could lead to stable bitumen-in-water emulsion with extremely small bitumen droplets which were unrecoverable in extraction.

CHAPTER 4 DEPOSITION AND SEPARATION OF CLAY PARTICLES AT THE BITUMEN-WATER INTERFACE

4.1 INTRODUCTION

The possible coagulation of fine clays is one of the mechanisms that account for the negative impact of clays on bitumen extraction from mined oil sands. In addition to that effect, the clay particles could also interact with other substances present in the system. Especially their interaction with bitumen is of great importance. When a clay particle is in contact with a bitumen droplet, it can attach to the droplet surface, unless prevented by sufficiently high energy barrier (Masliyah et al., 2011). Such coverage of a valuable mineral (i.e., bitumen in bitumen extraction) by fine gangue particles is called slime-coating (Fuerstenau, 1980; Sivamohan, 1990). When slime-coating occurs in bitumen extraction, the coalescence, aeration, and flotation of bitumen droplets become difficult (Liu et al., 2005b). It has been well documented that the presence of a large amount of fine clays could depress bitumen recovery and froth quality significantly (Wallace et al., 1989; Fong et al., 2004; Repka, 2007; Ding et al., 2006; Zhou et al., 2017b).

It has been found that the slurry water chemistry (such as pH and type and concentration of cations) affects slime-coating. A higher pH was found to alleviate slime-coating compared to the conditions at lower pH values (Liu et al., 2003, 2005b; Ding et al., 2006). This is because the surfaces of both bitumen and fine particles become more negatively charged at higher pHs, leading to stronger repulsion between them and thus creating a higher energy barrier to prevent unfavorable attachment between bitumen and fine particles (Schramm et al., 1984b). The pH of the oil sands slurry can be increased with the addition of NaOH (Flury et al., 2014; Srinivasa et al., 2012). In addition, the introduction of NaOH decreases the concentration of divalent cations via precipitation (Fong et al., 2004; Dai et al., 1992). This is also beneficial to reduce slime-coating (Kasongo et al.,

2000; Basu et al., 2004). Liu and his colleagues (Liu et al., 2002, 2003, 2004a, 2004b, 2005b) investigated the effect of calcium ions on bitumen-clay interactions and found that the presence of calcium ions decreased the long-range repulsive forces and increased the adhesion forces between bitumen and clay particles in aqueous media. This may be explained by the diminished negative charges on both bitumen and clay surfaces with the addition of calcium ions. A more severe slime-coating of bitumen droplets by clay particles was observed in the presence of calcium ions. Masliyah et al. (2011) proposed that positively charged calcium ions could serve as bridges between the negatively charged bitumen and clays to facilitate their attachments. Adding magnesium ions to the system led to a similar detrimental effect (Ding et al., 2006; Zhao et al., 2006). It is the valence not the type of the cations that matters. As a representative of monovalent cations, sodium ions in the oil sands slurry could come from the oil sands, the process water used or the addition of NaOH. In one oil sand operation, the sodium concentration in the tailings water increased by 75 mg/L per year from 1980 to 2001 (Allen, 2008). Takamura and Wallace (1988) reported a reduction of bitumen recovery by 40% with the addition of 1000 ppm NaCl. Basu et al. (1996, 1998) demonstrated a threshold value of sodium concentration in process water, above which bitumen liberation from a flat glass surface was badly hindered. Similar decrease in bitumen liberation with the addition of sodium ions was observed by Srinivasa et al. (2012). The negative effect of sodium addition on bitumen flotation was more pronounced at higher pH (Chen et al., 2017).

Another adverse impact of fine clays on oil sands processing is the formation of solid-stabilized emulsions in bitumen froth. Fine particles would remain in the water phase if they are water-wet and remain in the bitumen phase if they are oil-wet. However, partially oil-wet fine particles would stay at the bitumen-water interface to form rigid films on the emulsified water

droplets, hence acting as a steric barrier that prevents the coalescence of the water droplets (Rao et al., 2013). Extensive researches have been focused on the fine solids-stabilized emulsions (Boekel and Walstra, 1981; Gelot et al., 1984; Tambe and Sharma, 1993; Jacques et al., 1979). Generally, hydrophilic clays favor stabilizing oil-in-water (O/W) emulsions, while hydrophobic clays tend to stabilize water-in-oil (W/O) emulsions. It is a challenge to remove the micro-emulsified water droplets during froth treatment (Gu et al., 2003).

To achieve a satisfactory performance of bitumen extraction, it is essential to understand the interactions between bitumen and clays. The partitioning of fine clays between the aqueous phase and bitumen droplets and the tendency of the clay particles to deposit on the bitumen droplets need to be investigated. In our previous study, deposition of clays from an aqueous phase to a bitumen-water interface was tested to investigate the effect of clay concentration on bitumen slime-coating. It has been shown that the slime-coating of bitumen droplets by hydrophilic fine clays is governed by the clay concentration in the aqueous phase, and the clay concentrations leading to a monolayer coverage are suitable to be used as the critical concentrations for strong slime-coating to occur.

In the present study, we attempt to understand the factors that affect the partitioning of kaolinite particles between diluted bitumen and water. Since the collisions or interactions between bitumen and fine clays are responsible for the attachment to occur, it seems clear that the deposition of kaolinite particles at the bitumen-water interface can be affected by the chemistry of the aqueous phase. This study focuses on the roles of aqueous pH and the concentrations of sodium and calcium ions in the deposition process. The threshold concentrations for kaolinite particles to deposit onto bitumen droplets at different conditions will be established.

4.2 MATERIALS AND METHODS

4.2.1 Materials

Kaolinite particles (Edgar, Florida, USA) from Ward's Natural Science were used in the present study. After homogenization with a 500 ultrasonic dismembrator (Fisher) to prepare clay suspensions, the measured volume-based 50 and 90% passing sizes of the kaolinite particles were 1.7 and 5.3 μm , respectively. Coker feed bitumen was used as the bitumen source and was diluted by certified ACS grade toluene (Fisher Scientific). De-ionized water ($0.8 \mu\text{S}\cdot\text{cm}^{-1}$) with a pH of 5.0~5.6 was used as the aqueous phase. The pH of the aqueous phase was modified with the addition of NaOH (1N solution purchased from Fisher Scientific), while the sodium and calcium concentrations of the aqueous phase were adjusted by adding NaCl (ReagentPlus®, $\geq 99\%$, Sigma-Aldrich) and $\text{CaCl}_2 \cdot 2\text{H}_2\text{O}$ (ACS reagent, $\geq 99\%$, Sigma-Aldrich), respectively. Here, the cations were present in the form of chloride. The roles of other existence of cations may be different.

4.2.2 Methods

4.2.2.1 Emulsion preparation

A known amount of kaolinite particles was initially dispersed in 175 mL of de-ionized water and homogenized using an ultrasonic dismembrator for 15 min to prepare a clay suspension with kaolinite concentration at C_{wi} . The pH and the chemical composition of the de-ionized water were adjusted before the addition of clay particles. A solution of bitumen in toluene, referred to as diluted bitumen, was obtained by dissolving 450 g bitumen in toluene to an entire volume of 1 L. 25 mL of diluted bitumen was added to the prepared clay suspension and the mixture was sheared by a magnetic stirrer at 600 rpm for 20 min. The emulsified mixture was left to cream in a separation funnel for 10 min. The procedures for emulsion preparation are shown in Figure 4.1.

Photomicrographs of the bitumen droplets in the emulsion phase were observed using an optical microscopy. The diameters of the bitumen droplets, d , were determined by averaging 80~100 droplets.

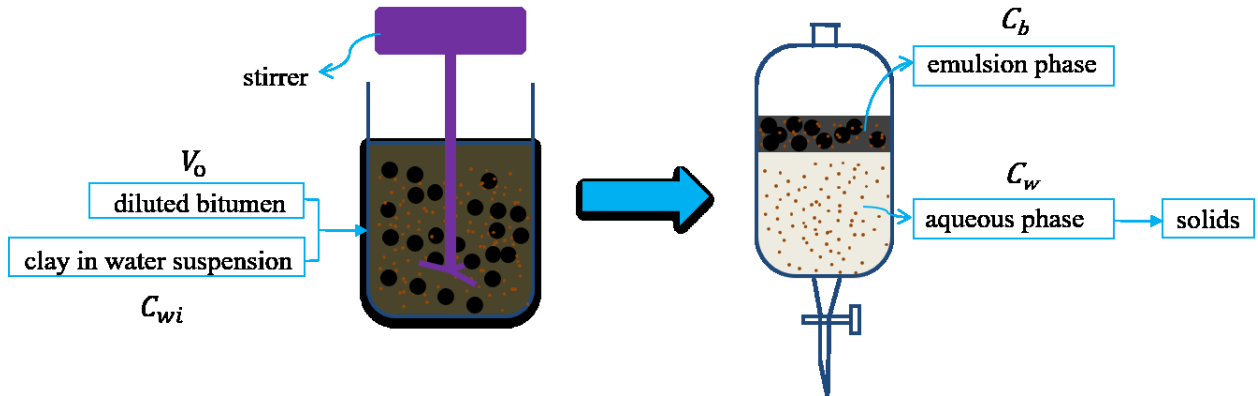


Figure 4.1. Schematic illustration for preparing diluted bitumen in water emulsion with kaolinite addition.

4.2.2.2 Deposition of kaolinite particles on bitumen surfaces

After the separation and collection of the two phases, the volumes of the emulsion phase (V_{ea}) and the aqueous phase (V_{wa}) were measured. The aqueous phase was then centrifuged to isolate the solids from the liquid, and then the weight of the solids (kaolinite particles) (W_w) was obtained by drying the solids in a vacuum oven overnight. The equilibrium clay concentration in the aqueous phase (C_w) was calculated by:

$$C_w = \frac{W_w}{V_{wa}} \quad (4.1)$$

For the emulsion phase, it is assumed that the clay concentration in the water entrained between the bitumen droplets was the same as that in the aqueous phase (Yan and Masliyah, 1994, 1995).

The weight of clays in the emulsion oil (W_o) was calculated by:

$$W_o = W_i - C_w V_w \quad (4.2)$$

where W_i was the weight of clays initially added into the water. V_w was the volume of water added prior to emulsification.

Finally, the equilibrium concentration (C_b in g/cm²) of clays on the bitumen droplets was given by:

$$C_b = \frac{W_o}{A} = \frac{W_o}{V_o} \cdot \frac{d}{6} = \frac{W_i - C_w V_w}{V_o} \cdot \frac{d}{6} \quad (4.3)$$

where V_o was the volume of the diluted bitumen added prior to emulsification and A was the total bitumen-water interfacial area. The deposition isotherm was given by plotting C_b vs. C_w .

4.2.2.3 Separation of kaolinite particles from bitumen surfaces

To determine how strong the kaolinite particles deposited on the bitumen droplets, an attempt was made to separate the particles as follows. The collected emulsion phase was redispersed into the make-up water of the same volume as the released aqueous phase. The pH and the chemical composition of the make-up water were kept the same as those of the initially prepared water. The diluted emulsion was stirred gently at 50 rpm for 10 min and left to cream for phase separation. This low stirring speed ensured no breakup of the bitumen droplets. After separation, the released aqueous phase was centrifuged for solid-liquid separation and the weight of the separated clay particles was obtained by drying the solids in an oven. This separation process was repeated multiple times until the released aqueous phase became colorless. The separation percent (SP) of the added clay particles was obtained from these measurements:

$$SP = \frac{W_o - W_{on}}{W_o} \times 100\% \quad (4.4)$$

where W_{on} was the weight of the clays in the emulsion oil after the separation procedures. The calculation process of W_{on} was similar to that for the deposition procedures.

4.3 THEORETICAL BASIS

Since the deposition of clay particles from the aqueous phase to the bitumen-water interface does not involve chemical reactions, it is considered to be a physisorption process. The forces involved in such a process are intermolecular forces (e.g. van der Waals forces). Following the BET multimolecular adsorption theory for the physisorption of gases onto a gas-solid interface, a multilayer adsorption model can be formulated to simulate the deposition of solids at an oil-water interface (Brunauer et al., 1938; Oscik, 1982; Yan and Masliyah, 1994). The deposition isotherm is fitted by:

$$\frac{C_b}{C_w} = \frac{k_1 C_m}{(1 - k_m C_w)(1 - k_m C_w + k_1 C_w)} \quad (4.5)$$

where k_1 , k_m and C_m are fitting parameters, and k_1 and k_m are the equilibrium constants of the first and subsequent layers, respectively, and C_m serves as the monolayer coverage of the clay particles on the bitumen droplets.

Theoretically, the deposition isotherm should be S-shaped. At large values of k_m where strong interactions exist between the deposited particles at adjacent layers, C_b would increase very rapidly with C_w .

4.4 RESULTS AND DISCUSSION

4.4.1 Effect of pH

The influence of pH on the partitioning of kaolinite particles between bitumen and water can be seen from Figure 4.2, which shows the results of deposition isotherms of kaolinite clays on bitumen surfaces with no pH control (pH=5.0~5.6) and at pH 8.0 and 10.8. It is clear that the concentration of clays attached to the bitumen surfaces increased with the increase of the initial clay contents in the aqueous phase. When the initial concentration of kaolinite clays in the aqueous phase increased from 1.1 to 28.6 g/L, the amount of clays deposited to the bitumen-water interface increased from 0.19 to $4.2(\times 10^{-5})$ g/cm² at pH 5.0~5.6. At the highest initial clay concentration of 28.6 g/L, the deposition amount of clays decreased from 4.2 to 3.0 and further to $2.1(\times 10^{-5})$ g/cm² when the aqueous pH was increased from 5.0~5.6 to 8.0 and further to 10.8, respectively. The reduced deposition of kaolinite particles onto the bitumen droplets at higher pH was not surprising because the particles and the droplets were more negatively charged at higher pH and, hence, it became more difficult for them to overcome the stronger repulsion to coagulate.

Using Eq. 4.5, one can fit the deposition isotherms with the BET multilayer adsorption model and the fitting parameters obtained are listed in Table 4.1. Clearly, both k_1 and k_m decreased with an increase in the aqueous pH, indicating that the probability of kaolinite particles to deposit on bitumen droplets was much higher at low pH than at high pH. It was also shown from the data in Table 4.1 that the monolayer coverage of clays on the bitumen droplets increased at higher pH values as indicated by the increase in C_m values. This may be attributed to the different states of the deposited particles at the bitumen-water interface. Figure 4.3 schematically describes two possible deposition states of the clay particles at the bitumen droplet surface. At low pH where a weak dispersion of clay particles occurred, clay aggregates tend to attach to the interface and the

relatively large lumps of clays hindered the contact between other clay particles/aggregates and the bare bitumen surface. This resulted in a thick clay film covered on the bitumen droplets, but the innermost layer was discrete (state A). While at high pH, a good dispersion of clay particles was achieved. A thinner clay film with more compact first layer was supposed to deposit on the bitumen surface (state B). This may account for the increase of C_m at high pH.

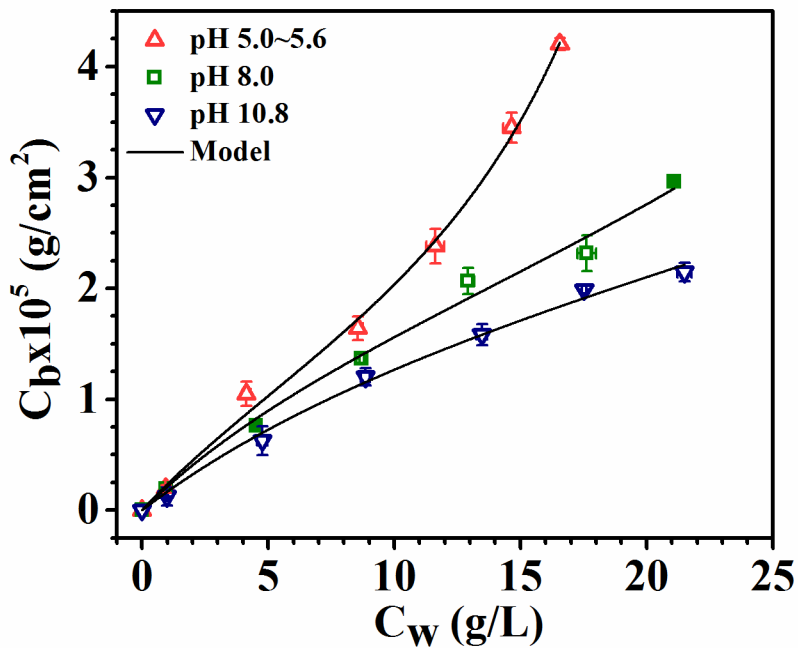


Figure 4.2. Deposition isotherms of kaolinite particles on diluted bitumen droplets in aqueous suspensions of different pH values.

The fifth column in Table 4.1 (C_w^m) summarizes the equilibrium clay concentrations in the aqueous phase at the monolayer coverage obtained from the fitted curves. The corresponding initial clay concentrations in the aqueous phase (C_{wi}^m) were calculated by linear interpolation between two adjacent experimental points, as listed in the last column. These concentrations, referred to as critical concentrations, provide guidelines for the deposition of kaolinite clays at the

bitumen-water interface. When the clay concentration in the aqueous phase exceeds the critical concentration, the deposition of clay particles at the interface goes beyond the monolayer coverage. In oil sands, it is possible to use these critical concentrations as indications of strong slime-coating of clays on bitumen droplets to occur. From this perspective, an important outcome of Figure 4.2 and Table 4.1 is that the required concentration for kaolinite clays to strongly slime-coat onto bitumen droplets increased from 12.9 to 42.3 g/L when the aqueous pH was increased from 5.0~5.6 to 10.8, indicating that increasing pH was able to alleviate bitumen slime-coating.

Table 4.1. Multilayer model parameters of particle deposition at different pH values

pH	Fitting parameters			Model prediction	
	$C_m \times 10^5 (\text{g}/\text{cm}^2)$	$k_1 (\text{L}/\text{g})$	$k_m (\text{L}/\text{g})$	$C_w^m (\text{g}/\text{L})$	$C_{wi}^m (\text{g}/\text{L})$
5.0~5.6	1.8902	0.1295	0.0374	9.346	12.90
8.0	2.4876	0.0901	0.0170	17.814	23.16
10.8	2.8988	0.0601	0.0090	31.001	42.26

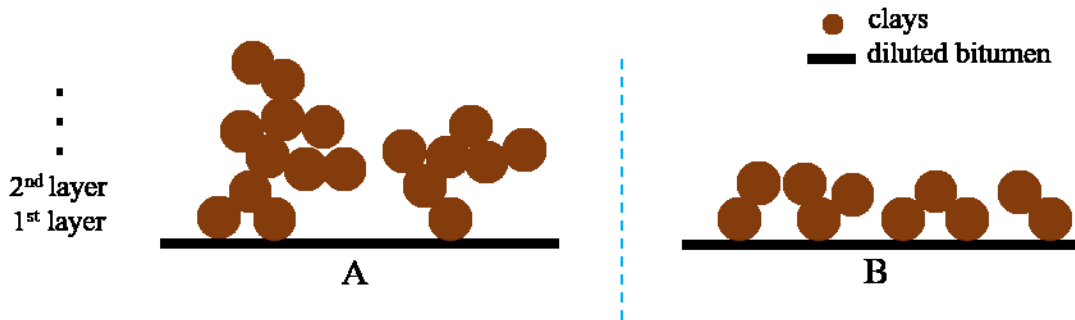


Figure 4.3. Deposition states of kaolinite particles on diluted bitumen droplets.

4.4.2 Effect of NaCl concentration

Figure 4.4 shows the deposition isotherms of kaolinite particles on bitumen droplets at pH 8.0 with 0, 30, and 60 mM of NaCl addition. The corresponding fitting parameters of BET model are

provided in Table 4.2. At pH 8.0, the deposition of kaolinite clays from an aqueous phase with clay concentrations of 1.1 to 28.6 g/L to a bitumen-water interface increased marginally from the baseline (no NaCl) at 0.19–3.0 to 0.28–3.3 and 0.29–3.4 ($\times 10^{-5}$) g/cm² with the addition of NaCl at 30 and 60 mM, respectively. The differences between the addition of 30 mM NaCl and 60 mM NaCl were non-significant. Solution sodium content affects the zeta potentials and the magnitude and thickness of the double layers surrounding the particles, and thus affecting the potential energy barrier between the particles (Takamura and Wallace, 1988). The less negative zeta potentials of clay particles and bitumen droplets at this pH with NaCl addition (Chen et al., 2017) caused an slightly enhanced coagulation tendency between clays and bitumen due to the reduced repulsive energy barrier and it could account for the minor increase of the deposition amount of kaolinite at the bitumen surfaces with NaCl addition compared to that without NaCl addition. As expected, k_1 and k_m increased marginally with the increase of NaCl concentrations. As for the decrease of C_m values, it is suitable to consider the effect of NaCl concentration on the dispersion of kaolinite clay particles. At the tested conditions, kaolinite particles can be well dispersed when the NaCl concentration is less than 20 mM (Takamura and Wallace, 1988). Poor dispersion of clay particles with NaCl concentration > 20 mM resulted in the transformation of deposition state of particles at the bitumen-water interface from tending to form state B to tending to form state A (Figure 4.3). In general, the effect of NaCl concentration on the deposition of clay particles from an aqueous phase to an oil-water interface was minor. Negligible effect of NaCl addition was shown on the particle-particle interactions between adjacent deposition layers as evident by the tiny variations of k_m values compared with the baseline.

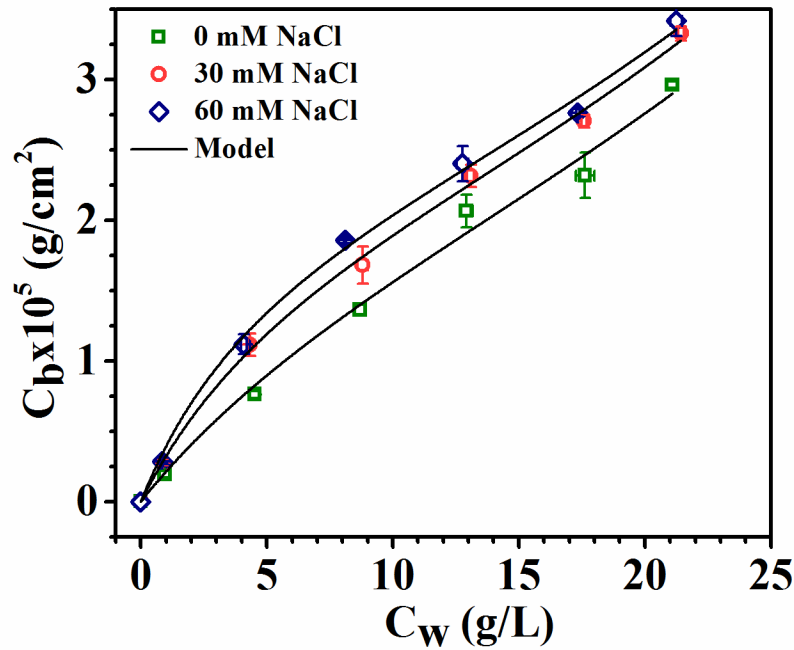


Figure 4.4. Deposition isotherms of kaolinite particles on diluted bitumen droplets in aqueous suspensions at pH 8.0 containing different levels of NaCl.

Table 4.2. Multilayer model parameters of particle deposition at pH 8.0 with NaCl addition

NaCl concentration	Fitting parameters			Model prediction	
	$C_m \times 10^5$ (g/cm ²)	k_1 (L/g)	k_m (L/g)	C_w^m (g/L)	C_{wi}^m (g/L)
0 mM	2.4876	0.0901	0.0170	17.814	23.16
30 mM	2.3967	0.1502	0.0180	14.286	18.66
60 mM	2.3886	0.1902	0.0180	13.070	17.53

The last two columns in Table 4.2 describe the equilibrium and initial clay concentrations in the aqueous phase at the monolayer coverage. The critical concentrations of kaolinite decreased slightly from the baseline (no NaCl) at 23.2 to 18.7 and 17.5 g/L when 30 and 60 mM NaCl were introduced into the system. This provides us an awareness that NaCl accumulation in water up to 60 mM at pH 8.0 is tolerable in oil sands production.

4.4.3 Effect of CaCl₂ concentration

In a solution containing 1 mM CaCl₂ at pH 8.0, the deposition amount of kaolinite clays from the aqueous phase onto the bitumen droplet surface increased from 0.35 to 3.4 ($\times 10^{-5}$) g/cm² with 1.1 to 28.6 g/L initial kaolinite concentration in the aqueous phase, as shown in Figure 4.5. The highest deposition amount of clays on the bitumen droplets at the initial clay concentration of 28.6 g/L increased from the baseline at 3.0 to 3.4 and further to 3.6 ($\times 10^{-5}$) g/cm² when the CaCl₂ concentration was increased from 0 to 1 and further to 2 mM, respectively. Again, the deposition isotherms can be reasonably fitted with the BET model. The parameters are listed in Table 4.3. The increased k_1 with increased CaCl₂ addition suggests that kaolinite particles can approach the bitumen surface easier with the existence of CaCl₂ than without CaCl₂ addition. Previous research has demonstrated a bridging effect of calcium ions between bitumen and clay particles to facilitate their coagulation (Liu, et al., 2004b). Also, calcium ions are supposed to affect the zeta potentials, double layer configurations and the dispersion of clay particles through a mechanism similar to sodium ions. Therefore, the reduction of C_m values with the addition of CaCl₂ was not surprising. The interaction between deposited particles and non-deposited particles was not affected much by calcium ions as indicated by the barely changed k_m values.

The role of calcium ions in promoting bitumen-clay attachment was confirmed by the reduced critical concentrations of kaolinite with the addition of calcium ions. As shown in the last column of Table 4.3, the critical concentrations of kaolinite reduced from the baseline at 23.2 to 16.7 and 13.8 g/L with 1 and 2 mM of calcium ions introduction, respectively. A comparison of Table 4.2 and Table 4.3 indicates that divalent cations are more pivotal than monovalent cations in efficient oil sands processing.

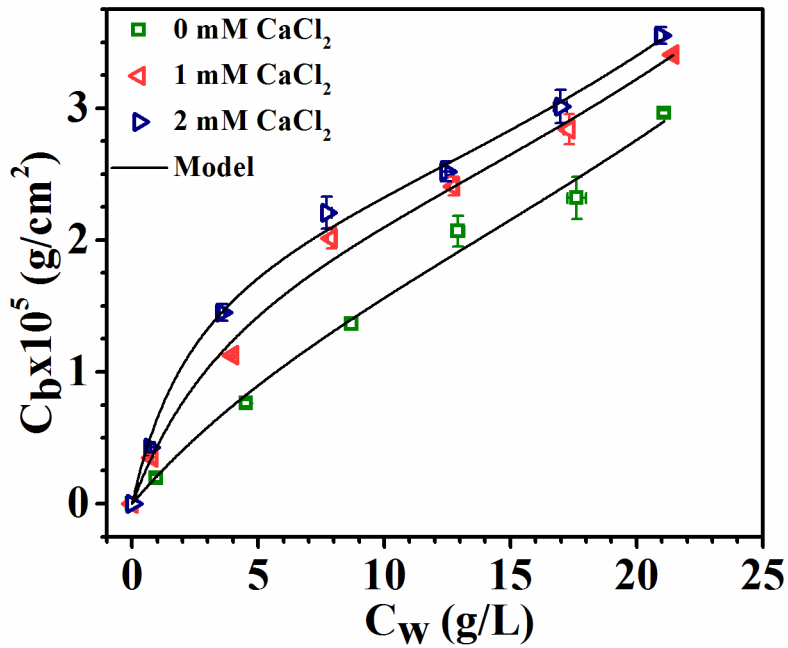


Figure 4.5. Deposition isotherms of kaolinite particles on diluted bitumen droplets in aqueous suspensions at pH 8.0 containing different levels of CaCl₂.

Table 4.3. Multilayer model parameters of particle deposition at pH 8.0 with CaCl₂ addition

CaCl ₂ concentration	Fitting parameters			Model prediction	
	$C_m \times 10^5$ (g/cm ²)	k_1 (L/g)	k_m (L/g)	C_w^m (g/L)	C_{wi}^m (g/L)
0 mM	2.4876	0.0901	0.0170	17.814	23.16
30 mM	2.3601	0.2202	0.0180	12.352	16.67
60 mM	2.2859	0.3804	0.0189	9.644	13.75

4.4.4 Separation

To understand whether the clay particles at the bitumen-water interface were weakly or strongly attached to the droplet surface, separation tests were conducted. Clay particles would be removed from the emulsion oil if they deposited weakly on the bitumen droplets, otherwise, they would remain in the emulsion phase due to strong attachments. Table 4.4 summarizes the results

of the separation tests at pH 5.0~5.6. Obviously, clay particles were strongly adhered to the surfaces of bitumen droplets at this condition since the separation percentages of the added clays were < 35%. On the other hand, other parameters being equal, the separation percent of extra clays decreased with the initial clay concentration increased. With 1.1 to 28.6 g/L clays addition, the separation percent decreased from 34 to 17%. This decreasing trend indicates that the attachments between bitumen droplets and clay particles and between adjacent clay layers are enhanced at higher clay concentrations. It is important to take clay concentration into consideration in oil sands or mining processes, especially when processing oil sands ores or coals with high clays content.

Table 4.4. Separation percent of added clay particles at various C_{wi} values at pH 5.0~5.6

C_{wi} (g/L)	SP (%)
1.1	33.5
5.7	30.9
11.4	29.9
17.1	28.6
22.8	19.3
28.6	17.1

The separation percentages of added clay particles at the initial clay concentration of 28.6 g/L in emulsification water of different chemistry are summarized in Table 4.5. Again, in all conditions tested here, clay particles were strongly attached to the bitumen droplet surface as was seen from the separation percent < 32%. It was shown that the separation of clay particles was easier in high pH than in low pH. The corresponding separation percent was increased from 17% at pH 5.0~5.6 to 32% at pH 10.8. This was in agreement with the previous results that k_1 and k_m decreased with increasing pH. Generally, k_1 and k_m represent the extent of difficulty of the deposition and

separation processes. Large k_1 and k_m describe a process that deposition is easy to take place while separation is hard to occur. k_1 is usually much higher than k_m since the tendency to form the first deposition layer is much higher than that of the second and subsequent layers. Or the separation of the outer layers is easier than the inner layers. Since the separation of clays from the bitumen-water interface at pH 8.0 is small, it is supposed to occur in outer layers and thus governed by the k_m values. This explained the observation that the separation percent remained unchanged at ~22% at pH 8.0 with and without the additions of sodium or calcium ions.

Table 4.5. Separation percent of added clay particles at $C_{wi} = 28.6$ g/L under various conditions

Condition	DP (%)
pH 5.0~5.6	17.1
pH 8.0	22.1
pH 10.8	31.6
pH 8.0 with 30 mM NaCl	22.3
pH 8.0 with 60 mM NaCl	22.4
pH 8.0 with 1 mM CaCl ₂	22.1
pH 8.0 with 2 mM CaCl ₂	22.4

4.5 INDUSTRIAL IMPLICATIONS

Based on the results obtained, Figure 4.6 shows the critical concentrations of kaolinite clays at different pH (a) and different sodium (b) and calcium (c) concentrations. The effects of other monovalent and divalent cations on the partitioning of kaolinite clays between bitumen and water may be only slightly different from those of sodium and calcium ions, so the y-axis of Figure 4.6 b and c could represent the total concentrations of monovalent and divalent cations, respectively. These critical concentrations could provide some guidance for industrial operations. It is noticeable

that the regions to the left of the curves indicate low coagulation tendency between bitumen and clays. The clay layers formed on oil droplets at the oil-water interface are expected to be unstable and below the monolayer coverage. On the other hand, the regions on the right side of the curves describe conditions where strong bitumen-clay attachments could occur.

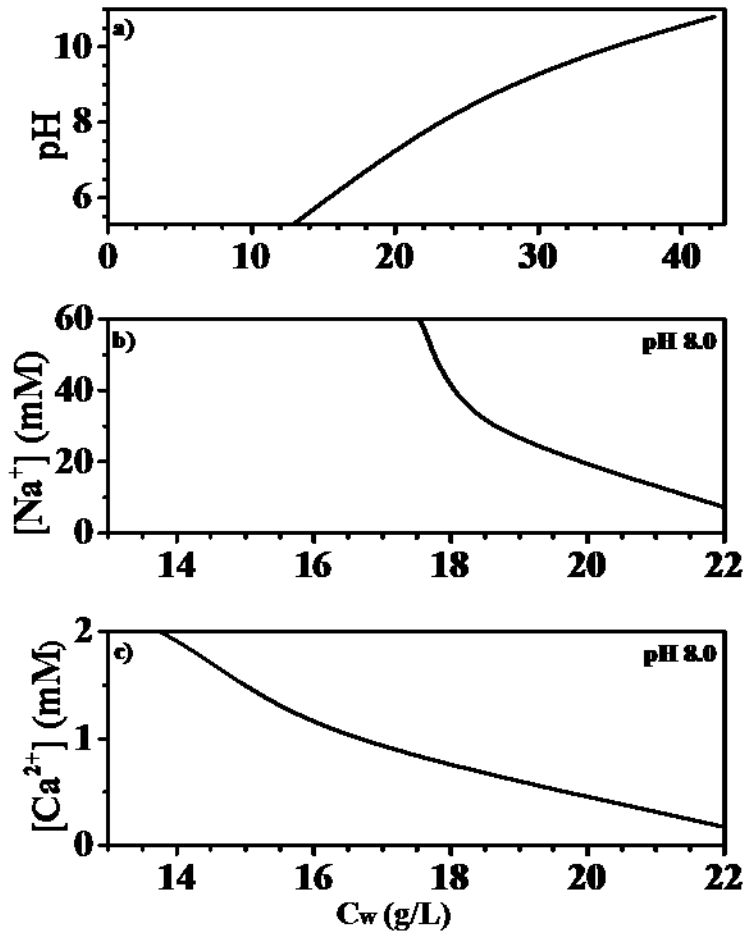


Figure 4.6. Critical concentration diagram for kaolinite clays a) at different pH; and at a given pH of 8.0 with the addition of b) sodium ions; or c) calcium ions.

4.6 CONCLUSIONS

- i. The deposition of kaolinite clays at the bitumen-water interface could be of multilayer type.

ii. With an increase in aqueous pH, the equilibrium constants of the deposition layers formation decreased and the monolayer coverage concentration of clays at the interface increased.

iii. The addition of cations increased the equilibrium deposition constants and reduced the interfacial clay monolayer coverage concentrations. These effects were more pronounced with divalent cations introduction than with monovalent cations introduction.

iv. The critical concentrations of kaolinite clays were determined to be 12.9, 23.2, and 42.3 g/L at pH 5.0~5.6, 8.0, and 10.8 without cations addition, respectively.

v. Extra cations in the system suppressed critical concentration values for kaolinite clays. At pH 8.0, the critical kaolinite concentrations were depressed to 18.7 and 17.5 g/L when 30 and 60 mM sodium ions were added. A more serious depression in critical kaolinite concentrations to 16.7 and 13.8 g/L were obtained with the addition of 1 and 2 mM calcium ions.

CHAPTER 5 DETERMINATION OF CLAY CONTENT IN CANADIAN OIL SANDS USING X-RAY FLUORESCENCE SPECTROSCOPY FOR DIAGNOSIS OF ORE PROCESSABILITY

5.1 INTRODUCTION

For Canadian oil sands, fines are traditionally referred to as the solid particles less than 44 μm in size while clays are particles of sizes smaller than 2 μm (Mercier et al., 2019). For typical oil sands ore, the solids (mostly sand and clays) make up ~85% of the total mass, while the fines and clay contents vary significantly, indicating variations in oil sands processability (Oil sands magazine, 2016). In bitumen extraction, clays could have a negative impact on bitumen-bitumen coalescence and bitumen-air bubble attachment due to slime-coating. Slime-coating, defined as the attachment of clays on bitumen droplets, could decrease the bitumen flotation rate and bitumen recovery while deteriorating froth quality by carrying the fine clays attached on the bitumen or air bubbles to the bitumen froth (Liu et al., 2004b). The degree of this impact varies with the type and content of the clays. Swelling clays such as montmorillonite can lead to the worst conditions for oil sands extraction. In addition to slime-coating, the viscosity of the bitumen extraction slurry would increase with increasing clays content, which inhibits bitumen flotation. On the other hand, the presence of clays could alter the emulsion stability in the subsequent froth treatment process. Furthermore, fine clays could remain suspended for an extended period in tailings streams, causing difficulties in tailings management (Rao and Liu, 2013; Jiang et al., 2011; Chalaturnyk et al., 2002). Finding a simple way to determine the type and content of problematic clays in oil sands processing is therefore highly desirable.

Kaolinite is the most abundant clay in oil sands (Masliyah et al., 2013). It is a two-layer type of clay consisting of one silicon-oxygen tetrahedron sheet (T) and one aluminum-oxygen-hydroxyl

octahedron sheet (O) as the building blocks (Masliyah et al., 2011). Kaolinite could carry different charges on the basal planes and edge surfaces. The charges on the edge surfaces are pH dependent as a result of the hydrolysis of broken Si/Al-oxygen bonds and pH dependent deprotonation or dissociation of hydroxyl groups. This pH dependent charging characteristics indicate that we could control the dispersion or coagulation of clays by adjusting the slurry pH (Moore and Reynolds, 1997). Since kaolinite exhibits a negligible swelling in water, the cation exchange capacity of kaolinite is very low and occurs mainly on the edges of the layers. Another important type of clay in oil sands is illite, which is a three-layer type of clay with one octahedral sheet sandwiched between two tetrahedral sheets. The isomorphic substitution in illite occurs mainly in the tetrahedral sheet where around 1/4 of Si atoms are replaced by Al atoms, causing its basal planes to be negatively charged. These charges are balanced mainly by compensating potassium ions. Illite is the second abundant clay in oil sands. Ding et al. (2006) showed a negative effect of illite on bitumen recovery. Using the QCM-D method, Bakhtiari et al. (2015) confirmed the slime-coating of illite on bitumen without or at low caustic addition. Mercier et al. (2008) developed an XRD-based method to characterize clays in unextracted oil sands and found that the amount of ultrathin illite was critical in bitumen extraction. Long et al. (2006) found that illite particles in Aurora recycle process water did not coagulate or flocculate, and hence settled slowly. The non-swelling illite could become swelling when it is degraded, making its cation exchange capacity significantly higher than kaolinite (Mitchell and Soga, 2005). After identifying the negative effect of illite on bitumen recovery, Wallace et al. (2004) suggested the use of soluble potassium as an indicator of illite degradation to account for the poor processing behavior of oil sands.

In the oil sands industry, methylene blue titration has been extensively used to characterize the fine solids, with the results being commonly expressed as MBI (Boxill, 2011). The measured MBI

provides an indication of the activity or cation exchange capacity, (Yener et al., 2012; Kahr and Madsen, 1995) and specific surface area (Hang and Brindley, 1970; Tewari and Thornton, 2010) of the solids in an oil sand ore, or in a froth or tailings stream. The correlation between the MBI of an ore and the predicted bitumen recovery allows oil sands researchers to use the MBI to evaluate ore processabilities (Kaminsky, 2014). However, the results obtained by the MBT measurements vary significantly from one laboratory to another. This is because its inherent operator-dependence of the end-point judgment of methylene blue titration. Furthermore, the surface contamination of clays by organic compounds as encountered in oil sands processing could lead to erroneous results. The quantitative phase analysis by XRD is also widely applied for mineralogy determination in solid samples (Kakali et al., 2001; Violante and Pigna, 2002; Bish et al., 2013). Liao et al. (2015) used XRD to reflect phase transformations of red mud under thermal treatment. Herald et al. (2017) performed XRD to quantitatively determine the content of struvite in struvite products thus confirming the contribution of brine water in magnesium concentration. Dittrich et al. (2014) used in-situ XRD to investigate the hydration of ordinary portland cement blended with siliceous fly ash and detected a retarding effect of fly ash on the silicate reaction. The limitations of XRD method exist in its complex and time-consuming sample preparation procedure (Omotoso and Eberl, 2009), taxing calibration curves fitting, and quantification methods selection, (Hillier, 2000; Hestnes and Sørensen, 2012) as well as its inherent deficiency that it detects crystalline phases only. In addition, automated mineralogy based on SEM and OIA are commonly utilized for estimating mineral grades (Parian et al., 2015). The method requires careful and tedious samples preparation and costs time and money (Lastra and Petruk, 2014).

Furthermore, instruments based on element analysis are used to characterize clay related properties in oil sands. To convert the measured element composition to the quantity of desired

minerals in bulk samples, a multicomponent mass balancing method, element to mineral conversion, is often used (Lamberg et al., 1997; Paktunc, 1998; Whiten, 2007). The method is restricted to the solution of multiple equations where the number of minerals must be no larger than the number of analyzed element components (Parian et al., 2015; Spencer et al., 2016). Mathematically it can be written in a matrix form as $M \cdot x=b$: (Parian et al., 2015; Lamberg et al., 1997)

$$\begin{bmatrix} M_{11} & \cdots & M_{1n} \\ \vdots & \ddots & \vdots \\ M_{n1} & \cdots & M_{nn} \end{bmatrix} \times \begin{bmatrix} x_1 \\ \vdots \\ x_n \end{bmatrix} = \begin{bmatrix} b_1 \\ \vdots \\ b_n \end{bmatrix} \quad (5.1)$$

where M is the matrix of the element composition of minerals; x is the vector of unknown weight percentage of minerals in bulk sample; and b is the vector representing analyzed element composition of the sample. Although the “element-to-mineral conversion” method has been proposed for decades, it is systematically applied in academic or industrial operations very rarely (Lamberg, 2011). More often, the element analysis was used as an evaluation strategy for estimating assay-dependent parameters. A gamma fines analyzer was developed by Syncrude Ltd. to correlate measured K40 with clay/fines content in processing streams. With an increasing clay/fines percentage, the responsive K40 levels increased (Dougan and McDowell, 1997). Limitations were found in its detection sensitivity and single element determination. Donkor et al. (1996) used instrumental neutron activation analysis (INNA) to establish correlations between fines content and 11 types of individual elements in 23 oil sands samples. This analysis required 120 min to obtain data for all the elements. However, the best fitting found in their study was only 0.81 for dysprosium. A more sensitive and faster technique for elements detection is needed to provide better relevance between mineral properties (single mineral content, clay content, or fines content) and element concentrations. Energy dispersive XRF analysis was considered for this

purpose due to its wide detection range from sodium to uranium with detection limits from ng/g to µg/g. Also, it is fast, nondestructive, and reliable, requires no or very little sample preparation, making it suitable for solid, liquid, and powdered samples (Cesareo, 2010). In general, the XRF technique has been widely used for the examination of chemical and element composition of samples in various fields (El-Nadi et al., 2009; Zhou et al., 2014; Rankin et al., 2016; Xu, 2018; Prado et al., 2018). With the determination of inorganic elements concentrations, XRF has been applied for the characterization of air particulate matter (PM_{2.5} and PM₁₀) in the Athabasca oil sands region (Wang et al., 2015; Landis et al., 2017). Chakrabarty and Longo (1994) used XRF for the identification of reactive minerals in cores based on evaluated photoelectric absorption (Pe) logs. Xiao et al. (2017) adopted XRF determined Hg and Br contents as indicators of mercury and bromine capture and the leaching capacity of thermal treated sorbents. XRF Solutions Ltd. (Spencer and Weedmark, 2015; Spencer et al., 2016; Weedmark et al., 2018) commercialized portable XRF as a technology to predict mineralogy, permeability, porosity, bitumen/water contents, and bitumen quality in heavy oil reservoirs. Researches up to this point lacks an exploration of solids extracted from processing streams. Experiments are required to determine the effects of cleaning methods on desired element contents in solid surfaces. In addition, complex calibrations or calculations were needed for quantitative analysis based on XRF in previous studies, therefore, a simpler model is of great importance.

As discussed above, potassium as a compensating element in illite can be used as an indicator of its presence. The hypothesis of the current study is that the potassium content determined by XRF could serve as a quantitative measure of the illite content in a given solid sample. The objective of this study is therefore to demonstrate that XRF can be used as a simple and robust method to determine the potassium content as a good indicator of illite content in mineral solids.

To achieve this, both the XRF analysis and MBT measurement are applied to various model clay samples composed of illite and other types of solids at variable ratios. To demonstrate the robustness of the XRF analysis for determining illite content in comparison with the MBT measurement, the model clay samples were contaminated with bitumen prior to XRF analysis and MBI determination. The contaminated samples with and without toluene washing or low temperature ashing were tested. Finally, the methods were tested with solids separated from oil sands processing streams.

5.2 MATERIALS AND METHODS

5.2.1 Materials

Three types of model solids were used in this study for clay content determination by both the XRF and MBI methods. Kaolinite (Edgar, Florida, U.S.A) was used as received. Illite (Rochester, New York, U.S.A) and oil sands fines provided by Teck Resource Ltd. (referred to as Teck fines 1 in this paper) were manually ground by pestle and mortar manually prior to use in the tests. The Teck fines 1 also went through toluene reflux in a Dean Stark apparatus to remove the contained bitumen and water. A Mastersizer 3000 was used to measure 50% passing sizes (d_{50}) of the solids used and the results are shown in Table 5.1. For bitumen contamination and toluene washing, coker feed bitumen provided by Syncrude Canada Ltd. and certified ACS grade toluene were used.

Table 5.1. 50% passing size (d_{50}) of model solids used in this study

Type	d_{50} (μm)
Kaolinite	5.9
Illite	5.8
Teck fines 1	15.6

Table 5.2. Ion concentration of process water used in this study

Na ⁺ (ppm)	K ⁺ (ppm)	Mg ²⁺ (ppm)	Ca ²⁺ (ppm)	F ⁻ (ppm)	Cl ⁻ (ppm)	NO ₃ ⁻ (ppm)	PO ₄ ²⁻ (ppm)	SO ₄ ²⁻ (ppm)
690.8	20.6	19.4	83.0	10.3	444.0	71.0	1215.8	957.3

Table 5.3. Composition of oil sands ores used in this study

Ore ID	Composition (wt.%)			
	Bitumen	Water	Solids	Fines (wt.% in solids)
Ore A	9.5	4.5	86.0	40.5
Ore B	9.7	4.3	86.0	13.7
Ore C	11.4	3.9	84.4	15.4
Ore D	9.3	6.5	84.1	33.1
Ore E	9.2	7.7	83.1	19.9
Ore F	10.0	3.2	86.8	18.7
Ore G	16.0	1.4	82.6	5.6
Ore H	12.1	3.8	84.1	7.8
Teck fines 1	3.4	9.9	86.7	79.5
Teck fines 2	0.7	10.3	89.0	89.2

For methylene blue titration, methylene blue trihydrate (USP grade, 373.9 g/mol) was used to prepare the 0.006 mol/L titrant (2.2436 g methylene blue powder in 1 L de-ionized water). Certified ACS grade sodium hydroxide and sodium bicarbonate powder or pellets were used to prepare the corresponding solutions. The 10 vol.% sulfuric acid solution used in this study was prepared by diluting a strong sulfuric acid (95.0–98.0%) of ACS reagent, purchased from Sigma-Aldrich. The properties of the process water and the oil sands ores used in oil sands extraction

experiments are summarized in Tables 5.2 and 5.3, respectively. Other chemicals used in this study were all of reagent grade, unless otherwise specified.

5.2.2 Methods

5.2.2.1 Methylene blue titration

A detailed description on the procedure of methylene blue index (MBI) measurement is available elsewhere (ASTM C837-09). To prepare the solid samples for MBI measurements, the procedure recently established by the CONRAD Clay Focus Group (2012) was used in this study:

i). Place 1–2 g solids (use 5 g if the sample is very sandy) in a clean dry beaker and add 50 mL 0.015 mol/L NaHCO₃ solution and 2 mL 10 wt.% NaOH solution (reduce the dosage of NaOH solution or eliminate its use if the pH exceeds 11.5);

ii). Soak the samples in the solution overnight for a minimum of 12 h;

iii). Use a mechanical stirrer and ultrasonic bath to fully disperse the samples before titration. The appearance of birefringence in the samples and the absence of solids remaining in the bottom of the beaker during stirring indicate a good dispersion;

iv). Adjust the pH of the sample suspension to 2.5–3.8 by 10 vol.% H₂SO₄ solution; and

v). Titrate the samples under continued stirring with 0.006 mol/L methylene blue solution carefully until the end point. The end point is indicated by a light blue halo formed around center drop on a Whatman 42 filter paper. According to the CONRAD Clay Focus Group, the titration results are expressed as the milliequivalent methylene blue adsorbed per 100 g of samples and known as the MBI (CONRAD Clay Focus Group, 2012). Based on this definition, MBI is calculated using the following equation:

$$MBI \left(\frac{meq}{100g} \right) = \frac{mLs \text{ of } MB \cdot mol/L \text{ of } MB}{mass \text{ of dried sample } (g)} \times 100 \quad (5.2)$$

It should be noted that the MBI results obtained by different researchers could vary significantly (e.g., as high as 20%). However, an experienced engineer could always obtain repeatable results (Yukselen and Kaya, 2008).

5.2.2.2 X-ray fluorescence analysis

The potassium contents of the solid samples were measured by an Orbis PC Micro-EDXRF Elemental Analyzer. A sample was placed in the sample holder which was then sealed with a paraffin film. A nitrogen gun was used to blow the entire sample holder to remove any loose particles and the test was conducted in vacuum to obtain good signal to noise ratios, i.e., good XRF peaks. X-ray optics of 2 mm was chosen and the spectrum collecting time was set for 30 s. The X-ray tube was typically operated at 40 kV and 750–950 μ A, depending on the nature of samples. A minimum of 5 spots were analyzed for each sample to obtain statistically representative results.

5.2.2.3 Bitumen contamination and toluene washing

A diluted-bitumen solution was prepared at a 0.7:1 of toluene to bitumen mass ratio. According to Khademi (2012), this bitumen concentration was sufficiently high to reach the maximum adsorption capacity of organics when contaminating solids. To remove the solids contained in the diluted bitumen prior to its use in contamination experiments, the prepared bitumen solution was first centrifuged at 20,000 g force for 3.5 h to obtain a solid-free bitumen solution (Gu et al., 2002). Then a sample of 2 g was placed in 20 mL diluted bitumen solution, with the mixture shaken for 24 h to ensure full contact of solid particles with bitumen. The solids were then separated from the bitumen solution by centrifugation at 20,000 g force for 1 h and decanting the supernatant. To remove the trapped bitumen solution in the wet cake, about 20 mL toluene was added to the wet

cake in the centrifuge tube, followed by shaking or sonication of the mixture to ensure full dispersion of the solids. The suspension was then centrifuged for 15 min at 20,000 g force to separate the solids from the liquid. The solids obtained after drying in a vacuum oven were referred to as contaminated. This toluene washing process was repeated multiple times until the supernatant became colorless and the solids obtained as such were referred to as contaminated + toluene washing.

5.2.2.4 Low temperature ashing (LTA)

In a previous study, low temperature ashing was shown to be able to remove organic contaminants from bitumen-contaminated solids (Adegoroye et al., 2009). An Emitech K1050X plasma asher was used in this study to remove the organic matters from the contaminated solid samples. The process was carried out at an oxygen level of 68.9 kPa and a maximum temperature of ~150 °C to avoid phase/structure change of the solids. A solid sample was placed in a ceramic petri dish and loaded into the chamber of the asher. Oxygen was then introduced into the system with an energizing RF power of 80 W applied. After a treatment of 1.5 h, the solids were stirred to move the bottom particles to the top and vice versa and reloaded into the instrument for another 1.5 h. The cycle was repeated several times until the weight loss was less than 0.002 g. The solids obtained as such were referred to as contaminated + LTA cleaning.

5.2.2.5 Contact angle measurement

Contact angle measurement was carried out with a Theta Optical Tensiometer (T200) using the sessile drop method (Drelich, 2013). To prepare a sample for contact angle measurement, 0.2 g clays were dispersed in 20 mL toluene by a 500 ultrasonic dismembrator (Fisher) for 15 min at 60% amplitude. A clean silica wafer was placed on a spin coater. Vacuum was applied to hold the silica wafer tightly in place. While spinning at 6,000 rpm, 10 drops of clay suspensions were

carefully placed on the silica wafer. After the evaporation of toluene, the sample was transferred with the help of tweezers to the Theta Optical Tensiometer to measure the contact angle of water on the clays deposited on the silica wafer.

5.2.2.6 Oil sands extraction

A modified Batch Extraction Unit (MBEU) was used to extract the bitumen from oil sands ores. Added along with 150 mL of process water (98 °C), 500 g of oil sands ore in a MBEU cell were conditioned by mixing the slurry with air addition at 150 mL/min for 10 min. Process aids (e.g., NaOH) were also added at this time if needed. Another 900 mL of process water (55 °C) was then added into the slurry and the bitumen extraction was proceeded without aeration for 10 min to collect the primary froth. After the primary froth collection, the air was turned on again at 50 mL/min for 5 more min and the secondary froth was collected. The mixing was achieved by an impeller that rotated at 600 rpm during conditioning and primary froth collection, and at 800 rpm during secondary froth collection. The suspension remained in the middle of MBEU cell was collected as the tailings stream and the bottom coarse solids were discarded. The obtained froth was then analyzed by a standard Dean Stark apparatus to determine the composition of the froth. Solids remained in thimbles after Dean Stark reflux were preserved for further measurements.

To separate the solids from the primary froth, toluene was added to the bitumen froth at 1:1 volume ratio and then the mixture was stirred for 24 h. Then the solids were separated from the liquid by centrifuging the mixture at 20,000 g force for 2 h. The solids obtained as such were referred to as primary froth solids. For the separation of the solids from the tailings stream, the tailings stream was placed still for 2 h to cause the coarse solids to settle down with the middle to top stream being collected. The suspension was centrifuged at 20,000 g force for 45 min to isolate the solids from water. The solids obtained as such were referred to as tailings solids. To compare

the results of different cleaning methods, toluene washing, standard Dean Stark reflux (primary froth went through Dean Stark reflux directly without any treatment), and low temperature ashing were used to treat the separated solids. The solids obtained as such were referred to as primary froth/tailings solids + toluene washing, primary froth/tailings solids + Dean Stark, and primary froth/tailings solids + LTA cleaning, respectively, as summarized in Table 5.4. Finally, the solids obtained from the Dean Stark reflux of the original oil sands ores (referred to as feed solids) were collected and preserved for further use.

Table 5.4. Solids extracted from oil sands processing streams used in this study

Primary froth solids			Tailings solids		
Treatment	Equipment	Media	Treatment	Equipment	Media
Toluene washing	Centrifuge	Cold toluene	Toluene washing	Centrifuge	Cold toluene
Dean Stark	Dean Stark apparatus	Hot toluene	Dean Stark	Dean Stark apparatus	Hot toluene
LTA	Plasma Asher	Oxygen	LTA	Plasma Asher	Oxygen

5.2.2.7 Wet sieving

To determine the content of < 44 μm fraction in oil sands solids, the Dean Stark procedure was applied to obtain bitumen-free dry solids. Agglomerates in solids were broken by lightly crushing the samples with a pestle and mortar. To disperse the solids, 1000 mL glass jars were used to contain the suspension of the solids in de-ionized water. Since the solids after the Dean-Stark reflux were initially hydrophobic, they were shaken overnight in water for good dispersion. After that, at least 1 h ultrasonic bath and sufficient stirring were conducted until the presence of streaming birefringence in the samples and the absence of particles at the bottom of the container during stirring was noted. Then, wet sieving for the solid samples was completed using 60, 140,

and 325 mesh cascade sieves and de-ionized water. A spray bottle was used to add fresh water during sieving to break up the remaining agglomerates. The sieving was stopped when the water from the bottom sieve appeared clear (Kaminsky, 2008). The solids retained on the 3 sieves were combined and dried for the determination of the coarse solids fraction, and the fines content of the solid samples were calculated by Eq. 5.3:

$$\begin{aligned}
 & \text{Fines content of solids (wt. \%)} \\
 &= \frac{\text{feed amount of solids (g)} - \text{coarse solids remaining (g)}}{\text{feed amount of solids (g)}} \quad (5.3) \\
 & \times 100\%
 \end{aligned}$$

5.3 RESULTS AND DISCUSSION

5.3.1 Sensitivity of potassium content to illite ratio in the mixture

The most abundant components in oil sand solids are sand, kaolinite and illite. Other types of solids such as montmorillonite, chlorite and some mixed-layer clays just contribute to ~3% of the total clay mass (Masliyah et al., 2011). In oil sands, potassium exists mainly in illite and K-feldspar. However, the content of K-feldspar in oil sands solids is usually relatively low (most likely less than 5%) (Kaminsky et al., 2008; Osacky et al., 2013). Hence, potassium content is often used as a marker for illite. For oil sands that contain comparable amounts of K-feldspar, the matrix equation (Eq. 5.1) should be used to estimate the illite content, which is beyond the scope of this study. Table 5.5 summarizes the XRF results of the determined potassium contents of the 4 typical solid types found in oil sands solids. Compared with illite, it is clear that the potassium contents of sand and kaolinite are negligible. As a representative of rare clay types, montmorillonite contains a slightly higher potassium content at 1.55% than sand and kaolinite, however, its potassium content is still very low compared to the 11.7% for illite. Furthermore, the presence of

montmorillonite and other rare clay types in oil sands solids is normally very low, leading to a negligible contribution of these clay types to the total potassium content of the solids. The results encourage us to use potassium content as an indicator of illite content in oil sands.

Table 5.5. K content (measured by XRF) of typical solid types in oil sands solids

Illite (g/100g, %)	Sand (g/100g, %)	Kaolinite (g/100g, %)	Montmorillonite (g/100g, %)
11.7	0.17	0.28	1.55

In order to test the sensitivity of using potassium content measured by XRF to determine the illite content in a mixed clay system, illite was mixed with sand, kaolinite, or Teck fines 1 at different ratios and the potassium contents of the mixtures were analyzed using the XRF technique. The results are shown in Figure 5.1. Here, each data point is an average value calculated from the data of 2 tests on 5 spots for each test. The standard deviations are calculated using the data from 10 spots and are found to be less than 0.5%. Based on the hypothesis that the potassium content of a mixture was the sum of potassium content measured in each component by weight fraction, the calculated value was obtained by Eq. 5.4, where x represented the mass fraction (wt.%) of A in the mixture:

$$\begin{aligned}
 &\text{Calculated } K \text{ content (wt. \%)} \text{ in } A\&B \text{ mixture} && (5.4) \\
 &= K \text{ content in } A \cdot x + K \text{ content in } B \cdot (1 - x)
 \end{aligned}$$

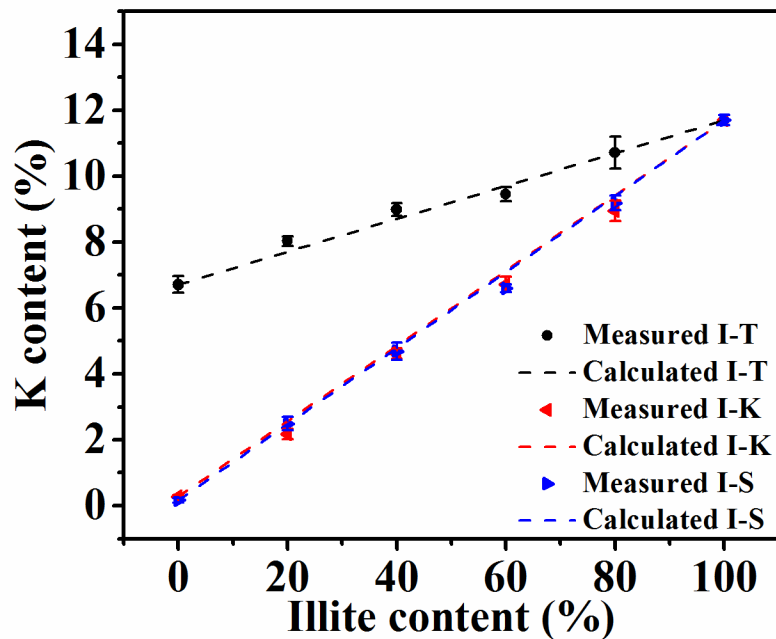


Figure 5.1. Correlation between the K content measured by XRF and illite ratios in the illite (I)-Teck fines 1(T), illite (I)-kaolinite (K), and illite (I)-sand (S) mixtures.

It was found that the potassium content determined by XRF is very sensitive to the illite content in the mixtures. Excellent matches between the measured values and the calculated values were obtained for all 3 mixtures that were tested. It supports our previous estimation that the potassium content of a mixture was a sum of the contributions from each component by mass fraction. Figure 5.1 also shows the potential matrix effect of measuring the illite content using K as the marker, i.e., the measured intensity of the K signal also depends on the type of other minerals in the sample. It is therefore important to construct the calibration curve of K signal with added illite into real samples to determine the slope of intensity variation with added illite content.

5.3.2 Correlation of potassium contents measured by XRF and MBI

To verify the suitability of using MBI to indicate illite content in a mixed clay system, the methylene blue index of the illite/Teck fines 1 and illite/kaolinite mixtures at different ratios was

measured and the results are shown in Figure 5.2. The standard deviations are calculated based on three replica experiments. The calculated values were obtained using Eq. 5.5 where x is the mass ratio of A in the mixture, as discussed before:

$$\text{Calculated MBI } \left(\frac{\text{meq}}{100\text{g}}\right) \text{ in A\&B mixture} = \text{MBI in A} \cdot x + \text{MBI in B} \cdot (1 - x) \quad (5.5)$$

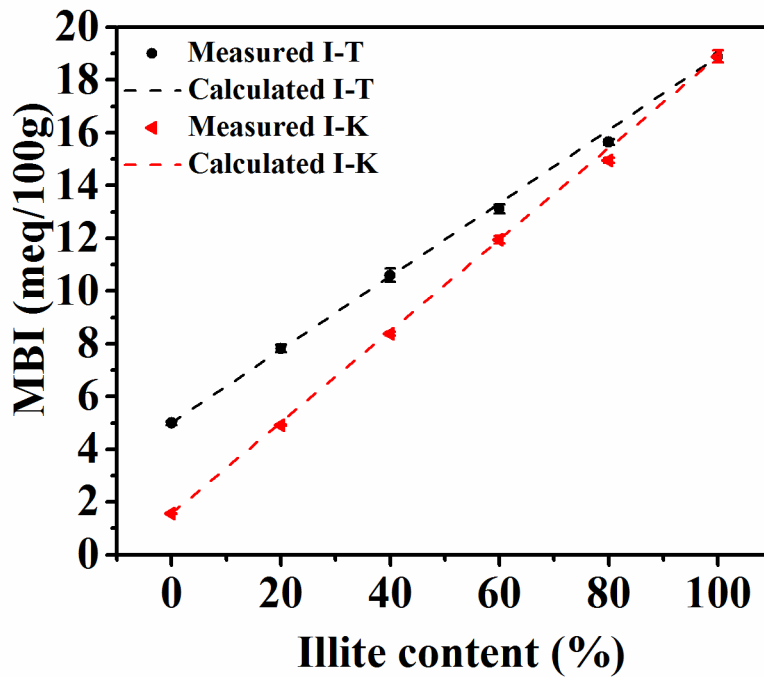


Figure 5.2. Correlation between MBI and illite ratios in the illite (I)-Teck fines 1 (T) and illite (I)-kaolinite (K) mixtures.

As expected, the methylene blue index is also very sensitive to illite content in the mixed clay systems. The calculated values by Eq. 5.5 agree well with the actual results of MBI in both the illite-Teck fines 1 and illite-kaolinite systems. This confirms the suitability of using the MBI to predict illite content in mixed clay systems. Figures 5.1 and 5.2 show that both potassium contents measured by XRF and MB titration are good indicators of the illite contents in illite/ Teck fines 1 and illite/kaolinite mixed clay systems. Figure 5.3 is obtained by replotting the data in Figures 5.1

and 5.2 to indicate the relationship between potassium content and methylene blue index of those model clay samples. As expected, there is a strong linear correlation between the potassium contents measured by XRF and the methylene blue index of the model mixed clay samples with $R^2 > 0.99$.

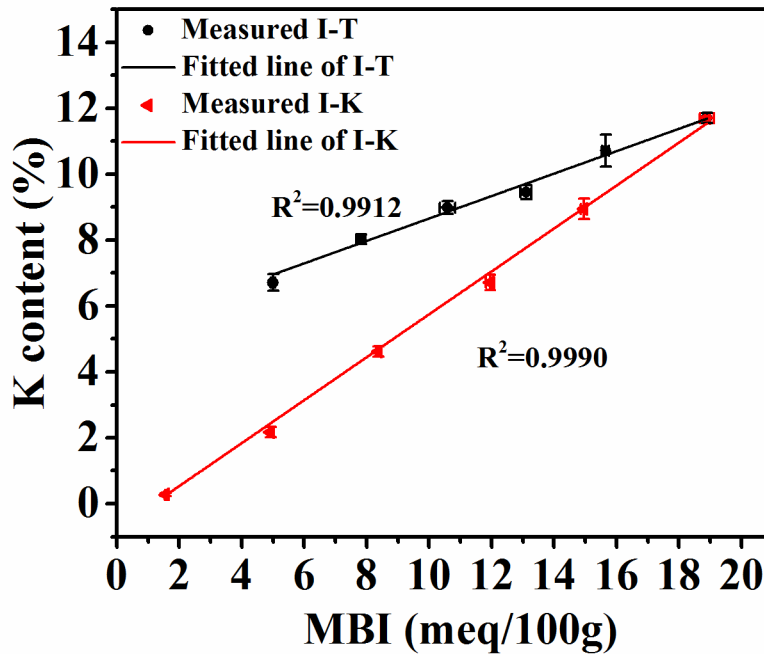


Figure 5.3. Correlation between the K content measured by XRF and MBI of illite (I)-Teck fines 1(T) and illite (I)-kaolinite (K) mixtures (linear fitting).

In summary, the potassium contents measured by XRF and methylene blue titration are both good candidates to indicate illite content in a clean system. Here, clean means no contamination of the clay surfaces by organic matters as encountered in real oil sands samples. In this regard, it is feasible to determine the potassium content or MBI and then calculate the illite content in the mixtures using Eq. 5.4 and Eq. 5.5. Considering no special needs of sample preparation for XRF measurements, it is convenient to use the XRF technique to determine the potassium contents as

an indicator of illite contents in oil sands ores and solids extracted from bitumen froth or tailings streams. This method also provides an opportunity to track illite variations during oil sands processing. More details are discussed in the following sections.

5.3.3 Effects of bitumen contamination

To further test the suitability of using potassium content measured by XRF for the determination of illite content in various oil sands processing streams or in fluid fine tailings (bottom layer in oil sands tailings pond), a toluene-diluted-bitumen solution was used to contaminate clay surfaces prior to their XRF analysis and MBT measurements. For this purpose, a set of four samples of the same chemical composition were used to test the robustness of the techniques. For example, a mixture of 20 wt.% illite (I) and 80 wt.% kaolinite (K) was used as one model sample (sample 1). The samples were first contaminated by a solids-free toluene-diluted-bitumen solution. Then toluene washing was applied to the samples, with one sample washed only once (referred to as “contaminated”) and the other washed thoroughly until the supernatant became colorless (referred to as “contaminated + toluene washing”). The third sample was prepared by cleaning the “contaminated” sample using low temperature ashing until the weight loss became negligible (referred to as “contaminated + LTA cleaning”).

As shown in Figure 5.4, the potassium contents of these four samples remained unchanged at 2.2% (the differences are within 5%, which could be regarded as instrument error). This indicates that bitumen contamination shows negligible effects on the potassium contents measured by XRF. It should be noted that XRF detects elements of atomic numbers >11 as such that the elements of atomic numbers <11 such as carbon is not detected despite their presence. As a result, the elements of atomic numbers <11 are not considered in the weight percent of elements or converted minerals analyzed by XRF. Although this limitation of using XRF for the detection of K-containing

minerals in oil sands or their process streams needs to be considered, such a limitation does not affect the use of XRF for determining illite content in oil sands solids if proper calibration or correction is made for the matrix effect, including carbon-containing minerals such as calcite, dolomite and siderite. During the contamination and cleaning procedures, the adsorption and removal of organic matters only affected the carbon contents of the samples. The results clearly show that X-ray could go through organic matters to reach underneath the samples so that the organic contaminants on the solid surfaces did not affect the potassium contents measured by XRF. This feature provides us with a chance to apply this methodology to oil sands processing streams systems since the major contaminants in those systems are organic compounds. In contrast, large variations in the measured MBI were observed among the four samples. It is shown that the MBI decreased significantly from 5.0 to 3.4 meq/100g when the sample was contaminated by diluted bitumen since the adsorbed organic compounds would inhibit the interactions between the methylene blue cations and the clay surfaces. Even if the sample was washed thoroughly by toluene, the measured MBI was much closer, but still statistically lower, at 4.0 meq/100g than the MBI of 5.0 meq/100g for the corresponding untreated sample. This finding indicates that washing by toluene cannot remove all organic matters coated on the clay surfaces. One possible reason for this phenomenon was that part of organic compounds attached on the clay surfaces were toluene-insoluble. When the contaminated sample was further cleaned by LTA, the measured MBI became the same as the original sample. Similar trends are found for sample 2, which were pure illite samples, also shown in Figure 5.4.

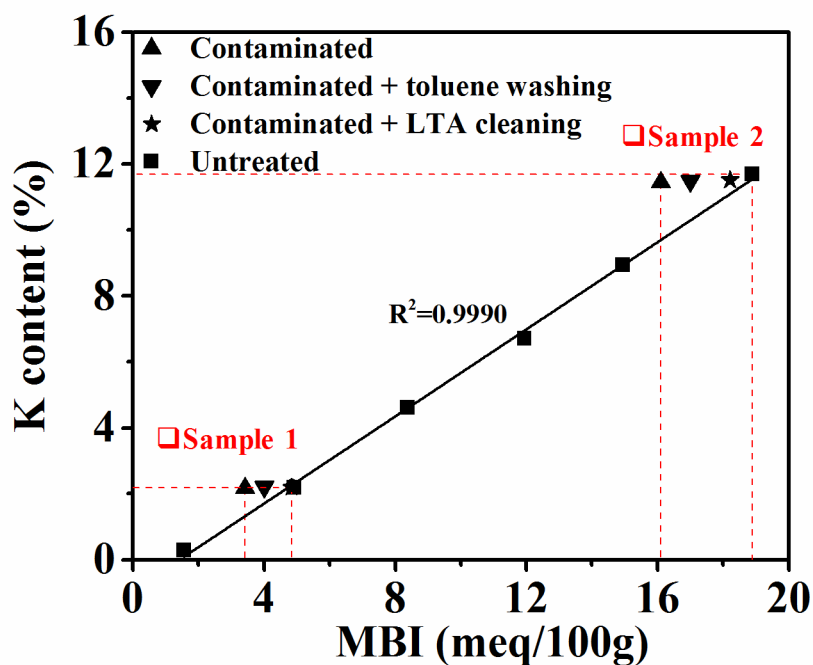


Figure 5.4. Effect of bitumen contamination, toluene washing, and LTA cleaning on K content measured by XRF and MBI of illite (I)-kaolinite (K) mixtures.

FTIR was used to confirm the results for contamination. In Figure 5.5a, peaks at around 2930 wavenumber in the FTIR spectrum show the adsorption of organic compounds by solid samples when contaminated by diluted bitumen solution. When the sample was washed by toluene until the supernatant became colorless, the adsorption peaks remained, yet became much weaker. This supports our results of MBT measurement that washing by toluene can only remove the toluene soluble bitumen components attached to the solids. When the sample was further cleaned by LTA, these peaks disappeared, indicating a complete removal of organic matters from the sample, further confirming the results of our MBT measurement. A similar phenomenon is shown in Figure 5.5b for sample 2.

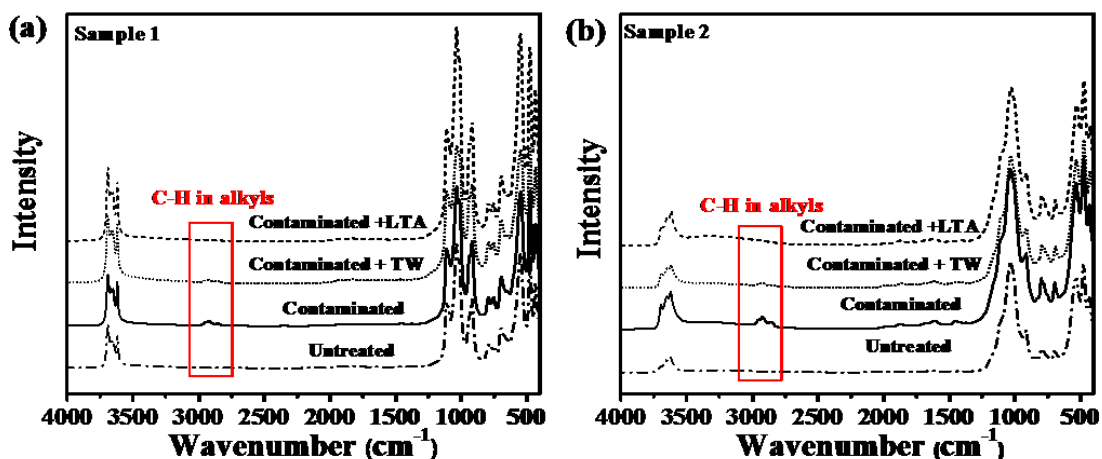


Figure 5.5. FTIR spectra of illite (I)-kaolinite (K) mixtures before and after various treatments (TW=toluene washing).

A thermal gravimetric analysis (TGA) was also performed to evaluate the adsorption of organic matters on the clay surfaces quantitatively. It measures the change in sample weight as a function of temperature by increasing the temperature from 100 °C to 700 °C. Here, 100 °C is chosen to be the starting temperature in order to eliminate the effect of uncontrolled moisture content on the measured weight loss. The evaporation/decomposition of organics causes a reduction in sample weight, and the amount of weight loss indicates the organic contaminants content on clay samples. The limit of this method is that the clay structure undergoes a change at around 400 °C where the O-H bond on the clay surface dehydrogenizes to form H₂O and also causes a change in the sample weight (Stoch and Waclawska, 1981). As a result, it is difficult to identify how much weight loss is due to the evaporation/decomposition of the organic contaminants. It is relatively safe to hypothesize that the amount of such O-H bonds on clay surfaces did not change during the contamination and various treatment processes. Then the differences between the weight loss of the untreated sample and that of samples after various treatments could be used to evaluate the adsorption of organic matters on the clay surfaces quantitatively, or at least semi-quantitatively.

The TGA curves of the pure illite samples before and after various treatments are shown in Figure 5.6. As expected, there was a significant weight loss at ~ 375 °C regardless of the existence of organic contaminants. Nevertheless, the weight loss of contaminated illite sample increased from the untreated value at 6.0 to 7.6%, indicating ~ 1.6 wt.% organic contaminants adsorbed on illite surfaces. The toluene washing was capable of removing 35% of organic contaminants on illite surfaces to reduce the weight loss from 7.6 to 7.0%. A more thoroughly removal of organic matters could be achieved by low temperature ashing, as revealed by the 0.5% difference between the TG curve of the untreated illite sample and that of “contaminated + LTA cleaning” illite sample in Figure 5.6.

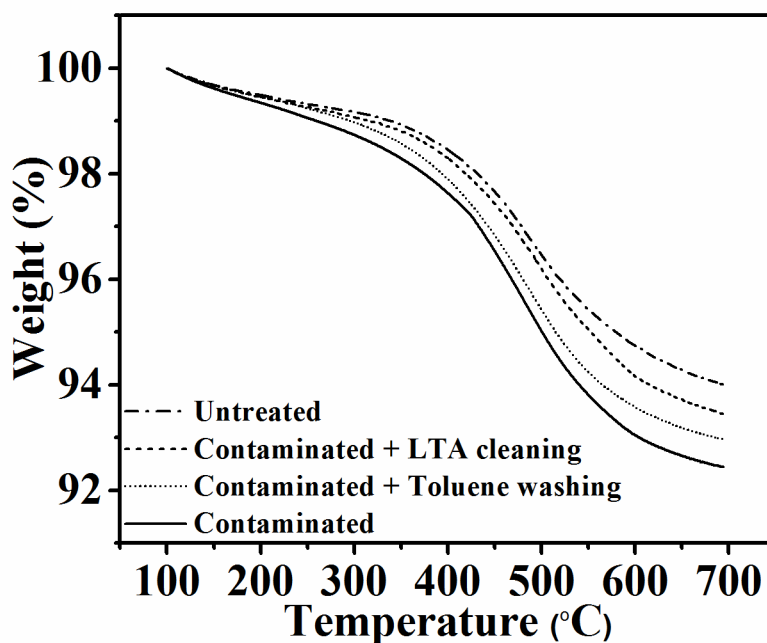


Figure 5.6. TGA spectra of illite samples before and after various treatments.

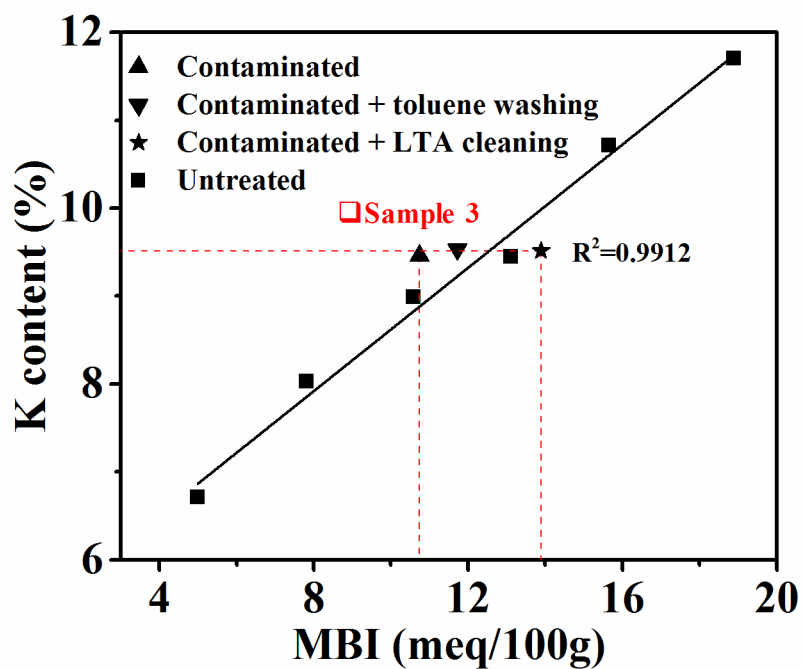


Figure 5.7. Effect of bitumen contamination, toluene washing, and LTA cleaning on K content measured by XRF and MBI of illite (I)-Teck fines 1 (T) mixtures.

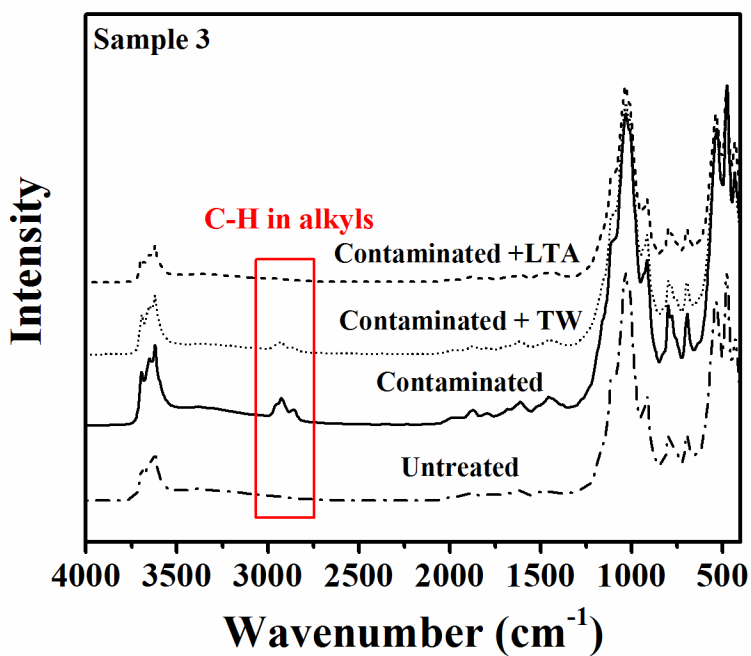


Figure 5.8. FTIR spectra of illite (I)-Teck fines 1 (T) mixtures before and after various treatments (TW=toluene washing).

To further illustrate the robustness of the XRF method for determining K content and hence the illite content in a complex solid mixture, a mixture of 60 wt.% illite (I) and 40 wt.% Teck fines 1 (T), referred to as sample 3, underwent the same bitumen contamination, toluene washing, and LTA cleaning processes. The same procedure was repeated twice for each type of sample (contaminated, toluene washing and LTA cleaning) with differences all within a 5% error. The corresponding average of the two repeating experiments is shown in Figure 5.7 and the FTIR spectra are shown in Figure 5.8.

Similar to the results of the kaolinite-illite mixtures, a unique K-content value of 9.5% was obtained from the XRF analysis regardless of the contamination or the toluene washing/LTA cleaning, as shown in Figure 5.7. Similarly, the MBI decreased significantly from the original value of 13.1 meq/100g for the untreated mixture to 10.7 meq/100g for the bitumen contaminated mixture. A thorough toluene washing of the bitumen-contaminated mixture led to a significant increase in the MBI value to 11.7 meq/100g, which further increased to 13.9 meq/100g by LTA cleaning. The results clearly illustrate that the XRF technique is a robust and hence more preferred method than the MBT measurement for determining illite content in oil sands ores and relevant processing streams. The results further confirm that low temperature ashing is an effective method to remove organic compounds coated on solid samples, as also shown by the corresponding FTIR spectra in Figure 5.8.

5.3.4 Hydrophobicity of clays

To investigate the impact of solid hydrophobicity on MBT measurement, the contact angles of water on the model illite samples before and after bitumen contamination were measured. Table 5.6 summarizes the contact angle values of water on the illite samples of three different treatments. As expected, illite without bitumen contamination was hydrophilic with a contact angle value of

0°. After bitumen contamination, the illite became strongly hydrophobic with a water contact angle of 135°. Washing by toluene slightly reduced the contact angle of the water to 100°. In contrast, the LTA treatment led to the complete removal of organic matters and hence a hydrophilic solid surface of contact angle 0° was obtained.

To evaluate whether particle aggregation/dispersion due to the change in illite particle hydrophobicity affect MBT measurement, ethanol and toluene/IPA (isopropyl alcohol) at 7/3 (g/g) were used to disperse the illite samples before dispersing the particles in 0.015 mol/L NaHCO₃ solution prior to MBT measurement. In addition, untreated illite was treated by toluene using a similar procedure of bitumen contamination process to eliminate the effect of toluene adsorption and/or particle dispersion on the MBT measurement. The results of the MBT measurements are summarized in Table 5.7. It is evident that the wetting of illite by ethanol and toluene/IPA has a negligible effect on the MBT measurement. Also shown is a negligible effect of toluene washing on the MBT measurement of untreated illite samples, illustrating the inability of volatile toluene adsorbing on clay surfaces. These findings confirm that the decrease in the MBI of the clay samples after bitumen contamination is indeed due to the adsorption of organic compounds onto clay surfaces, not from particle aggregation in the MBT measurement solutions due to the increase in particle hydrophobicity.

Table 5.6. Water contact angle of model illite before and after bitumen contamination

Condition of model illite	Contact angle (degree)
Untreated	0
Contaminated	135
Contaminated + toluene washing	100
Contaminated + LTA cleaning	0

Table 5.7. Methylene blue index of model illite after several treatments

Condition of model illite	Methylene blue index (meq/100g)
Untreated	18.89
Contaminated	16.10
(Wetted by ethanol)	16.00
(Wetted by toluene/IPA)	15.48
Contaminated + toluene washing	17.00
(Wetted by ethanol)	16.92
(Wetted by toluene/IPA)	16.80
Treated by toluene	19.09

5.3.5 Application to oil sands

To confirm the suitability of using potassium content as an indicator of illite content in oil sands solids, solid samples from bitumen froth as well as from the corresponding tailings stream were also tested. Toluene washing, the commonly used Dean Stark apparatus, and low temperature ashing were applied to clean the solid surfaces prior to the XRF analysis and MBT measurement. The results shown in Figure 5.9 are generalized to determine a more robust method to indicate the illite content in the oil sands and determine a preferable technique to clean solid surfaces.

As anticipated, the potassium contents remained consistent at 6.8% and 7.5% for primary froth solids and tailings solids, respectively, after various treatments. This supports our previous hypothesis that potassium contents measured by the XRF method are not affected by surface contaminations and could be a simple and robust way to determine illite content in oil sands solids. On the contrary, there were significant variations in the measured MBI data among the samples with different treatments. Toluene washing was found to be able to increase the MBI of

solids by around 10–20% by removing the trapped bitumen in the solids, while the Dean Stark reflux of hot toluene caused a non-significant further improvement of MBI data. LTA cleaning, as effective as discussed before, increased the MBI of the solids by 20–30% with the help of burning out all the organic matters on the solids. This finding demonstrates the preferential performance of removing organic contaminants from oil sands solids by low temperature ashing. The overall conclusion is that XRF is a robust way to determine illite content in oil sands solids since it is tolerant to surface contaminants. For the traditionally used MBT method, low temperature ashing is found to be a suitable way to clean the solid surface prior to measurement.

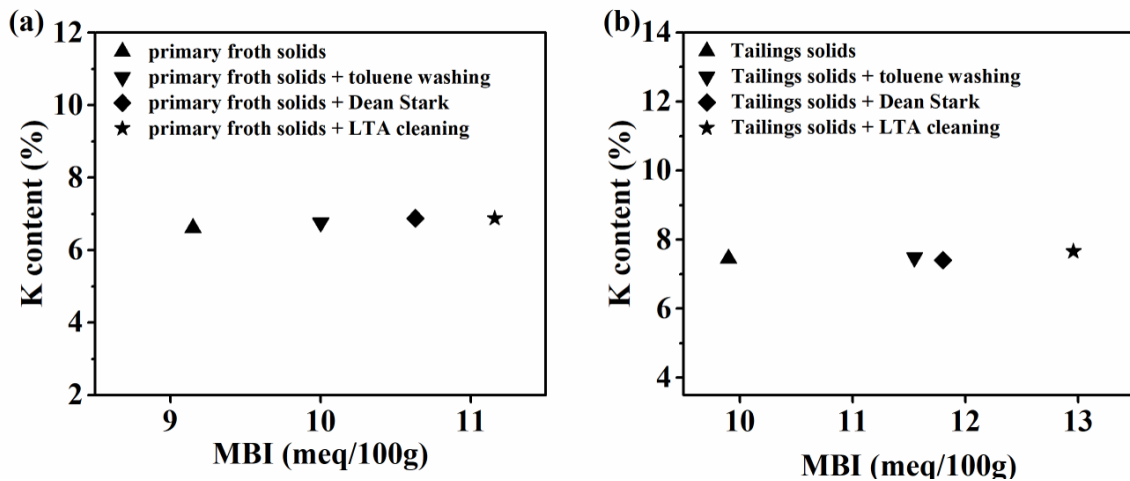


Figure 5.9. Effect of toluene washing, Dean Stark, and LTA cleaning on the K content measured by the XRF and MBI of (a) primary froth solids and (b) tailings solids of ore A.

Figure 5.10 shows the presence of a linear correlation between the measured potassium contents by the XRF method used in this study and the measured fines contents in the oil sands solids. This indicates the potential to apply the XRF method in the oil sand industry for the estimation of fines/clay contents.

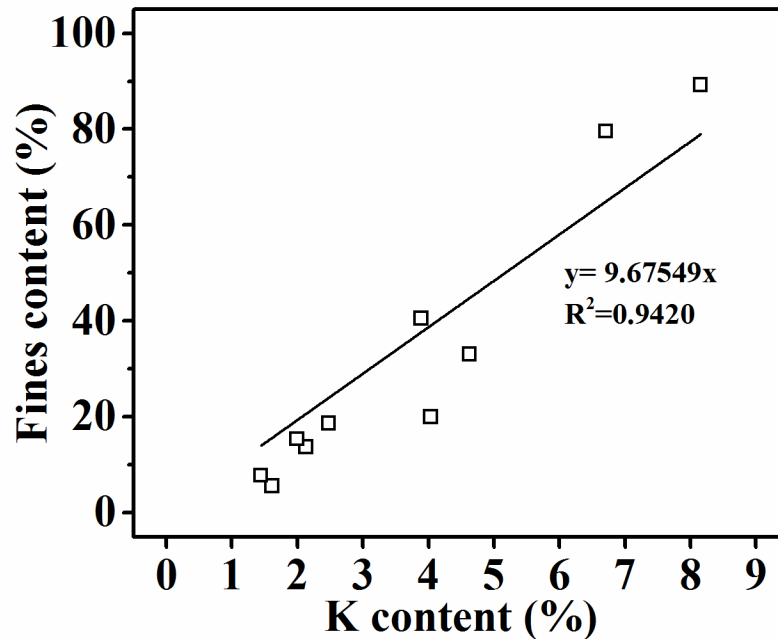


Figure 5.10. Correlation between the fines content and K content measured by XRF.

In order to quantitatively apply the methodology used in this study to determine illite content, the following matters require special attention: a) the selection of a standard illite sample; and b) the variation in the potassium content in oil sands illite as a result of isomorphous substitution or degradation.

5.4 CONCLUSIONS

In this study, the XRF technique was used to determine the potassium content as an indicator of the illite content in a solids sample from an oil sand ore or related stream. Strong linear correlations between the potassium content determined by XRF and illite content and between the methylene blue index and illite content were obtained for non-contaminated (clean) samples, indicating that both XRF and MBT were sensitive to illite content in mixed clay systems if no contaminants were adsorbed on the clay surfaces. When the samples were contaminated with a

diluted bitumen solution, the organic matters were adsorbed on the clay surfaces. Such adsorption decreased the measured methylene blue index significantly. After removing the entrapped bitumen by toluene washing, the methylene blue index was much closer to, though still lower, than the original data. The total removal of the organic matters was achieved by low temperature ashing, after which the MBI results were comparable to the values of the original clean samples. The potassium contents measured by XRF in the fine solids samples remained unchanged for the samples after the contamination, toluene washing and organic matter removal processes. The results of various oil sands processing solids confirmed our hypothesis that XRF is more appropriate to determine illite content than the MBT method since it is more tolerant to surface contamination. This study demonstrates that the XRF method provides a simple and efficient way of determining illite/fines content in oil sands ores and relevant processing streams.

CHAPTER 6 STRATEGIES FOR IMPROVING THE PROCESSABILITY OF OIL SANDS ORES OF HIGH FINES CONTENT

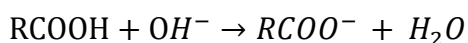
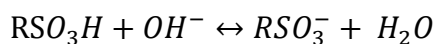
6.1 INTRODUCTION

The bituminous oil sands were first discovered and documented as a natural source of petroleum centuries ago (Pilote et al., 2018). Canadian oil sands deposits differ from conventional oil reservoirs in two ways. First, the oil sands reserves are orders of magnitude larger than conventional oil reservoirs. Second, the physical properties of oil sands bitumen differ greatly from those of conventional crude oil (Mossop, 1980). Since bitumen is imbedded in the oil sands formations, it must be extracted from the oil sands before it can be further processed. In the oil sands industry, bitumen recovery and froth quality are key performance indicators to evaluate an extraction process. Fines (<44 μm) content plays an important role in determining the ore processability (Chong et al., 2003).

Fundamentally, the bitumen extraction process can be considered to occur in three stages: bitumen liberation, bitumen aeration, and bitumen flotation (Hepler and His, 1989; Hepler and Smith, 1994). For the separation of bitumen from the sand grains, solids wettability is a contributing factor. The more hydrophilic the solids, the easier the detachment of bitumen from the solid matrix. Dang-Vu et al. (2009) used contact angle, critical surface tension, water drop penetration time and solids partitioning to investigate the wettability of solids isolated from oil sands. Their results showed that for weathered ore, poor processing ore, and good processing ore, the hydrophilicity of the solids increased in the same order, with a similar increasing trend of bitumen recovery. In this regard, clay plays a less significant role. Basu et al. (1998) used a microscope glass slide model to monitor the dynamic/static contact angles in bitumen separation process in the presence and absence of clays. Their results proved that clays, no matter hydrophilic

or hydrophobic, have little effect on the bitumen detachment and displacement from the sand/glass slide surfaces. In the aeration and flotation processes, fine solids have a significant impact on the bitumen-bitumen coalescence and bitumen-air bubble attachment due to slime-coating. The coverage of bitumen by fines is detrimental to bitumen recovery (Masliyah, et al., 2004, 2011, 2013). The presence of various surfactants and metal ions in the oil sands slurry were found to be able to promote the bitumen-fines hetero-coagulations by altering the solid surface properties and thus attributed to fine solids carryover to the froth product (Zhou et al., 1999; Zhao et al., 2006). Gu et al. (2003) used induction time to indicate the efficiency of bitumen-air bubble attachment. Their results showed an increased induction time with the addition of fine solids along with calcium ions into the measurement media, suggesting a detrimental effect of fine solids and calcium ions on bitumen flotation.

In industrial operations, chemical aids such as NaOH are often used in the extraction process to enhance bitumen recovery (Flury et al., 2014; Schramm, 2000; Hupka et al., 1983; Long et al., 2011; Li et al., 2008). The amount of NaOH needed has been shown to be related to the fines content of the ore. The higher the fines content, the more NaOH is needed (Sanford, 1983). The following reactions (Hepler and Smith, 1994) illustrate how NaOH promotes the release of natural surfactants from bitumen, which has been demonstrated to be qualitatively correlated with bitumen recovery (Schramm et al., 1984b; Schramm and Smith, 1985, 1987).



The increase of pH with the addition of NaOH alters the surface properties of bitumen and solids and as a result facilitates bitumen liberation (Flury et al., 2014; Srinivasa et al., 2012). In

addition, the introduction of NaOH to the extraction slurry was capable of consuming divalent cations and alleviating bitumen slime-coating (Schramm and Smith, 1987; Fong et al., 2004; Liu et al., 2005b). The presence of divalent cations such as calcium and magnesium were found to be problematic to bitumen extraction (Kasongo et al., 2000). At sufficiently high pH, the precipitation of divalent cations in the form of carbonates or hydroxides were promoted and the concentration of free divalent cations in the processing stream was reduced. Bitumen recovery and froth quality were then less affected (Fong et al., 2004; Dai et al., 1992). Using AFM, Liu et al. (2005b) confirmed the significant impact of solution pH and calcium ions on the colloidal interactions between bitumen-bitumen and between bitumen-fines. The increase of pH led to a weaker attraction between bitumen and fines, resulting in a depression in unwanted slime-coating. While divalent cations were observed to show an adverse impact.

In 1985, Schramm et al. put forward the idea of binary mixture of oil sands. In their systematic approach, various poor oil sands ores were blended with rich oil sands ores at different ratios and resulted in better bitumen recovery than the weight addition of two individual ores. A governing rule was proposed based on the correlation between the maximum bitumen recovery and the concentration of free carboxylic surfactants. Similar promotions in bitumen recovery by ore blending have been reported elsewhere (Takamura and Wallace, 1988; Chen et al., 2017). Recently, Zhou et al. (2013) proposed “carrier flotation” as one of the mechanisms for improving bitumen recovery of poor ores by ore blending. The apparent bitumen droplet size was increased by using hydrophobic carrier materials to piggyback small bitumen droplets.

The objective of this chapter is to find coping technologies to improve the processability of oil sands ores of high fines content. Doping fine solids to a good processing ore in extraction tests was conducted to identify the detrimental role of fine solids in bitumen extraction. Slime-coating

phenomenon was confirmed using ζ potential distribution measurement. NaOH addition and ore blending were tested as coping strategies to mitigate the negative impact of fine solids on bitumen extraction. And in this chapter, the effects of NaOH addition and ore blending have been investigated by considering water chemistry and surfactant concentrations. Furthermore, high potassium content of froth solids measured by XRF was examined to be a marker for low bitumen recovery in oil sands.

6.2 MATERIALS AND METHODS

6.2.1 Materials

Three Athabasca oil sands were supplied by Syncrude Canada Ltd. The compositions of these three ores identified as Ore G, HF, and MF are given in Table 6.1. The difference between the last two ores was their fines content. Fine solids were provided by Tech Resource Ltd.

Table 6.1. Composition of three oil sands ore samples used in this study

Ore ID	Composition (wt.%)			
	Bitumen	Water	Solids	Fines (wt.% in solids)
Ore G	11.4	3.9	84.4	15.4
Ore HF	9.5	4.5	86.0	40.5
Ore MF	9.7	4.3	86.0	13.7

Coker feed bitumen was used to prepare bitumen emulsions for ζ potential distribution measurement. High purity KCl (>99.999%, Aldrich) was used as a background electrolyte in preparing aqueous solutions while NaOH (1N, Fisher Scientific) was used as a pH modifier. NaOH was also added as a process aid in extraction tests.

The ions contents of the Aurora process water used in the bitumen extraction tests are summarized in Table 6.2. Its original pH was measured to be ~8.0.

Table 6.2. Ion concentration of process water used in this study

Na ⁺ (ppm)	K ⁺ (ppm)	Mg ²⁺ (ppm)	Ca ²⁺ (ppm)	F ⁻ (ppm)	Cl ⁻ (ppm)	NO ₃ ⁻ (ppm)	PO ₄ ²⁻ (ppm)	SO ₄ ²⁻ (ppm)
690.8	20.6	19.4	83.0	10.3	444.0	71.0	1215.8	957.3

6.2.2 Methods

6.2.2.1 Bitumen extraction test

A modified Batch Extraction Unit (MBEU) was used for bitumen extraction tests. After complete thaw of oil sands ore at room temperature, 500 g ore and 150 mL process water (98 °C) were placed in the MBEU cell and conditioned with 150 mL/min air flow for 10 min. NaOH (expressed as wt.% of the ore) was also added in this step by dissolving in water. Then another 900 mL process water (55 °C) was added into the slurry without aeration for 10 min. Primary froth was collected during this step. After that, air was introduced again at 50 mL/min for another 5 min with the secondary froth collected during agitation. The impeller for dispersing the oil sands was set to rotate at 600 rpm for conditioning stage and primary froth collection and at 800 rpm for secondary froth collection. After each test, the suspension remained in the MBEU cell was collected as tailings water and the bottom coarse solids were discarded. A Dean Stark refluxing method was used to determine the contents of bitumen, water and solids in the bitumen froth. The cumulative bitumen recovery over a flotation period was calculated by:

Overall Bitumen Recovery (%)

$$= \frac{\text{Bitumen in primary and secondary froth (g)}}{\text{Bitumen in feed (g)}} \times 100\% \quad (6.1)$$

Solids retained on extraction thimbles after Dean Stark analysis were dried and preserved for further measurement.

6.2.2.2 ζ potential distribution measurement

ζ potential distribution measurement was carried out with a ZetaphoremeterIII (SEPHY/CAD). 1 g of bitumen was emulsified in 100 mL electrolyte solution using a 500 ultrasonic dismembrator (Fisher). The suspension of fine solids was prepared in the same manner. To prepare binary mixtures of bitumen-fines, bitumen emulsion and fines suspension were mixed at a specific ratio and conditioned in an ultrasonic bath for ~5 min prior to the measurement. For ζ potential measurement, samples were transferred to a testing solution with the same chemical composition to reach a concentration of 0.01~0.1 wt.% particles. The movements of around 50–100 particles were traced simultaneously by laser illuminating and video viewing system. The captured images were analyzed and converted to ζ potential distribution histograms by a built-in imaging processing software. ζ potential distributions of bitumen emulsion and solids suspension, individually or as a mixture, were obtained to provide a good estimation of the hetero-coagulation phenomenon in aqueous medium for a two-component system. A detailed description of using this method to estimate slime-coating phenomenon was reported elsewhere (Liu et al., 2002).

6.2.2.3 Carboxylic surfactant analysis

The FTIR method (Jivraj et al., 1995; Clemente and Fedorak, 2005; Scott et al., 2008) was used to determine the concentrations of carboxylic surfactants in tailings water. The collected tailings water was first centrifuged at 20,000 g force for 30 min to remove solids. After further removal of fine particles by vacuum filtration (0.1 μm), 50 g tailings water was acidified by reagent grade HCl to adjust the pH to 2.3. Then 25 mL dichloromethane (DCM) (Optima™) was added to the sample to extract the natural surfactants out. After liquid-liquid extraction process, surfactants-in-DCM solution was collected from the bottom of the separatory funnel. The extraction was repeated three times to recover the carboxylic surfactants as full as possible. The total solution

collected was placed in a fume hood to evaporate the solvent (DCM) under air. The remaining residue was redissolved in 20 g carefully weighted fresh DCM. FTIR (Agilent Cary-670) spectrum of the solution was obtained using a KBr super-sealed liquid transmission cell (International Crystal Laboratories) and a deuterated triglycine sulfate (DTGS) detector. The measurements were performed at a resolution of 4 cm⁻¹, an infrared range of 4000–400 cm⁻¹ and 128 co-added scans. The intensities of the peaks at ~1743 and ~1706 cm⁻¹ which corresponding to the carboxylic functional groups in the form of monomers and dimers were used to calculate the concentration of carboxylic surfactants. A quantification standard curve obtained using known model compounds of naphthenic acids was applied (Bakhtiari, 2015):

$$y = 0.0047x + 0.0001 \quad (6.2)$$

where x was the total intensity at ~1743 and ~1706 cm⁻¹ and y was the carboxylic surfactant concentration in solution (mol/L).

6.2.2.4 Surface tension

Surface tensions of tailings water were determined by a Kruss K12 process tensiometer using flat Wilhelmy plate method. The presence of surface-active materials (surfactants) is able to lower the surface tension of the solution, hence surface tension serves as a qualitative marker for concentration of total surfactants in tailings water. The accuracy of the instrument was validated using Milli-Q water (72.8 mN/m at room temperature) before each series of tests.

6.2.2.5 X-ray fluorescence

An Orbis PC Micro-EDXRF Elemental Analyzer was used to measure the potassium contents of Dean Stark solids. Samples sealed with a paraffin film were placed in the sample holder with caution. A nitrogen gun was used to blow away any loose particles prior to the measurement. The

tests were conducted in vacuum to obtain fine XRF peaks. X-ray optics of 2 mm was used and the spectrum collecting time was set at 30 s. Depending on the properties of the samples, the X-ray tube was operated at 40 kV and 400~800 μ A. A minimum of 5 distributed spots were collected for each sample to obtain statistically representative results.

6.3 RESULTS AND DISCUSSION

6.3.1 Effect of doped fines on extraction performance

The presence of a large amount of fines in the “poor processing” ore is one of the primary causes for its poor processability. Addition of fine solids to the ore was previously used to investigate the roles of fines in bitumen extraction (Kasongo et al., 2000). To confirm the detrimental effects of fines on bitumen extraction, different levels of fines were added to ore G in bitumen extraction tests. Mixing of the fines and the ore sample was conducted prior to their addition into the flotation cell to ensure full dispersion of the added fine particles in the slurry. De-ionized water was used as water source to eliminate the complex effect of process water chemistry.

The results are shown in Figure 6.1. The standard deviations of three replica experiments were less than 5%. As expected, cumulative bitumen recovery of ore G decreased from the 88% of the base case with no fines addition to 79 and further to 65% with fines addition at 1 and 2% (Figure 6.1a). A sharp decrease of the bitumen recovery to 46% was observed when fines addition was increased to 5%, indicating that the negative effect of fine particles on bitumen recovery was more significant at higher fines content. Such decreases should be mainly due to the slime-coating effect. Previous research (Liu et al., 2004b, 2005b; Dang-Vu et al., 2009) has revealed that slime-coating imposed the most detrimental impact on bitumen recovery, and this effect should become severer if higher content of fines was present in the oil sands slurry. Slime-coating could not only decrease bitumen flotation rate and bitumen recovery but also deteriorate froth quality by carrying fine

solids to the froth product (Liu et al., 2004b). As shown in Figure 6.1b, both the bitumen content and bitumen/solids ratio in bitumen froth decreased when extra fines were added into the system, with bitumen/solids ratio shown to depress more by as large as 56% (from 3.4 to 1.5). This supported our analysis that fine slimes in bitumen froth increased with increasing fines addition. Other possible factors that could account for the fine particles reporting to the bitumen froth including the entrainment of fine particles in water and the entrapment of fine particles between bitumen droplets. These effects were found to be dependent on the size of the particles. Small particles were preferentially entrained or entrapped than large particles (Zhou et al., 2017; Dai and Chung, 1995). In general, Figure 6.1 confirmed the negative effects of added fines on bitumen recovery and froth quality.

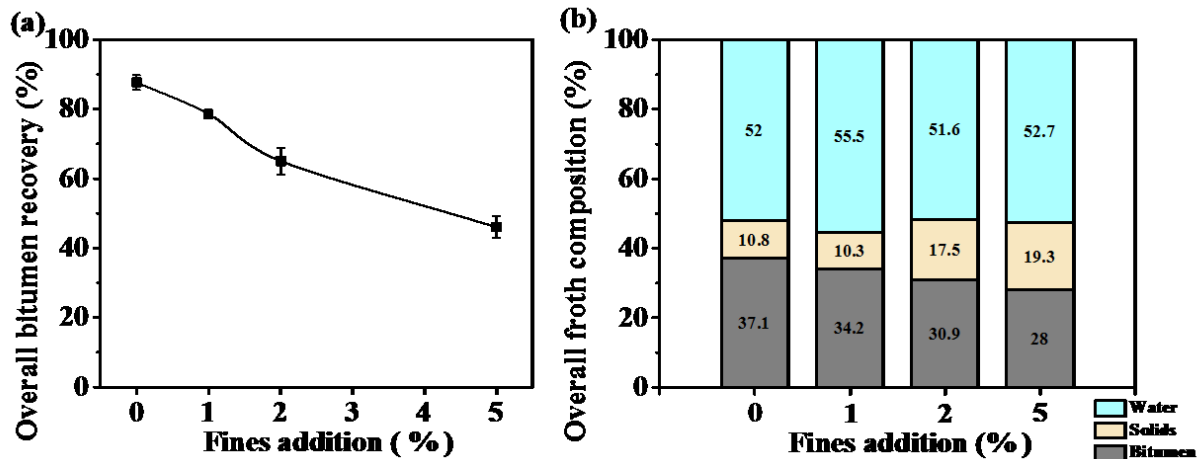


Figure 6.1. Effect of fines on (a) bitumen recovery and (b) froth quality of ore G.

6.3.2 Effect of caustic addition on extraction performance

Sodium hydroxide (NaOH), or commercially called caustic, is often used as a process aid to help optimize bitumen recovery as well as froth quality. Optimal conditions of water-based bitumen extraction process have been studied extensively by researchers to find preferred

temperature, caustic dosage, air injection rate, and so on. One of the challenges lies as to why different oil sands response differently to caustic addition. As an important indicator of the processability of Canadian oil sands, fines content varies among different ores. Figures 6.2 and 6.3 show the results of bitumen recovery and froth quality for two median grade oil sands (HF and MF) as a function of caustic addition. According to Figure 6.2a, bitumen recovery of a high fines ore (ore HF) was increased dramatically from 11 to 82% with an increase in caustic addition from 0 to 0.08%. With higher caustic addition, bitumen recovery improvement became insignificant and even started to decrease, indicating an overdose of caustic. Froth quality data are consistent with the recovery results. As shown in Figure 6.2b, bitumen content and bitumen/solids ratio in bitumen froth increased from 8.5 to 56.4 and from 0.8 to 4.2, respectively, with increased caustic addition from 0 to 0.1%. After that, the improvement in froth quality was not pronounced, and froth bitumen content showed an ‘overdose’ phenomenon at concentrations above 0.2%. To sum up, caustic addition at 0.08~0.1% was optimal to this high fines ore. On the other hand, for ore MF with similar composition but lower fines content, the optimal caustic addition appeared to be much lower as compared to the high fines ore. Figure 6.3a shows that 0.05% caustic addition was sufficient for the medium fines ore (ore MF) to obtain the maximum bitumen recovery at 94%. Similar results were found for the froth quality, as presented in Figure 6.3b. Bitumen/solids ratio in collected froth reached a desirable value at 4.6 with 0.05% caustic addition, after which the bitumen content in froth increased at about the same rate as the solids content. In other words, for this medium fines ore, 0.05% caustic dosage was able to help reach satisfying bitumen recovery and froth quality.

In summary, a higher fines content requires more caustic to achieve optimal bitumen recovery and froth quality. Moreover, the improvement of bitumen recovery and froth quality with the introduction of caustic was more pronounced for ores of high fines content.

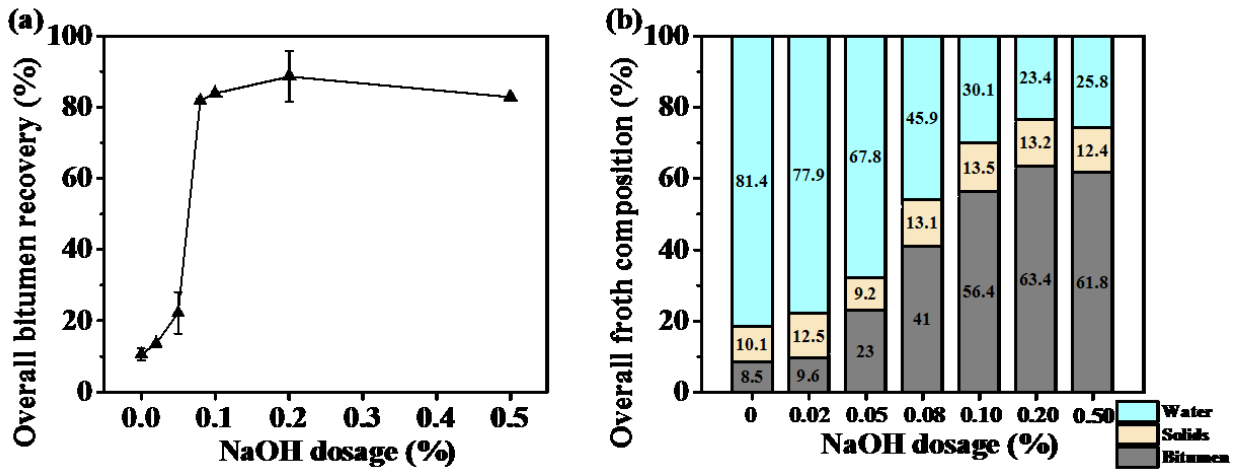


Figure 6.2. Effect of NaOH addition on (a) bitumen recovery and (b) froth quality of ore HF.

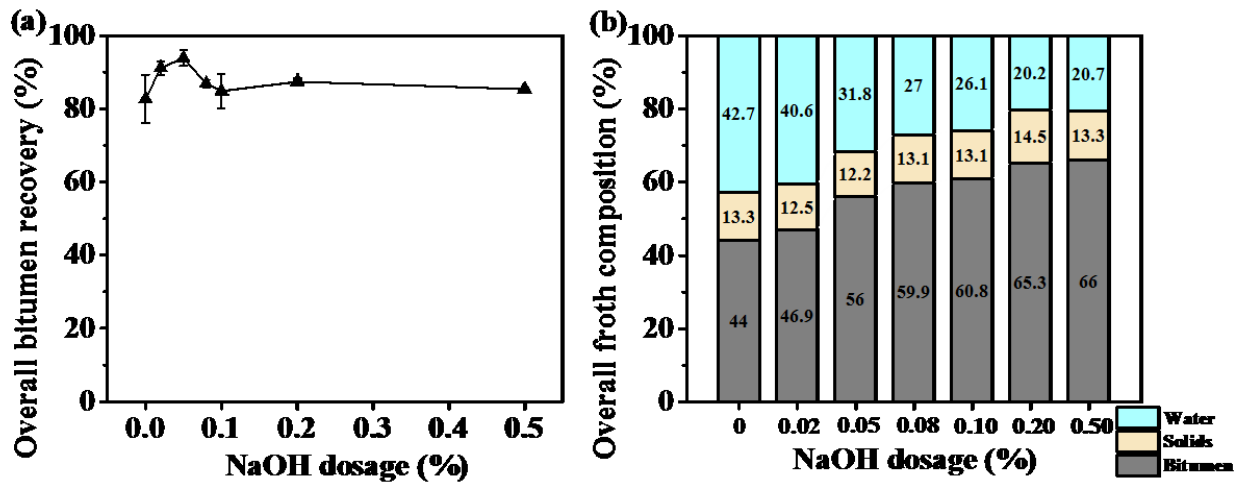


Figure 6.3. Effect of NaOH addition on (a) bitumen recovery and (b) froth quality of ore MF.

6.3.2.1 Slime coating

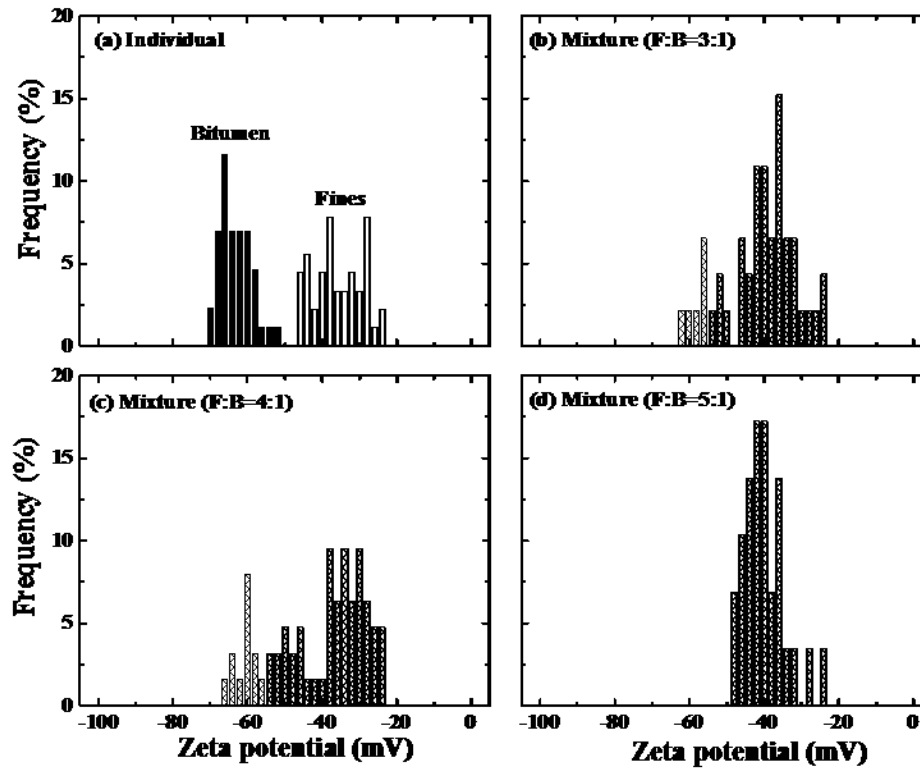


Figure 6.4. ζ potential distributions of bitumen emulsion and fines suspension (a) and their mixtures at 3:1(b), 4:1(c), and 5:1 (d) fines to bitumen mass ratios in 1 mM KCl aqueous solutions without pH control.

ζ potential distribution measurement has been used to investigate the slime-coating phenomenon in oil sands processing (Liu et al., 2002, 2004a, 2004b; Ding et al., 2006). Figure 6.4a shows ζ potential distributions of bitumen emulsion and fines suspension measured individually in 1 mM KCl solution with no pH control. Both bitumen and fine particles displayed a negative ζ potential with the distributions peaked at -64 and -37 mV, respectively. For the binary mixtures, as shown in Figure 6.4 b–c, two distinct ζ potential distribution peaks were observed at the fines to bitumen ratios no bigger than 4. Small shifts of ζ potentials of bitumen and fines from their original values were obtained as a result of partial coverage. Then a single ζ potential

distribution peak was observed in Figure 6.4d when the fines to bitumen ratio was high at 5. The obtained distribution peak centered at -40 mV, which was close to the original value of the fines alone, revealing a complete coverage of the bitumen droplets by the fine particles in this condition. The results indicate that without caustic addition, a significant coverage of fine particles on bitumen surface can be obtained at a fines concentration of ~ 8 g/L. In general, Figure 6.4 shows the occurrence of slime-coating phenomenon of fine solids on bitumen droplets with the deposited fine slimes increased as the fines to bitumen ratio increased. This supported the results in Figure 6.1 that worse slime-coating with increased fines addition hindered bitumen-bitumen coagulation and bitumen-air attachment and as a result reduced bitumen recovery and froth quality.

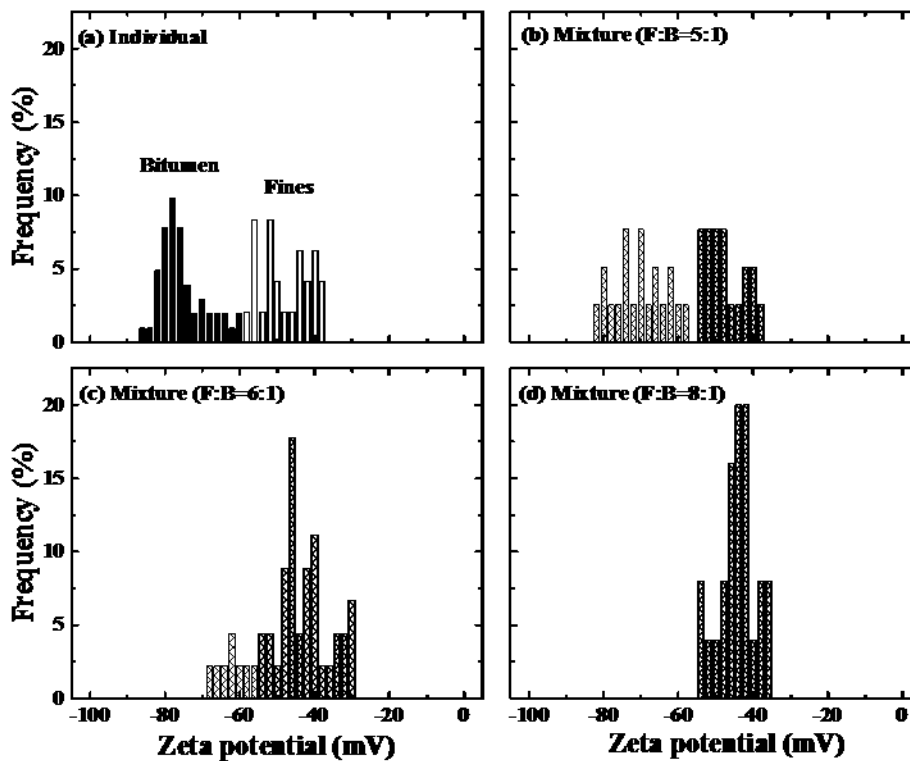


Figure 6.5. ζ potential distributions of bitumen emulsion and fines suspension (a) and their mixtures at 5:1(b), 6:1(c), and 8:1 (d) fines to bitumen mass ratios in 1 mM KCl aqueous solutions of pH 8.0.

Then caustic was added into the solution to increase the solution pH. As expected, ζ potentials of bitumen and fines became more negative at higher pHs. The observed ζ potential distribution peaks of bitumen and fines shifted from -64 and -37 mV to -76 and -49 mV, respectively, as described in Figure 6.5a. In this case, two distinct ζ potential distribution peaks were obtained in a mixture with fines to bitumen ratio at 5, as shown in Figure 6.5b. The positions of these two peaks were similar to those of original bitumen and fines measured separately. At pH 8.0, strong slime-coating of bitumen droplets by fine particles appeared at the fines to bitumen ratio of 6 (Figure 6.5c), and full coverage was observed at the ratio of 8 (Figure 6.5d). These findings demonstrated that the addition of caustic was able to alleviate the slime-coating phenomenon of bitumen droplets by fine particles at normal operation pH.

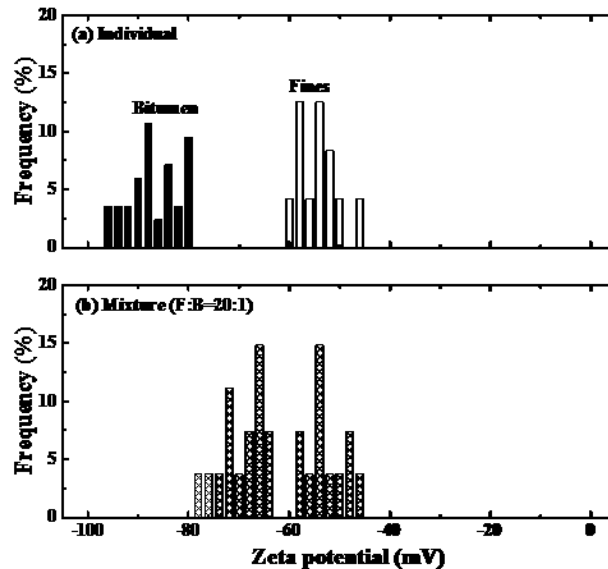


Figure 6.6. ζ potential distributions of bitumen emulsion and fines suspension (a) and their mixture at 20:1 fines to bitumen mass ratio (b) in 1 mM KCl aqueous solutions of pH 10.8.

When the solution pH was further increased to 10.8, satisfactory condition was achieved for the control of slime-coating. As illustrated in Figure 6.6, two distinct ζ potential distribution peaks

were observed in the binary mixture at a fines to bitumen ratio of 20, although the peak corresponding to the original bitumen droplets shifted toward the value of fine particles. Considering the effect of clay concentration on slime-coating, the observed shift in peak position may be accounted for very weak slime-coating. This indicated a drastic depression of slime-coating between fine particles and bitumen droplets at systems with high pH values. To sum up, it was clearly shown in Figures 6.5 and 6.6 that the addition of caustic was able to reduce slime-coating of bitumen by fine particles, even at high fines to bitumen ratios. The more caustic added, the better the performance of slime-coating control. Furthermore, the lower sensitivity of low fines ores to caustic addition than that of high fines ores may be qualitatively related to the less occurrence of slime-coating.

6.3.3 Effect of ore blending on extraction performance

A hypothesis was established that mixing or blending of a high fines ore with a lower fines ore can be used as an alternative method to control the high fines content of the ore and effectively improve the overall processing performance.

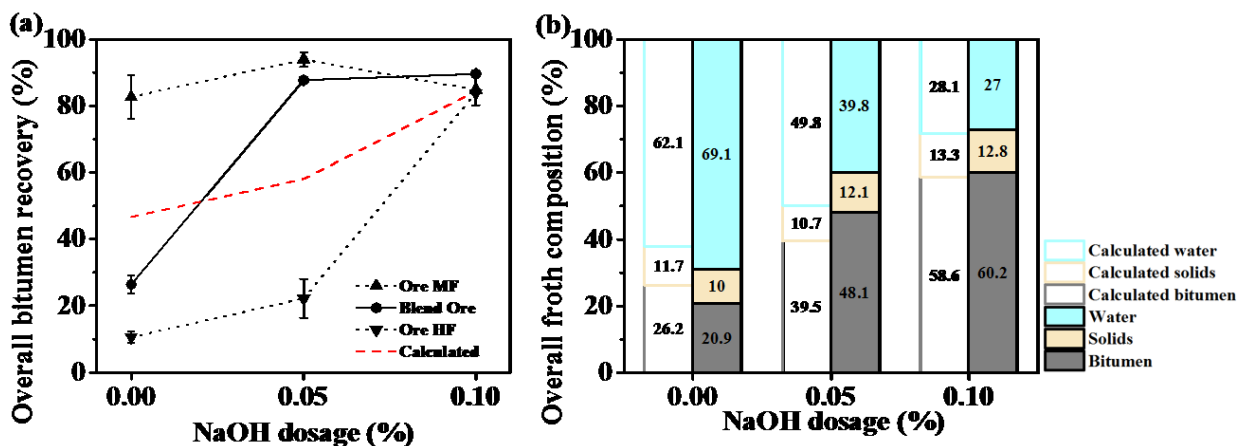


Figure 6.7. Effect of ore blending on (a) bitumen recovery and (b) froth quality of ore MF and ore HF with the addition of NaOH.

Bitumen recovery results of a 1:1 (wt.: wt.) blend of ore HF and ore MF as well as the individual recovery of these two ores are shown in Figure 6.7a. The calculated recovery was the sum of bitumen recovery obtained using each ore by weight fraction. At zero caustic dosage, ore blending did not seem to improve the bitumen recovery performance, since the recovery of the blend at 26% was much lower than the average recovery value of these two ores at 47%. When caustic addition was increased to 0.05%, the overall bitumen recovery of this blend increased dramatically to 88%, which was comparable to that of ore MF at 94%. This confirmed that ore blending can enhance the bitumen recovery of the high fines ore. When caustic concentration was further increased to 0.1%, the bitumen recovery of the blend was 90%. The corresponding froth quality results are shown in Figure 6.7b. As expected, bitumen content and bitumen/solids ratio in the froth improved from the calculated values at 39.5 and 3.7 to 48.1 and 4, respectively, for the blend with 0.05% caustic addition. Combining the results of bitumen recovery and froth quality, 0.05% caustic addition appeared to be optimal to achieve the best overall performance.

The effect of blending ratios on the performance of bitumen extraction was further tested with a fixed caustic content at 0.05%. As shown in Figure 6.8a, the enhancement of bitumen recovery reached a maximum from the calculated value at 58 to 88% at the 50% blending ratio of ore MF. Further increase of ore MF content did not appear to improve bitumen recovery much. Froth quality results shown in Figure 6.8b confirmed the optimal content of ore MF at 50%. Compared to calculated values, bitumen content and bitumen/solids ratio in froth product increased by 22 and 8% at 50% of ore MF content. These increases in froth bitumen content and froth bitumen/solids ratio were 8 and -4% with 25% of ore MF in the blend and were 7 and 2% with 75% of ore MF in the blend. In other word, the negative impacts of high fines content of ore HF can be effectively depressed by blending it with the medium fines ore at 1:1 mass ratio, as the blend reached almost

the performance of the high quality ore (i.e., the MF ores). The overall outcome of Figures 6.7 and 6.8 is that ore blending can be used as an efficient way to improve the processability of ores of high fines content.

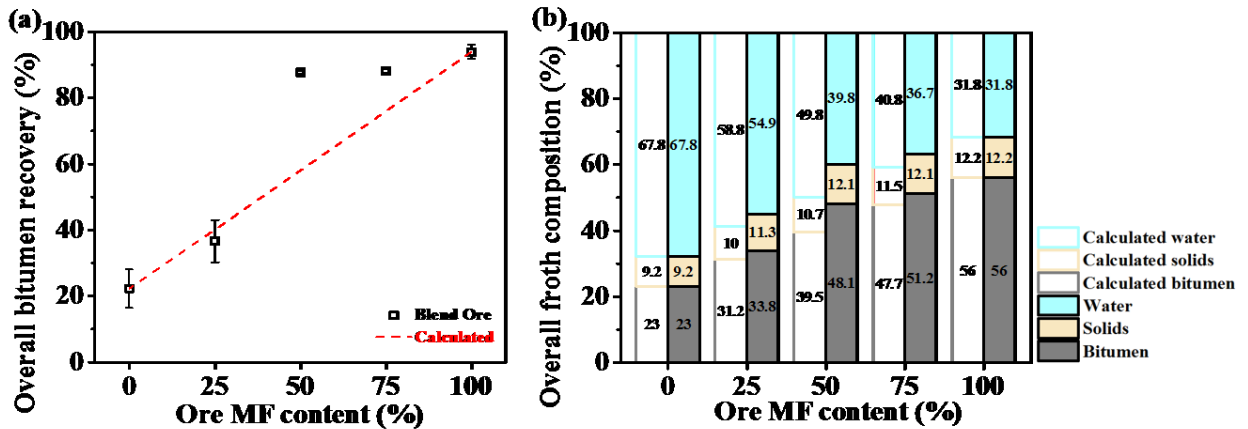


Figure 6.8. Effect of blending ratio on (a) bitumen recovery and (b) froth quality of ore MF and ore HF at 0.05% caustic level.

6.3.3.1 Water chemistry

In order to identify the factors that contribute to the increased bitumen recovery and froth quality of the blended ore, laboratory extracted tailings waters were analyzed to characterize the water chemistry. According to Schramm and Smith (1987), there was a critical surfactant concentration (CSC) which corresponded to the maximum bitumen recovery. If the concentration of carboxylic surfactants was lower than the CSC, bitumen recovery was found to be positively correlated with carboxylic surfactant concentration. While the presence of excess carboxylic surfactants was detrimental to bitumen extraction since they altered surface properties of bitumen and fine solids and resulted in favorable conditions for slime-coating (Bakhtiari et al., 2015).

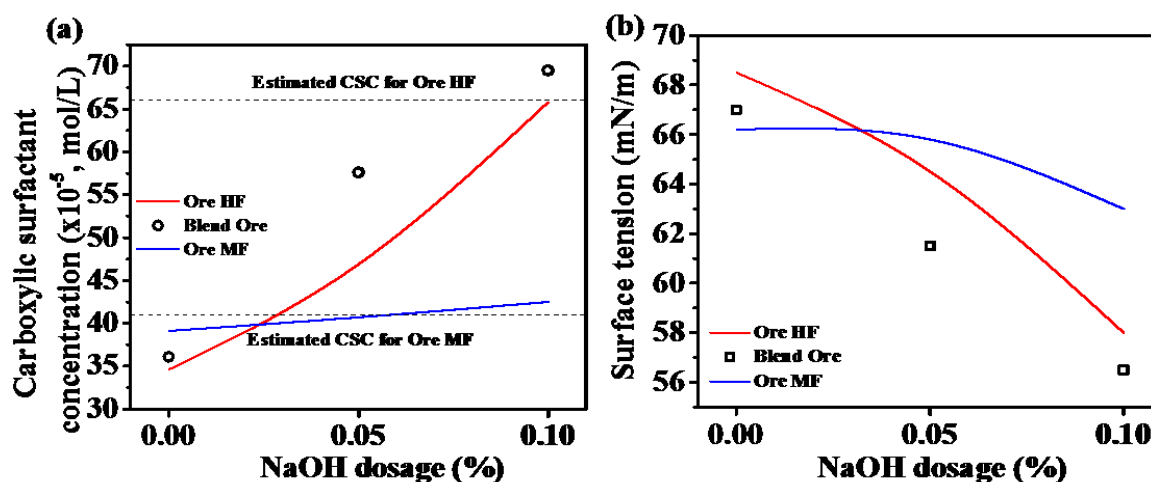


Figure 6.9. Effect of ore blending on (a) carboxylic surfactant concentration and (b) surface tension of tailing water at 3 caustic levels.

Figure 6.9a shows the concentrations of carboxylic surfactants for the corresponding tailings water of ore HF, ore MF, and their 1:1 blend at 3 caustic levels. As expected, an increase in carboxylic surfactant concentration was obtained by increasing the caustic addition regardless of the type of ores. This trend is in good agreement with previous data (Schramm and Smith, 1987; Wik et al., 2008). The estimated CSC for ore HF was $\sim 66 \times 10^{-5}$ mol/L according to the optimal bitumen recovery found in the vicinity of 0.1% caustic addition. Similarly, CSC for ore MF was speculated at $\sim 41 \times 10^{-5}$ mol/L. An interesting phenomenon was indicated in Figure 6.9a that the blend was able to provide carboxylic surfactants at a concentration of 57.6×10^{-5} mol/L in the presence of 0.05% caustic. This value located between the CSCs of two ores. Extra carboxylic surfactants appeared in the process water when as much as 0.1% caustic was added into the system. These findings were consistent with the results of bitumen recovery shown in Figure 6.7a. At 0.05% caustic addition, the bitumen recovery of the blend was significantly improved from the simple average of the two ore recoveries. When 0.1% caustic was added to the system, the increase in bitumen recovery of the blend was insignificant. Also, the difference between the measured and

calculated bitumen recovery values of the blend became smaller than that at 0.05% caustic dosage, indicating less improvement in bitumen recovery by ore blending at 0.1% caustic level. Results in Figure 6.9a revealed that bitumen recovery improvement by ore blending may be related to a facilitated release of carboxylic surfactants.

In order to understand the amount of other types of surfactants such as sulfonic acids in tailings water, surface tensions of the well filtered tailings waters were measured. As expected as shown in Figure 6.9b, surface tensions of tailings water decreased as caustic addition increased. Since the variation trend of surface tensions matched well to that of carboxylic surfactant concentrations, a hypothesis can be obtained that carboxylic surfactants were the major surfactants found in tailings water. In general, Figure 6.9 shows that ore blending is capable of providing suitable surfactants concentrations for both two ores and this improvement in water chemistry may be qualitatively correlated with the enhanced bitumen extraction of the blend. Systematic studies should be conducted in the future to investigate the detailed mechanisms for ore blending to improve bitumen recovery performance. Nevertheless, ore blending was shown to be able to alleviate the negative effects of fine solids on bitumen extraction by mixing with lower fines ores to reduce the apparent fines content of high fines ores.

6.4 EVALUATION STRATEGY: XRF DETERMINED POTASSIUM CONTENT

Figure 6.10 shows a liner correlation between the overall bitumen recovery and the measured potassium content in solids recovered in bitumen froth. The higher the potassium content in froth solids determined by XRF, the less bitumen recovered from the oil sands. The data related to ore G were conducted under the same conditions discussed in the experimental section, no extra fines were added. This indicates that high potassium content in froth solids determined by XRF was a marker for low bitumen recovery in oil sands operations.

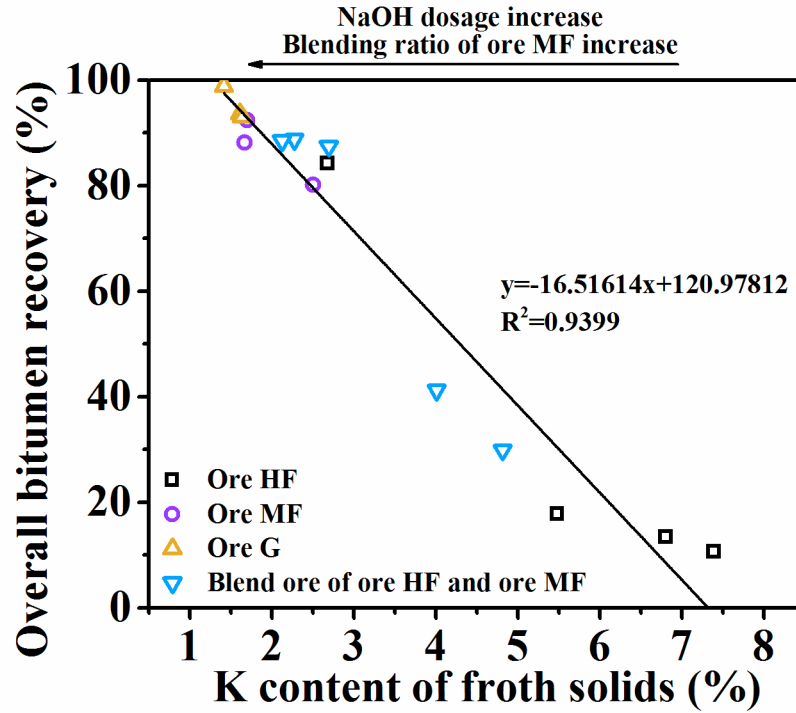


Figure 6.10. Correlation between overall bitumen recovery and XRF determined potassium content in froth solids.

6.5 CONCLUSIONS

Three types of oil sands ores were tested to investigate the role of fine solids in bitumen extraction. Caustic addition and ore blending as coping technologies for high fines ore processing were evaluated and discussed. The followings are found:

- Fines were detrimental to bitumen recovery and froth quality. The more fines added, the worse the performance of bitumen extraction process.
- Results of ζ potential distribution measurement showed that fine particles slime-coated on bitumen droplets at high fines concentrations.
- Addition of caustic reduced the negative effects of fine solids on bitumen extraction. Slime-coating of bitumen droplets by fine particles was diminished at pH 8.0 and removed at pH 10.8.

The required caustic dosage to achieve optimum process conditions increased with increasing fines content in the ores.

- Blending a high fines ore with a lower fines ore seemed to be a promising technique to reduce the detrimental effect of fine solids on bitumen extraction. The suitable blending ratio of the binary mixture depends on the processabilities of two individual ores.
- Optimized surfactant concentration was found to be one of the reasons accounting for improved bitumen recovery and froth quality by ore blending.
- XRF determined potassium content correlated with bitumen recovery discussed in this chapter. The higher the potassium content measured in froth solids, the lower the bitumen recovery obtained.

CHAPTER 7 OVERALL CONCLUSIONS AND FUTURE WORK

7.1 OVERALL CONCLUSIONS

This thesis presents the results of studies on the roles of fine solids (clays) in the water-based bitumen extraction process. The focus was on the effects of clays on bitumen recovery and froth quality. Fundamentally, the effects of clay type, concentration, and wettability on bitumen-bitumen coalescence, bitumen-clay interaction, and bitumen-air bubble attachment were studied.

Experimentally, clays including kaolinite, illite, and montmorillonite were added to an oil sands ore of good processability in the extraction tests. It was found that these clays were detrimental to bitumen extraction and montmorillonite was the worst. Attachment of organic contaminants changed the surfaces of these clays from being hydrophilic to hydrophobic. After contamination, the extraction performance was not affected by the clay type due to the coverage of their surfaces by similar organic matters.

It was found that the detrimental effect of clays in extraction was mainly due to slime-coating. The hetero-coagulation between bitumen and hydrophilic clays was governed by clay concentration. Strong slime-coating of all 3 types of clays, including kaolinite, on bitumen droplets was observed when the clay concentration exceeded a critical value. The critical concentrations of clays in aqueous suspension were suitable to be evaluated by clay deposition between an aqueous phase and a bitumen-water interface. The results showed that the deposition isotherms of the clay particles at the oil-water interface are of the BET multilayer type. By fitting the model parameters, estimates of critical clay concentrations in the process water were obtained. The effects of water chemistry on the deposition of clays on bitumen surfaces were investigated. When the pH of the aqueous phase increased from 5.0~5.6 to 10.8, the critical clay concentrations increased by > 200%. Monovalent (sodium) cations up to 60 mM marginally affected the deposition characteristics of

kaolinite clays on the bitumen droplet surface at pH 8.0. While a more pronounced reduction in the critical clay concentrations was measured with the addition of divalent (calcium) cations at 1–2 mM to the emulsifying water. The low separation levels of added clay particles from oil-water interface at less than 35% confirmed a strong attachment between clays and bitumen at high clay concentrations. Strong slime-coating of hydrophobic clays on bitumen droplets was mainly due to the long-range attractive hydrophobic forces, which led to strong adhesions between bitumen and solids. It was also found that the existence of extra hydrophobic clays in extraction system resulted in small emulsified bitumen droplets, which were difficult to be recovered.

The type and amount of clays in oil sands play an important role in determining the processability of oil sands ores. An attempt was made to use energy dispersive XRF spectroscopy for determination of illite content in oil sands as a first step in developing a viable technique for clay/fines content measurement. Compared with the existing mineralogical methods (e.g. XRD, SEM, other element-based analysis) which often require careful and tedious sample preparation, the analysis by XRF technique is fast, nondestructive, reliable, and robust, requiring no or very little sample preparation. Both potassium contents determined by XRF method and traditional MBT method were shown to be sensitive to illite content in clay mixtures. However, the determination of illite content by XRF method was tested to be more robust and tolerant to contamination of clay surfaces by heavy oil than MBT method. A good correlation between the fines contents and potassium contents was also observed. The XRF method was demonstrated to provide a simple and efficient solution for determination of illite/fines content in oil sands ores and relevant processing streams, and can be potentially used as a diagnosis tool for assessing ore processability. A high potassium content determined by XRF for froth solids was shown to be a marker for low bitumen recovery in extraction tests.

NaOH was often added into the extraction system as a process aid to optimize bitumen extraction performance. It was found that increasing pH of the extraction solution resulted in reduced slime-coating and improved the release of natural surfactants. Increasing NaOH addition could improve bitumen recovery and froth quality when processing high fines ores.

Ore blending was also tested and found to be an effective way to mitigate the negative impact of high fines content on extraction.

7.2 FUTURE WORK

There are several expansions of the present research to be studied in the future:

- In this study, clay concentration was identified to be a governing factor in determining bitumen-clay interactions in the absence of cations. The role of clay concentration in slime-coating in the presence of cations, especially divalent cations, should be discussed.
- Interaction forces between bitumen and real basal planes and edges of clays are worthwhile to be investigated.
- Interactions between clay particles and air bubbles in the extraction system are of great importance. It is suggested to study the slime-coating of clays on air bubbles and its implication in bitumen recovery, froth quality and froth stability.
- Theoretically, the existence of hydrophobic particles in bitumen extraction system would deteriorate froth quality without reduction in bitumen recovery. However, the ability of hydrophobic solids to depress bitumen recovery was shown in previous studies as well as in this research. The detailed mechanisms need to be fully understood.

– A technique based on the XRF determined potassium content was developed as a diagnose tool for clay/fines content in oil sands. It would be worthwhile to investigate the correlations between more elements contents (K, Al, Si, Fe, Cu...) measured by XRF and the oil sands process variables (clay/fines content, bitumen grade, bitumen recovery, water content...). Also, XRF element analysis has potential to be applied in other areas such as process control, pharmacy, and agriculture.

– Two types of oil sands ores vary in fines content were shown to respond differently to NaOH addition. It is suggested to further investigate why different oil sands react differently to chemical aids (NaOH).

– In this thesis, ore blending was shown to optimize the surfactant concentration in bitumen extraction. The behind mechanisms require further exploration.

REFERENCE

Abnet, C. C.; Lai, B.; Qiao, Y.; Vogt, S.; Luo, X.; Taylor, P. R.; Dong, Z.; Mark, S. D.; Dawsey, S. M. (2005). Zinc Concentration in Esophageal Biopsy Specimens Measured by X-ray Fluorescence and Esophageal Cancer Risk. *Journal of the National Cancer Institute*, vol. 97, no. 4, pp. 301-306.

Adegoroye, A.; Uhlik, P.; Omotoso, O.; Xu, Z.; Masliyah, J. (2009). A Comprehensive Analysis of Organic Matter Removal from Clay- Sized Minerals Extracted from Oil Sands Using Low Temperature and Hydrogen Peroxide. *Energy & Fuels*, vol. 23, pp. 3716-3720.

Alagha, L., Wang, S.; Xu, Z.; Masliyah, J. (2011). Adsorption Kinetics of a Novel Organic-Inorganic Hybrid Polymer on Silica and Alumina Studied by Quartz Crystal Microbalance. *The Journal of Physical Chemistry C*, vol. 115, pp. 15390-15402.

Alassane, T.; Mouhamadou, D.; Omar, G. P. E. H.; Ahmadou, W.; Pierre, L.; Ousmane, S.; Souleymane, M. (2013). Characterization of Element and Mineral Content in *Artemisia Annu* and *Camellia Sinensis* Leaves by Handheld X-ray Fluorescence. *African Journal of Biotechnology*, vol. 12, no. 26, pp. 4179-4186.

Alberta Energy Regulator (AER). (2018). Alberta's Energy Reserves and Supply/Demand Outlook. Calgary, Alberta, Canada, ST98-2018.

Alexander, K. L.; Li, D. (1996). Effects of Bitumen Films Over Air Bubble Surfaces on Bitumen Drop – Air Bubble Attachment. *Colloids and Surfaces A: Physicochemical and Engineering Aspects*, vol. 106, pp. 191-202.

Alexandre, T. L.; Bueno, M. I. M. S. (2006). Classification of Some Species, Genera and Families of Plants by X-ray Spectrometry. *X-Ray Spectrometry*, vol. 35, pp. 257-260.

Allen, E. W. (2008). Process Water Treatment in Canada's Oil Sands Industry: 1. Target Pollutants and Treatment Objectives. *Journal of Environmental Engineering and Science*, vol. 7, pp. 123-138.

Allen, J. G.; Mcclean, M. D.; Stapleton, H. M.; Webster, T. F. (2008). Linking PBDEs in House Dust to Consumer Products Using X-ray Fluorescence. *Environmental Science & Technology*, vol. 42, pp. 4222-4228.

Aronson, M. P.; Petko, M. F.; Princen, H. M. (1978). On the Stability of Aqueous Films Between Oil and Silica. *Journal of Colloid and Interface Science*, vol. 65, pp. 296-306.

ASTM C837-09. (Reapproved 2014). *Standard Test Method for Methylene Blue Index of Clay*. ASTM International, West Conshohocken, PA.

Ayling, B.; Rose, P.; Petty, S.; Zemach, E.; Drakos, P. (2012). QEMSCAN[®] (Quantitative Evaluation of Minerals by Scanning Electron Microscopy): Capability and Application to Fracture Characterization in Geothermal Systems. Proceeding of 37th Workshop on Geothermal Reservoir Engineering, Stanford University, Stanford, California.

Bakhtiari, M. T.; Harbottle, D.; Curran, M.; Ng, S.; Spence, J.; Siy, R.; Liu, Q.; Masliyah, J.; Xu, Z. (2015). Role of Caustic Addition in Bitumen-Clay Interactions. *Energy Fuels*, vol. 29, pp. 58-69.

Bakhtiari, M. T. (2015). Role of Sodium Hydroxide in Bitumen Extraction: Production of Natural Surfactants and Slime Coating. Ph.D. Thesis, University of Alberta, Edmonton, Alberta, Canada.

Bakraji, E. H. (2006). Application of Multivariate Statistical Methods to Classify Archaeological Pottery from Tel-Alramad Site, Syria, Based on X-ray Fluorescence Analysis. *X-Ray Spectrometry*, vol. 35, pp. 190-194.

Ball, M. W. (1935). Athabasca Oil Sands: Apparent Example of Local Origin of Oil. *Bulletin of the American Association of Petroleum Geologists*. vol. 19, no. 2, pp. 153-171.

Baptista, M. V.; Bowman, C. W. (1969). The Flotation Mechanism of Solids from the Athabasca Oil Sands. In *19th Canadian Chemical Engineering Conference*, Edmonton, Alberta, Canada.

Basu, S.; Kanda, W. C.; Nandakumar, K.; Masliyah, J. (1998). Effect of Hydrophobic and Hydrophilic Clays on Bitumen Displacement by Water on a Glass Surface. *Industrial & Engineering Chemistry Research*, vol. 37, pp. 959-965.

Basu, S.; Nandakumar, K.; Lawrence, S.; Masliyah, J. (2004). Effect of Calcium Ion and Montmorillonite Clay on Bitumen Displacement by Water on a Glass Surface. *Fuel*, vol. 83, no. 1, pp. 17-22.

Basu, S.; Nandakumar, K.; Masliyah, J. H. (1996). A Study of Oil Displacement on Model Surfaces. *Journal of Colloid and Interface Science*, vol. 182, pp. 82-94.

Basu, S.; Nandakumar, K.; Masliyah, J. H. (1998). Effect of NaCl and MIBC/Kerosene on Bitumen Displacement by Water on a Glass Surface. *Colloids and Surfaces A: Physicochemical and Engineering Aspects*, vol. 136, pp. 71-80.

Basu, S.; Nandakumar, K.; Masliyah, J. H. (1997). On Bitumen Liberation from Oil Sands. *The Canadian Journal of Chemical Engineering*, vol. 75, pp. 476-479.

- Batten, G. D. (2002). Relating Minerals in Rice Shoots and Grain to Soil Tests, Yield and Grain Quality. *A report for Rural Industries Research and Development Corporation*, pp. 1-32.
- Berkowitz, N and Speight, J. G. (1975). The Oil Sands of Alberta. *Fuel*, vol. 54, pp. 138-149.
- Berrezueta, E.; Casado, B. O.; Bonilla, W.; Banda, R.; Castroviejo, R.; Carrión, P.; Puglla, S. (2016). Ore Petrography Using Optical Image Analysis: Application to Zaruma- Portovelo Deposit (Ecuador). *Geoscience*, vol. 6, no. 2, pp. 30.
- Berrezueta, E.; Cuesta, M. J. D.; Casado, B. O.; Medina, C.; Molinero, R. (2017). Pore Space Quantification of Sedimentary Rocks Before-After Supercritical CO₂ Interaction by Optical Image Analysis. *Energy Procedia*, vol. 114, pp. 4382-4393.
- Bish, D. L.; Blake, D. F.; Vaniman, D. T.; Chipera, S. J.; Morris, R. V.; Ming, D. W.; Treiman, A. H.; Sarrazin, P.; Morrison, S. M.; Downs, R. T.; Achilles, C. N.; Yen, A. S.; Bristow, T. F.; Crisp, J. A.; Morookian, J. M.; Farmer, J. D.; Rampe, E. B.; Stolper, E. M.; Spanovich, N.; MSL Science Team (2013). X-ray Diffraction Results from Mars Science Laboratory: Mineralogy of Rocknest at Gale Crater. *Science*, vol. 341, pp. 1238932.
- Bloch, J. M. (1985). Concentration Profile of a Dissolved Polymer Near the Air-Liquid Interface: X-Ray Fluorescence Study. *Physical Review Letters*, vol. 54, no. 10, pp. 1039-1042.
- Boekel, M. V.; Walstra, P. (1981). Stability of Oil-in-Water Emulsions with Crystals in the Disperse Phase. *Colloids and Surfaces*, vol. 3, pp. 109-118.
- Bonizzoni, L.; Galli, A.; Gondola, M.; Martini, M. (2013). Comparison Between XRF, TXRF and PXRF Analysis for Provenance Classification of Archaeological Bricks. *X-Ray Spectrom*, vol. 42, pp. 262-267.

Bortoleto, G. G.; Pataca, L. C. M.; Bueno, M. I. M. S. (2005). A New Application of X-ray Scattering Using Principal Component Analysis – Classification of Vegetable oils. *Analytica Chimica Acta*, vol. 539, pp. 283-287.

Bowman, C. W. (1967). Molecular and Interfacial Properties of Athabasca Tar Sands. In *7th World Petroleum Congress*, Mexico City, Mexico, April 2-9.

Boxill, L. (2011). Potential for Use of Methylene Blue Index Testing to Enhance Geotechnical Characterization of Oil Sands ores and Tailings. *Proceedings Tailings and Mine Waste*, Vancouver, Canada, November 6-9.

Bragg, W. (1913). The Diffraction of Short Electromagnetic Waves by A Crystal. *Proceedings of the Cambridge Philosophical Society*, vol. 17, pp. 43-57.

Brunauer, S.; Emmett, P. H.; Teller, E. (1938). Adsorption of Gases in Multimolecular Layers. *Journal of the American Chemical Society*, vol. 60, no. 2, pp. 309-319.

Calza, C.; Anjos, M. J.; Bueno, M. I. M. S.; Lima, T. A.; Lopes, R. T. (2007). EDXRF Analysis of Marajoara Public Covers. *Nuclear Instruments and Methods in Physics Research B*, vol. 263, pp. 245-248.

Calza, C.; Anjos, M. J.; De Souza, S. M. F. M.; Brancaglion, A. Jr.; Lopes, R. T. (2007). X-ray Microfluorescence Analysis of Pigments in Decorative Paintings from the Sarcophagus Cartonnage of an Egyptian Mummy. *Nuclear Instruments and Methods in Physics Research B*, vol. 263, pp. 249-252.

Carlisle, J. A.; Shirley, E. L.; Hudson, E. A.; Terminello, L. J.; Callcott, T. A.; Jia, J. J.; Ederer, D. L.; Perera, R. C. C.; Himpsel, F. J. (1995). Probing the Graphite Band Structure with Resonant Soft-X-Ray Fluorescence. *Physical Review Letters*, vol. 74, no. 7, pp. 1234-1237.

Carter, W. P. and Mitterer, R. M. (1978). Amino Acid Composition of Organic Matter Associated with Carbonate and Non-carbonate Sediments. *Geochimica et Cosmochimica Acta*, vol. 42, pp. 1231-1238.

Cenens, J. and Schoonheydt, R. A. (1988). Visible Spectroscopy of Methylene Blue on Hectorite, Laponite B, and Barasym in Aqueous Suspension. *Clays and Clay Minerals*, vol. 36, no. 3, pp. 214-224.

Cesareo, R. (2010). X-Ray Fluorescence Spectrometry. *Ullmann's Encyclopedia of Industrial Chemistry*, vol. 39, 595-631.

Chahid, A.; Hilali, M.; Benhachimi, A.; Bouzid, T. (2014). Contents of Cadmium, Mercury and Lead in Fish from the Atlantic Sea (Morocco) Determined by Atomic Absorption Spectrometry. *Food Chemistry*, vol. 147, pp. 357-360.

Chakrabarty, T.; Longo, J. M. (1994). Production Problems in the Steam- Stimulated Shaley Oil Sands of the Cold Lake Reservoir: Cause and Possible Solutions. *The Journal of Canadian Petroleum Technology*, vol. 33, no. 10, pp. 34-39.

Chalaturnyk, R. J.; Scott, J. D.; Özü, B. (2002). Management of Oil Sands Tailings. *Petroleum Science and Technology*, vol. 20, no. 9-10, pp. 1025-1046.

Chave, K. E. (1965). Carbonates: Association with Organic Matter in Surface Seawater. *Science*, vol. 148, pp. 1723-1724.

Chen, Q.; Liu, J.; Thundat, T.; Gray, M. R.; Liu, Q. (2017). Spatially Resolved Organic Coating on Clay Minerals in Bitumen Froth Revealed by Atomic Force Microscopy Adhesion Mapping. *Fuel*, vol. 191, pp. 283-289.

Chen, T.; Lin, F.; Primkulov, B.; He, L.; Xu, Z. (2017). Impact of Salinity on Warm Water-Based Mineable Oil Sands Processing. *The Canadian Journal of Chemical Engineering*, vol. 95, pp. 281-289.

Chenu, C.; Bissonnais, Y. L.; Arrouays, D. (2000). Organic Matter Influence on Clay Wettability and Soil Aggregate Stability. *Soil Science Society of America Journal*, vol. 64, pp. 1479-1486.

Chenu, C. (2006). *Soils: Basic Concepts and Future Challenges*. Cambridge University Press, Cambridge, UK.

Chew, K. J. (2014). The Future of Oil: Unconventional Fossil Fuels. *Philosophical Transactions of the Royal Society A*, vol. 372, pp. 20120324.

Chong, J.; Ng, S.; Chung, K. H.; Sparks, B.D.; Kotlyar, L. S. (2003). Impact of Fines Content on a Warm Slurry Extraction Process using Model Oilsands. *Fuel*, vol. 82, pp. 425-438.

Clapera, R. S. (2006). Energy Dispersive X-Ray Fluorescence: Measuring Elements in Solids and Liquid Matrices. Final Degree Project (Enginyeria Tèc. Ind. Química Industrial). Universitat de Girona (Escola Politècnica Superior).

Clark, K. A. (1929). The Separation of the Bitumen from Alberta Bituminous Sands. *Bulletin of the Canadian Institute of Mining and Metallurgy*, vol. 22, pp. 1385-1395.

Clark, K. A. (1944). Hot Water Separation of Alberta Bituminous Sand. *Transactions of the Canadian Institute of Mining and Metallurgy*, vol. 47, pp. 257-274.

Clark, K. A. and Pasternack, D. S. (1932). Hot Water Separation of Bitumen from Alberta Bituminous Sand. *Industrial and Engineering Chemistry*. vol. 24, pp. 1410-1416.

Clemente, J; Fedorak, P. (2005) A Review of the Occurrence, Analyses, Toxicity and Biodegradation of Naphthenic Acids. *Chemosphere*, vol. 60, pp. 585-600.

CONRAD Clay Focus Group. (2012). Methylene Blue Procedure for Dean Stark Solis.

Cuddy, G. (2004). Oil Sands Geology. *Guest Lecture Notes for Chemical Engineering 534, Fundamentals of Oil Sands Extraction*, University of Alberta, Edmonton, Canada, January 7-9.

Cui, Y.; Vogt, S.; Olson, N.; Glass, A. G.; Rohan, T. E. (2007). Levels of Zinc, Selenium, Calcium, and Iron in Benign Breast Tissue and Risk of Subsequent Breast Cancer. *Cancer Epidemiology, Biomarkers & Prevention*, vol. 16, no. 8, pp. 1682-1685.

Currie, R.; Bansal, S.; Khan, I.; Mian, H. (2014). An Investigation of the Methylene Blue Titration Method for Clay Activity of Oil Sands Samples. Oil Sands Research and Information Network, University of Alberta, School of Energy and the Environment, Edmonton, Alberta. *OSRIN Report No. TR-60*. 50 pp.

Dai, Q.; Chung, K. H. (1995). Bitumen-Sand Interaction in Oil Sand Processing. *Fuel*, vol. 74, pp. 1858-1864.

Dai, Q.; Chung, K. H.; Czarniecki, J. (1992). Formation of Calcium Carbonate in the Bitumen/Aqueous Sodium Hydroxide System. *AOSTRA Journal of Research*, vol. 8, no. 2, pp. 95-101.

- Dang-Vu, T.; Jha, R.; Wu, S.; Tannant, D. D.; Masliyah, J.; Xu, Z. (2009). Wettability Determination of Solids Isolated from Oil Sands. *Colloids and Surfaces A: Physicochemical and Engineering Aspects*, vol. 337, pp. 80-90.
- Debye, P. and Hückel, E. (1923). The Theory of Electrolytes. I. Lowering of Freezing Point and Related Phenomena. *Physikalische Zeitschrift*, vol. 24, pp. 185-206.
- Devi, K. N.; Sarma, H. N.; Kumar, S. (2008). Estimation of Essential and Trace Elements in Some Medicinal Plants by PIXE and PIGE Techniques. *Nuclear Instruments and Methods in Physics Research*, vol. 266, pp. 1605-1610.
- De Vries, J. L.; Vrebos, B. A. R. (2002). Quantification of Infinitely Thick Specimens by XRF Analysis. In *Handbook of X-Ray Spectrometry*, 2nd Edition, Marcel Dekker, New York, pp. 341-405.
- Dik, J.; Janssens, K.; Snickt, G. V. D.; Loeff, L. V. D.; Rickers, K.; Cotte, M. (2008). Visualization of a Lost Painting by Vincent Van Gogh Using Synchrotron Radiation Based X-ray Fluorescence Elemental Mapping. *Analytical Chemistry*, vol. 80, pp. 6436-6442.
- Ding, M.; Zhang, Y.; Liu, J.; Jia, W.; Hu, B.; Ren, S. (2014). Application of Microbial Enhanced Oil Recovery Technology in Water-Based Bitumen Extraction from Weathered Oil Sands. *AIChE Journal*, vol. 60, no. 8, pp. 2985-2993.
- Ding, X.; Repka, C.; Xu, Z.; Masliyah, J. (2006). Effect of Illite Clay and Divalent Cations on Bitumen Recovery. *The Canadian Journal of Chemical Engineering*, vol. 84, pp. 643-650.
- Di Stefano, C.; Ferro, V.; Mirabile, S. (2010). Comparison Between Grain-Size Analyses Using Laser Diffraction and Sedimentation Methods. *Biosystems Engineering*, vol. 106, pp. 205-215.

Dittrich, S.; Neubauer, J.; Goetz-Neunhoeffler, F. (2014). The Influence of Fly Ash on The Hydration of OPC Within the First 44 h – A Quantitative in situ XRD and Heat Flow Calorimetry Study. *Cement and Concrete Research*, vol. 56, pp. 129-138.

Doesthale, Y. G.; Devara, S.; Rao, S.; Belavady, B. (1979). Effect of Milling on Mineral and Trace Element Composition of Raw and Parboiled Rice. *Journal of the Science of Food and Agriculture*, vol. 30, pp. 40-46.

Donkor, K. K.; Kratochvil, B.; Duke, M. J. M. (1996). Estimation of the Fines Content of Athabasca Oil Sands Using Instrumental Neutron Activation Analysis. *Canadian Journal of Chemistry*, vol. 74, pp. 583-590.

Donskoi, E.; Manuel, J. R.; Austin, P.; Poliakov, A.; Peterson, M. J.; Hapugoda, S. (2013). Comparative Study of Iron Ore Characterization Using a Scanning Electron Microscope and Optical Image Analysis. *Applied Earth Science*, vol. 122, no. 4, pp. 217-229.

Donskoi, E.; Poliakov, A.; Manuel, J. R. (2015). Automated Optical Image Analysis of Natural and Sintered Iron Ore. *Iron Ore*, pp. 101-159.

Donskoi, E.; Poliakov, A.; Manuel, J. R.; Peterson, M.; Hapugoda, S. (2015). Novel Developments in Optical Image Analysis for Iron Ore, Sinter and Coke Characterisation. *Applied Earth Science*, vol. 124, no. 4, pp. 227-244.

Dos Anjos, M. J.; Lopes, R. T.; De Jesus, E. F. O.; Assis, J. T.; Cesareo, R.; Barradas, C. A. A. (2000). Quantitative Analysis of Metals in Soil Using X-ray Fluorescence. *Spectrochimica Acta Part B*, vol. 55, pp. 1189-1194.

Dougan, P. and McDoWell, K. (1997). Sensor Development in Oil Sands Processing. In: M. Kothare, M. Tade, A. V. Wouwer, I. Smets (Eds.), Proceedings of the Dynamic Modelling Control Application for Industry Workshop, IEEE Industry Applications Society, Leuven, Belgium, pp. 68-73.

Drelich, J. (2013). Guidelines to Measurements of Reproducible Contact Angles Using a Sessile-Drop Technique. *Surface Innovations*, vol. 1, no. 4, pp. 248-254.

Ducker, W. A.; Senden, T. J. (1992). Measurement of Forces in Liquids Using a Force Microscope. *Langmuir*, vol. 8, pp. 1831-1836.

Edzwald, J. K.; Upchurch, J. B.; O'Melia, C. R. (1974). Coagulation in Estuaries. *Environmental Science & Technology*, vol. 8, pp. 58-63.

El-Nadi, Y. A.; Awwad, N. S.; Nayl, A. A. (2009). A Comprehensive Study of Vanadium Extraction by Aliquat-336 from Acidic and Alkaline Media with Application to Spent Catalyst. *International Journal of Mineral Processing*, vol. 90, pp. 115-120.

Essington, M. E. (2004). *Soil and Water Chemistry: An Integrative Approach*. CRC Press, Boca Raton.

Evans, L. T. and Russell, E. W. (1959). The Adsorption of Humic and Fulvic Acids by Clays. *Journal of Soil Science*, vol. 10, pp. 119-132.

Falconer J. G. and Mattson, S. (1933). The Laws of Soil Colloidal Behavior: XIII. Osmotic Imbibition. *Soil Science*, vol. 36, no. 4, pp. 317.

Fandrich, R.; Gu, Y.; Burrows, D.; Moeller, K. (2007). Modern SEM-Based Mineral Liberation Analysis. *International Journal of Mineral Processing*, vol. 84, no. 1-4, pp. 310-320.

Figuerola, G.; Moeller, K.; Buhot, M.; Gloy, G.; Haberla, D. (2012). Advanced Discrimination of Hematite and Magnetite by Automated Mineralogy. *Proceedings of the 10th International Congress for Applied Mineralogy (ICAM)*, pp. 197-204.

Fityus, S. G.; Smith, D. W.; Jennar, A. M. (2000) Surface Area Using Methylene Blue Adsorption as a Measure of Soil Expansivity. In *Geo 2000 Conference*, Melbourne, Australia (on CD).

Flury, C.; Afacan, A.; Bakhtiari, M. T.; Sjoblom, J.; Xu, Z. (2014). Effect of Caustic Type on Bitumen Extraction from Canadian Oil Sands. *Energy Fuels*, vol. 28, pp. 431-438.

Flynn, M.; Bara, B.; Czarnecki, J.; Masliyah, J. (2001). An Investigation of the Effect of Air Addition During Oil Sand Conditioning. *The Canadian Journal of Chemical Engineering*, vol. 79, pp. 468-470.

Fong, N.; Ng, S.; Chung, K.; Tu, Y.; Li, Z.; Sparks, B.; Kotlyar, L. (2004). Bitumen Recovery from Model System Using a Warm Slurry Extraction Process: Effect of Oilsands Components and Process Water Chemistry. *Fuel*, vol. 83, no. 14-15, pp. 1865-1880.

Fornili, S.L.; Sgroi, G.; Izzo, V. (1981). Solvent Isotope Effect in the monomer-Dimer Equilibrium of Methylene Blue. *Journal of the Chemical Society, Faraday Transactions 1*, vol. 77, pp. 3049-3053.

Franzini, M.; Leoni, L.; Saitta, M. (1972). A Simple Method to Evaluate the Matrix Effects in X-ray Fluorescence Analysis. In *X-ray Spectrometry*, 1st Edition, Institute of Mineralogy and Petrology, University of Pisa, Italy, pp. 151-154.

Freitas, R. P.; Calza, C.; Lima, T. A.; Rabello, A.; Lopes, R. T. (2010). EDXRF and Multivariate Statistical Analysis of Fragments from Marajoara Ceramics. *X-Ray Spectrometry*, vol. 39, pp. 307-310.

Friedrich, W.; Knipping, P.; Laue, M. (1912). Sitzungsberichte Der Mathematisch-Physikalischen Klasse Der Koeniglich Bayerischen Akademie Der Wissenschaften Zu Muenchen. *Proceedings of Bavarian Academy of Science*, pp.303-322.

Fu, D.; Woods, J. R.; Kung, J.; Kingston, D. M.; Kotlyar, L. S.; Sparks, B. D.; Mercier, P. H. J.; McCracken, T.; Ng, S. (2010). Residual Organic Matter Associated with Toluene-Extracted Oil Sands Solids and Its Potential Role in Bitumen Recovery via Adsorption onto Clay Minerals. *Energy Fuels*, vol. 24, pp. 2249-2256.

Fuerstenau, D. W. (1980). Fine Particle Flotation. In *Fine Particle Processing*, Somasundaran, P., Eds., The Society of AIME, New York, pp. 669-705.

Gaudette, H. E.; Eades, J. L.; Grim, R. E. (1966). The nature of illite. In *13th National Conference on Clays and Clay Minerals*, pp. 33-48.

Gelot, A.; Friesen, W.; Hamza, H. A. (1984). Emulsification of Oil and Water in the Presence of Finely Divided Solids and Surface-Active Agents. *Colloids and Surfaces*, vol. 12, pp. 271-303.

Geraki, K.; Farquharson, M. J.; Bradley, D. A. (2002). Concentrations of Fe, Cu and Zn in Breast Tissue: A Synchrotron XRF study. *Physics in Medicine and Biology*, vol. 47, pp. 2327-2339.

Giacomo, F. D.; Signore, A. D.; Giaccio, M. (2007). Determining the Geographic Origin of Potatoes Using Mineral and Trace Element Content. *Journal of Agricultural and Food Chemistry*, vol. 55, pp. 860-866.

- Giesy, J. P.; Anderson, J. C.; Wiseman, S. B. (2010). Alberta Oil Sands Development. *Proceedings of the National Academy of Sciences of the United States of America*, vol. 107, no. 3, pp. 951-952.
- Gillott, J. E. (1987). *Clay in Engineering Geology*. Elsevier, New York.
- Gomes, O. F. M.; Iglesias, J. C. A.; Paciornik, S.; Vieira, M. B. (2013). Classification of Hematite Types in Iron Ores Through Circularly Polarized Light Microscopy and Image Analysis. *Minerals Engineering*, vol. 52, pp. 191-197.
- Goodall, W. R. (2008). Automated Mineralogy in the Prediction of Acid Rock Drainage: Accessible Mineralogy Using QEMSCAN. Proceedings of the 2008 Society for Mining, Metallurgy and Exploration (SME) Annual Meeting and Exhibit, Salt Lake City, Utah, Society for Mining, Metallurgy and Exploration Inc., United States.
- Greenland, D. J. (1971). Interactions Between Humic and Fulvic Acids and Clays. *Soil Science*, vol. 111, pp. 34-41.
- Gribble, C. D.; Hall, A. J. (1992). *Optical Mineralogy: Principles and Practice*. CRC Press, London, NY.
- Grim, R. E. (1953). *Applied Clay Mineralogy*. McGraw Hill Book Company Inc., New York.
- Grim, R. E. (1968). *Clay Mineralogy*, 2nd Edition, McGraw-Hill Book Company Inc., New York.
- Gu, G.; Sanders, R.; Nandakumar, K.; Xu, Z.; Masliyah, J. (2004). A Novel Experimental Technique to Study Single Bubble-Bitumen Attachment in Flotation. *International Journal of Mineral Processing*, vol. 74, pp. 15-29.

Gu, G.; Xu, Z.; Nandakumar, K.; Masliyah, J. (2003). Effects of Physical Environment on Induction Time of Air-Bitumen Attachment. *International Journal of Mineral Processing*, vol. 69, pp. 235-250.

Gu, G.; Xu, Z.; Nandakumar, K.; Masliyah, J. H. (2002). Influence of Water-Soluble and Water-Insoluble Natural Surface Active Components on the Stability of Water-In-Toluene-Diluted Bitumen Solution. *Fuel*, vol. 81, pp. 1859-1869.

Gu, G.; Zhou, Z.; Xu, Z.; Masliyah, J. H. (2003). Role of Fine Kaolinite Clay in Toluene-Diluted Bitumen/Water Emulsion. *Colloids and Surfaces A: Physicochemical and Engineering Aspects*, vol. 215, pp. 141-153.

Gu, Y. (2003). Automated Scanning Electron Microscopy Based Mineral Liberation Analysis: An Introduction to JKMRC/FEI Mineral Liberation Analyser. *Journal of Minerals & Materials Characterization & Engineering*, vol. 2, no. 1, pp. 33-41.

Hall, A. C.; Collins, S. H.; Melrose, J. C. (1983). Stability of Aqueous Wetting Films in Athabasca Tar Sands. *Society of Petroleum Engineers Journal*, vol. 23, no. 2, pp. 249-258.

Hang, P. T. and Brindley, G. W. (1970). Methylene Blue Adsorption by Clay Minerals: Determination of Surface Areas and Cation Exchange Capacities (Clay Organic Studies XVIII). *Clay and Clay Minerals*, vol. 18, pp. 203-212.

Harhira, A.; Haddad, J. E.; Blouin, A.; Sabsabi, M. (2018). Rapid Determination of Bitumen Content in Athabasca Oil Sands by Laser-Induced Breakdown Spectroscopy. *Energy Fuels*, vol. 32, pp. 3189-3193.

He, F.; Espen, P. J. V. (1991). General Approach for Quantitative Energy Dispersive X-ray Fluorescence Analysis Based on Fundamental Parameters. *Analytical Chemistry*, vol. 63, pp. 2237-2244.

Hepler, L. G.; Hsi, C. (1989). AOSTRA Technical Handbook on Oil Sands, Bitumen and Heavy Oils. In *AOSTRA Technical Publication Series #6*, Alberta Oil Sands Technology and Research Authority, Edmonton, AB, Canada.

Hepler, L. G. and Smith, R. G. (1994). The Alberta Oil Sands: Industrial Procedures for Extraction and Some Recent Fundamental Research, In *AOSTRA technical publication series # 14*, Alberta Oil Sands Technology and Research Authority, Edmonton, Alberta.

Heckel, J.; Haschke, M.; Brumme, M. (1992). Principles and Applications of Energy-Dispersive X-ray Fluorescence Analysis with Polarized Radiation. *Journal of Analytical Atomic Spectrometry*, vol. 7, pp. 281- 286.

Helsen, J. A.; Kuczumow, A. (1993). Wavelength-Dispersive X-ray Fluorescence. In *Handbook of X-ray Spectrometry: Methods and Techniques*, Marcel Dekker, Inc., New York, pp. 75-149.

Hendrickson, T. A. (1975). *Synthetic Fuels Data Handbook*. Cameron Engineers, the United State.

Henley, K. J. (1992). A Review of Recent Developments in the Process Mineralogy of Gold. Extractive Metallurgy of Gold and Base Metals, Kalgoorlie, Proceedings, pp. 177-194.

Henriques, C. B.; Alves, J. C. L.; Poppi, R. J.; Filho, R. M.; Bueno, M. I. M. S. (2013). X-ray Spectroscopy and Chemometric Methods for Real-Time Characterization of Petroleum for the Refining Process Through True Boiling Point Curve and American Petroleum Institute Gravity. *Energy Fuels*, vol. 27, pp. 3014-3021.

Heraldy, E.; Rahmawati, F.; Heryanto; Putra, D. P. (2017). Application of Quantitative XRD on the Precipitation of Struvite from Brine Water. *IOP Conference Series: Materials Science and Engineering*, vol. 172, pp. 012015.

Hestnes, K. H.; Sørensen, B. E. (2012). Evaluation of Quantitative X- ray Diffraction for Possible Use in the Quality Control of Granitic Pegmatite in Mineral Production. *Minerals Engineering*, vol. 39, pp. 239-247.

Heyes, A.; Leach, A.; Mason, C. F. (2018). The Economics of Canadian Oil Sands. *Review of Environmental Economics and Policy*, vol. 12, pp. 242-263.

Hillier, S. (2000). Accurate Quantitative Analysis of Clay and Other Minerals in Sandstones by XRD: Comparison of a Rietveld and a Reference Intensity Ratio (RIR) Method and The Importance of Sample Preparation. *Clay Minerals*, vol. 35, pp. 291-302.

Hogg, R.; Healy, T. W.; Fuerstenau, D. W. (1966). Mutual Coagulation of Colloidal Dispersions. *Transactions of the Faraday Society*, vol. 62, pp. 1638-1651.

Hupka, J.; Miller, J. D.; Cortez, A. (1983). Importance of Bitumen Viscosity in the Hot Water Processing of Domestic Tar Sands. *Mining Engineering*, vol. 35, no.12, pp. 1635-1641.

Hutton, A. C.; Mandile, A. J. (1996). Quantitative XRD Measurement of Mineral Matter in Gondwana Coals Using the Rietveld Method. *Journal of African Earth Sciences*, vol. 23, no. 1, pp. 61-72.

Itokumbul, M. T.; Kosaric, N.; Bulani, W.; Cairns, W. L. (1985). Froth Flotation for the Beneficiation of Heavy Minerals from Oil Sand Tailings. *AOSTRA Journal of Research*. vol. 2, pp. 59-66.

- Jacks, G. V. (1963). The Biological Nature of Soil Productivity. *Soils Fert*, vol. 26, pp. 147-150.
- Jacques, M. T.; Hovarongkura, A. D.; Henry Jr, J. D. (1979). Feasibility of Separation Processes in Liquid-Liquid Solid Systems: Free Energy and Stability Analysis. *AIChE Journal*, vol. 25, pp. 160-170.
- Jada, A and Debih, H. (2009). Hydrophobation of Clay Particles by Asphaltenes Adsorption. *Composite Interfaces*, vol. 16, no. 2-3, pp. 219-235.
- Janeth, L. (2005). Fundamental Study of the Role of Fines in Upgrading. M.S. Thesis. University of Alberta, Edmonton, Alberta, Canada.
- Jenkins, R. (1999). *X-Ray Fluorescence Spectrometry*. 2nd Edition, John Wiley & Sons, Inc., New York.
- Jiang, S. L.; Wu, J. G.; Feng, Y.; Yang, X. E.; Shi, C. H. (2007). Correlation Analysis of Mineral Element Contents and Quality Traits in Milled Rice. *Journal of Agricultural and Food Chemistry*, vol. 55, pp. 9608-9613.
- Jiang, T.; Hirasaki, G. J.; Miller, C. A.; Ng, S. (2011). Effects of Clay Wettability and Process Variables on Separation of Diluted Bitumen Emulsion. *Energy & Fuels*, vol. 25, pp. 545-554.
- Jivraj, M.; Mackinnon, M.; Fung, B. (1995) Naphthenic Acids Extraction and Quantitative Analysis with FT-IR Spectroscopy. *Syncrude Analytical Manuals*, 4th Edition, Research Department, Syncrude Canada, Ltd., Edmonton, Alberta, Canada.
- Jones, M. P.; Gravidovic, J. (1970). Automatic Quantitative Mineralogy in Mineral Technology, *Rudy*, vol. 5, pp. 189-197.

Jordán, A. (2014). Lightening the Clay (I). EGU blog network.
<https://blogs.egu.eu/divisions/sss/2014/09/05/lightening-the-clay-i/>

Kahle, M.; Kleber, M.; Jahn, R. (2002). Review of XRD-Based Quantitative Analyses of Clay Minerals in Soils: The Suitability of Mineral Intensity Factors. *Geoderma*, vol. 109, pp. 191-205.

Kahr, G., and Madsen, F. T. (1995). Determination of the Cation Exchange Capacity and the Surface Area of Bentonite, Illite and Kaolinite by Methylene Blue Adsorption. *Applied Clay Science*, vol. 9, pp. 327-336.

Kakali, G.; Perraki, T.; Tsvivilis, S.; Badogiannis, E. (2001). Thermal Treatment of Kaolin: The Effect of Mineralogy on the Pozzolanic Activity. *Applied Clay Science*, vol. 20, pp. 73-80.

Kaminsky, H.A.W. (2008). Characterization of an Athabasca Oil Sands Ore and Process Streams. Ph.D. Thesis, University of Alberta, Edmonton, Alberta, Canada.

Kaminsky, H.A.W. (2010). Clay Minerals and Why They're Important in Oil Sands. In *CONRAD Clay Workshop*, Edmonton, AB, Canada, March 8.

Kaminsky, H. A. W. (2014). Demystifying the Methylene Blue Index. Proceedings of the 4th International Oil Sands Tailings Conference, Lake Louise, AB, Canada, December 7-10.

Kaminsky, H. A. W.; Etsell, T. H.; Ivey, D. G.; Omotoso, O. (2008). Characterization of Heavy Minerals in the Athabasca Oil Sands. *Minerals Engineering*, vol. 21, pp. 264-271.

Kasongo, T. (2006). Role of Fine Clays and Ionic Species in Bitumen Extraction from Oil Sands Ores Using the Hot Water Extraction Process. Ph.D. Thesis, University of Alberta, Edmonton, Alberta, Canada.

- Kasongo, T.; Zhou, Z.; Xu, Z.; Masliyah, J. (2000). Effect of Clays and Calcium Ions on Bitumen Extraction from Athabasca Oil Sands Using Flotation. *The Canadian Journal of Chemical Engineering*, vol. 78, pp. 674-681.
- Katari, J. E. B.; Colvin, V. L.; Alivisatos, A. P. (1994). X-ray Photoelectron Spectroscopy of CdSe Nanocrystals with Applications to Studies of the Nanocrystal Surface. *The Journal of Physical Chemistry*, vol. 98, no. 15, pp. 4109-4117.
- Kelly, W.J. (1984). Review of the Methylene Blue Test. *Ceramic Engineering Science Proceedings*, vol. 5, no. 11-12, pp. 886-894.
- Khademi, S. (2012). Effect of Solid Contamination on Stability of Model Oil-Water Emulsions. M.S. Thesis, University of Alberta, Edmonton, Alberta, Canada.
- Klein, C., Harbottle, D.; Alagha, L.; Xu, Z. (2013). Impact of Fugitive Bitumen on Polymer-Based Flocculation of Mature Fine Tailings. *The Canadian Journal of Chemical Engineering*, vol. 91, pp. 1427-1432.
- Kotlyar, L. S.; Kodama, H.; Sparks, B. D.; Grattan-Bellew, P. E. (1987). Non-Crystalline Inorganic Matter-Humic Complexes in Athabasca Oil Sand and Their Relationship to Bitumen Recovery. *Applied Clay Science*, vol. 2, pp. 253-271.
- Kotlyar, L. S.; Ripmeester, J. A.; Sparks, B. D. (1988). Comparative Study of Organic Rich Solids Present in Utah and Athabasca Oil Sands. In *The Future of Heavy Crude and Tar Sands*, UNITAR, Paper No. 16, Preprint 1, pp.10.
- Kotlyar, L. S. and Sparks, B. D. (1985). Isolation of Inorganic Matter-Humic Complex from Athabasca Oil Sands. *AOSTRA Journal of Research*, vol. 2, pp. 103-111.

Kotlyar, L. S.; Sparks, B. D.; Kodama, H. (1984a). Isolation and Characterization of Various Types of Organic Matter in Oil Sands Tailings Sludge. *AOSTRA Journal of Research*, vol. 1, pp. 99-106.

Kotlyar, L. S.; Sparks, B. D.; Kodama, H. (1984b). Some Chemical and Mineralogical Properties of Fine Solids Derived from Oil Sands. *AOSTRA Journal of Research*, vol. 1, no. 2, pp. 99-106.

Kwitko-Ribeiro, R. (2012). New Sample Preparation Developments to Minimize Mineral Segregation in Process Mineralogy. Proceedings of the 100th International Congress for Applied Mineralogy (ICAM). pp. 411-417.

Lamberg, P. (2011). Particles—The Bridge Between Geology and Metallurgy. In *Conference in Mineral Engineering*, Luleå, Sweden, February 8-9, Proceedings, pp. 1-16.

Lamberg, P.; Hautala, P.; Sotka, P.; Saavalainen, S. (1997). Mineralogical Balances by Dissolution Methodology. In *Short Course on 'Crystal Growth in Earth Science'*, S.Mamede de Infesta, Portugal, September 8-10, Proceedings, pp. 1-29.

Lamberg, P.; Paria, M.; Mwangi, A.; Rosenkranz, J. (2013). Mineralogical Mass Balancing of Industrial Circuits by Combining XRF and XRD analyses. In *Conference in Mineral Engineering*, Luleå, Sweden, February 8-9, Proceedings, pp. 1-16.

Landis, M. S.; Pancras, J. P.; Graney, J. R.; White, E. M.; Edgerton, E. S.; Legge, A.; Percy, K. E. (2017). Source Apportionment of Ambient Fine and Coarse Particulate Matter at the Fort McKay Community Site, in the Athabasca Oil Sands Region, Alberta, Canada. *Science of the Total Environment*, vol. 584-585, pp. 105-117.

Lastra, R.; Petruk, W. (2014). Mineralogical Characterization of Sieved and Un-Sieved Samples. *Journal of Minerals and Materials Characterization and Engineering*, vol. 2, pp. 40-48.

- Lavina, B.; Dera, P.; Downs, R. T. (2014). Modern X-ray Diffraction Methods in Mineralogy and Geosciences. *Reviews in Mineralogy & Geochemistry*, vol. 78, pp. 1-31.
- Leake, B. E.; Hendry, G. L.; Kemp, A.; Plant, A. G.; Harrey, P. K.; Wilson, J. R.; Coats, J. S.; Aucott, J. W.; Lünel, T.; Howarth, R. J. (1969/1970). The Chemical Analysis of Rock Powders by Automatic X-ray Fluorescence. *Chemical Geology*, vol. 5, pp. 7-86.
- Li, H.; Long, J.; Xu, Z.; Masliyah, J. (2008). Novel Polymer Aids for Low-Grade Oil Sands Ore Processing. *Canadian Journal of Chemical Engineering*, vol. 86, no. 2, pp. 168-176.
- Li, H.; Wei, S.; Qing, C.; Yang, J. (2003). Discussion on the Position of the Shear Plane. *Journal of Colloid and Interface Science*, vol. 258, pp. 40-44.
- Li, S.; Pang, X.; Jin, Z.; Yang, H.; Xiao, Z.; Gu, Q.; Zhang, B. (2010). Petroleum Source in the Tazhong Uplift, Tarim Basin: New Insights from Geochemical and Fluid Inclusion Data. *Organic Geochemistry*, vol. 41, pp. 531-553.
- Li, Z.; Wang, C. J.; Jiang, W. T. (2010). Interaction of Methylene Blue in a High-charge Calcium Montmorillonite –An indication of Surface Charge Determination. *Adsorption Science & Technology*, vol. 28, no. 4, pp. 297-312.
- Liao, C.; Zeng, L.; Shih, K. (2015). Quantitative X-ray Diffraction (QXRD) analysis for Revealing Thermal Transformations of Red Mud. *Chemoshpere*, vol. 131, pp. 171-177.
- Little, L.; Becker, M.; Wiese, J.; Mainza, A. N. (2015). Auto-SEM Particle Shape Characterisation: Investigating Fine Grinding of UG2 Ore. *Minerals Engineering*, vol. 82, pp. 92-100.

- Liu, J.; Xu, Z.; Masliyah, J. (2004a). Interaction Between Bitumen and Fines in Oil Sands Extraction System: Implication to Bitumen Recovery. *Canadian Journal of Chemical Engineering*, vol. 82, no. 4, pp. 655-666.
- Liu, J.; Xu, Z.; Masliyah, J. (2005a). Colloidal Forces Between Bitumen Surfaces in Aqueous Solutions Measured with Atomic Force Microscope. *Colloids and Surfaces A: Physicochemical and Engineering Aspects*, vol. 260, pp. 217-228.
- Liu, J.; Xu, Z.; Masliyah, J. (2005b). Interaction Forces in Bitumen Extraction from Oil Sands. *Journal of Colloid and Interface Science*, vol. 287, no. 2, pp. 507-520.
- Liu, J.; Xu, Z.; Masliyah, J. (2005c). Processability of Oil Sand Ores in Alberta. *Energy Fuels*, vol. 19, pp. 2056-2063.
- Liu, J.; Xu, Z.; Masliyah, J. (2004b). Role of Fine Clays in Bitumen Extraction from Oil Sands. *AIChE J.*, vol. 50, no. 8, pp. 1917-1927.
- Liu, J.; Xu, Z.; Masliyah, J. (2003). Studies on Bitumen-Silica Interaction in Aqueous Solutions by Atomic Force Microscopy. *Langmuir*, vol. 19, pp. 3911-3920.
- Liu, J.; Zhou, Z.; Xu, Z.; Masliyah, J. (2002). Bitumen-Clay Interactions in Aqueous Media Studied by Zeta Potential Distribution Measurement. *Journal of Colloidal and Interface Science*, vol. 252, pp. 409-418.
- Long, J. (2016). Optimized Caustic Control Based on Ore Grade and Fines Content for Bitumen Extraction from Mined Oil Sands. U.S. Patent 9,458,386B2, October 4.

Long, J.; Drelich, J.; Xu, Z.; Masliyah, J. H. (2007). Effect of Operating Temperature on Water-Based Oil Sands Processing. *The Canadian Journal of Chemical Engineering*, vol. 85, pp. 726-738.

Long, J.; Li, H.; Xu, Z.; Masliyah, J. (2011). Improving Oil Sands Processability Using a Temperature –Sensitive Polymer. *Energy Fuels*, vol. 25, pp. 701-707.

Long, J.; Xu, Z.; Masliyah, J. (2006). Role of Illite-illite Interactions in Oil Sands Processing. *Colloids and Surfaces A: Physicochemical and Engineering Aspects*, vol. 281, pp. 202-214.

Lu, X.; Wang, L.; Lei, K.; Huang, J.; Zhai, Y. (2009). Contamination Assessment of Copper, Lead, Zinc, Manganese and Nickel in Street Dust of Baoji, NW China. *Journal of Hazardous Materials*, vol. 161, pp. 1058-1062.

Lund, C. (2013). Mineralogical, Chemical and Textural Characterisation of the Malmberget Iron Ore Deposit for a Geometallurgical Model. Ph.D. Thesis, Luleå University of Technology, Luleå, Sweden.

Madge, D. N.; Romero, J.; Strand, W. L. (2004). Hydrocarbon Cyclones in Hydrophilic Oil Sand Environments. *Minerals Engineering*, vol. 17, pp. 625-636.

Mantler, M.; Schreiner, M. (2000). X-ray Fluorescence Spectrometry in Art and Archaeology. *X-ray Spectrometry*, vol. 29, pp. 3-17.

Mao, L.; Yoon, R. H. (1997). Predicting Flotation Rates Using a Rate Equation Derived from the First Principles. *International Journal of Mineral Processing*, vol. 51, no. 1-4, pp. 171-181.

Marjan, T. B.; Harbottle, D.; Curran, M.; Ng, S.; Spence, J.; Siy, R.; Liu, Q.; Masliyah, J.; Xu, Z. (2015). Role of Caustic Addition in Bitumen-Clay Interactions. *Energy Fuels*, vol. 29, pp. 58-69.

Martin, M. J. S.; Cruz, M. S. R.; Andrades, M. S.; Camazano, M. S. (2006). Efficiency of Different Clay Minerals Modified with A Cationic Surfactant in the Adsorption of Pesticides: Influence of Clay Type and Pesticide Hydrophobicity. *Applied Clay Science*, vol. 31, pp. 216-228.

Martines, E.; Csaderova, L.; Morgan, H.; Curtis, A. S. G.; Riehle, M. O. (2008). DLVO Interaction Energy Between a Sphere and a Nano-patterned Plate. *Colloids and Surfaces A: Physicochemical and Engineering Aspects*, vol. 318, pp. 45-52.

Marwick, B. (2005). Element Concentrations and Magnetic Susceptibility of Anthrosols: Indicators of Prehistoric Human Occupation in the Inland Pilbara, Western Australia. *Journal of Archaeological Science*, vol. 32, pp. 1357-1368.

Masliyah, J. H.; Czarnecki, J; Xu, Z. (2011). *Handbook on Theory and Practice of Bitumen Recovery form Athabasca Oil Sands*. Volume I : Theoretic Basis, Kingsley Knowledge Publishing, Canada.

Masliyah, J. H.; Czarnecki, J; Xu, Z. (2013). *Handbook on Theory and Practice of Bitumen Recovery form Athabasca Oil Sands*. Volume II : Industrial Practice, Kingsley Knowledge Publishing, Canada.

Masliyah, J. H.; Zhou, Z.; Xu, Z.; Czarnecki, J; Hamza, H. (2004). Understanding Water-Based Bitumen Extraction from Athabasca Oil Sands. *The Canadian Journal of Chemical Engineering*, vol. 82, 628-654.

Meel, K. V.; Smekens, A.; Behets, M.; Kazandjian, P.; Grieken, R. V. (2007). Determination of Platinum, Palladium, and Rhodium in Automotive Catalysts Using High-Energy Secondary Target X-ray Fluorescence Spectrometry. *Analytical Chemistry*, vol. 79, pp. 6383-6389.

Melquiades, F. L.; Bortoleto, G. G.; Marchiori, L. F. S.; Bueno, M. I. M. S. (2012). Direct Determination of Sugar Cane Quality Parameters by X-ray Spectrometry and Multivariate Analysis. *Agricultural and Food Chemistry*, vol. 60, pp. 10755-10761.

Melquiades, F. L.; Santos, F. R. D. (2015). Preliminary Results: Energy Dispersive X-Ray Fluorescence and Partial Least Squares Regression for Organic Matter Determination in Soil. *Spectroscopy Letters*, vol. 48, pp. 286-289.

Mercier, P. H. J.; Ng, S.; Moran, K.; Sparks, B. D.; Kingston, D.; Kotlyar, L. S.; Kung, J.; Woods, J.; Patarachao, B.; McCracken, T. (2012). Colloidal Clay Gelation: Relevance to Current Oil Sands Operations. *Petroleum Science and Technology*, vol. 30, pp. 915-923.

Mercier, P. H. J.; Pararachao, B.; Kung, J.; Kingston, D.M.; Woods, J. R.; Sparks, B. D.; Kotlyar, L. S.; Ng, S.; Moran, K.; McCracken, T. (2008). X-Ray Diffraction (XRD)-Derived Processability Markers for Oil Sands Based on Clay Mineralogy and Crystallite Thickness Distributions. *Energy & Fuels*, vol. 22, pp. 3174-3193.

Mercier, P. H. J.; Tyo, D. D.; Zborowski, A.; Kung, J.; Patarachao, B.; Kingston, D. M.; Couillard, M.; Robertson, G.; McCracken, T.; Ng, S. (2019). First Quantification of <2 μm clay, <0.2 μm Ultrafines and Solids Wettability in Process Streams from Naphthenic Froth Treatment Plant at Commercial Mined Oil Sands Operations. *Fuel*, vol. 237, pp. 961-976.

Mikula, R. J.; Omotoso, O.; Friesen, W. I. (2007). Interpretation of Bitumen Recovery Data from Batch Extraction Tests. *Canadian Journal of Chemical Engineering*, vol. 85, no. 5, pp. 765-772.

Millington, D. (2018). Canadian Oil Sands Supply Costs and Development Projects (2018-2038). ISBN 1-927037-55-3, Canadian Energy Research Institute, Calgary, May 2018.

Mistra, M.; Aguilar, R.; Miller, J. D. (1981). Surface Chemistry Futures in the Hot Water Processing of Utah Tar Sand. *Separation Science Technology*, vol. 16, no. 10, pp. 1523-1544.

Mitchell, J. K. (1993). *Fundamentals of Soil Behavior*. 2nd Edition, John Wiley & Sons, Inc., New York.

Moore, D. M.; Reynolds, R. C. (1997). *X-ray Diffraction and the Identification and Analysis of Clay Minerals*. 2nd Edition, Oxford University Press, Oxford, New York.

Moran, K.; Yeung, A.; Masliyah, J. (2000). Factors Affecting the Aeration of Small Bitumen Droplets. *The Canadian Journal of Chemical Engineering*, vol. 78, pp. 625-634.

Mossop, G. D. (1980). Geology of the Athabasca Oil Sands. *Science*, vol. 207, pp. 145-152.

Mulligan, C. N.; Yong, R. N.; Gibbs, B. F. (2001). Surfactant-Enhanced Remediation of Contaminated Soil: A Review. *Engineering Geology*, vol. 60, pp. 371-380.

Musílek, L.; Čechák, T.; Trojek, T. (2012). X-ray Fluorescence in Investigations of Cultural Relics and Archaeological Finds. *Applied Radiation and Isotopes*, vol. 70, pp. 1193-1202.

Nayak, P. S.; Singh, B. K. (2007). Instrumental Characterization of Clays by XRF, XRD and FTIR. *Bulletin of Materials Science*, vol. 30, no. 3, pp. 235-238.

Neumann, C.; Eichinger, P. (1991). Ultra-Trace Analysis of Metallic Contaminations on Silicon Wafer Surfaces by Vapour Phase Decomposition/ Total Reflection X-ray Fluorescence (VPD/TXRF). *Spectrochimica Acta*, vol. 46B, no. 10, pp. 1369-1377.

Nguyen, A. V.; Nalaskowski, J.; Miller, J. D.; Butt, H. J. (2003). Attraction Between Hydrophobic Surfaces Studied by Atomic Force Microscopy. *International Journal of Mineral Processing*, vol. 72, pp. 215-225.

Norrish, K. (1954). The Swelling of Montmorillonite. *Discussions of the Faraday Society*, vol. 18, pp. 120-134.

Oats, W. J.; Ozdemir, O.; Nguyen, A. V. (2010). Effect of Mechanical and Chemical Clay Removals by Hydrocyclone and Dispersants on Coal Flotation. *Mineral Engineering*, vol. 23, pp. 413-419.

Oil sands magazine. (2016) "Oil Sands Physical & Chemical Properties," accessed on 22 November 2016, <http://www.oilsandsmagazine.com/oil-sands-deposit/>

Omotoso, D. (2011). Clay Characterization in the Oil Sand Industry. In *CONRAD Clay Workshop*, Edmonton, Canada, March 9-10.

Omotoso, O.; Eberl, D. (2009). Sample Preparation and Data Collection Strategies for X-Ray Diffraction Quantitative Phase Analysis of Clay-Bearing Rocks. Proceedings of the 46th Annual Meeting of the Clay Minerals Society, Billings, Montana, June 5-11.

Osacky, M.; Geramian, M.; Ivey, D. G.; Liu, Q.; Etsell, T. H. (2013). Mineralogical and Chemical Composition of Petrologic End Members of Alberta Oil Sands. *Fuel*, vol. 113, pp. 148-157.

Oscik, J. (1982). *Adsorption*. John Wiley & Sons, Inc., New York, pp.42.

Paktunc, A. D. (1998). Modan: An Interactive Computer Program for Estimating Mineral Quantities Based on Bulk Composition. *Computers & Geosciences*, vol. 24, no. 5, pp. 425-431.

- Parian, M.; Lamberg, P.; Möckel, R.; Rosenkranz, J. (2015). Analysis of Mineral Grades for Geometallurgy: Combined Element-to-Mineral Conversion and Quantitative X-Ray Diffraction. *Minerals Engineering*, vol. 82, pp. 25-35.
- Pauling, L. (1930). The Structure of Micas and Related Minerals. *Proceedings of the National Academy of Sciences of the United States of America*, vol. 16, pp. 123-129.
- Paunesku, T.; Vogt, S.; Maser, J.; Lai, B.; Woloschak, G. (2006). X-Ray Fluorescence Microprobe Imaging in Biology and Medicine. *Journal of Cellular Biochemistry*, vol. 99, pp. 1489-1502.
- Petruk, W. (2000). Applied Mineralogy in the Mining Industry. Elsevier, Ottawa, Canada.
- Pilote, M.; André, C.; Turcotte, P.; Gagné, F.; Gagnon, C. (2018). Metal Bioaccumulation and Biomarkers of Effects in Caged Mussels Exposed in the Athabasca Oil Sands Area. *Science of the Total Environment*, vol. 610-611, pp. 377-390.
- Poliakov, A.; Donskoi, E. (2014). Automated Relief-Based Discrimination of Non-Opaque Minerals in Optical Image Analysis. *Minerals Engineering*, vol. 55, pp. 111-124.
- Poppe, L. J.; Paskevich, V. F.; Hathaway, J. C.; Blackwood, D. S. (2001). A Laboratory Manual for X-Ray Powder Diffraction. *U. S. Geological Survey (USGS) Open-File Report 01-041*, <https://pubs.usgs.gov/of/2001/of01-041/>
- Potgieter, J. H. (1990). An Experimental Study of the Adsorption Behavior of Methylene Blue on Activated Carbon. *Colloids and Surfaces*, vol. 50, pp. 393-399.
- Potgieter, J. H. and Strydom, C. A. (1999). Determination of the Clay Index of Limestone with Methylene Blue Adsorption Using A UV-VIS Spectrophotometric Method. *Cement and Concrete Research*, vol. 29, pp. 1815-1817.

Prado, G. H. C.; Riya; Hyrve, M.; Klerk, A. D. (2018). Role of Metal Halides in Coke Formation During Bitumen Upgrading, *Fuel*, vol. 211, pp. 775-782.

Primkulov, B. K. (2014). Bitumen Liberation Dynamics. Ph.D. Thesis, University of Alberta, Edmonton, Alberta, Canada.

Querry, M. R. (1987). Optical Constants of Minerals and Other Materials from the Millimeter to the Ultraviolet. Contractor Report CRDEC-CR-88009.

Rabinovich, Y. I.; Yoon, R. H. (1994). Use of Atomic Force Microscopy for the Measurement of Hydrophobic Forces Between Silanated Silica Plate and Glass Sphere. *Langmuir*, vol. 10, pp. 1903-1909.

Raju, G. J. N.; Sarita, P.; Rao, J. C. S.; Rao, K. C. B.; Reddy, S. B. (2013). Correlation of Trace Elemental Content in Selected Anticancer Medicinal Plants with Their Curative Ability Using Particle Induced X - Ray Emission (PIXE). *Journal of Medicinal Plants Research*, vol. 7, no. 16, pp. 1081-1086.

Ralston, J.; Fornasiero, D.; Hayes, R. A. (1999). Bubble-Particle Attachment and Detachment in Flotation. *International Journal of Mineral Processing*, vol. 56, pp. 133-164.

Ralston, J.; Fornasiero, D.; Mishchuk, N. (2001). The Hydrophobic Force in Flotation – a Critique. *Colloids and Surfaces A: Physicochemical and Engineering Aspects*, vol. 192, pp. 39-51.

Ramasamy, V. and Anandalakshmi, K. (2008). The Determination of Kaolinite Clay Content in Limestones of Western Tamil Nadu by Methylene Blue Adsorption Using UV-VIS Spectroscopy. *Spectrochimica Acta Part A*, vol. 70, pp. 25-29.

- Ramsey, M. H.; Pottes, P. J.; Webb, P. C.; Watkins, P.; Watson, J. S.; Coles, B. J. (1995). An Objective Assessment of Analytical Method Precision: Comparison of ICP-AES and XRF for the Analysis of Silicate Rocks. *Chemical Geology*, vol. 124, pp. 1-19.
- Rankin, J.; Litz, K.; Briggs, S.; McCaskill, T.; Scudder, M.; Khalid, S.; Budhani, R. (2016). Selective Desulfonylation of Oxidized Sulfur Compounds in Crude Oil by Alcohol-Mediated Nucleophilic Attack Studied by XANES and XRF Spectroscopy. *Preprints*, pp. 2016090075.
- Rao, F.; Liu, Q. (2013). Froth Treatment in Athabasca Oil Sands Bitumen Recovery Process: A Review. *Energy Fuels*, vol. 27, pp. 7199-7207.
- Reinhardt, J. (2004). Optical Mineralogy in a Modern Earth Sciences Curriculum. *Journal of Geoscience Education*, vol. 52, pp. 60-67.
- Ren, S.; Dang-Vu, T.; Zhao, H.; Long, J.; Xu, Z.; Masliyah, J. (2009a). Effect of Weathering on Surface Characteristics of Solids and Bitumen from Oil Sands. *Energy Fuels*, vol. 23, no. 1, pp. 334-341.
- Ren, S.; Zhao, H.; Dang-Vu, T.; Xu, Z.; Masliyah, J. H. (2009b). Effect of Weathering on Oil Sands Processability. *The Canadian Journal of Chemical Engineering*, vol. 87, pp. 879-886.
- Ren, S.; Zhao, H.; Long, J.; Xu, Z.; Masliyah, J. (2009c). Understanding Weathering of Oil Sands Ores by Atomic Force Microscopy. *AIChE Journal*, vol. 55, no. 12, pp. 3277-3285.
- Repka, C. C. (2007). Bitumen-Montmorillonite Interactions in Aqueous Media. M.S. Thesis, University of Alberta, Edmonton, Alberta, Canada.
- Rietveld, H. M. (1967). Line Profiles of Neutron Powder Diffraction Peaks for Structure Refinement. *Acta Crystallographica*, vol. 22, pp. 151-152.

Rihawy, M. S.; Bakraji, E. H.; Aref, S.; Shaban, R. (2010). Elemental Investigation of Syrian Medicinal Plants Using PIXE Analysis. *Nuclear Instruments and Methods in Physics Research B*, vol. 268, pp. 2790-2793.

Robertson, J.; Thomas, C. J.; Caddy, T. B.; Lewis, A. J. M. (1984). Particle Size Analysis of Soils – A Comparison of Dry and Wet Sieving Techniques. *Forensic Science International*, vol. 24, no. 3, pp. 209-217.

Robinson, D. A. (2004). Measurement of the Solid Dielectric Permittivity of Clay Minerals and Granular Samples Using a Time Domain Reflectometry Immersion Method. *Vadose Zone Journal*, vol.3, pp.705-713.

Romanova, U. G.; Valinasab, M.; Stasiuk, E. N.; Yarranton, H. W.; Schramm, L. L.; Shelfantook, W. E. (2006). The Effect of Oil Sands Bitumen Extraction Conditions on Froth Treatment Performance. *Journal of Canadian Petroleum Technology*, vol. 45, no. 9, pp. 36-45.

Rosa, L.; Davis, K. F.; Rulli, M. C.; D'Odorico, P. (2017). Environmental Consequences of Oil Production from Oil Sands. *Earths Future*, vol. 5, pp. 158-170.

Rouzaud, J. N.; Oberlin, A. (1989). Structure, Microtexture, and Optical Properties of Anthracene and Saccharose-Based Carbons. *Carbon*, vol. 27, no. 4, pp. 517-529.

Rowe, H.; Hughes, N.; Robinson, K. (2012). The Quantification and Application of Handheld Energy-Dispersive X-ray Fluorescence (ED-XRF) in Mudrock Chemostratigraphy and Geochemistry. *Chemical Geology*, vol. 324-325, pp. 122-131.

Rui, Z.; Wang, X.; Zhang, Z.; Lu, J.; Chen, G.; Zhou, X.; Patil, S. (2018). A Realistic and Integrated Model for Evaluating Oil Sands Development with Steam Assisted Gravity Drainage Technology in Canada. *Applied Energy*, vol. 213, pp. 76-91.

Ryan, P. C.; Wall, A. J.; Hillier, S.; Clark, L. (2002). Insights into Sequential Chemical Extraction Procedures from Quantitative XRD: A Study of Trace Metal Partitioning in Sediments Related to Frog Malformities. *Chemical Geology*, vol. 184, pp. 337-357.

Ryland, A. L. (1958). X-ray Diffraction. *Journal of Chemical Education*, vol. 35, no. 2, pp. 80-83.

Saada, A.; Siffert, B.; Papirer, E. (1995). Comparison of the Hydrophilicity/Hydrophobicity of Illites and Kaolinites. *Journal of Colloid and Interface Science*, vol. 174, pp. 185-190.

Sanford, E. (1983). Processability of Athabasca Oil Sand: Interrelationship between Oil Sand Fine Solids, Process Aids, Mechanical Energy and Oil Sand Age after Mining. *Canadian Journal of Chemical Engineering*, vol. 61, pp. 554-567.

Sanford, E. C. and Seyer, F. A. (1979). Processability of Athabasca Tar Sand Using a Batch Extraction Unit: The Role of NaOH. *CIM Bulletin*, vol. 72, pp. 164-179.

Schramm, L. L. (2000). *Surfactants: Fundamentals and Applications in the Petroleum Industry*. Cambridge University Press, United Kingdom.

Schramm, L.L. (1989). The Influence of Suspension Viscosity on Bitumen Rise Velocity and Potential Recovery in the Hot Water Flotation Process for Oil Sands. *Journal of Canadian Petroleum Technology*, vol. 28, no. 3, pp. 73-80.

Schramm, L. L.; Smith, R. G. (1985). Influence of Natural Surfactants on Interfacial Charges in the Hot Water Process for Recovering Bitumen from the Athabasca Oil Sands. *Colloids and Surfaces*, vol. 14, no. 1, pp. 67-85.

Schramm, L. L.; Smith, R. G. (1987). Two Classes of Anionic Surfactants and Their Significance in Hot Water Processing of Oil Sands. *Canadian Journal of Chemical Engineering*, vol. 65, no. 5, pp. 799-811.

Schramm, L. L.; Smith, R. G.; Stone, J. A. (1984a). A Surface Tension Method for the Determination of Anionic Surfactants in Hot Water Processing of Athabasca Oil Sands. *Colloids and Surfaces*, vol. 11, no. 3-4, pp. 247-263.

Schramm, L. L.; Smith, R. G.; Stone, J. A. (1985). On the Processibility of Mixtures of Oil Sands. *AOSTRA Journal of Research*, vol. 1, no. 3, pp. 147-161.

Schramm, L. L.; Smith, R. G.; Stone, J. A. (1984b). The Influence of Natural Surfactants Concentration on the Hot Water Process for Recovering Bitumen from the Athabasca Oil Sands. *AOSTRA Journal of Research*, vol. 1, pp. 5-14.

Schramm, L. L.; Stasiuk, E. N.; Turner, D. (2003). The Influence of Interfacial Tension in the Recovery of Bitumen by Water-Based Conditioning and Flotation of Athabasca Oil Sands. *Fuel Processing Technology*, vol. 80, pp. 101-118.

Scott, A. C.; Young, R. F.; Fedorak, P. M. (2008) Comparison of GC-MS and FTIR Methods for Quantifying Naphthenic Acids in Water Samples. *Chemosphere*, vol. 73, pp. 1258-1264.

Scrivener, K. L.; Füllmann, T.; Gallucci, E.; Walenta, G.; Bermejo, E. (2004). Quantitative Study of Portland Cement Hydration by X-ray Diffraction/Rietveld Analysis and Independent Methods. *Cement and Concrete Research*, vol. 34, pp. 1541-1547.

Searle, A. B. (1960). *The Chemistry and Physics of Clay and Other Ceramic Materials*, 3rd Edition, Ernest Benn Ltd., London.

Sharma, R.; Bisen, D. P.; Shukla, U.; Sharma, B. G. (2012). X-ray Diffraction: A Powerful Method of Characterizing Nanomaterials. *Recent Research in Science and Technology*, vol. 4, no. 8, pp. 77-79.

Shaw, R. C.; Czarnecki, J.; Schramm, L. L.; Axelson, D. (1994). Bituminous Froths in the Hot-Water Flotation Process. In *Foams: Fundamentals and Applications in the Petroleum Industry*, Elsevier, Washington, DC, the United States.

Sivamohan, R. (1990). The Problem of Recovering Very Fine Particles in Mineral Processing—A Review. *International Journal of Mineral Processing*, vol. 28, pp. 247-288.

Siy, R.; Cymerman, G.; Long, J.; Vandenberghe, J. (2011). Oil Sand Slurry Solids Reduction to Enhance Extraction Performance for Problem Ores. U.S. Patent 20,110,127,198A1, June 2.

Smith, A. M.; Johnston, K. A.; Crawford, S. E.; Marbella, L. E.; Millstone, J. E. (2017). Ligand Density Quantification on Colloidal Inorganic Nanoparticles. *Analyst*, vol. 142, pp. 11-29.

Sparks, B. D.; Kotlyar, L. S.; O'Carroll, J. B.; Chung, K. H. (2003). Athabasca Oil Sands: Effect of Organic Coated Solids on Bitumen Recovery and Quality. *Journal of Petroleum Science and Engineering*, vol. 39, pp. 417-430.

Spencer, R.; Weedmark, T. (2015). Application of X-Ray Fluorescence (XRF) Analyses to the Characterization of Oil Sands Reservoirs. In *GeoConvention: New Horizons*, Calgary, AB, Canada, May 4 to 8.

Spencer, R.; Weedmark, T.; Besplug, J. (2016). Determination of Reservoir Properties in Bitumen Saturated Core from XRF Analyses. In *CSPG Poster Oil Sands 2016*, XRF Solutions.

Spencer, R.; Weedmark, T.; Besplug, J. (2016). Determination of Reservoir Properties in Bitumen Saturated Core from XRF Analysis. In *GeoConvention: Optimizing Resources*, Calgary, AB, Canada, Marth 7 to 11.

Srinivasa, S.; Flury, C.; Afacan, A.; Masliyah, J.; Xu, Z. (2012). Study of Bitumen Liberation from Oil Sands Ores by Online Visualization. *Energy Fuels*, vol. 26, no. 5, pp. 2883-2890.

Stevenson, F. J. (1982). *Humans Chemistry-Genesis, Composition, Reactions*. John Wiley and Sons, Inc., New York.

Stoch, L.; Waclawska, I. (1981). Dehydroxylation of Kaolinite Group Minerals 1. Kinetics of Dehydroxylation of Kaolinite and Halloysite. *Journal of Thermal Analysis*, vol. 20, pp. 291-304.

Studart, A. R.; Amstad, E.; Antoni, M.; Gauckler, L. J. (2006). Rheology of Concentrated Suspensions Containing Weakly Attractive Alumina Nanoparticles. *Journal of the American Ceramic Society*, vol. 89, no. 8, pp. 2418-2425

Stumm, W. and Morgan, J. J. (1996). *Aquatic Chemistry*. John Wiley and Sons, Inc., New York.

Suárez, M. H.; Rodríguez, E. M.; Romero, C. D. (2007). Mineral and Trace Element Concentrations in Cultivars of Tomatoes. *Food Chemistry*, vol. 104, pp. 489-499.

Sury, K. N. (1990). Low Temperature Bitumen Recovery Process. U.S. Patent 4,946,597A, August 7.

Sutherland, D. (2007). Estimation of Mineral Grain Size Using Automated Mineralogy. *Minerals Engineering*, vol. 20, pp. 452-460.

Sutherland, D. N.; Gottlieb, P. (1991). Application of Automated Quantitative Mineralogy in Mineral Processing. *Minerals Engineering*, vol. 4, no. 7-11, pp. 753-762.

Takamura, K. (1982). Microscopic Structure of Athabasca Oil Sand. *The Canadian Journal of Chemical Engineering*, vol. 60, pp. 538-545.

Takamura, K.; Wallace, D. (1988). The Physical Chemistry of the Hot Water Process. *The Journal of Canadian Petroleum Technology*, vol. 27, pp. 98-106.

Tambe, D. E.; Sharma, M. M. (1993). Factors Controlling the Stability of Colloid-Stabilized Emulsions: I. An Experimental Investigation. *Journal of Colloid and Interface Science*, vol. 157, pp. 244-253.

Taylor, R. K. (1985). Cation Exchange in Clays and Mudrocks by Methylene Blue. *Journal of Chemical Technology & Biotechnology*, vol. 35A, pp. 195-207.

Taylor, S. D.; Czarnecki, J.; Masliyah, J. (2001). Refractive Index Measurements of Diluted Bitumen Solutions. *Fuel*, vol. 80, pp.2013-2018.

Tewari, B. B. and Thornton, C. O. (2010). Use of Basic Methylene Blue Dye for Specific Surface Area Measurement of Metal Hexacyanoferrate (II) Complexes, *Revista de la Sociedad Química del Perú.*, vol. 76, no. 4, pp. 330-335.

Theng, B. K. G. and Scharpenseel, H. W. The Adsorption of ¹⁴C-Labeled Humic Acid by Montmorillonite. Proceedings of the International Clay Conference, Applied Publishing Wilmette, pp. 643-653.

Tipman, R. (2000). Muskeg Pilot Plant: Experience with Poorly Processing Ores. In *CONRAD Extraction Fundamentals Seminar*, Fort McMurray, AB, Canada, March 28.

Tombácz, E.; and Szekeres, M. (2006). Surface Charge Heterogeneity of Kaolinite in Aqueous Suspension in Comparison with Montmorillonite. *Applied Clay Science*, vol. 34, no. 1-4, pp. 105-124.

Torelli, M. D.; Putans, R. A.; Tan, Y.; Lohse, S. E.; Murphy, C. J.; Hamers, R. J. (2015). Quantitative Determination of Ligand Densities on Nanomaterials by X-ray Photoelectron Spectroscopy. *ACS Applied Materials & Interfaces*, vol. 7, pp. 1720-1725.

Tu, Y.; O'Carroll, J. B.; Kotlyar, L. S.; Sparks, B. D.; Ng, S.; Chung, K. H.; Cuddy, G. (2005). Recovery of Bitumen from Oilsands: Gelation of Ultra-fine Clay in the Primary Separation Vessel. *Fuel*, vol. 84, pp. 653-660.

Tu, Y.; Kingston, D.; Kung, J.; Kotlyar, L. S.; Sparks, B. D.; Chung, K. H. (2006). Adsorption of Pentane Insoluble Organic Matter from Oilsands Bitumen Onto Clay Surfaces. *Petroleum Science and Technology*, vol. 24, no. 3-4, pp. 327-338.

Twining, B. S.; Baines, S. B.; Fisher, N. S.; Maser, J.; Vogt, S.; Jacobsen, C.; Sanchez, A. T.; Wilhelmy, S. A. S. (2003). Quantifying Trace Elements in Individual Aquatic Protist Cells with a Synchrotron X-Ray Fluorescence Microprobe. *Analytical Chemistry*, vol. 75, pp. 3806-3816.

Usui, S. (1973). Interaction of Electrical Double Layers at Constant Surface Charge. *Journal of Colloid and Interface Science*, vol. 44, pp. 107-113.

Valiño, V.; Román, M. F. S.; Ibáñez, R.; Benito, J. M.; Escudero, I.; Ortiz, I. (2014). Accurate Determination of Key Surface Properties That Determine the Efficient Separation of Bovine Milk BSA And LF Proteins. *Separation and Purification Technology*, vol. 135, pp. 145-157.

van Olphen, H. (1963). *An Introduction to Clay Colloid Chemistry*. John Wiley and Sons, Inc., New York.

Vietti, D. (2011). Clay Mineralogy and Water Chemistry on Tailings Settling and Rheology. In *CONRAD Clay Workshop*, Edmonton, Canada, March 9-10.

Violante, A.; Pigna, M. (2002). Competitive Sorption of Arsenate and Phosphate on Different Clay Minerals and Soils. *Soil Science Society of America Journal*, vol. 66, pp. 1788-1796.

Wallace, D. (2015). Clay Behavior and Influence on Oil Sands Extraction. In *COSIA Clay Workshop*, Edmonton, Canada, April 28-29.

Wallace, D.; Henry, D.; Takamura, K. (1989). A Physical Chemical Explanation for Deterioration in the Hot Water Processability of Athabasca Oil Sand Due to Aging, *Fuel Science and Technology International*, vol. 7, no. 5-6, pp. 699-725.

Wallace, D.; Kadatz, B.; Tipman, R.; Snaychuck, S. (2001). Problem Ores: Application of BEU Units to the Simulation of Continuous Processes. In *CONRAD Oil Sands Extraction Fundamentals and Process Water Chemistry*, Fort McMurray, AB, Canada, May 7-8.

Wallace, D.; Tipman, R.; Komishke, B.; Wallwork, V.; Perkins, E. (2004). Fines/Water Interactions and Consequences of the Presence of Degraded Illite on Oil Sands Extractability. *The Canadian Journal of Chemical Engineering*, vol. 82, pp. 667-677.

Wallwork, V.; Xu, Z.; Masliyah, J. (2003). Bitumen Recovery with Oily Air Bubbles. *Canadian Journal of Chemical Engineering*, vol. 81, no. 5, pp. 993-997.

- Wallwork, V.; Xu, Z.; Masliyah, J. (2004). Processibility of Athabasca Oil Sand Using A Laboratory Hydrotransport Extraction System (LHES). *Canadian Journal of Chemical Engineering*, vol. 82, no. 4, pp. 687-695.
- Wang, L.; Dang-Vu, T.; Xu, Z.; Masliyah, J. H. (2010). Use of Short-Chain Amine in Processing of Weathered/Oxidized Oil Sands Ores. *Energy Fuels*, vol. 24, pp. 3581-3588.
- Wang, X.; Chow, J. C.; Kohl, S. D.; Percy, K. E.; Legge, A. H.; Watson, J. G. (2015). Characterization of PM_{2.5} and PM₁₀ Fugitive Dust Source Profiles in the Athabasca Oil Sands Region. *Journal of the Air & Waste Management Association*, vol. 65, no. 12, pp. 1421-1433.
- Wan, J. and Tokunaga, T. K. (2002). Partitioning of Clay Colloids at Air-Water Interface. *Journal of Colloid and Interface Science*, vol. 247, no. 1, pp. 54-61.
- Warren, L. J. (1975). Shear-Flocculation of Ultrafine Scheelite in Sodium Oleate Solutions. *Journal of Colloid and Interface Science*, vol. 50, pp. 307-318.
- Weedmark, T.; Spencer, R.; Besplug, J.; Wright, H. (2018). Deriving Mineralogy and Reservoir Properties in the Oil Sands Using X-Ray Fluorescence (XRF). In *CSPG Core Conference: in Conjunction with Geoconvention*, Calgary, AB, Canada, May 10-11.
- Weltje, G. J.; Tjallingii, R. (2008). Calibration of XRF Core Scanners for Quantitative Geochemical Logging of Sediment Cores: Theory and Application. *Earth and Planetary Science Letters*, vol. 274, pp. 423-438.
- White, C. E.; Provis, J. L.; Riley, D. P.; Kearley, G. J.; van Deventer, J. S. J. (2009). What Is the Structure of Kaolinite? Reconciling Theory and Experiment. *The Journal of Physical Chemistry B*, vol. 113, no. 19, pp. 6756-6765.

Whiten, B. (2007). Calculation of Mineral Composition from Chemical Assays. *Mineral Processing and Extractive Metallurgy Review*, vol. 29, no. 2, pp. 83-97.

Wik, S.; Sparks, B. D.; Ng, S.; Tu, Y.; Li, Z.; Chung, K. H.; Kotlyar, L. S. (2008). Effect of Process Water Chemistry and Particulate Mineralogy on Model Oilsands Separation Using a Warm Slurry Extraction Process Simulation. *Fuel*, vol. 87, pp. 1394-1412.

Winburn, R. S.; Lerach, S. L.; Jarabek, B. R.; Wisdom, M. A.; Grier, D. G.; McCarthy, G. J. (2000). Quantitative XRD Analysis of Coal Combustion By-Products by the Rietveld Method. Testing with Standard Mixtures. *Advances in X-ray Analysis*, vol. 42, pp. 387-396.

Wobrauschek, P.; Aiginger, H. (1975). Total-Reflection X-Ray Fluorescence Spectrometric Determination of Elements in Nanogram Amounts. *Analytic Chemistry*, vol. 47, no. 6, pp. 852-855.

Xiao, Y.; Pudasainee, D.; Gupta, R.; Xu, Z.; Diao, Y. (2017). Bromination of Petroleum Coke for Elemental Mercury Capture. *Journal of Hazardous Materials*, vol. 336, pp. 232-239.

Xie, M.; Bohlen, A. V.; Klockenkämper, R.; Jian, X.; Günther, K. (1998). Multielement Analysis of Chinese Tea (*Camellia Sinensis*) by Total-Reflection X-ray Fluorescence. *Z Lebensm Unters Forsch A*, vol. 207, pp. 31-38.

Xu, G. (2018). Atmospheric Benzo [a] pyrene and Vanadium Evidence for the Presence of Petroleum Coke Dust in the Athabasca Oil Sands Region, Alberta, *Canadian Journal of Cleaner Production*, vol. 171, pp. 592-599.

Xu, S. and Boyd, S. A. (1995). Cationic Surfactant Adsorption by Swelling and Nonswelling Layer Silicates. *Langmuir*, vol. 11, pp. 2508-2514.

Xu, Z.; Liu, J.; Choung, J. W.; Zhou, Z. (2003). Electrokinetic Study of Clay Interactions with Coal in Flotation. *International Journal of Mineral Processing*, vol. 68, pp. 183-196.

Yan, N.; Masliyah, J. H. (1994). Adsorption and Desorption of Clay Particles at the Oil-Water Interface. *Journal of Colloid and Interface Science*, vol. 168, pp. 386-392.

Yan, N.; Masliyah, J. H. (1995). Characterization and Demulsification of Solids-Stabilized Oil-in-Water Emulsions Part 1. Partitioning of Clay Particles and Preparation of Emulsions. *Colloids and Surfaces A: Physicochemical and Engineering Aspects*, vol. 96, pp. 229-242.

Yang, H.; Wang, Y.; Ding, M.; Hu, B.; Ren, S. (2012). Water-Assisted Solvent Extraction of Bitumen from Oil Sands. *Industrial & Engineering Chemistry Research*, vol. 51, no. 7, pp. 3032-3038.

Yariv, S. (2002). *Organo-Clay Complexes and Interactions*. Marcel Dekker, Inc., New York.

Yener, N.; Biçer, C.; Önal, M.; Sarikaya, Y. (2012). Simultaneous Determination of Cation Exchange Capacity and Surface Area of Acid Activated Bentonite Powders by Methylene Blue Adsorption. *Applied Surface Science*, vol. 258, no. 7, pp. 2534-2539.

Yeung, T. and Moran, K. (2000). Surface Heterogeneities and the Coalescence/Aeration of Bitumen Drops, In *N SERC Research Chair in Oil Sands Review Meeting*, University of Alberta, Edmonton, AB, pp. I1-I13.

Yeung, Z. L. L.; Kwok, R. C. W.; Yu, K. N. (2003). Determination of Multi-Element Profiles of Street Dust Using Energy Dispersive X-ray Fluorescence (EDXRF). *Applied Radiation and Isotopes*, vol. 58, pp. 339-346.

- Yoon, R. H. and Luttrell, G. H. (1989). The Effect of Bubble Size on Fine Particle Flotation. *Mineral Processing and Extractive Metallurgy Review*, vol. 5, no. 1, pp. 101-122.
- Young, R. A. (Eds.) (1993). *The Rietveld Method*. Oxford University Press. Oxford, New York.
- Yu, Y.; Ma, L.; Cao, M.; Liu, Q. (2017). Slime Coatings in Froth Flotation: A Review. *Minerals Engineering*, vol. 114, pp. 26-36.
- Yu, Y.; Ma, L.; Xu, H.; Sun, X.; Zhang, Z.; Ye, G. (2018). DLVO Theoretical Analyses Between Montmorillonite and Fine Coal Under Different pH and Divalent Cations. *Powder Technology*, vol. 330, pp.147-151.
- Yukselen, Y. and Kaya, A. (2008). Suitability of the Methylene Blue Test for Surface Area, Cation Exchange Capacity and Swell Potential Determination of Clayey Soils. *Engineering Geology*, vol. 102, pp. 38-45.
- Zhao, H.; Long, J.; Masliyah, J. H.; Xu, Z. (2006). Effect of Divalent Cations and Surfactants on Silica-Bitumen Interactions. *Industrial and Engineering Chemistry Research*, vol. 45, no. 22, pp. 7482-7490.
- Zhou, F.; Wang, L.; Xu, Z.; Liu, Q.; Deng, M.; Chi, R. (2014). Application of Reactive Oily Bubbles to Bastnaesite Flotation, *Minerals Engineering*, vol. 64, pp. 139-145.
- Zhou, Z.; Li, H.; Chow, R.; Roberge, K. (2013). Role of Carrier Flotation in Accelerating Bitumen Extraction Recovery from Mineable Athabasca Oil Sands. *The Canadian Journal of Chemical Engineering*, vol. 91, pp. 1340-1348.

Zhou, Z.; Kasongo, T.; Xu, Z.; Masliyah, J. (2004). Assessment of Bitumen Recovery from the Athabasca Oil Sands Using a Laboratory Denver Flotation Cell. *The Canadian Journal of Chemical Engineering*, vol. 82, 696-703.

Zhou, Z.; Li, H.; Chow, R.; Adeyinka, O. B.; Xu, Z.; Masliyah, J. (2017a). Impact of Fine Solids on Mined Athabasca Oil Sands Extraction I. Floatability of Fine Solids. *The Canadian Journal of Chemical Engineering*, vol. 95, pp. 111-119.

Zhou, Z.; Li, H.; Chow, R.; Adeyinka, O. B.; Xu, Z.; Masliyah, J. (2017b). Impact of Fine Solids on Mined Athabasca Oil Sands Extraction II. Effect of Fine Solids with Different Surface Wettability on Bitumen Recovery. *The Canadian Journal of Chemical Engineering*, vol. 95, pp. 120-126.

Zhou, Z.; Xu, Z.; Masliyah, J. H.; Czarnecki, J. (1999). Coagulation of Bitumen with Fine Silica in Model Systems. *Colloids and Surfaces A: Physicochemical and Engineering Aspects*, vol. 148, pp. 199-211.

APPENDIX A: EFFECT OF CLAYS ON FROTH SOLIDS PARTICLE SIZE DISTRIBUTION

A.1 Hydrophilic clays addition

To understand how the addition of different clays affected the froth solids particle size distribution (PSD), Figure A.1 shows the measured PSDs for the froth solids obtained. Table A.1 lists the key fractions of the PSD results. Without any clay addition (the baseline), the solids showed a narrow distribution with the peak centering around 170 μm . The introduction of 2 wt.% illite reduced the peak frequency values at $\sim 170 \mu\text{m}$ from 10 to 8% and led to slightly higher percentages of coarse particles in the froth than the baseline. When illite addition was increased to 5 wt.%, the froth solids PSD shows a bimodal distribution with the second peak centering around 1800 μm , indicating a further increased concentration of coarse particles. In contrast, kaolinite addition showed different trends as shown in Figure A.1. The highest peak shifted towards smaller sizes from 170 to 110 μm and a small PSD peak at 0.6 μm appeared when 2 wt.% kaolinite was added. Also, more smaller particles existed as compared to the baseline conditions. With 5 wt.% kaolinite addition, a trimodal distribution was observed for the froth solids and more small particles were obtained than 2 wt.% kaolinite addition. In general, kaolinite addition to the ore feed resulted in more fines and less coarse particles in the froth than illite addition.

The PSD results of the combined froth solids presented in Table A.1 indicate the different effects of illite and kaolinite. Addition of illite had little impact on froth fines content but led to more coarse particles (especially $>350 \mu\text{m}$ particles) in the froth. With 2 and 5 wt.% illite addition, froth coarse particles ($>175 \mu\text{m}$) fraction increased from the baseline at 28.6 to 33.3 and 38.6 vol.%, respectively. With kaolinite addition, the froth fines content ($<44 \mu\text{m}$) was significantly increased from the baseline of 16.3 to 43.6 and 57.5 vol.% for 2 and 5 wt.% addition, respectively. Also,

the content of coarse particles in froth solids were reduced from the baseline of 28.6 to ~10 vol.% when 5 wt.% kaolinite was added.

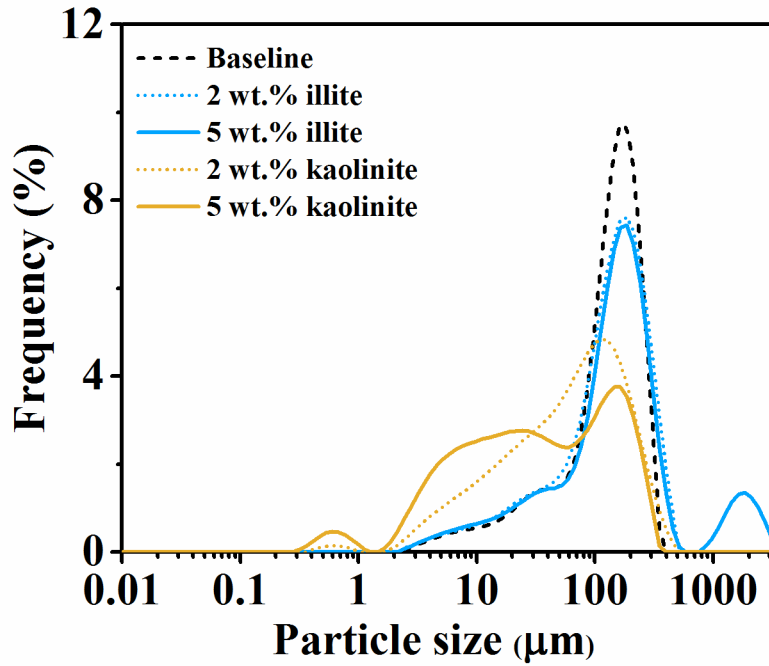


Figure A.1. Froth solids PSDs for the tests with hydrophilic clays addition.

Table A.1. Key size fractions for combined froth solids obtained for tests with hydrophilic clays addition

Condition	Combined PSD (vol.%)				
	Fine		Medium	Coarse	
	<2 μm	2~44 μm	44~175 μm	175~350 μm	>350 μm
Baseline	0	16.3	55.1	28.6	0
2% illite	0	17.8	48.9	30.3	3.0
5% illite	0	17.3	44.1	27.6	11.0
2% kaolinite	1.1	42.5	46.3	10	0.1
5% kaolinite	3.6	53.9	32.6	9.9	0

The results presented in Figure A.1 and Table A.1 show that:

- Clay addition significantly affected the PSD of froth solids.
- Kaolinite addition increased the content of fines ($< 44 \mu\text{m}$) and reduced the content of coarse particles ($>175 \mu\text{m}$) in the froth. Illite addition had little impact on the fines content but led to high content of coarse particles in the froth. Two possible fundamentals for such phenomenon are: 1) kaolinite is less hydrophilic than illite (Saada et al., 1995), therefore, kaolinite is more competitive to go to froth while illite is more likely to go with tailings; 2) kaolinite is unstable relative to illite (Edzwald et al., 1974) and expected to locate upstream from illite.
- Froth PSD is important for froth transportation, especially for the cases where the extraction and froth treatment facilities are far away from each other. A high content of coarse particles would lead to the settling of solids in a froth pipeline (Siy et al., 2011). Increasing fines content and reducing coarse particles content are important to ensure the proper transport of froth. This study indicates that addition of kaolinite is an effective way to improve froth transportability.

A.2 Hydrophobic solids addition

The PSDs of froth solids with the addition of hydrophobized solids are shown in Figure A.2. Compared to the baseline with a narrow distribution centering around $170 \mu\text{m}$, the addition of hydrophobized solid particles broaden the solids PSDs and shifted the peak toward smaller sizes. When 2 wt.% solids were added, the measured froth solids PSD had the highest peaks at around $100 \mu\text{m}$. More fines and fewer coarse particles existed in the froth. A lower peak appeared at $\sim 800 \mu\text{m}$ in the case of 2 wt.% hydrophobic silica addition. When 5 wt.% hydrophobic solids were added, the highest peaks shifted to $10\sim 20 \mu\text{m}$. This shows a higher fines content and a lower coarse

particles content than 2 wt.% hydrophobic solids addition. In general, clay mineralogy was less important due to similar surface coverage as expected.

The key fractions of froth solids PSD with hydrophobic solids addition are summarized in Table A.2. The addition of hydrophobic particles resulted in larger fraction of fine particles and smaller fraction of coarse particles in froth solids. Fines content (<44 μm) in froth solids increased from the baseline of 16.3 to ~46 and ~81 vol.% with 2 and 5 wt.% hydrophobic solids addition, respectively. While coarse particles content (>175 μm) in the froth solids decreased from the baseline of 28.6 to ~11 and 0.4 vol.% with 2 and 5 wt.% hydrophobic solids addition, respectively. Solids type had negligible impact. A comparison of Table A.2 and Table A.1 shows that hydrophobic solids addition to the ore feed resulted in more fines and less coarse particles in the froth than hydrophilic solids addition and solids mineralogy became less important because the surfaces were covered by organic matter.

Table A.2. Key size fractions for combined froth solids obtained for tests with hydrophobic solids addition

Condition	Combined PSD (vol.%)				
	Fine		Medium	Coarse	
	<2 μm	2~44 μm	44~175 μm	175~350 μm	>350 μm
Baseline	0	16.3	55.1	28.6	0
2% ho. illite	2.1	43.1	43.0	10.1	1.7
2% ho. silica	1.6	45.5	43.2	6	3.7
5% ho. illite	5.2	78	16.8	0	0
5% ho. kaolinite	4.4	74.3	20.5	0.8	0

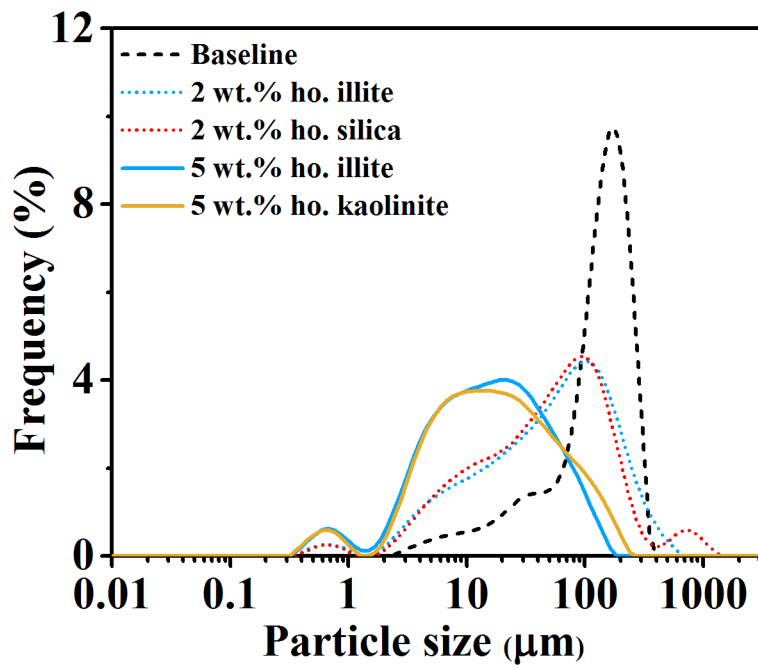


Figure A.2. Froth solids PSDs for the tests with hydrophobic solids addition (ho.= hydrophobic).

APPENDIX B: ZETA POTENTIAL DISTRIBUTIONS

ζ potential distributions of bitumen and clay particles at different conditions, individually or as a mixture, were shown in this appendix. The results were previously summarized in Table 3.5.

B.1 Bitumen-clay interactions without pH control

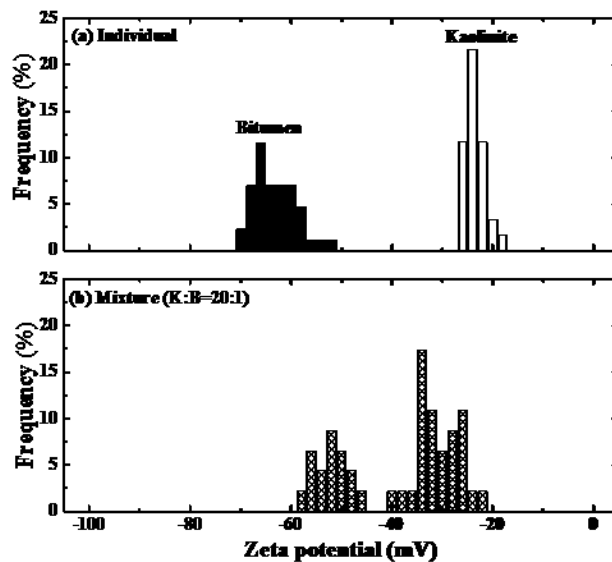


Figure B.1. ζ potential distributions of bitumen emulsion and kaolinite suspension (a) and their mixture at 20:1 (b) clay to bitumen mass ratio in 1 mM KCl aqueous solutions without pH control.

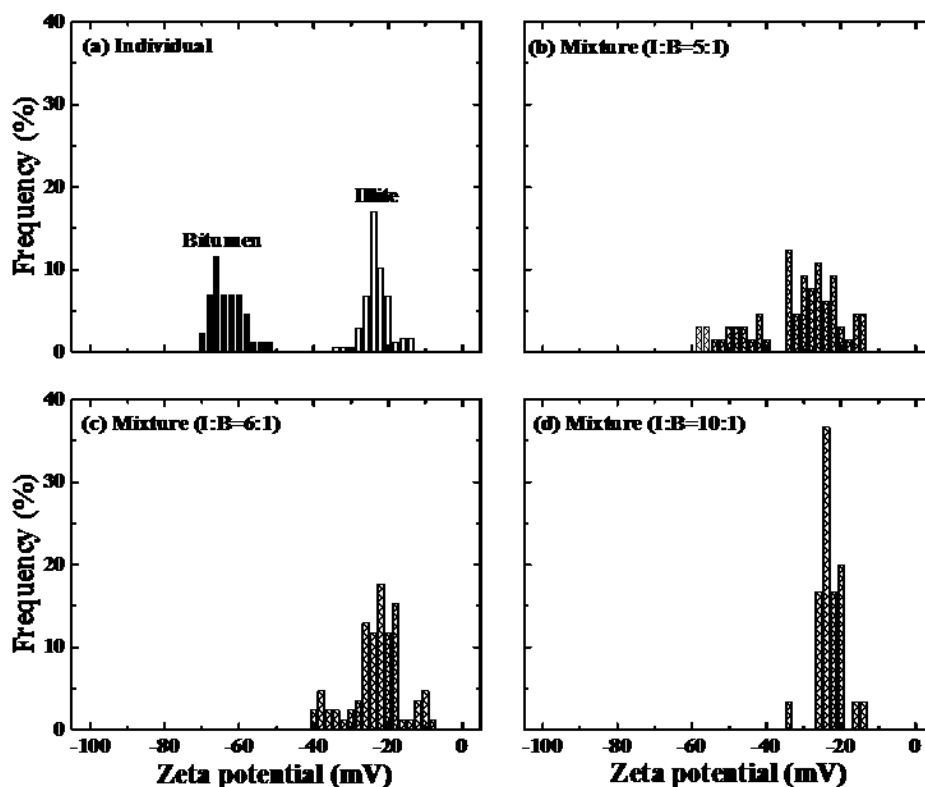


Figure B.2. ζ potential distributions of bitumen emulsion and illite suspension (a) and their mixtures at 5:1 (b), 6:1 (c), and 10:1 (d) clay to bitumen mass ratios in 1 mM KCl aqueous solutions without pH control.

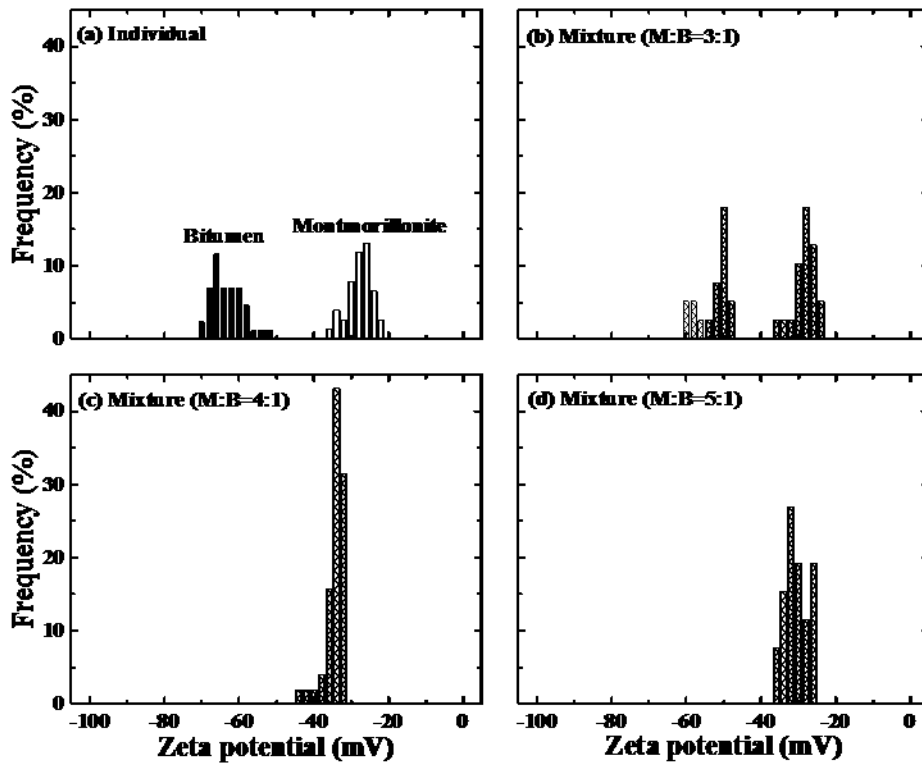


Figure B.3. ζ potential distributions of bitumen emulsion and montmorillonite suspension (a) and their mixtures at 3:1 (b), 4:1 (c), and 5:1 (d) clay to bitumen mass ratios in 1 mM KCl aqueous solutions without pH control.

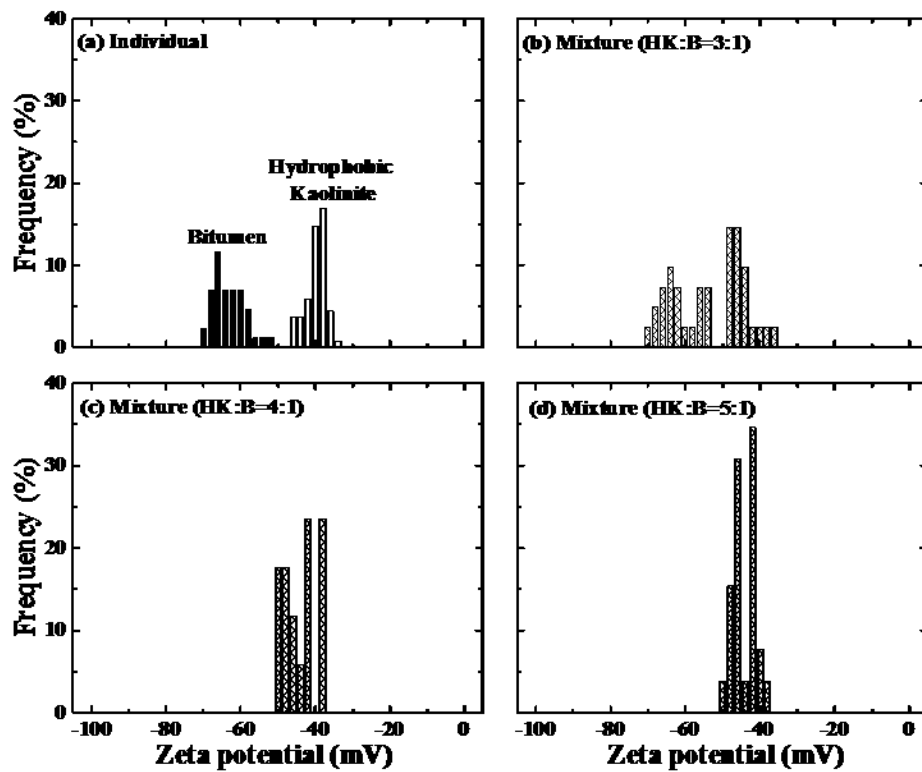


Figure B.4. ζ potential distributions of bitumen emulsion and hydrophobic kaolinite suspension (a) and their mixtures at 3:1 (b), 4:1 (c), and 5:1 (d) clay to bitumen mass ratios in 1 mM KCl aqueous solutions without pH control.

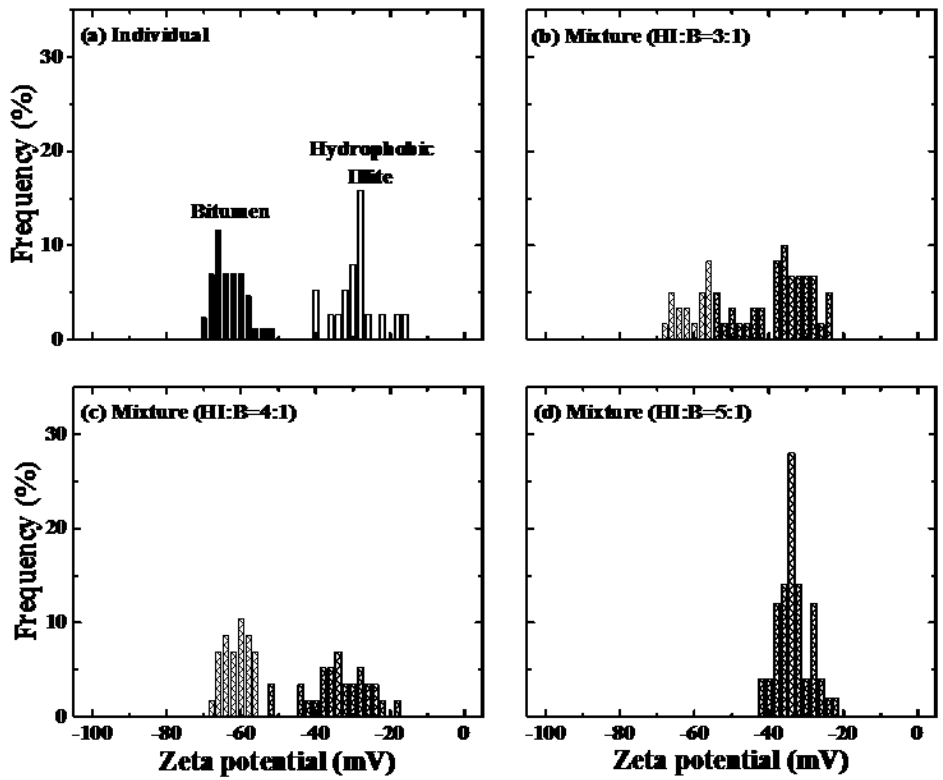


Figure B.5. ζ potential distributions of bitumen emulsion and hydrophobic illite suspension (a) and their mixtures at 3:1 (b), 4:1 (c), and 5:1 (d) clay to bitumen mass ratios in 1 mM KCl aqueous solutions without pH control.

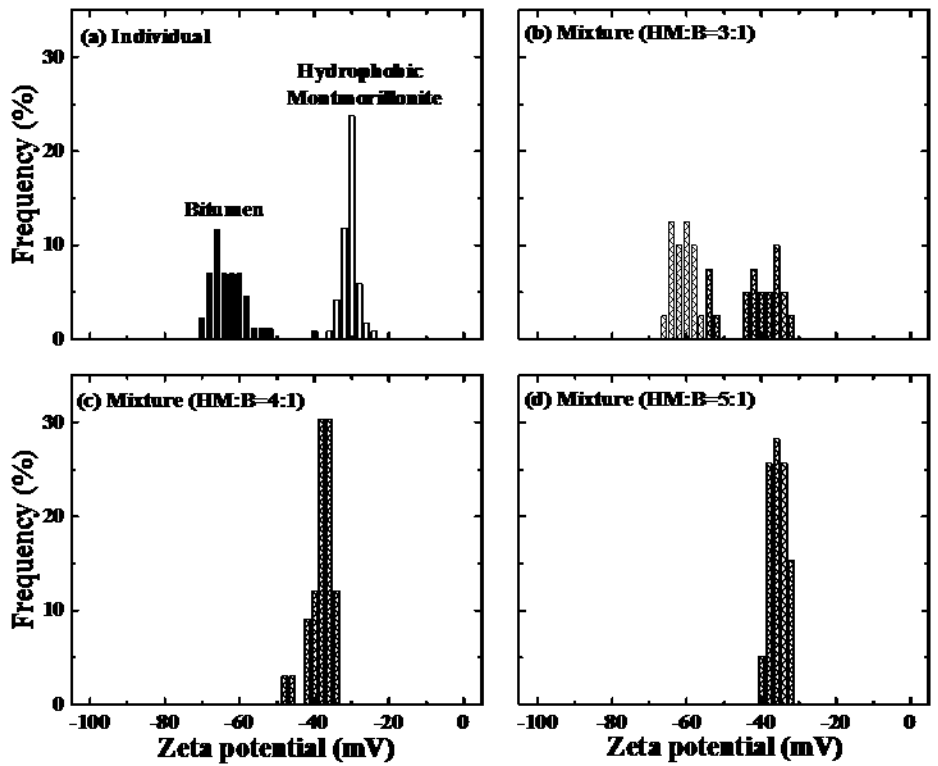


Figure B.6. ζ potential distributions of bitumen emulsion and hydrophobic montmorillonite suspension (a) and their mixtures at 3:1 (b), 4:1 (c), and 5:1 (d) clay to bitumen mass ratios in 1 mM KCl aqueous solutions without pH control.

B.2 Bitumen-clay interactions at pH 8.0

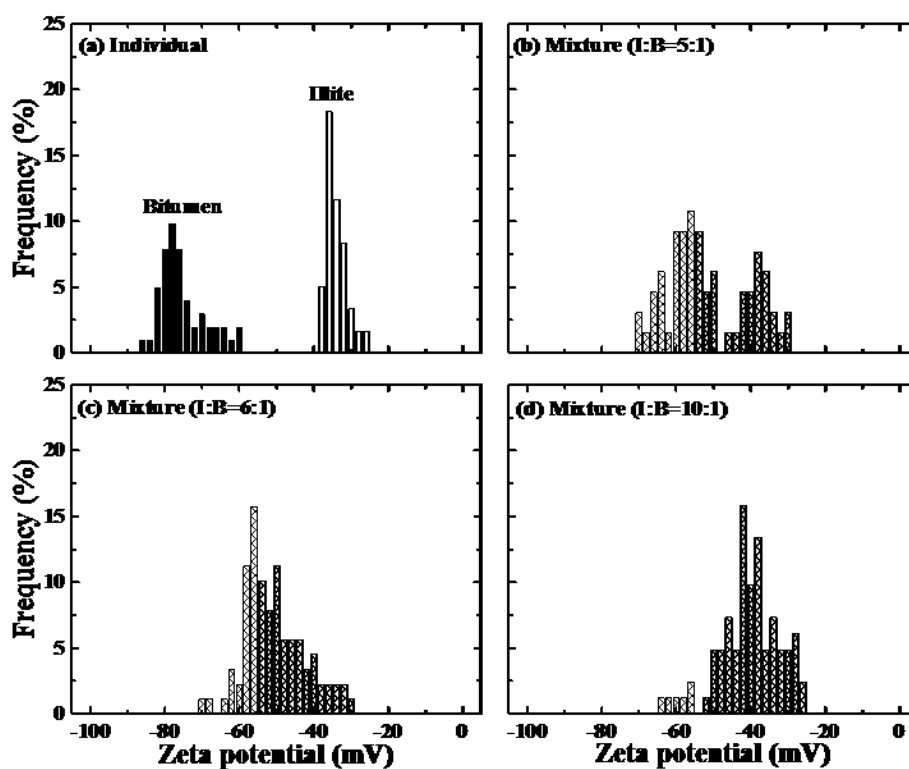


Figure B.7. ζ potential distributions of bitumen emulsion and illite suspension (a) and their mixtures at 5:1 (b), 6:1 (c), and 10:1 (d) clay to bitumen mass ratios in 1 mM KCl aqueous solutions of pH 8.0.

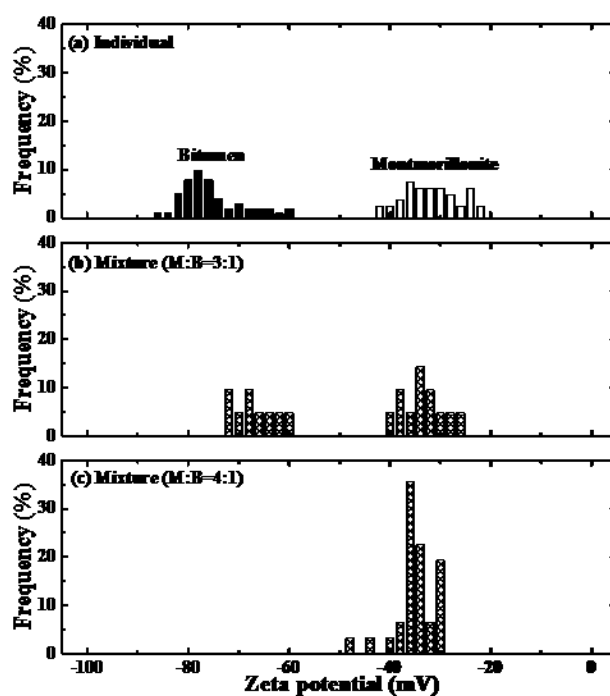


Figure B.8. ζ potential distributions of bitumen emulsion and montmorillonite suspension (a) and their mixtures at 3:1 (b) and 4:1 (c) clay to bitumen mass ratios in 1 mM KCl aqueous solutions of pH 8.0.

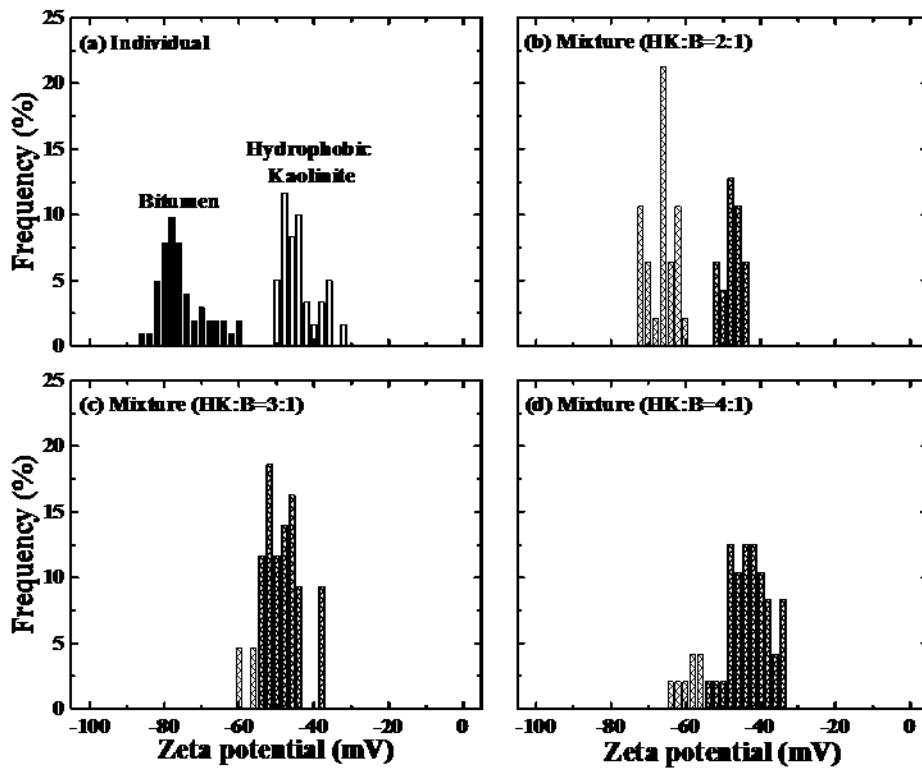


Figure B.9. ζ potential distributions of bitumen emulsion and hydrophobic kaolinite suspension (a) and their mixtures at 2:1 (b), 3:1 (c), and 4:1 (d) clay to bitumen mass ratios in 1 mM KCl aqueous solutions of pH 8.0.

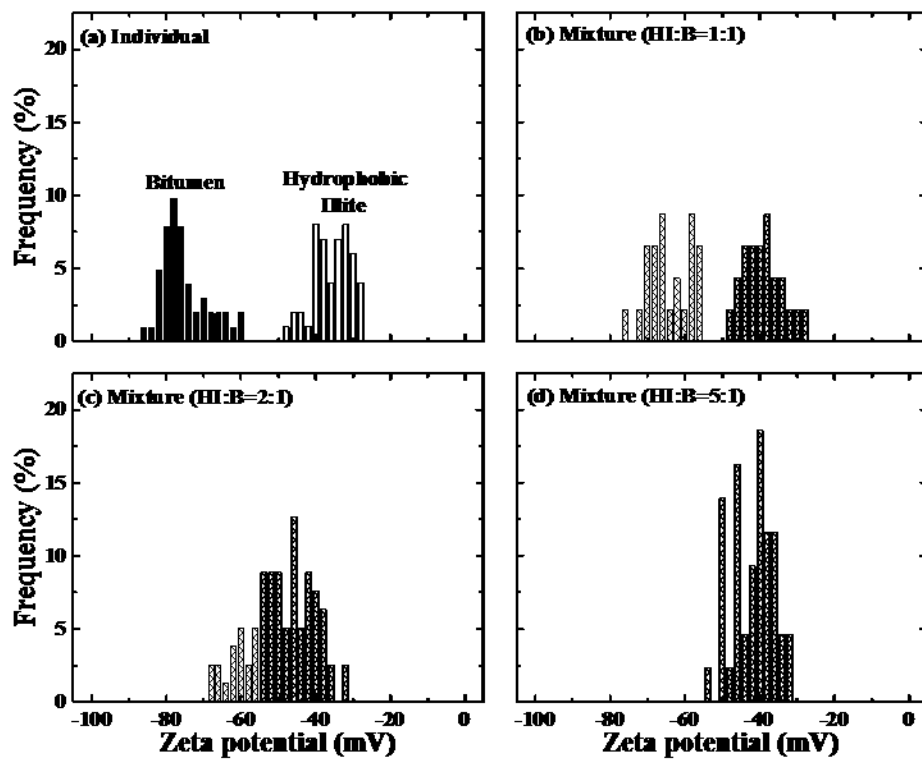


Figure B.10. ζ potential distributions of bitumen emulsion and hydrophobic illite suspension (a) and their mixtures at 1:1 (b), 2:1 (c), and 5:1 (d) clay to bitumen mass ratios in 1 mM KCl aqueous solutions of pH 8.0.

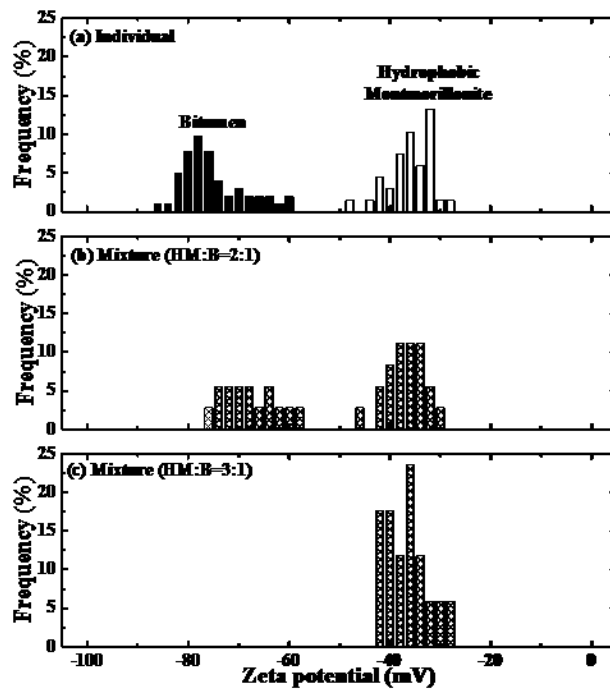


Figure B.11. ζ potential distributions of bitumen emulsion and hydrophobic montmorillonite suspension (a) and their mixtures at 2:1 (b) and 3:1 (c) clay to bitumen mass ratios in 1 mM KCl aqueous solutions of pH 8.0.

B.3 Bitumen-clay interactions at pH 10.8

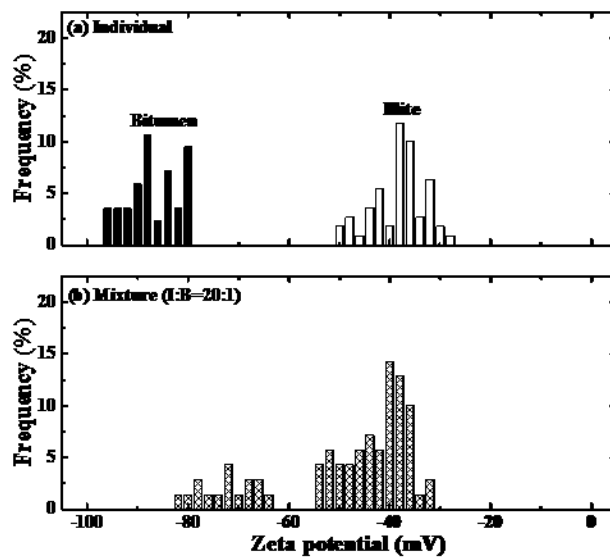


Figure B.12. ζ potential distributions of bitumen emulsion and illite suspension (a) and their mixture at 20:1 (b) clay to bitumen mass ratio in 1 mM KCl aqueous solutions of pH 10.8.

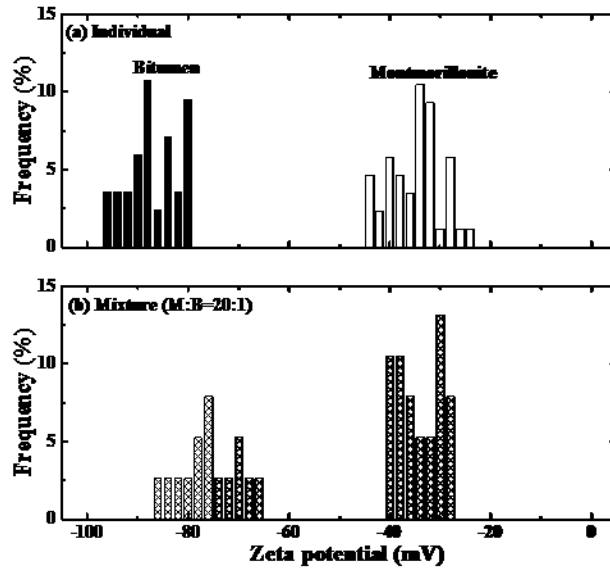


Figure B.13. ζ potential distributions of bitumen emulsion and montmorillonite suspension (a) and their mixture at 20:1 (b) clay to bitumen mass ratio in 1 mM KCl aqueous solutions of pH 10.8.

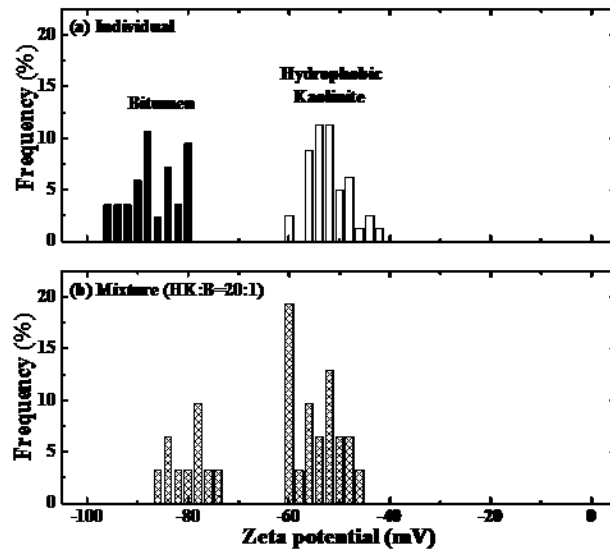


Figure B.14. ζ potential distributions of bitumen emulsion and hydrophobic kaolinite suspension (a) and their mixture at 20:1 (b) clay to bitumen mass ratio in 1 mM KCl aqueous solutions of pH 10.8.

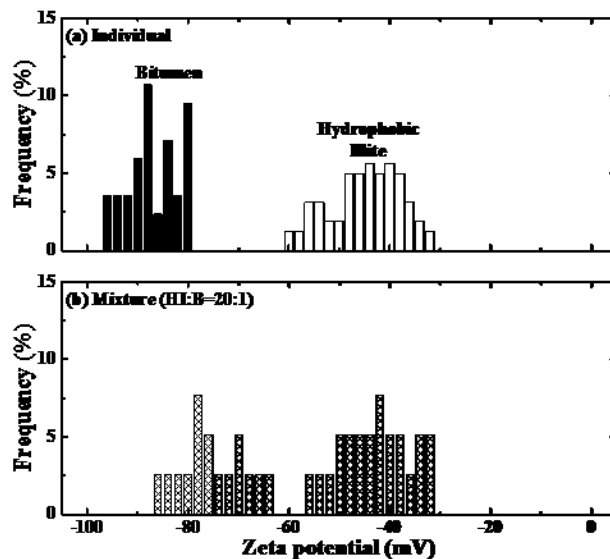


Figure B.15. ζ potential distributions of bitumen emulsion and hydrophobic illite suspension (a) and their mixture at 20:1 (b) clay to bitumen mass ratio in 1 mM KCl aqueous solutions of pH 10.8.

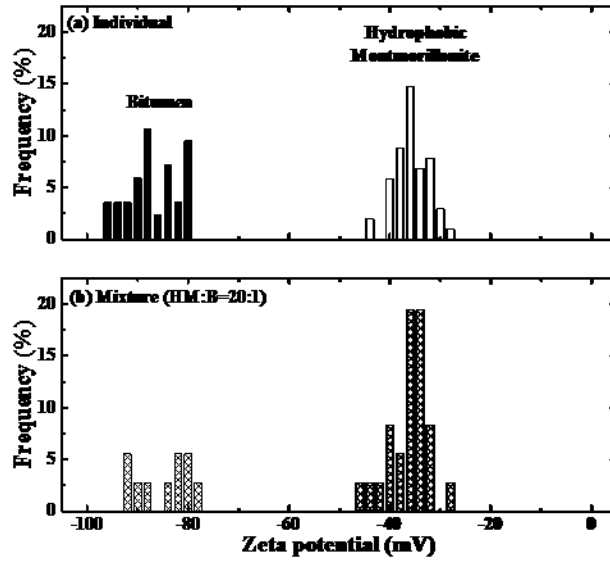


Figure B.16. ζ potential distributions of bitumen emulsion and hydrophobic montmorillonite suspension (a) and their mixture at 20:1 (b) clay to bitumen mass ratio in 1 mM KCl aqueous solutions of pH 10.8.

APPENDIX C: DLVO/EDLVO FITTING EQUATIONS AND PARAMETERS

C.1 Theoretic analysis

In this study, the analysis of bitumen clay interactions was performed in terms of the classical and extended DLVO theory. In hydrophilic clay system, the classical DLVO theory was adopted to simulate the interaction forces between bitumen and the basal planes of clays at different pH environments. The interaction force is determined by the sum of the van der Waals forces (F_{vdw}) and the electrostatic double layer force (F_{edl}) (Hogg et al., 1966).

$$F_{DLVO} = F_{vdw} + F_{edl} \quad (C.1)$$

The van der Waals forces can be calculated by Eq. (C.2) (Hogg et al., 1966):

$$\frac{F_{vdw}}{R} = -\frac{A_{132}}{6D^2} \quad (C.2)$$

where R is the radius of probe particles, D is the separation distance between two substances and A_{132} is the Hamaker constant for substances 1 and 2 interacting in the presence of medium 3.

According to Lifshiz approach, A_{132} can be evaluated by Hamaker constant values of interacting substances:

$$A_{132} \approx (\sqrt{A_{11}} - \sqrt{A_{33}})(\sqrt{A_{22}} - \sqrt{A_{33}}) \quad (C.3)$$

Hamaker constants for bitumen, water, silica and alumina were reported to be 6×10^{-20} , 3.7×10^{-20} , 6.5×10^{-20} (Liu, et al., 2003) and $1.52 \times 10^{-19}J$ (Studart et al., 2006), respectively. Then the combined Hamaker constant values calculated for bitumen-water-silica (A_{b-w-s}) and bitumen-water-alumina (A_{b-w-a}) were 3.3×10^{-21} and $1.0 \times 10^{-20}J$, respectively, as shown in Table C.1

The electrostatic double layer force is (Usui, 1973; Martines et al., 2008):

$$\frac{F_{edl}}{R} = 2\pi\epsilon\epsilon_0\kappa \left\{ 2\psi_1\psi_2 \frac{1}{e^{\kappa D} - e^{-\kappa D}} - (\psi_1^2 + \psi_2^2) \frac{e^{-\kappa D}}{e^{\kappa D} - e^{-\kappa D}} \right\} \quad (C.4)$$

Here, ψ_1 and ψ_2 are the surface potentials of substances 1 and 2, which are fitted using the measured ζ potentials for initial values. κ^{-1} is the Debye length (9.6 nm in 1 mM KCl).

To monitor bitumen-hydrophobic clay interactions, an extra attractive force referred to as long-range hydrophobic force (F_H) was supposed to exist between two hydrophobic surfaces in aqueous solution (Rabinovich and Yoon, 1994; Nguyen et al., 2003; Ralston et al., 2001), which could be described by an exponential form given below (Ralston et al., 2001):

$$\frac{F_H}{R} = C_0 \exp\left(\frac{-D}{D_0}\right) \quad (C.5)$$

where C_0 and D_0 are fitting parameters depend on the hydrophobicity of interacting substances. The introduction of the hydrophobic force in the classical DLVO theory leads to a so-called extended DLVO (EDLVO) theory:

$$F_{EDLVO} = F_{vdw} + F_{edl} + F_H \quad (C.6)$$

Table C.1. Hamaker constants

Substance	Bitumen	Water	Silica	Alumina	b-w-s	b-w-a
A ($\times 10^{-20}J$)	6	3.7	6.5	15.2	0.33	1.0

C.2 Bitumen-hydrophilic clays interactions

The force profiles of the interactions between bitumen and silica/alumina planes are shown in Figure 3.5 and Figure 3.6. DLVO fitting parameters based on the equations of C.1, C.2, and C.4 are obtained and listed in Table C.2 and Table C.3.

Table C.2. DLVO fitting parameters for bitumen-silica

pH	$\kappa^{-1}(\text{nm})$	$\psi_b(\text{mV})$	$\psi_s(\text{mV})$
5.6	9.4	-48	-29
8.0	9.4	-71	-50
10.8	9.2	-82	-64

*b=bitumen, s=silica

Table C.3. DLVO fitting parameters for bitumen-alumina

pH	$\kappa^{-1}(\text{nm})$	$\psi_b(\text{mV})$	$\psi_a(\text{mV})$
5.6	9.2	-48	12
8.0	8.8	-72	-12
10.8	8.2	-81	-31

*b=bitumen, a=alumina

C.3 Bitumen-hydrophobic clays interactions

The force profiles for bitumen-hydrophobic silica and bitumen-hydrophobic alumina interactions are shown in Figure 3.9 and Figure 3.10, respectively. The corresponding EDLVO fitting parameters (using Eq. C.2, C.4, C.5, and C.6) are listed in Table C.4 and Table C.5, respectively.

Table C.4. EDLVO fitting parameters for bitumen-hydrophobic silica

pH	$\kappa^{-1}(\text{nm})$	$\psi_b(\text{mV})$	$\psi_{hs}(\text{mV})$	$C_0(\text{mN/m})$	$D_0(\text{nm})$
5.6	9.2	-47	-34	6.0	11.8
8.0	9.2	-70	-54	5.2	8.1
10.8	9.1	-80	-68	5.0	6.5

*b=bitumen, hs=hydrophobic silica

Table C.5. EDLVO fitting parameters for bitumen-hydrophobic alumina

pH	$\kappa^{-1}(\text{nm})$	$\psi_b(\text{mV})$	$\psi_{ha}(\text{mV})$	$C_0(\text{mN/m})$	$D_0(\text{nm})$
5.6	9.1	-45	4	5.9	11.2
8.0	8.4	-74	-22	4.6	7.4
10.8	7.6	-81	-40	4.2	6.6

*b=bitumen, ha=hydrophobic alumina

APPENDIX D: XRF ELEMENT ANALYSIS FOR ESTIMATING ORE PROCESSABILITY

D.1 Correlations of elemental results in oil sands and fines content

Seven elements concentrations were determined using XRF technique. As shown in Figure D.1, with the exception of silicon, all elements were positively correlated with fines content, yielding correlation coefficients R^2 -values ranging from 0.84 to 0.94. The obtained good correlations ($R^2 > 0.8$) could be used as models for estimating the fines content in oil sands.

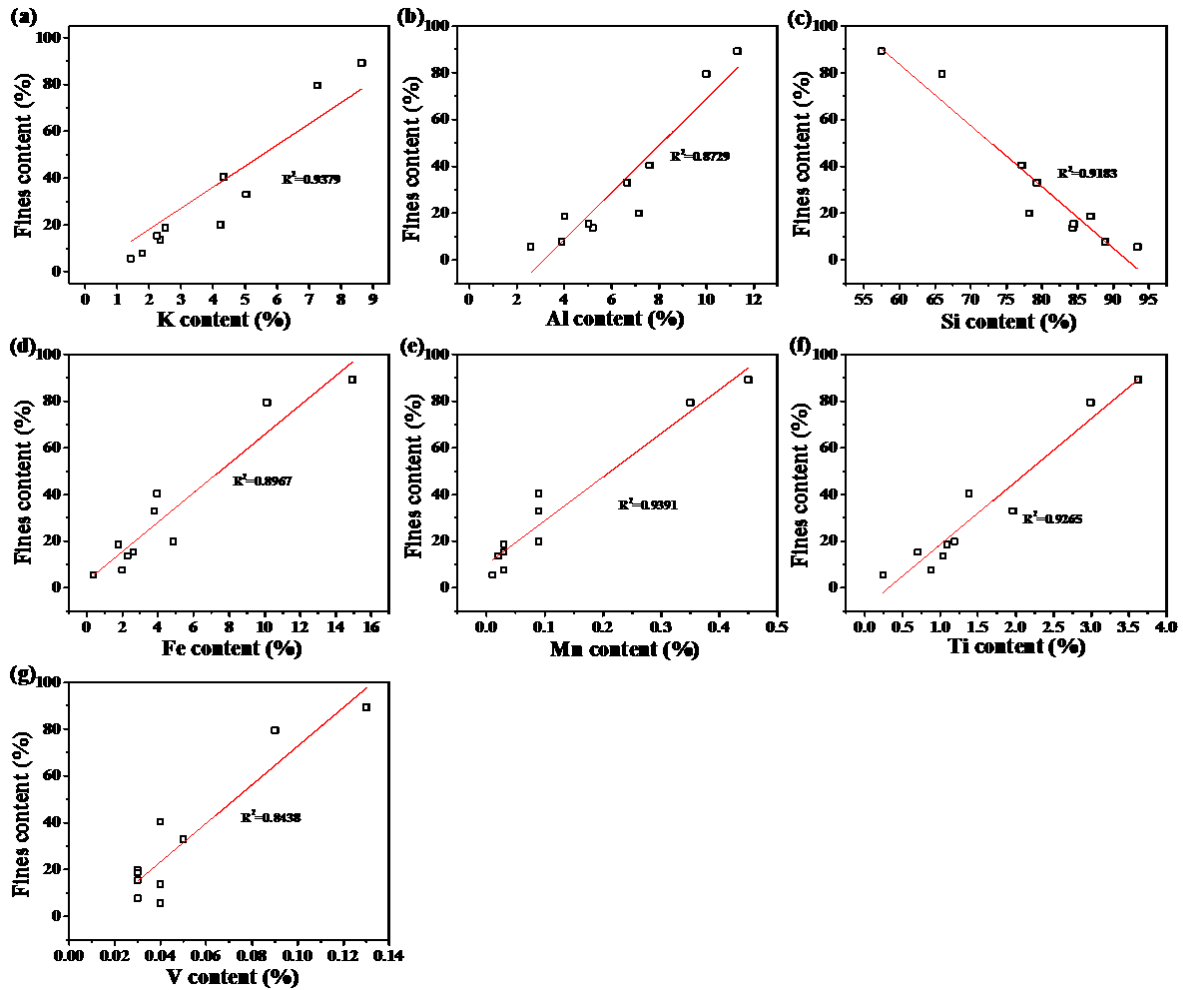


Figure D.1. Correlation plots for fines content versus (a) potassium, (b) aluminum, (c) silicon, (d) iron, (e) manganese, (f) titanium, and (g) vanadium concentrations for oil sands.

D.2 Correlations of elemental results in oil sands and bitumen grade

In oil sands regions with high bitumen grade, the content of fine solids tends to be lower. An inverse relationship between bitumen grade and fines content is expected since a high fines content would reduce sediment permeability, therefore hindering bitumen infiltration (Donkor et al., 1996). The plots of bitumen grade versus elemental concentrations are presented in Figure D.2. As expected, the relationships between element contents and bitumen grade were opposite to that between element contents and fines content. In addition to vanadium, correlation coefficients of other element concentrations with bitumen grade were greater than 0.8.

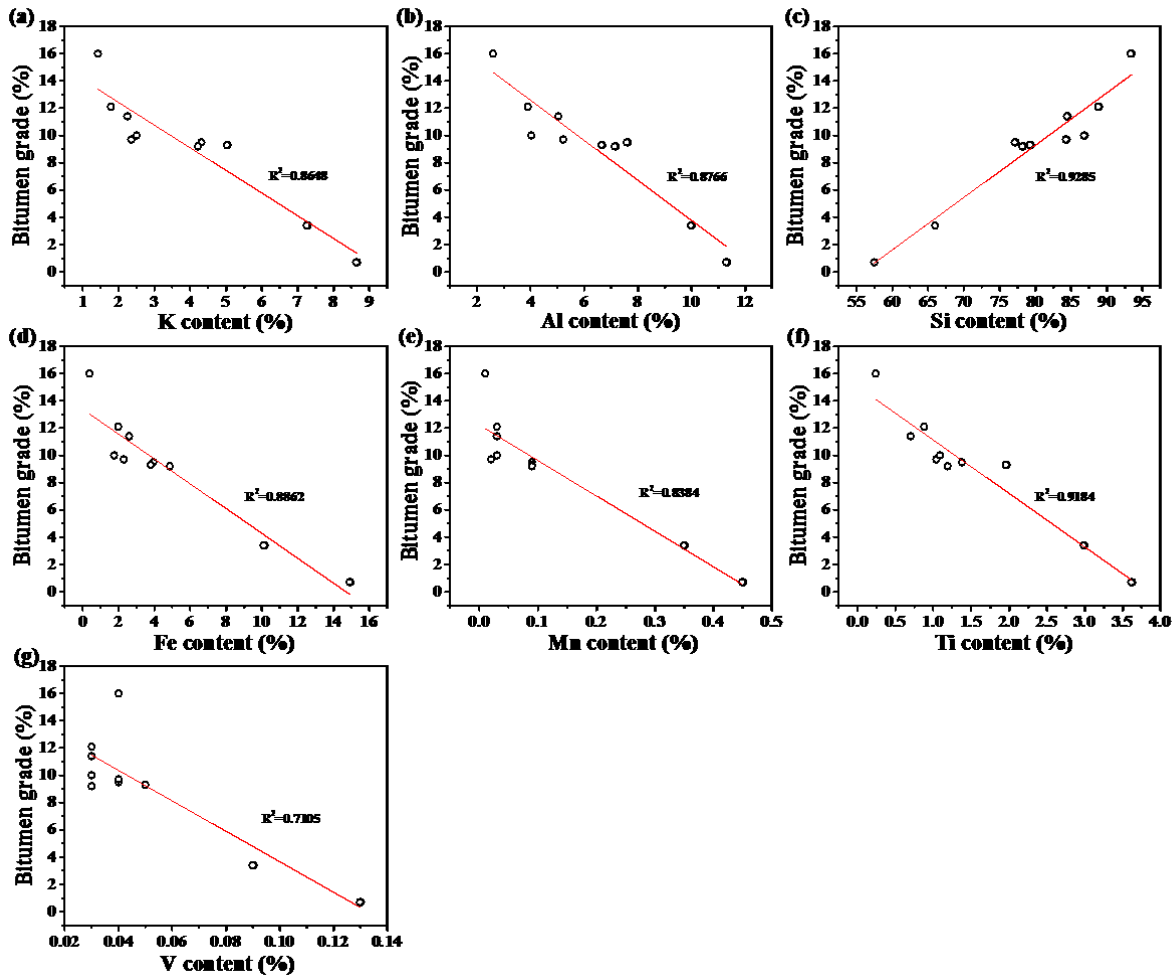


Figure D.2. Correlation plots for bitumen grade versus (a) potassium, (b) aluminum, (c) silicon, (d) iron, (e) manganese, (f) titanium, and (g) vanadium concentrations for oil sands.

D.3 Evaluation of bitumen recovery

In section 6.4, potassium contents of froth solids determined by XRF were observed to correlate negatively with bitumen recovery in oil sands extraction testes performed in Chapter 6. Figure D.3 shows aluminum and zirconium as alternative elements to evaluate bitumen recovery with tolerable precision.

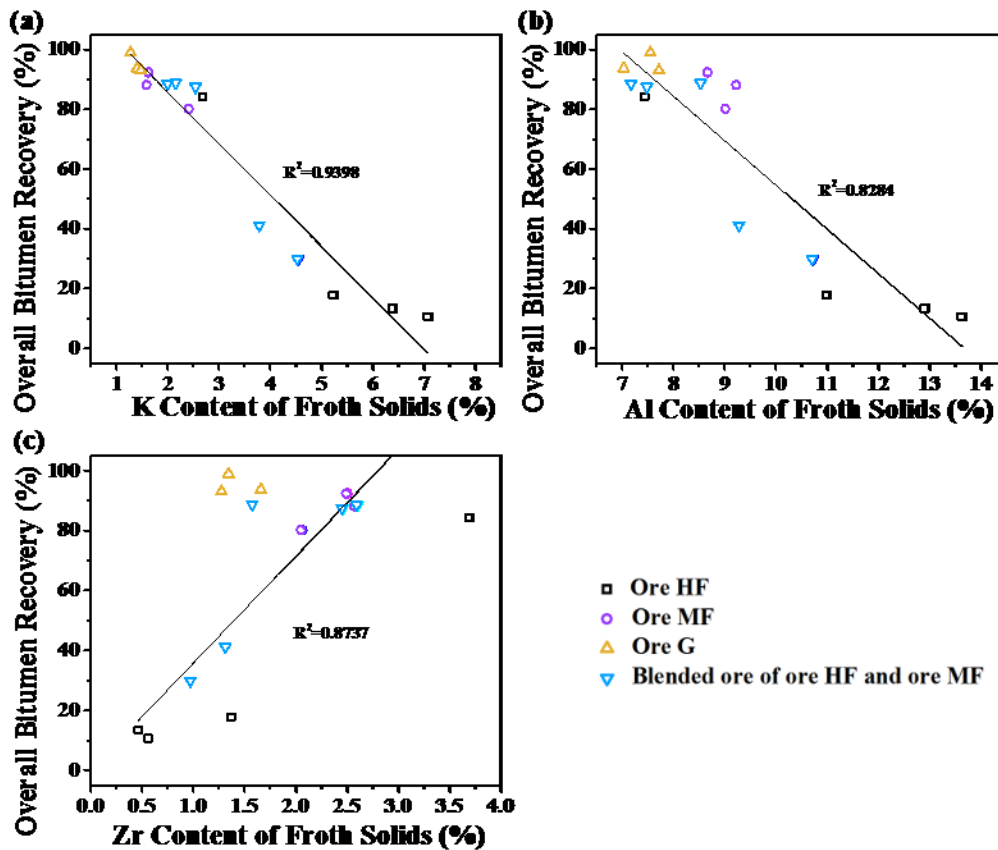


Figure D.3. Correlation plots for bitumen recovery versus (a) potassium, (b) aluminum, and (c) zirconium concentrations for oil sands.